**V. P. ROMBAKH**

# NON-INVASIVE MONITORING OF ATOMIC REACTIONS AND ITS APPLICATIONS

Catastrophes Prevention Research Laboratory

EDMONDS, WA USA

vrombakh@yahoo.com

2019

**Abstract**

This book contains 847[1] photographs, similar to those shown in the annotation. Photos were taken using simple devices for all types of deformations, plant growth and the functioning of cells of a living organism. These and 66 photographs taken by other authors in the study of nanomaterials using modern high-precision highly sensitive equipment and published confirm the author's conclusion that atomic reactions in a substance are accompanied by radiation of electromagnetic waves, called p-radiation, the frequency of which is comparable to X-ray radiation, but the penetrating power of the rays in this substance exceeds the penetrating ability of X-rays in millions of times**.**

*The use of radiation from atomic reactions can prevent technological disasters, predict earthquakes, tsunamis and pathological changes in plant cells and living organisms.*

[1] See Attachment No. 1

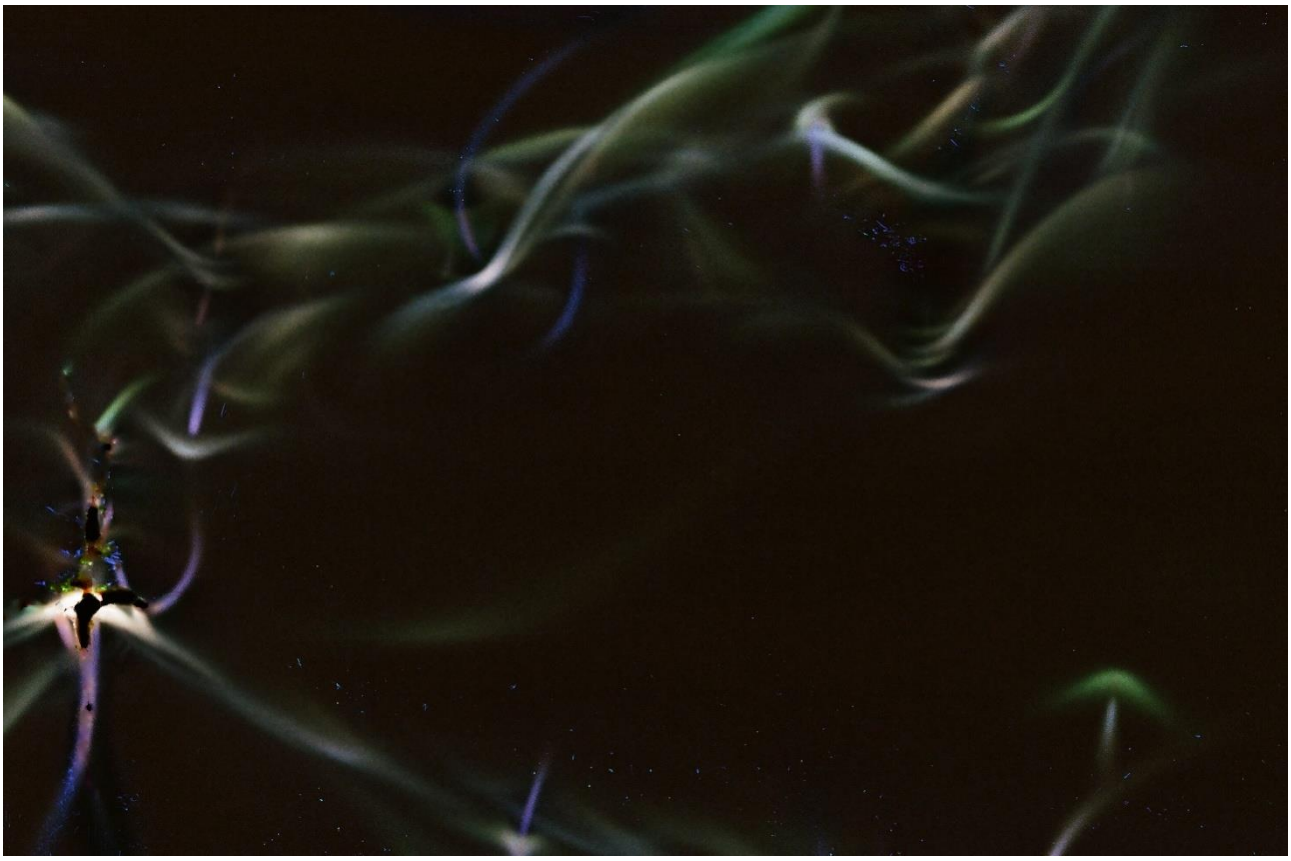

Photograph of the author’s heart, blood vessels and stents, obtained using p-radiation due to atomic reactions

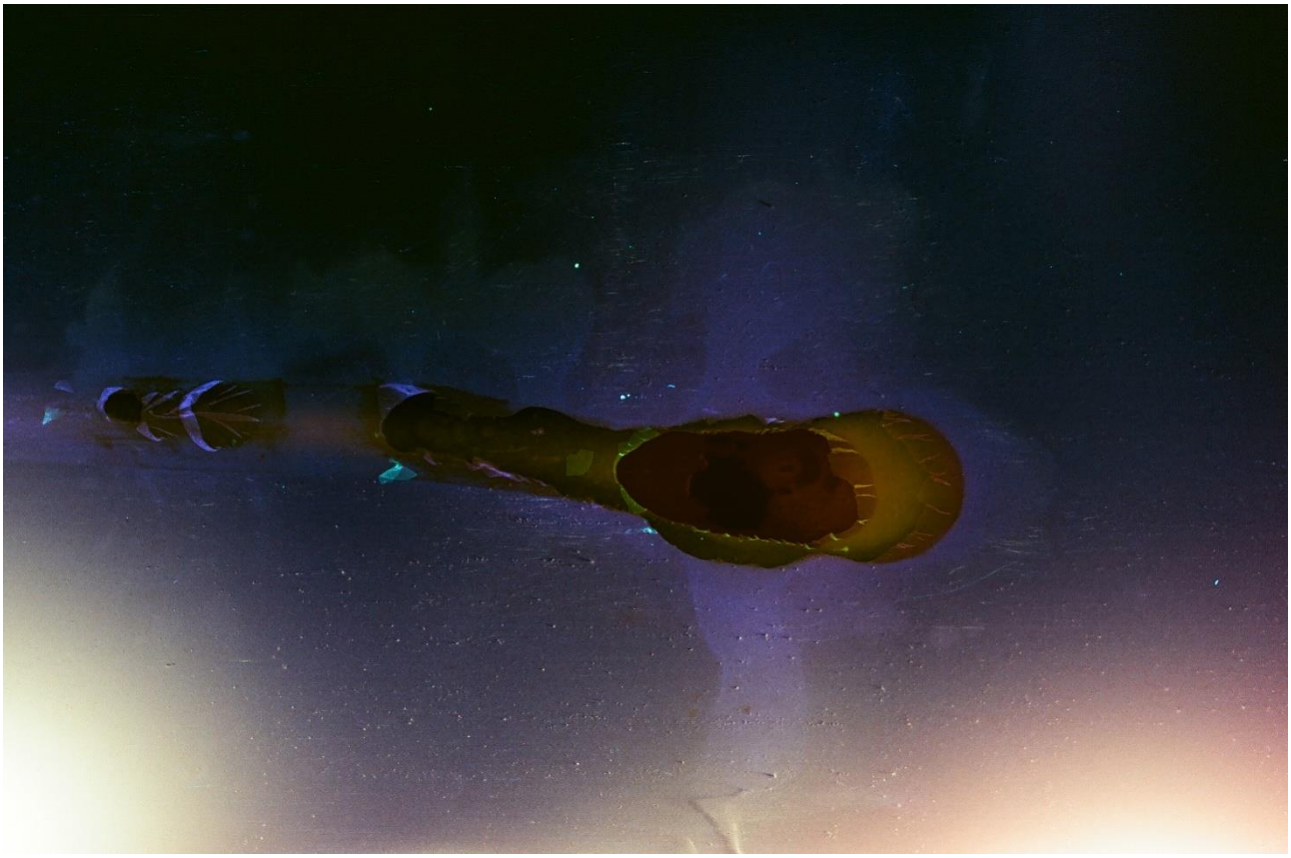

One of the images of the process of nucleation and growth of a green fly larva in rotting fish obtained using p-radiation.

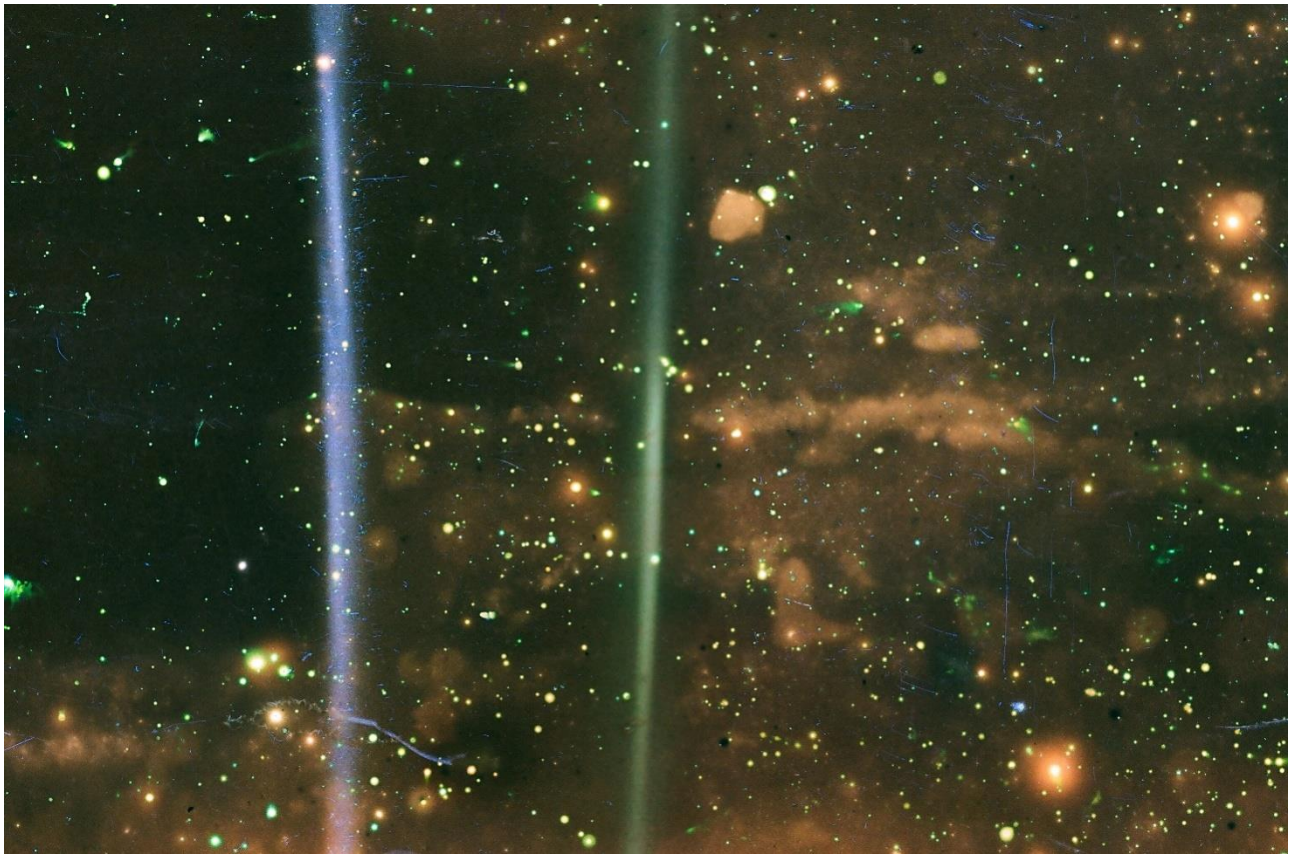

One of the photographs of the bottom of the Puget Sound Bay, obtained using p-radiation. The film was located on the surface of the water at a distance of 30 cm from the bottom.

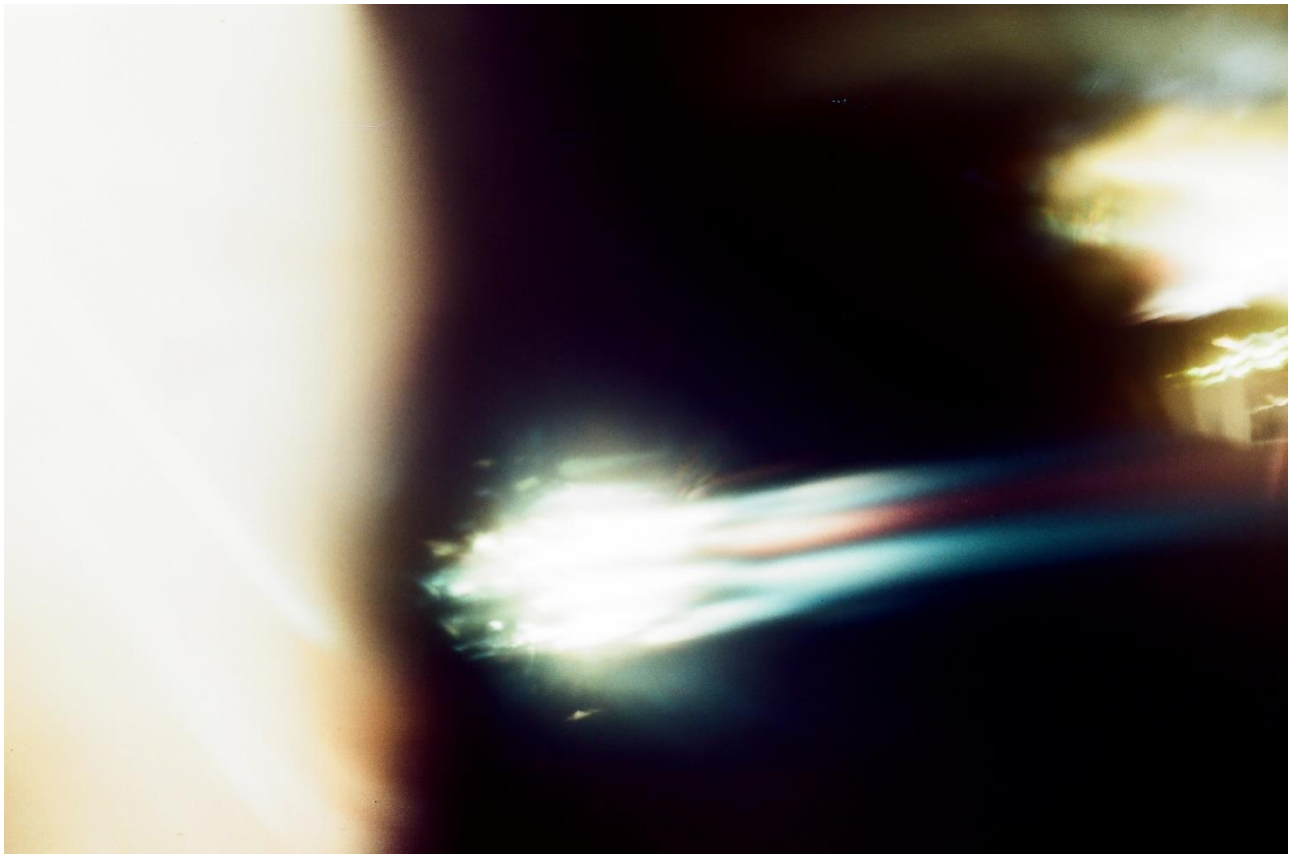

Photograph of the response of the rail to the braking process of a locomotive, obtained using p-radiation at a distance of 800 meters from the breaking point.

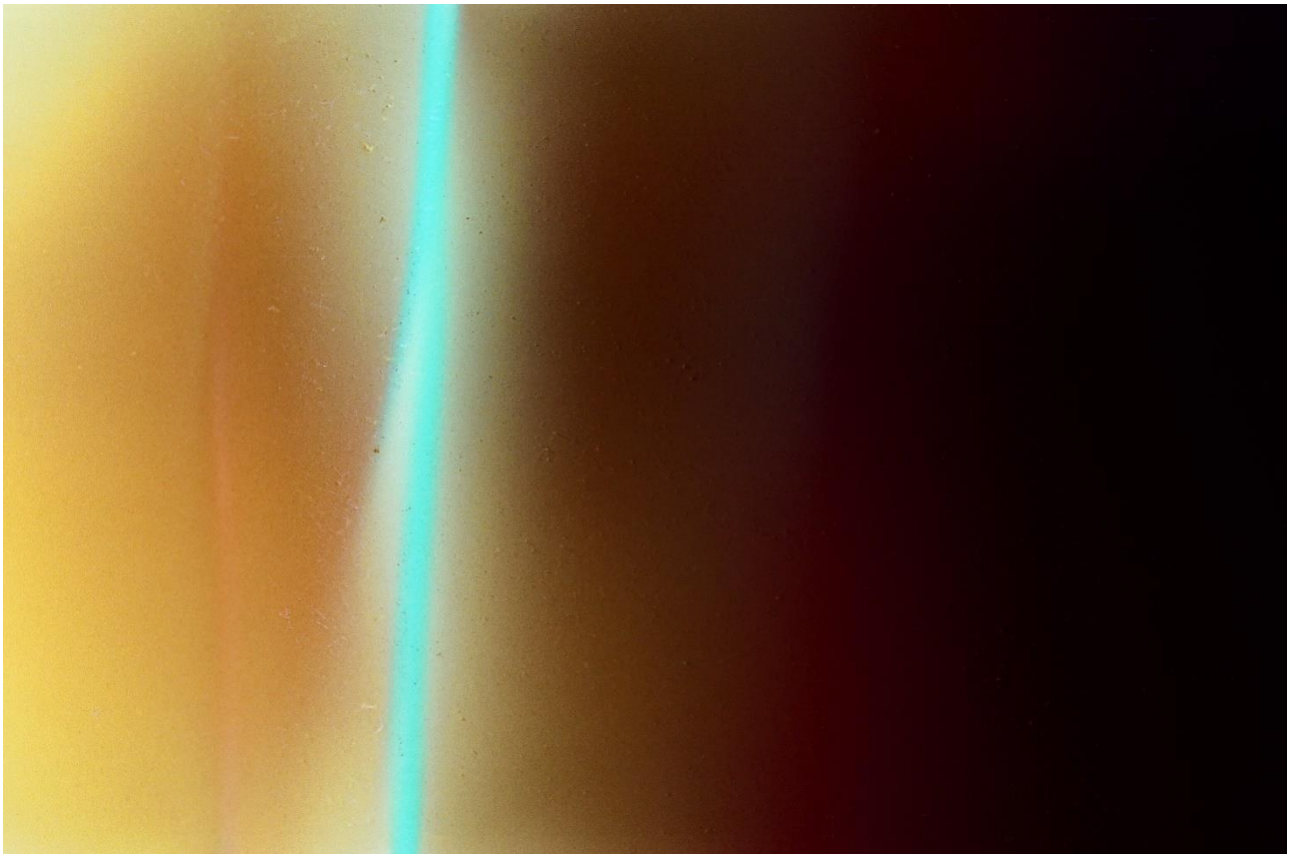

A photograph is illustrating the intense p-radiation recorded on a film located on the surface of the Earth.

## FOREWORD

Dear Reader, you opened this book by accident or intentionally, without realizing that it is intended for you because you want to live and stay healthy, you want man-made and natural disasters not to affect you, but now it depends only on you. You will learn from this foreword that the bridge you crossed did not collapse, not because it was designed and built correctly, but contrary to this. This conclusion is based on a comparative analysis of calculations performed by modern methods based on classical mechanics with calculations performed based on quantum mechanics. Note that the calculations are performed using a computer that was created thanks to quantum mechanics, and we trust the calculations performed by the methods of quantum mechanics everywhere.

But you cannot make any calculations and use any of the color photographs obtained as a result of experimental studies by the author. Each image obtained as a result of electromagnetic, including high-frequency radiation caused by an atomic reaction, refutes all the standards and methods that are proposed today to ensure the safe operation of aircraft, oil and gas pipelines, bridges, etc.

The basis of the industry and its development has always been physics. The technical progress of the twenty-first century is due to the creation of quantum electrodynamics, which is the most accurate physical theory, based on which the humanity masters outer space and an area called nanoscale. Space flights, the creation, and operation of thousands of kilometers of oil and gas pipelines, railway tracks, bridges, giant hydroelectric power stations, nuclear reactors, etc. are impossible without security. However, technological progress does not reduce but increases the risk of multi-functional high-speed and high-energy structures and devices exploitation.

Three catastrophes in three years (the Sayano-Shushenskaya hydropower plant, Russia, 2009; the Oil platform in the Gulf of Mexico, the USA, 2010; the Fukushima nuclear power plant, Japan, 2011) indicate that prevention of catastrophic destruction becomes a worldwide trial, which should be solved by the joint efforts of the world's most developed countries. All scientific and technical achievements should be used to ensure the safe operation of structures and devices.

An analysis of the risk of operating structures and devices shows that one of the most important causes of technological disasters is the lack of a quantum theory of strength and fracture. It is impossible to justify the fact that scientific academies of all countries did not pay attention to the fact that the most important branch of technology, such as the strength of materials and their destruction, is still trying to explain from the standpoint of classical mechanics.

The main error of modern fracture mechanics lies in the hypothesis that the stress state in a solid exists by itself, but it is since the interaction between the atoms has changed. The release of elastic

energy is not the cause of destruction since it is a consequence of the formation of local groups of metastable atoms.

The paradox of the situation is that the study of the properties of a solid and its destruction is performed using tunnel electronic and atomic force microscopes, an X-ray structural analysis, etc., but the analysis of the results is shown based on classical mechanics and the physical parameters of atom, electron, and photon are not used. The creation of the quantum theory of strength and fracture lagged behind the creation of the quantum theory: thermal conductivity, electrical conductivity, electronics, chemistry, optics, biology for 75-85 years, and from the creation of quantum electrodynamics for about 50 years.

This book, like the other works of the author, is written for professionals who are supposed to ensure the safety of human activity in nature and objects created by man.

Lee Davis, a well-known investigator of disasters, believes that the cause of man-made disasters is due to human factors associated with Stupidity, Carelessness, and Greed. The author of the book is convinced that the human factor is due to ignorance of the laws of nature or disregard for them when they are discovered. The scientists should eliminate the first cause, and the authorities should address the second and the third ones.

All existing theories of strength, which are more than one hundred, are based on the hypothesis that the loss of integrity of a solid (formation of pores, cracks, destruction) is due to the elastic energy accumulated in the stress concentrators.

The refutation of the fundamental hypothesis, based on which the theory of the strength of a solid is written, is sufficient to reject them, to invalidate all those methods that are based on the erroneous assumptions, as it also happened not only in technology, but in chemistry, biology, and medicine.

The first chapter of this book is devoted to experimental evidence that any external influence on a substance is accompanied by an atomic reaction due to the exchange of atoms by electrons and photons, which can only be described from the standpoint of quantum mechanics. The methods of classical mechanics end when the bodies approach at a distance of no more than two nanometers.

*Only electromagnetic and gravitational fields affect the atom. The gravitational effect is neglected since it is 38 orders of magnitude weaker than the electromagnetic one.*

The author used simple equipment to prove this fact. The reader can easily repeat any of the above experiments. Such an author's confidence is because the

test is based on the law of nature, which cannot be changed. The formulation of this law is given in the second chapter, along with an interpretation of the mechanism of this phenomenon. All experiments were performed according to a plan, compiled based on the achievements of modern physics, following the instructions of its founders I. Newton, D.C. Maxwell, A. Einstein, and their followers, L. Pauling and R. Feynman. The experiments were designed to refute the assumption that the problem of strength and fracture of a solid can be solved without taking into account interatomic interaction; to confirm that the energy source is local groups of metastable atoms.

The first experiments were carried out with a rotating grinding stone because the author was familiar with the work of J. C. Maxwell, in which he described the mechanism for the destruction of grinding stone in 1850.

The first calculations showed that the photon energy is 50 keV. Therefore, it is X-ray radiation, known from the publications. But a beautiful photograph was taken when a hammer hit a steel beam, in which the radiation passed 38 mm without attenuation.

It caused many questions:

- Why is this possible?
- Will I get a photo if I hit a stone instead of metal?
- How about a block of wood or water?
- Not with a hammer, but with steam?
- Not on a short beam, but a long rail?

Nature has answered the questions posed, demonstrating an increase in penetration up to two meters, six meters, 800 meters, 1600 meters, in the rail, 100 meters in water, 3 meters in soil. Therefore, this is not X-rays, but high-frequency radiation resulting from an atomic reaction without a high voltage that accelerates electrons. Also, the penetrating power of this radiation, excited in a substance, is millions of times greater than the penetrating power of X-rays. This area of electromagnetic radiation is **conditionally called p-radiation or p-rays.** The mechanism for formatting this radiation is described in Chapter III.

The reader will see 537 of 883 photographs in the first chapter, each of which is due to this radiation.

The plant growth and the birth of a living organism's cell growth, aging, and pathological changes occur as a result of atomic reactions, which are accompanied by p-radiation. The reader will see in the second chapter 135 photographs characterizing the growth of plant cells, the

functioning of human cells, and the birth of an insect. All of them require an explanation. Such an attempt has been made in the third chapter, although collective efforts are needed. The number of photographs can be increased indefinitely, but studies of this phenomenon on modern high-precision equipment are necessary to utilize the information that p-rays send us. We need specialists who can understand it.

The experiments showed that p-radiation is observed in all substances regardless of the composition, structure, shape, size, and nature of the external influence. In deciding to describe the mechanism of this phenomenon, I have realized that I am not a specialist in all those areas in which it can be used.

Lectures played a unique role in the development of biology, and the book by E. Schrödinger, "What is life? The Physical Aspect of the Living Cell". The following is what he wrote at the beginning of his book:

"A scientist is supposed to have a complete and thorough I of knowledge, at first hand, of some subjects and, therefore, is usually expected not to write on any topic of which he is not a life, master. It is regarded as a matter of noblesse oblige. For the present purpose, I beg to renounce the noblesse, if any, and to be the freed of the ensuing obligation. My excuse is as follows: We have inherited from our forefathers the keen longing for unified, all-embracing knowledge. The very name given to the highest institutions of learning reminds us that from antiquity to and throughout many centuries, the universal aspect has been the only one to be given full credit. But the spread, both in and width and depth, of the various branches of knowledge by during the last hundred-odd years, has confronted us with a queer dilemma. We feel that we are only now beginning to acquire reliable material for welding together the sum of all that is known into a whole; but, on the other hand, it has become next to impossible for a single mind fully to command more than a small specialized portion of it. I can see no other escape from this dilemma (lest our true who aim to be lost forever) than that some of us should venture to embark on a synthesis of facts and theories, albeit with second-hand and incomplete knowledge of some of them -and at the risk of making fools of ourselves. So much for my apology."

Now, I am solving the problem, following A. Poincare's advice: "it is better to predict without being completely sure than not to predict at all."

The absolute reliability of the use of this phenomenon guarantees success in its practical application to prevent catastrophic destruction of structures and devices, earlier prediction of earthquakes and tsunamis, and the quality improvement of medical care.

It is useful for the reader, who will take this as a fantasy, to learn that the basis of this phenomenon is the processes that the primitive man has used to produce fire, striking a piece of the iron against flint, inventing an ax; B. Franklin used it to tame the lightning. The creators of the laser solved the opposite problem by increasing the rate of energy storage in the active substance.

Each time you slide your finger across the screen of a mobile phone, you reproduce what is called an electromagnetic impulse.

Fantastic, not yet unraveled energy processes occur in the cells of our bodies, which p-radiation will help to understand.

But for this, it is necessary to abandon modern theories of strength, which the experiment refutes; create a new industry based on the use of p-radiation, write new state standards for the prevention of disasters.

The history of physics indicates that new ideas do not immediately break their way. The period of recognition of the fact that the Earth is not in the center of the universe was tragic. In the figurative expression of A. Einstein, the evolution of physics is a drama of ideas. Such an omission occurred at the beginning of the last century when relativistic and quantum mechanics was born, but only now has it touched all those who must abandon the theory of strength based on classical mechanics.

ACKNOWLEDGMENTS

The author is deeply grateful to S. S. Batsanov for discussions, useful advice, and the provision of published and unpublished studies of him that helped to understand the mechanism of the observed phenomenon and describe it.

Thanks to my son Pavel for help in conducting experiments, searching, and analyzing literature.

The pilot study, launched in January 2016, ended in November 2019. More than a hundred photographic films are using for this. Fifty-nine discs are recording. The author thanks Dale Sutton for his help in this study.

## CHAPTER I. EXPERIMENTAL PROOF THE POSSIBILITIES OF PREVENTING THE MAN-MADE CATASTROPHES

*Everything we know about reality begins with*

*an experiment and ends with it.*

A. Einstein

### Introduction

A study of the causes of such lag in strength theory showed that it began after the death of J.C. Maxwell. Biographers did not appreciate Maxwell's work [1.1], and today it is almost not mentioned. This work starts with the statement, "THERE are few parts of mechanics in which theory has differed more from experiment than in theory of elastic solids." This conclusion refers to those theories and models that are published today. The solution of each equation, obtained by Maxwell in analyzing the thirteen problems caused by deformation in the fulfillment of Hooke's law, was experimentally verified.

Maxwell considered the energy of the destruction of a solid in his letter to Thomson (Lord Kelvin) [1.2]. The letter was found in the archives only in 1937. An analysis of the article [1.1] and the letter was published S.P. Timoshenko in the review in 1953 [1.3].

Timoshenko writes: "We see that Maxwell already had the theory of yielding which we now call maximum distortion energy theory. But he never came back again to this question, and his ideas became known only after publication Maxwell's letters. It took engineers a considerable time before they finally developed the theory identical to that of Maxwell's."

A comparison of the interpretation of Maxwell's work, given by Timoshenko, with the original showed that the interpretation contains several fundamental errors. Timoshenko wrote, "We see that Maxwell already had the theory of elasticity, which we now call maximum distortion energy theory. But he never came back again to this question, and his ideas became known only after publication Maxwell's letters. It took engineers a considerable time before they finally developed the theory identical to that of Maxwell's."

First, Timoshenko ignores the fact that Maxwell analyzes the results of the mechanical impact with the help of interference of polarized rays. Secondly, he ignores the equation linking the potential deformation energy with displacement, the proportionality coefficients in which are characterized as follows: "... where A & B are coeffits, the nature of which is foreign to our inquiry. Now we may write $U = U_1 + U_2$ where $U_1$ is due to symmetrical compression, and $U_2$, to distortion

without compression..." Thirdly, he does not pay attention to the fact that these coefficients have the dimension of the surface energy density.

Fourthly, Maxwell writes three times, '*strain*' not to the 'stresses.' Fifth, Maxwell's equation fundamentally differs from the equations proposed after him, for example, from equations proposed by Mises. Maxwell ends the letter with the phrase: "I think this notion will bear working out into a mathematical theory of plasticity when I have time to compare with experiment when I know the right experiments to make."

The phrase, which Maxwell completes the letter to Thomson, illustrates the fact that an idea can be recognized by theory only when the experiment confirms it. He was not only a brilliant theorist but also an excellent experimenter. His concept, about some unknown form of energy, formulated ten years before the creation of electrodynamics was a brilliant foresight. But the electromagnetism, predicted by Maxwell, remained a hypothesis before the experiments of H. Hertz. Timoshenko knew about R. Mises's article [1.4]. He had an opportunity to compare it with Maxwell's works and draw attention to the fundamental difference but concluded that they are identical. Why?

Significantly noteworthy is the fact that Maxwell's works on mechanics are, practically, not quoted, but in those cases when the authors of the articles refer to Maxwell's work, they do it not by the original, but by the publication of Timoshenko.

The dishonesty of scientists has led to the fact that the national standards of the USA, Russia, and possibly other states, used to design structures and devices and their functioning, are based on erroneous hypotheses. Maxwell's idea was ahead of the development of physics for 70-80 years.

The experiment that he dreamed about can be completed by anyone today by reading this publication of mine.

I will give two phrases from that part of Maxwell's letter, which Timoshenko does not quote.

"In my paper on elasticity I produce instances (not new phenomena) to show that in this case the pressure could not exist as the effects where in the same direction over the whole body & could not balanced. At the same time, I stated that gutta percha when heated to a certain point goes back to its original form.

G. Wertheim has the best experiment I have seen on compressed glass. He maintains & I think with truth that the effects are due to the '*strain*' not to the 'stresses'. As far as I know glass is not capable of maintaining strain without stress at least. When it is cut, the strain disappears for want of stress.

If you examine any plane section of a piece of unannealed glass, you will find that $\sum pdS = 0$ where *p* is the stress perp to *dS*. That is the whole pressure=whole tension in the section."

"The reduction to double refraction is Fresnels.

That of Heat to mechanical action –Herschel.

*Proof that this action is not stress- Maxwell.*

Proof that this is strain with numerical data for various kinds of glass-Wertheim."

I allowed myself to emphasize in italics in the letter Maxwell's proof that the cause of birefringence is not mechanical stress. Today we know more about atom and electromagnetism than Maxwell knew. We can interpret his conclusions from the perspective of this knowledge.

Richard Feynman was already a Nobel laureate when the head of NASA invited him to the commission to investigate the causes of the death of the shuttle Challenger. It was Feynman, guided by a deep understanding of physical processes, which established the cause of the disaster and demonstrated an experiment confirming the correctness of his conclusion, but the head of the commission, William Rogers, did not include his report in the commission's report. Feynman signed the commission report only after his conclusion was included as an appendix. He, being seriously ill, published a book, "What do you care what other people think?" Understanding the meaning of his recommendations and the low probability that they would be read without a book. An analysis of the documents [1.5-1.7] related to the Columbia shuttle crash that occurred 17 years after the Challenger shuttle crash indicates that Feynman's fears were justified: his report is mentioned only once.

Modern methods should provide continuous remote monitoring of the technical condition of all structural elements of structures or devices, the damage of which can cause a technogenic catastrophe. Assessment of the technical state of the structural component and its changes is possible only based on measuring the difference in the physical parameters characterizing the technical state, transferring information to memory devices, analyzing and deciding on further using or its termination. Only a computer program based on the physical law provides a realistic opportunity to predict changes in the measured physical parameter and to stop the operation of the structure or device before when this parameter reaches a critical value, the excess of which leads to a catastrophe.

The absence of a quantum theory of strength and a quantum criterion of destruction led to the fact that all theories based on classical mechanics do not allow to formulate the law of destruction.

The problem of the energy source is the cornerstone of any physical theory. Modern strength theories proceed from the fact that the primary source of energy, the radiation of which leads to the formation of cracks and destruction, are stress concentrators. The equations proposed based on this hypothesis are empirical. The probabilistic nature of the assessment of the technical state does not exclude those events, the probability of which is minuscule, occur at the beginning of exploitation in the form of a catastrophe.

It has been established that four types of atomic interactions determine all processes in nature: strong, which is taken as unity, electrometry, equal to 1/137, weak, constituting $1\times 10^{-12,}$ and gravitational = $1\times10^{-40}$. The strong interaction is due to the existence of atomic nuclei. Therefore, when the energy release of nuclear reactions can be neglected, then all processes between atoms in a solid can be described using the electromagnetic interaction. There is no mechanical interaction between atoms, but solids consist of atoms. The question arises: how do they interact?

*There is only one answer: Kinetic energy in contact is converted into electromagnetic energy, and then the electromagnetic energy is converted into kinetic energy.*

That means that for another 65 years, humanity has only lost because the first part of Maxwell's letter was not carefully read and understood.

This book summarizes the results of the author's many years of research aimed at discovering the physical laws of solids' destruction causes.

This hypothesis was first reported at international conferences [1.11, 1.12] and published [1.8, 1.9, 1.10, 1.13, 1.14].

### 1.1. Investigation of the processes of destruction of solid

All mechanical effects on the solid can be reduced to seven types of deformation: shear, stretching, compression, torsion, bending, impact, and temperature gradient.

The shear deformation at which the destruction has occurred was accomplished by contacting the material with a grinding stone rotating at a frequency of 57.5 revolutions/second (Fig. 1 a, b), and drilling of glass, concrete, plastic, and wood with a diamond-coated hollow and of high-strength steel drill. Alloys based on Fe, Al, Cu, Zn, Pb-Sn, glass, concrete, flagstone, granite, marble, cobblestone, polymers and wood, were studied at room temperature or a liquid nitrogen temperature for various types of deformation.

Electromagnetic radiation was captured on a KODAK 400 or FUJIFILM SUPERIA X-TRA 400 color photographic film. The film was placed in a PENTAX camera (Fig. 1a, Fig.2), the lens and mirror from which were removed, and the shutter is closed. Particles of metal and stone formed during the destruction fell into the capsule (Fig. 2 a, 3), placed in the camera. The lower part of the capsule (Fig. 2a, 5) was replaced after each experiment. Instead of the camera, a bicycle rubber inner tube (container, Fig.2, Fig.2a, and Fig.2 b), which allows performing various studies, was often used. The film was placed in a container above a steel plate 3 mm thick. A Pb-Sn alloy wire (Fig.2a, 2) with a diameter of 4 mm, curved in the form of a wave, was located inside the container above the emulsion layer.

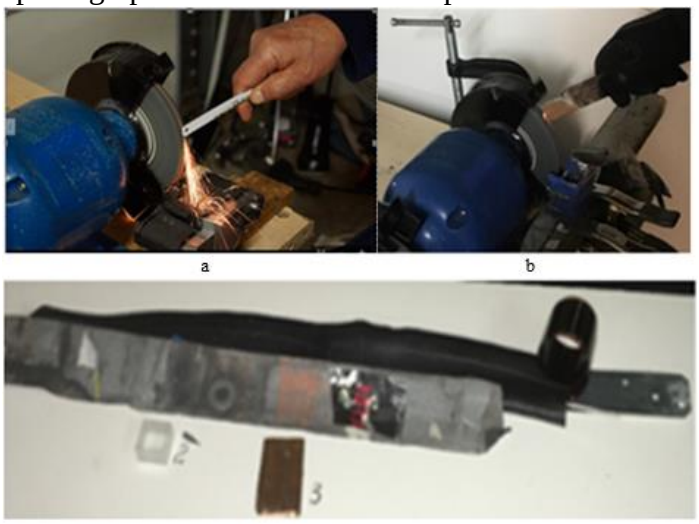

**Fig. 1**

**Fig. 2**

Particles of alloys, glass, plastic, and wood formed as a result of the destruction, fell into a "trap," located on the surface of the container, covered with a sticky tape to which they stuck. The flux of particles was directed above the surface of the container or perpendicular to the surface, but beyond its boundary, to record the direct radiation at the time of destruction and to exclude the effect of radiation from the particles.

The experiment has been completed in such a way that the interaction of visible and ultraviolet radiation to the photographic film is eliminated.

Therefore, the film recorded radiation that arose at the time of destruction and from fragments formed as a result of destruction located outside the visible and ultraviolet range.

The radiation caused a photochemical reaction in the entire visible range. This meant that the electromagnetic spectrum contains radiation with a higher frequency, in which the p-ray region is located.

*However, an analysis of the results of numerous studies of the properties of this radiation showed that they differ from the properties of electromagnetic radiation excited by electron impact at high voltage.*

*This electromagnetic radiation is conditionally called p-radiation (or p-ray) to emphasize this difference. The mechanism for the formation of p-radiation is described in Chapter III.*

The photos illustrate the importance of effective detection. We confine ourselves to describing the most relevant results of the study, which are used as examples.


**Fig. 1d**

### 1.1.1. P-ray radiation at a tensile strain

Six photographs of p-radiation during the tensile deformation of aluminum plates (Fig. 2, sample 7 and Fig. 2, sample 8) and copper (Fig. 2, sample 9) shown in Fig. 3 were obtained using a Wilton Bench vise (Fig. 1d), adapted for stretching. The thickness of the aluminum plates is 0.8 mm; the width is 22 mm, the depth of cuts is 5 and 2 mm; the thickness of the copper plate is 1.4 mm, the width is 27 mm, and the depth of cuts is 9 and 4 mm.

The plates with one upper and one lower bolt hole (Fig. 2, simple 7 and Fig. 2, simple 8) were pressed additionally with bolts through the right and left end holes. The left hole is not shown. The container with the film was located above the specimen.

Note: A comparative analysis of the size of the images does not make sense since the photographs are given at different magnifications.

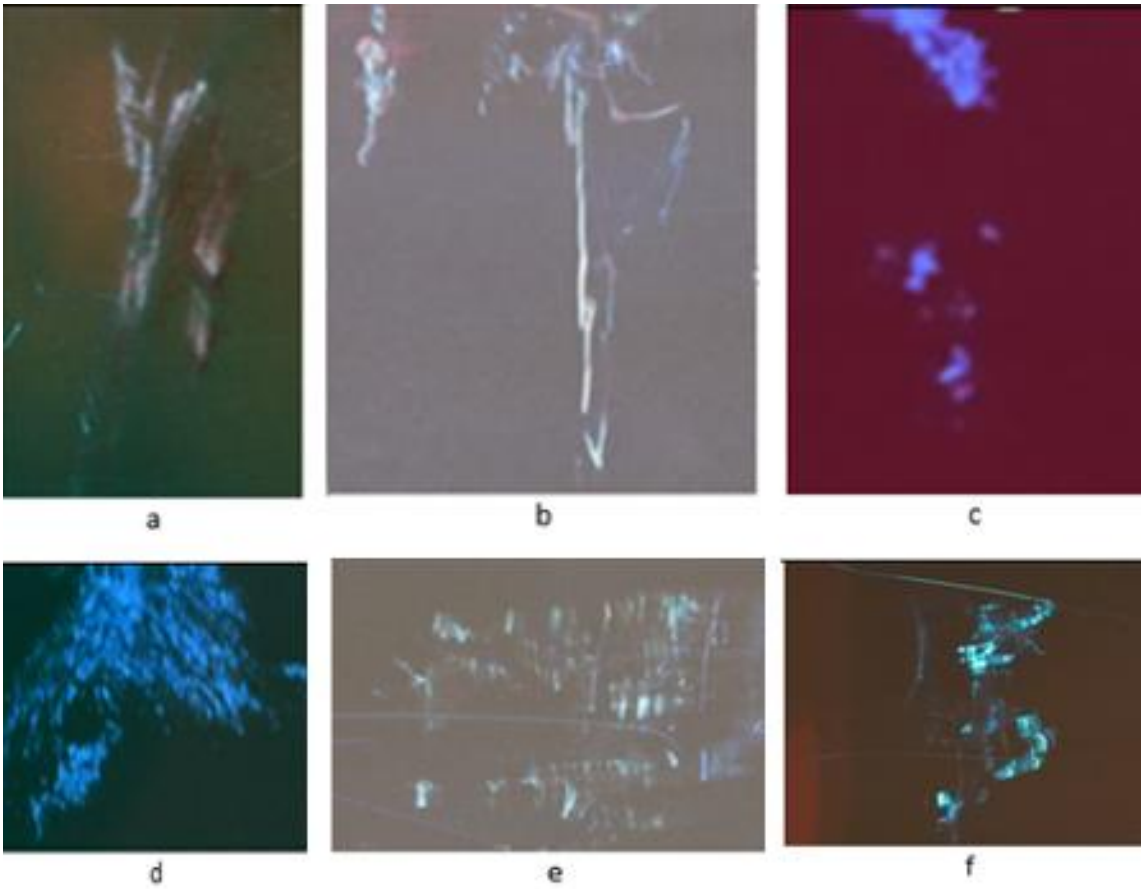


**Fig. 3**

Fig. 3 a and Fig. 3 b. Two of these photographs were obtained by examining the plates Fig. 2, 7. The gap, as we see, occurred at the point of attachment, but not between the notches. One of the notches is visible in Fig. 3 a. The radiation of p-rays near the left fixing bolt is captured in Fig. 3 b. The aluminum alloy plate is shown in Fig. 3 d, having holes, was stretched along the diagonal. It was torn in two, but in the photo Fig. 3 d, the radiation of only one of the parts is recorded, due to the displacement of the container, at which the lower part of the plate was outside the frame. The photographs of radiation when the aluminum plates are divided into two parts are shown in Fig. 3 c and Fig. 3 e. The radiation of an aluminum plate fastened with two bolts like a copper plate (Fig. 2a, 9), is recorded in Fig. 3 f. The horizontal strip in Fig. 3 e and two bands in Fig. 3 f corresponds to the boundary of the vice.

A characteristic feature of radiation from the plates that were divided into two parts at the points of incisions, or radiation from plates with damaged fastening is that *there is no radiation at the edges of destruction.*

*The spatial distribution of the intensity of electromagnetic radiation during the deformation of a solid established experimentally is proof that the destruction is caused to the stimulated emission of photons by atoms.*

Stimulated emission of atoms and its absorption lasts no more than $10^{-7} \div 10^{-8}$ seconds, while the delayed spontaneous emission in the visible region, determined in a specially performed experiment, was 6-30 microseconds

Photons spontaneously emitted before breaking bonds between atoms are witnesses to the fact that there was an increase in energy due to the transition of electrons to higher metastable energy levels. The change in the energy state of the atoms is accompanied by a difference in the forces of interaction between them, as a result of which the arrangement of the atoms changes. These changes are perceived as a stress state, *but it is a consequence*.

The change in the energy state of atoms is due to a change in the structure of the electron shell of atoms, under which anisotropy of the polarizability of atoms arises. However, the difference in polarizability also occurs in those cases when the energy state has not changed, or the changes have turned out to be such that the accumulation of energy occurs at such a rate that the critical state is not reached during the entire exploitation.

### 1.1.2. P- radiation with compression, torsion and bending deformation

The photos are shown in Fig. 4 a and Fig. 4 b were obtained in the first experiment that was performed in January 2016. The particles (sparks) formed as a result of the contact of the saw blade with the rotating stone flew over the surface of the container without being adsorbed to it. The experiment was carried out to register direct radiation at the time of destruction, proceeding from the fact that the photon velocity is many times greater than the particle velocity.

The images obtained in this case are significantly different from those recorded in radiation from particles adsorbed on the container surface, but the experiment does not allow to register the radiation moment: whether it occurred before or after destruction.

The drill, which diameter is 5 mm (Fig.2, simple 10), captured in the upper and middle parts, was split into three fragments. The split occurred at the point of the lower anchorage and the position of application of the force acting from left to right. The nature of the destruction can be seen in the photograph (Fig. 4, c) from the variation in the brightness of the radiation along with the entire drill. Let's pay attention to the fact that the drill was not only destroyed but also deformed.

Photo Fig. 4 d serves as an additional confirmation of the absence of radiation at the time of destruction.

An investigation of the deformation of torsion was performed with a copper tube (Fig.2, simple 13), which diameter is 29 mm, and the metal thickness is 1.5 mm.

The tube, which the holes have weakened strength, was located in that part of the vice (Fig.1 d, 2), which is intended for fastening the pipes so that the damaged area is outside the attachment. The lever's rotation caused the deformation of torsion. The response to p- radiation registered in the photographic film is shown in Fig. 4 d.

Let us draw attention to a transparent interface between the moving and fixed parts of the tube. The color difference indicates that the stationary section emits electromagnetic waves from the entire surface subject to compression, and not only at a place where the deformation is unusually large, but the wavelength of the radiation is different. The blue radiation at the tube attachment point indicates higher photon energy.

The contour of the rotating part of the copper tube, especially the upper boundary, can be seen with an additional magnification. Consequently, this part of the tube radiates in the p-radiation region also, since the container is opaque for visible and ultraviolet rays.

The effect of infrared rays is eliminated, because, firstly, the surface temperature did not change much, and secondly, infrared radiation cannot cause luminescence in the violet region.

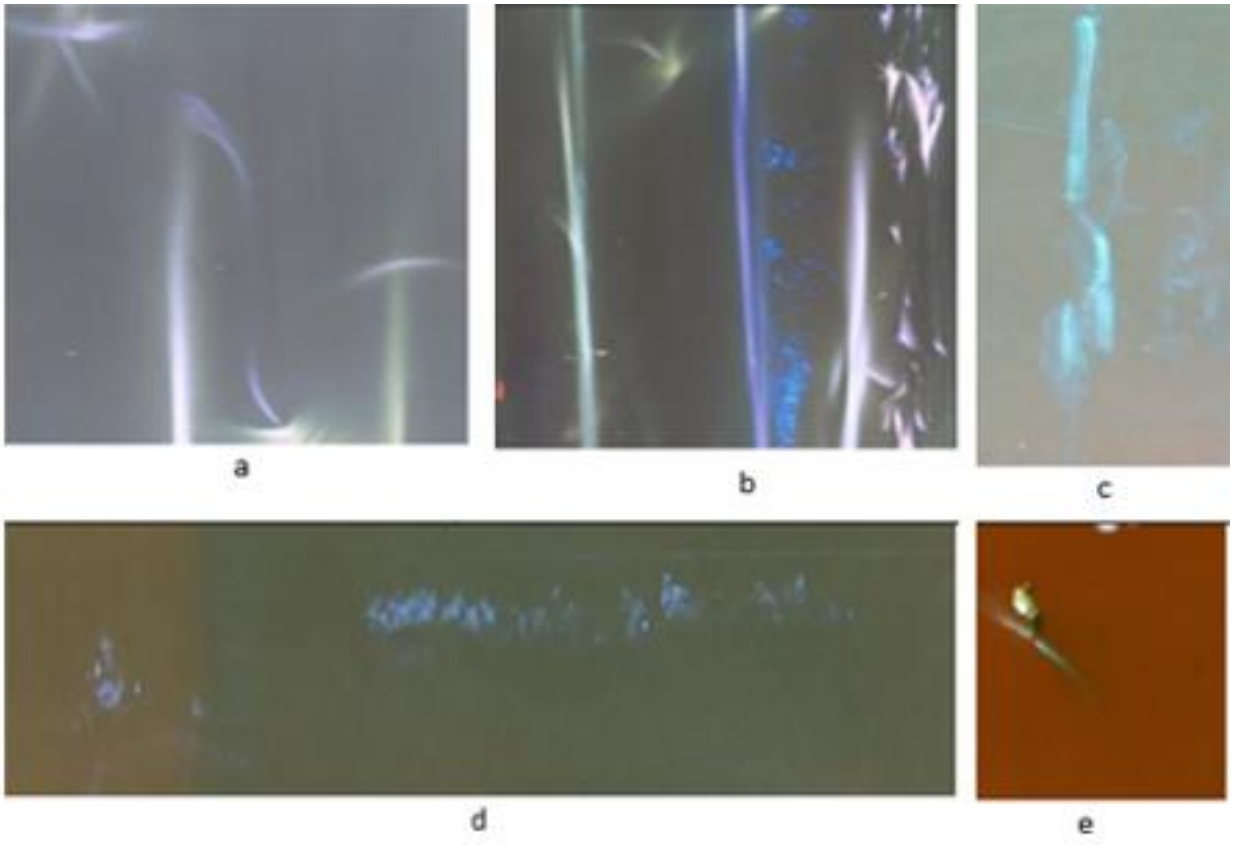


**Fig. 4**

.

The destruction of the drill is of particular interest. This experiment allows us to investigate the process of deformation and destruction of a solid. The features of this process can be traced with a fivefold increase. Detailed analysis is beyond the scope of this study. We pay attention to the regions located between the upper and middle fragment and between the middle and lower fragments. The nature of the radiation in these regions refutes those models of fracture in which stress distribution is considered before the tip of the crack, to which a particular role is assigned.

All these processes can be investigated by modern spectral, including high-speed, methods.

A fragment of an arcuate-shaped article of silumin, shown in Fig. 2, sample11, was compressed along the chord. A brittle failure occurred at low load, but p-radiation, as we see in Fig. 4 e, was bright enough. A small fragment, captured in the photo, was not found.

We pay attention to the fact that the gap between the fragments is dark, and the glow comes from a very small part of the body being destroyed.

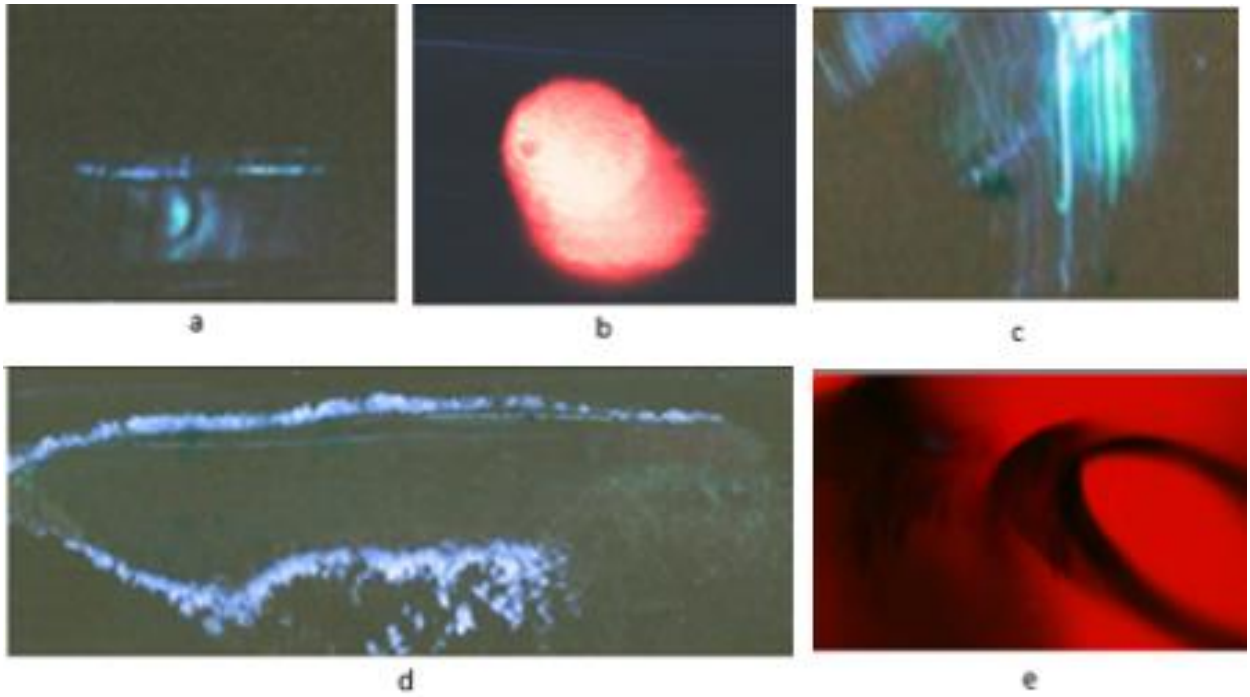


**Fig. 5**

### 1.1.3. P- radiation with shear strain and impact

The five photographs of the destruction of mirror glass, shown in Fig. 5, were obtained under the following conditions: a- when drilling with a diamond-coated hollow drill at room temperature; b- when drilling with the same drill, but at a temperature of liquid nitrogen; c-when the edge of the glass is chipped at room temperature; d- when struck by a thin punch at a temperature of liquid nitrogen; e-in friction with a rotating grindstone, as shown in Fig. 1b.

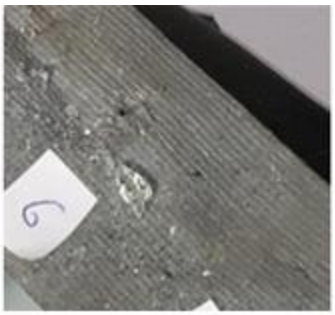

**Fig. 5 (1)**

The white color of the two cracks shown in Fig. 5d indicates delayed radiation from fragments formed after destruction.

The photograph of two large fragments of the glass, the radiation of which is recorded in Fig. 5 e are shown in Fig. 5 (1) near the number 6. These photographs illustrate the moment when the destruction occurred; the dark edge of the glass characterizes the place where the split occurred.

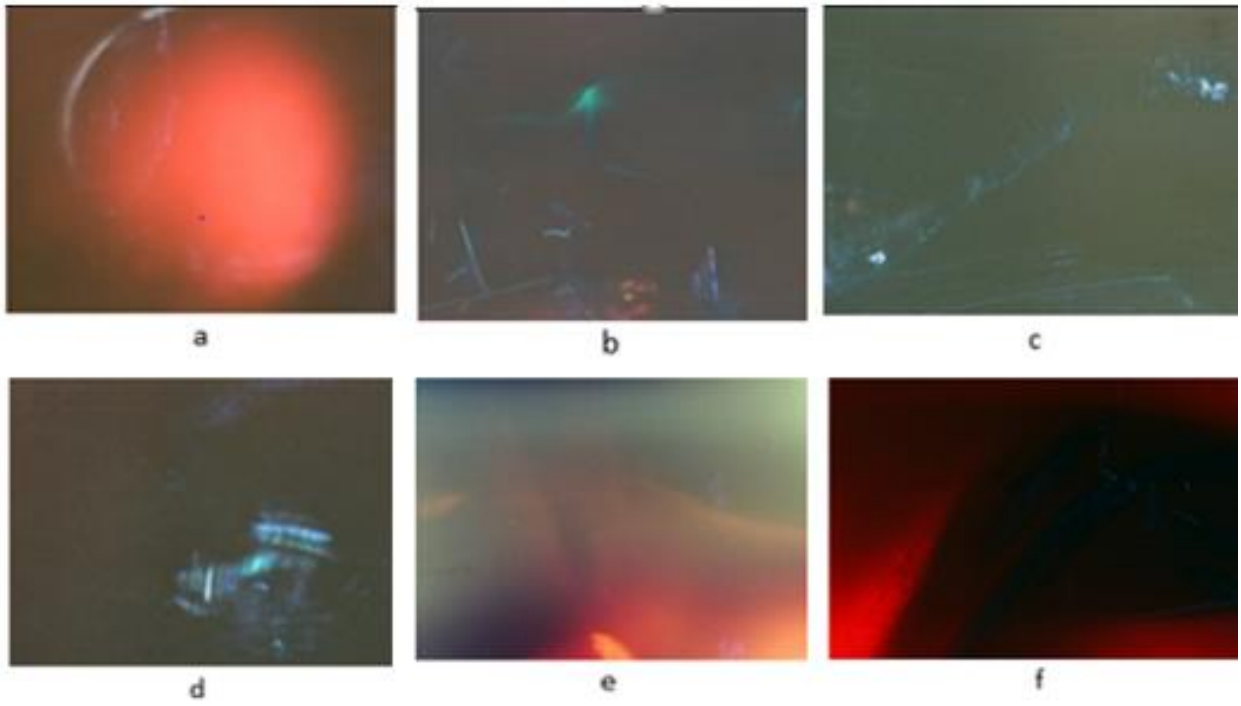


**Fig. 6**

The photos are shown in Fig. 6, were obtained with the following experiments: a-drilling holes in concrete (Fig. 2b, simple 14); b-destruction of the plastic rod (Fig.2 b, simple 15), cooled by liquid nitrogen, in contact with a rotating grindstone; c-destruction of the Pb-Sn alloy cooled by liquid nitrogen upon contact with a rotating grinding stone; the photograph shows a section of the Pb-Sn alloy wire located inside the container; d- when an aluminum-based alloy is destroyed upon contact with a rotating grinding stone; e- when the copper-based alloy is broken upon contact with a rotating grindstone (a section of Pb-Sn alloy wire located inside the container is visible in the photograph); f- upon irradiation of the Pb-Sn alloy located inside the container with particles formed during the destruction of glass, as shown in the lower part of Fig. 6 c. the double image is due to engine's vibration.

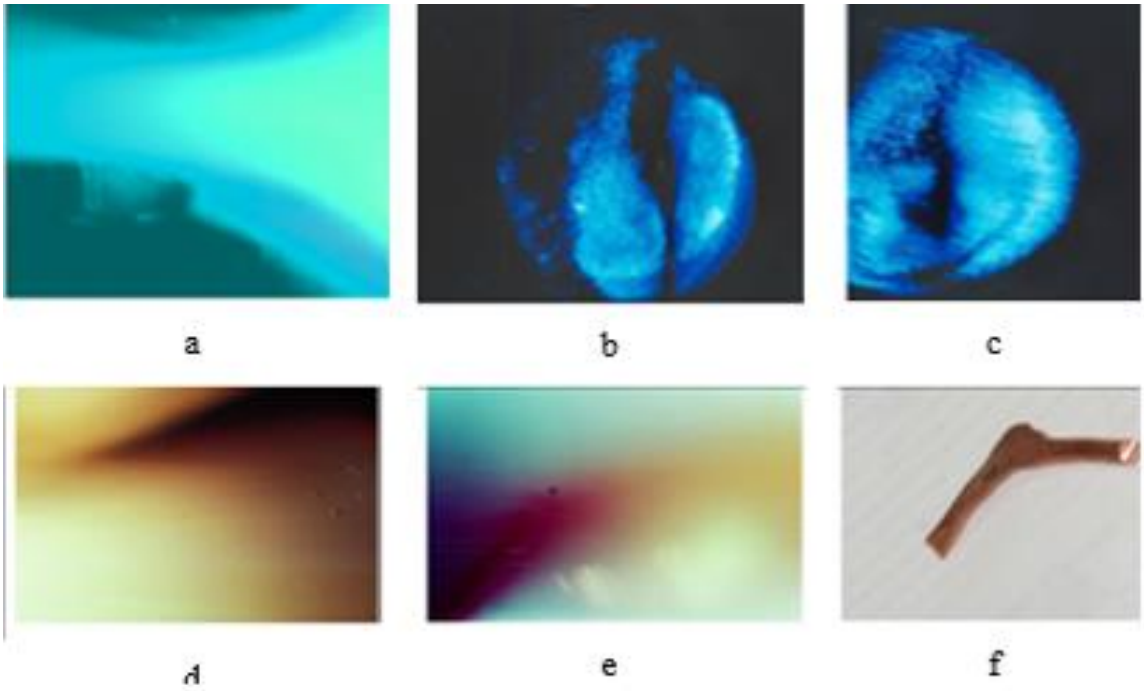


**Fig. 7**

The photos are shown in Fig. 7, were obtained with the following experiments:

a-when a zinc alloy breaks down on contact with a rotating grindstone (radiation limited to steel screens); b- when a Pb-Sn alloy wire located on the surface of a container is irradiated with radiation from particles of steel adsorbed on its surface after failure (a wire 3 mm in diameter is flattened in the upper part to a thickness of 0.004 mm); c-analogous experiment with more extended irradiation; d-irradiation of phrase 12 (Fig.2) by radiation from particles of the same web, but from another company; e-when irradiating a copper alloy wire shown on frame f.

### 1.1.4. Glass fracture during temperature gradient

The mirror glass plate is shown in Fig. 8, 1 was heated by the flame of a gas burner. Two cracks originated in the area with maximum temperature. The p- radiation during the formation of a vertical crack 1 is captured in the photograph (Fig. 9 a).


**Fig. 8**

As we see, the photograph shows only the radiation of the regions located on the edges of the crack in which the fragments were formed.

The glow in the crack region is not recorded, similar to the one shown in Fig. 3 e.

Fig. 9 a

The bottom of the crystal vase, the thickness of which exceeded two centimeters, was divided into four fragments with concentrated point heating. Two pieces 2 and 3 are shown in Fig. 8. The p-radiation from these fragments is captured in the photographs Fig. 9 a,

Fig. 9b. Four frames of the destruction a crystal vase during point heating bottom using a gas burner flame

The crack birth in the left fragment

The crack birth in the right fragment

Three glowing areas in the right fragment

We draw your attention to the fact that, firstly, the radiation from the region between the fragments is not captured, and secondly, the pieces that split off from the left and in the center flew out of the frame.

### 1.1.5. Destruction of the adhesive layer

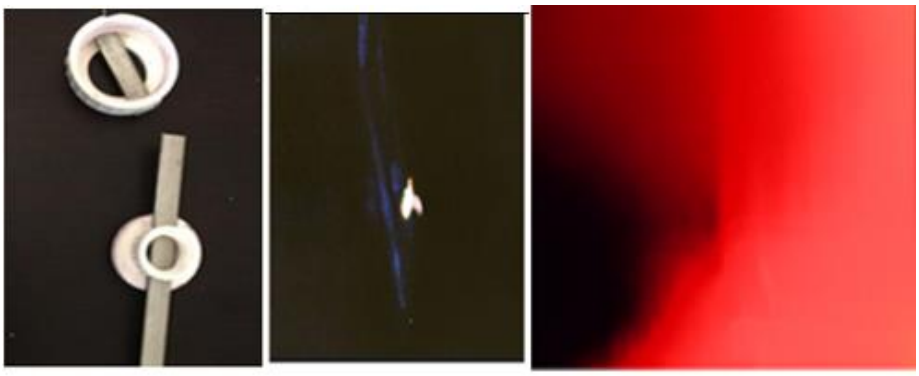

1 2 3

**Fig. 10**

Fig. 10, frame (2) illustrates Y- radiation caused by the destruction of the adhesive layer that filled the coupling thread, Fig. 10 frame 1, by 40%. The experiment showed that the torque at unscrewing was ~ 4000 times higher than when it was screwed on. A white spot in the photograph is associated with p-rays caused by deformation at the point of contact between the lever and the screw.

Fig. 10, frame 3 illustrates p- radiation caused by the destruction of aluminum alloy plates 1 mm thick glued together. The contact area was 3 $cm^2$. The experiment was terminated after a crack forming in one of the plates. The plate shift is not set.

.

### 1.1.6. P- radiation caused under single impact

The fact that the container, which is not transparent to visible and ultraviolet rays, transmits some radiation, allowed the author to conclude that the frequency of this radiation corresponds to the x-ray range. The properties of X-ray radiation are well understood. This region of the electromagnetic spectrum is in the energy region of 100 eV-100 keV, or the frequency range from $3\times10^{16}$ Hz to $3\times10^{19}$ Hz.

Photos are shown in Fig. 7, indicate that the radiation energy corresponds to the range of 50-100 keV. It was found that the x-ray intensity decreases according to the exponential $I_{xR}=I_0e^{-\mu x}$, where μ is the linear absorption coefficient, measured in $cm^{-1}$ which depends on the nuclear charge $Z$ and the radiation wavelength λ according to the law $\mu = \eta Z^4 \lambda^3$, where $\eta$- coefficient of proportionality.

A lead nucleus charge 82, corresponding to the number of protons. This element is used in practice as an X-ray absorber most often.

Photo Fig. 7d illustrates the fact that sample 12 (Fig. 2), whose thickness is 0.5 mm, is opaque to Y-rays emitted from particles formed upon the destruction of such an alloy.

The variety of the solid response demonstrated above required an experimental verification of any plausible hypothesis built on the previous concept of the properties of a solid.

Experiment No. 1. Verification of the transparency of a steel beam to p-radiation

The photo-container is located under the steel beam, as shown in Fig. 11 (1), frame 1 illustrates experiments in which the metal serves as a shield for the rays emitted as a result of the hammer blow on the upper surface of the steel beam, while the film is located below it.

Fig. 11 (1), frame 4 shows that the p-rays freely pass through the screen with the thickness 76 times the greater of the previous sample. Moreover, we see in frames 5 and 6 an additional response to the blow.

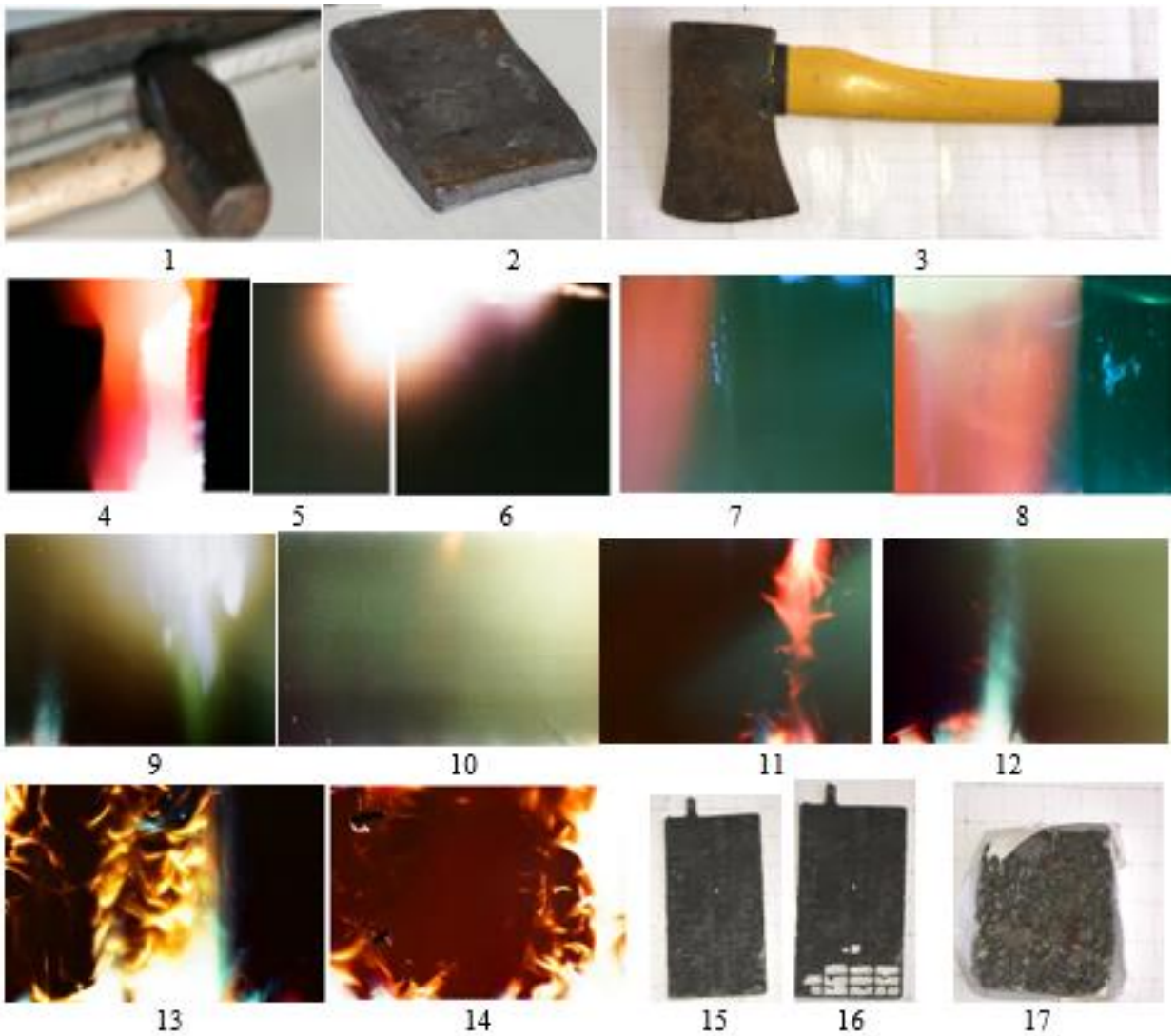


**Fig. 11(1)**

The lead plates, one of which is shown in Fig 11 (1), frame 2, were used as screens in the experiment, as shown in frames 7 and 8. An impurity region could explain the luminous areas in the plates with a small atomic number numerically equal to the charge of the nucleus.

Experiment No. 2. Study of lead electromagnetic radiation

a) A lead battery separator plate is shown in Fig. 11 (1), frame 15, was located on the surface of the container and was subjected to an impact, as a result of which the filler fell off (frame 16). The frames 9 and 10 here demonstrate radiation caused by the impact.

b) The two lead nets without filler were twisted together to form a tourniquet that was placed on the container and subjected to impact. The radiation caused by the impact is shown in frames 11 and 12.

c) Pieces of lead shown in frame 17 were poured into a wooden mold (Fig. 24). The blow was made through a rectangular aluminum alloy parallelepiped. The radiation caused by the impact is shown in frames 13 and 14.

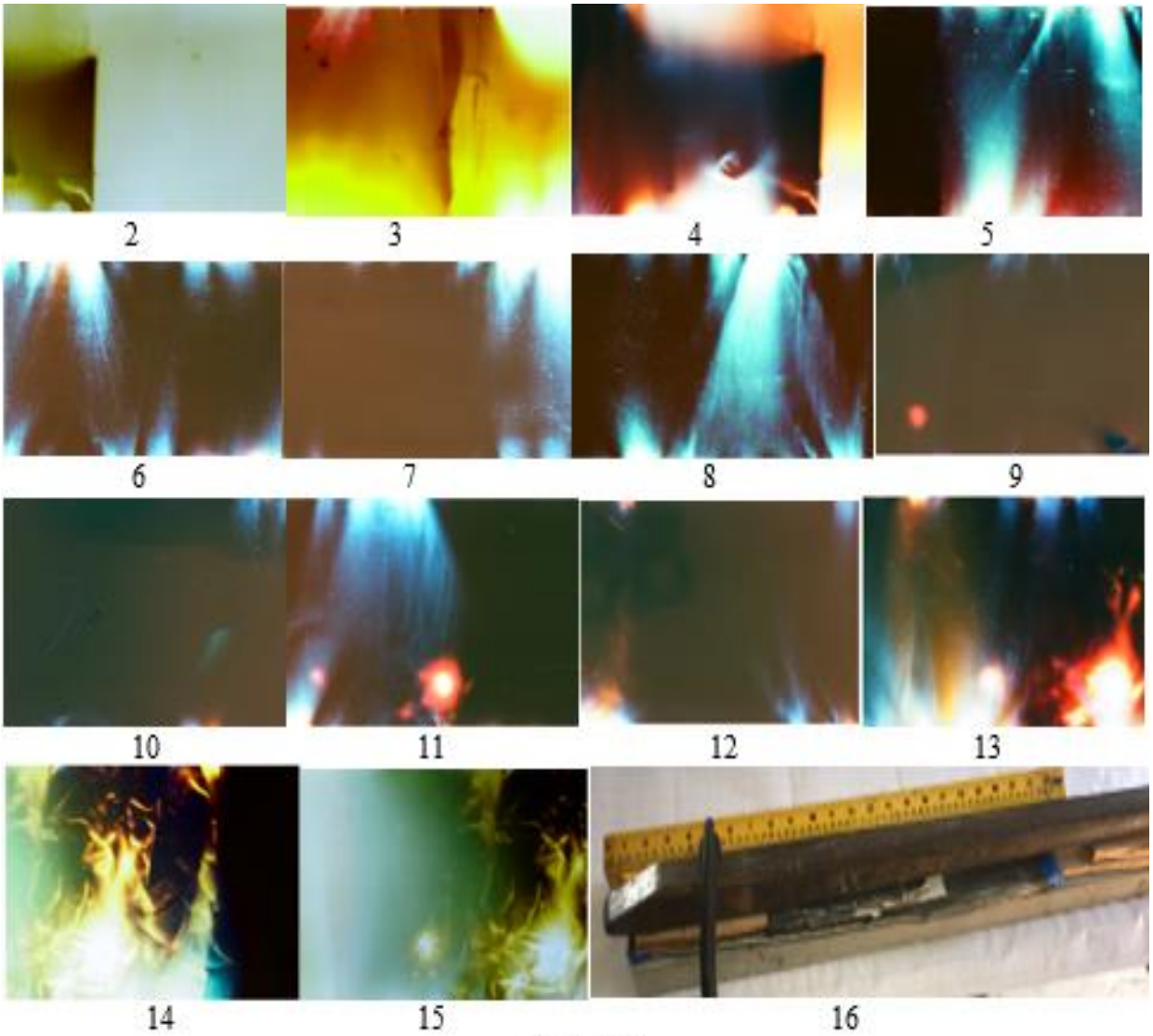


**Fig. 11 (2)**

Experiment No. 3. Study of lead transparency

The lead plates 2.5 mm thick were laid on the surface of the container with six stacks so that the number of plates decreased from six to one. The missing plate was replaced with a laminate of the same thickness, so that the stack height was the same, as shown in Fig. 11 (2) frame 16. The sixth stack, consisting of one plate, is partially flattened to a thickness of 0.03 mm.

The location of the radiation source (steel bar), absorber (lead) and detector (film) have the following dimensions:

1) the total length of the absorber 210 mm, height 15 mm,

2) the useful length of the container is 550 mm,

3) the total length of the gap between the lower surface of the timber and the container is 340 mm.

Two hits with the sharp points of the ax shown in fig. 11 (1), frame 3, were applied to the corner of the beam in the area of the first and second (left) piles of lead. Fig. 11 (2) shows 14 frames out of 15, but only for six the radiation caused by the impact passed through the absorber. However, a significant difference in intensity is not observed in frames 2-3, and 10-15, which are located outside the absorber, and (4-9) where the absorber is located. Frames 4-13 illustrate fan-shaped radiation, the source of which is outside the frame. This radiation has been observed many times, as will be shown below. The red spots that are observed in frames 9, 11, and 13 are due to radiation when drilling holes before the experiment with impact. The unique picture recorded on frames 14 and 15 is probably associated with a change in the structure of the plate during hardening.

Conclusions.

1) The mechanism of electromagnetic radiation of lead caused by shock, the frequency of which corresponds to the frequency of x-ray radiation, is no different from the radiation mechanism in other materials.

2) The brightness of the photographs obtained after the radiation passed through the lead absorber does not differ from the one received when the radiation passed through the air gap.

3) The high transparency of lead allows us to conclude that the mechanism of excitation of this radiation is different from the one of x-ray radiation utilizing electron impact accelerated by high voltage.

4) The experiments convince me that my recognition of this radiation as X-ray, as it was generally accepted, was erroneous. These differences allow us to state that another mechanism of electromagnetic energy emission of 50-100 keV, which corresponds to a frequency of $10^{18}$ -$10^{19}$ Hz, is realized in nature. This phenomenon is called p-radiation.

5) It is known that one experiment cannot refute the results of another one. That means that the experiment, the result of which is shown in Fig. 7 does not contradict the test result shown in Fig. 11, since in the first case, delayed radiation from particles formed as a result of destruction was used, while in the second case, direct radiation was used, the frequency and, probably, the formation mechanism of which is different.

6) Experiment No. 4 demonstrated the possibility of detecting signals at a distance from the radiating surface, which can be used to analyze the damage in places where the installation of the sensors is impossible. The results of the experiments confirm that the conclusion is given below.

### 1.1.7. Self-emission transparency

The following experiment was carried out in such a way that the radiation caused by the impact with the tip of the ax was recorded simultaneously on two films. One of the films was located under the bar, as shown in Fig. 11 (1), the second one was wound spirally around the metal beam, the film under it, and the wooden substrate. It recorded radiation at various angles to the direction of impact. Twelve of the twenty-eight photographs illustrating p-radiation recorded on the film located under the beam are shown in Fig. 11(2).

The next experiment was carried out in such a way that radiation caused by the impact of the tip of the ax was recorded simultaneously on two films. One of the films was under the beam, as shown in Fig. 11 (1), frame 1. The second film was wound spirally around a metal beam, the film under it, and the wooden substrate. The ax hit the top surface, and the radiation was recorded at different angles with the direction of impact.

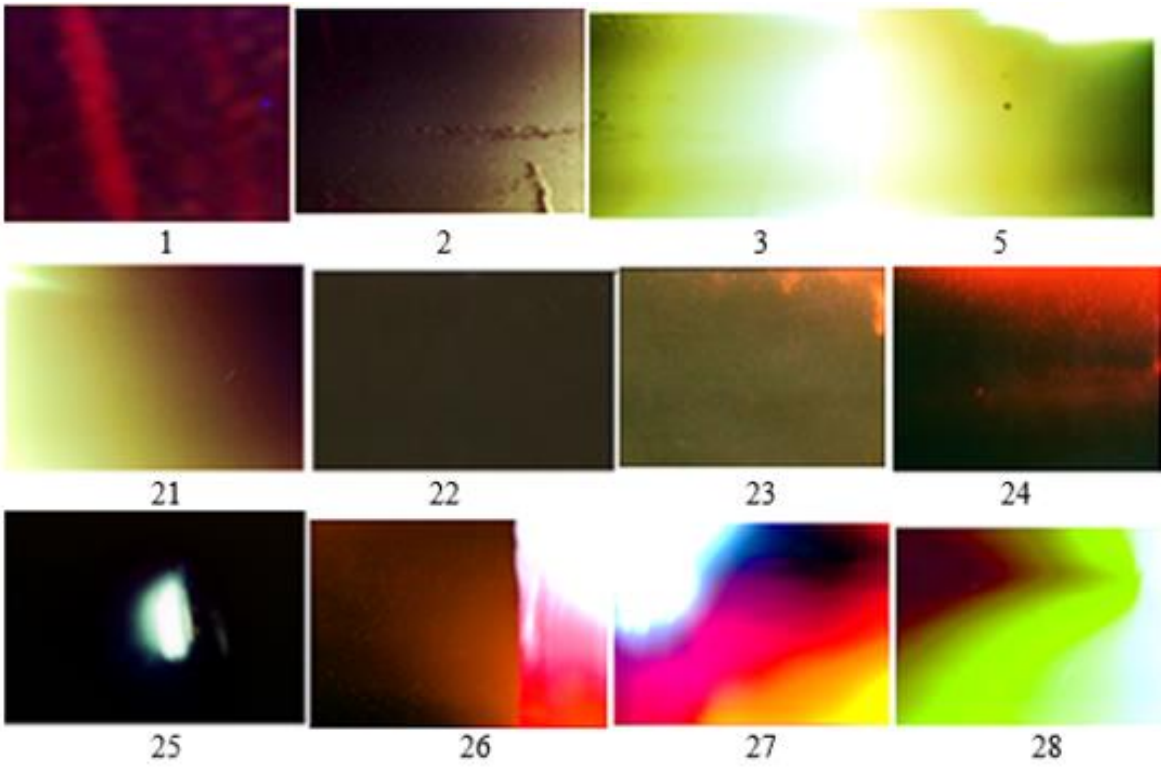


**Fig. 12**

Twelve of the twenty-eight photographs illustrating the p-radiation recorded on the film under the beam are shown in Fig. 12. One blow of the ax tip on the surface has caused the radiation that was recorded on the frame No. 1.

Let us pay attention to some features of the response of the entire beam to impact.

1) Frame 1 illustrates two (possibly three) images of the impact;

2) Frame 2 shows one more (maybe two) image of the impact of lower intensity.

3) The frame width is 1.38″ (35 mm). Therefore, the distance from the frame No. 1 Fig. 11 (2) to the frame No. 28, Fig. 11 (2) is 37.2″ (945 mm).

4) Frames 26, 27, and 28 illustrate bright radiation, the color of which changes with distance from the radiation source. The figure, which three frames represent something that looks like a crack, as it is depicted in fracture mechanics.

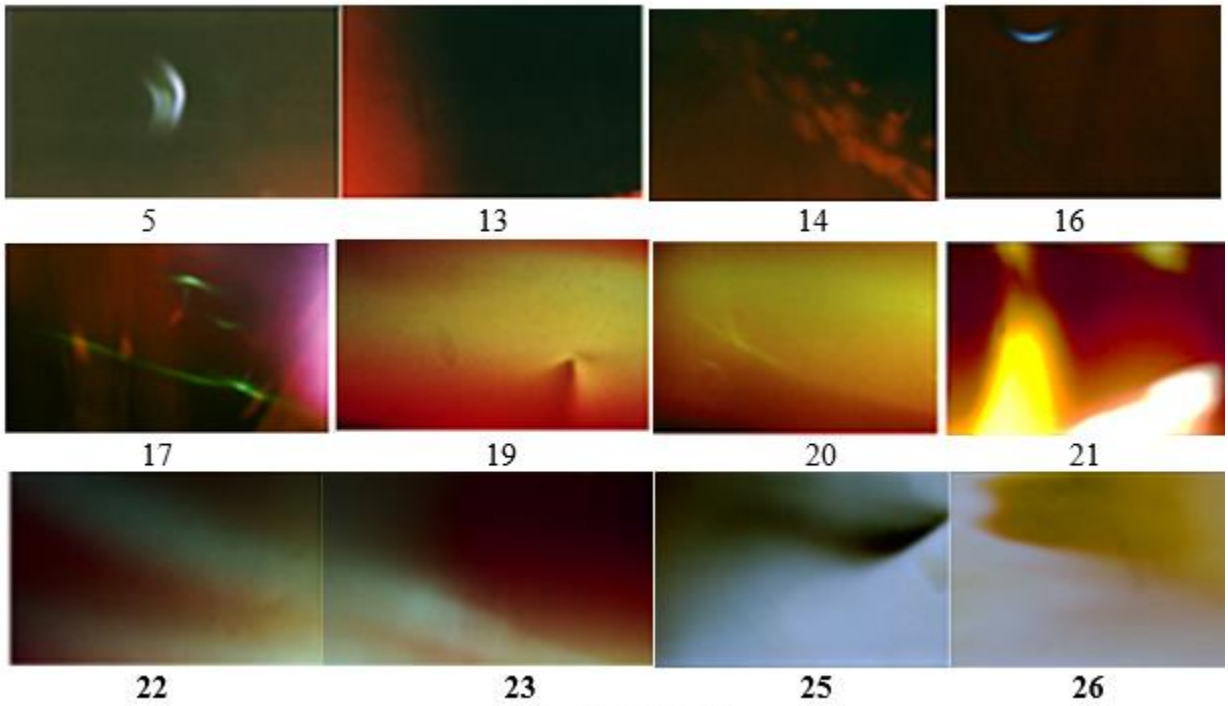


**Fig. 12 (Spiral)**

The 12 out of the 26 frames, illustrating radiation caused by the same impact, but captured on a film arranged in a spiral around the beam and the first container, are shown in Fig. 12. A strike was made on the upper surface *xy* in the direction of the *z*-axis. The photos show in Fig. 11 (2), obtained on a film located along the *x* axis on the lower surface, 1.5″ (38 mm) apart from the upper one.

The photos show in Fig. 12 (Spiral), are obtained at various angles to the direction of impact. Frame 5 illustrates the emission of p-rays in the direction of the y-axis, at the moment of impact captured at approximately the place where Fig. 11 (2) frame 1. Frame 14 is captured on a film located at an angle of ~ 40° to the *z*-axis.

The photographs analysis showed that there is a natural phenomenon similar to self-induced transparency caused by exposure to a femtosecond laser, but with a higher frequency of electromagnetic radiation, corresponding to the frequency of X-ray radiation caused by high-speed electron blow.

Four films were placed on eight parts of the 4×9.5 I-steel beam surfaces, as shown in Fig. 13.

Fig. 13

Forty-seven photographs illustrating p- radiation are shown in Fig. 14 (1) - 14. (4). The blow of the ax tip was applied at a point spaced from the edges of the beam at a distance of 14″ (355.6 mm) and 70″ (1778 mm). The blow point is shown in Fig. 14(4), frame 11. The photographs were taken on all surfaces of the beam, including the butts, as it is shown in Fig.13, Fig.14 (2), frame 1, and Fig. 14 (3) frame 7. That means that the maximum propagation distance of the pulse is 70″ (1778 mm).

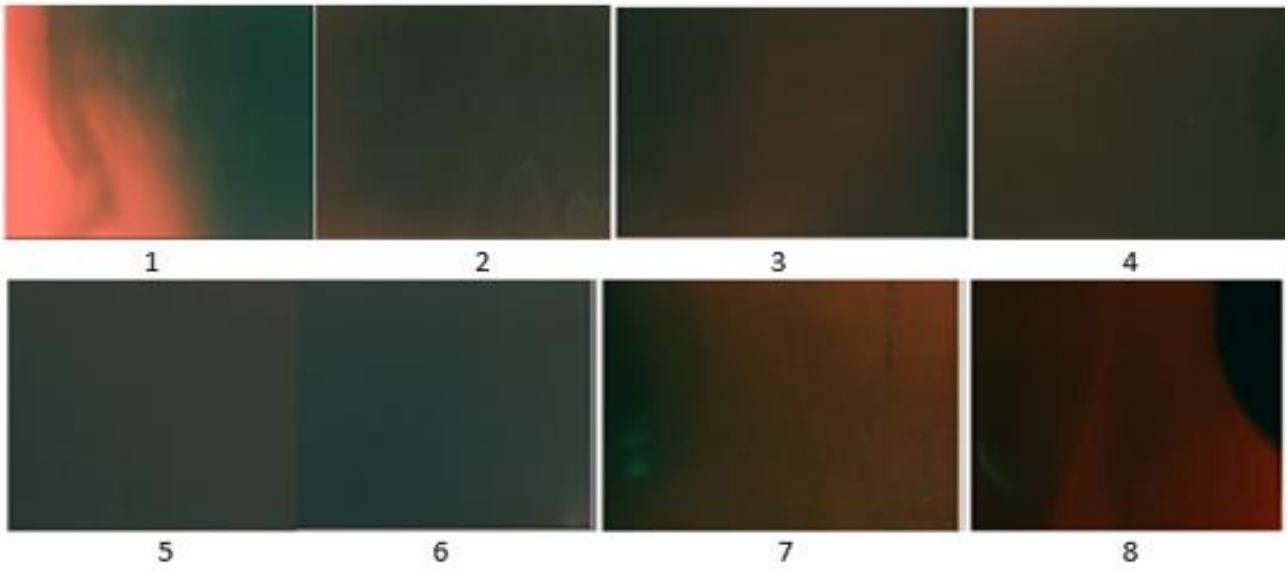


**Fig. 14 (1)**

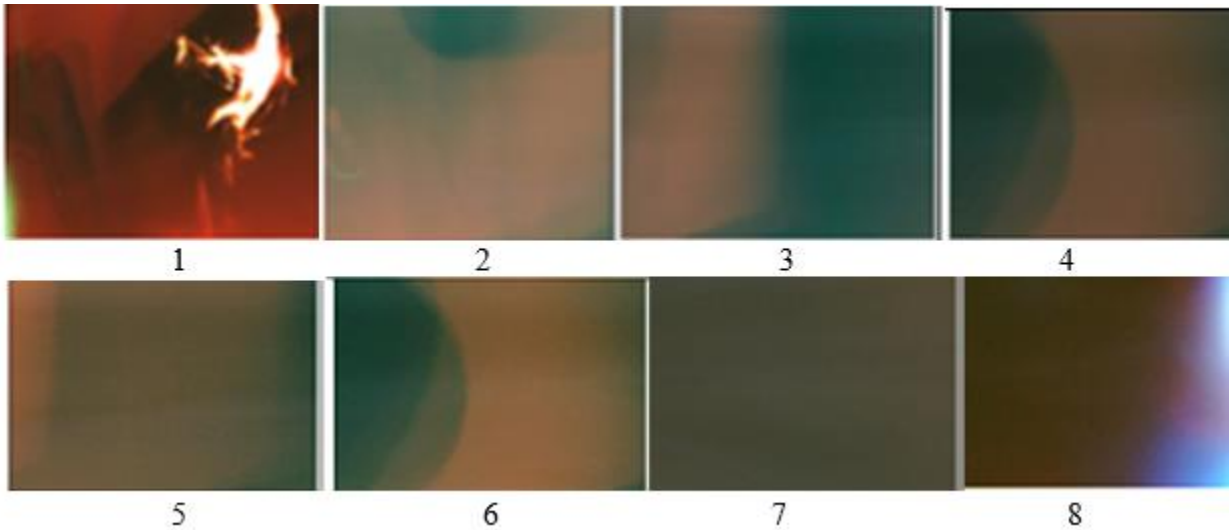


**Fig. 14 (2)**

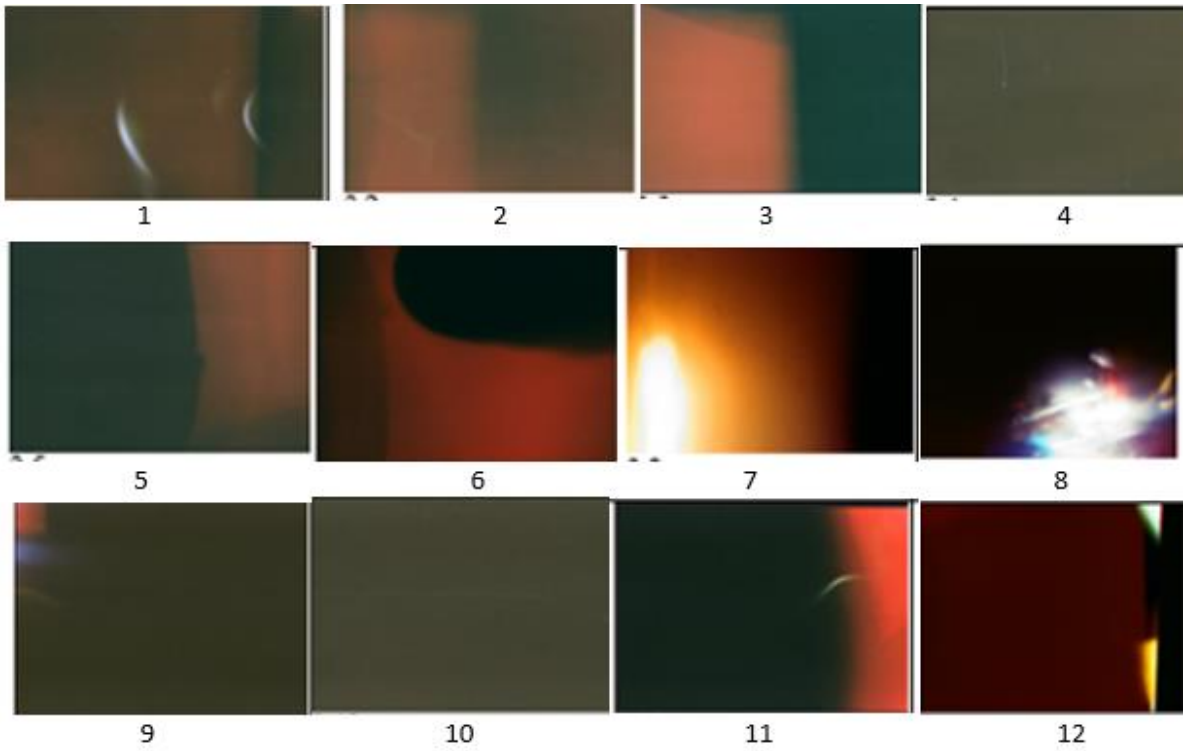


**Fig. 14 (3)**

Photo Fig. 14 (3), frame 7 illustrates a blow response recorded on a film located on a lower surface 101.6 mm apart from the upper one.

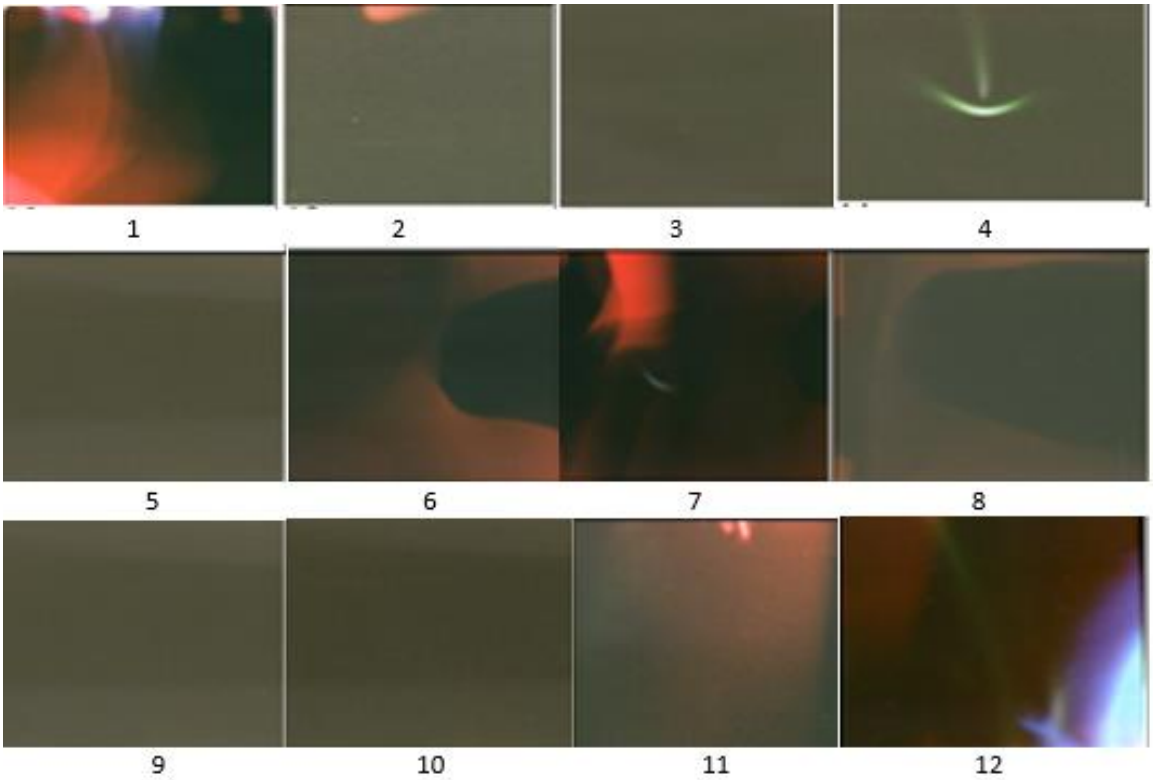


**Fig. 14 (4)**

*This phenomenon is called self-emissive transparency, by analogy with self-induced transparency*.

One hundred and two frames recorded after a single impact indicates a natural phenomenon, which determines the possibility of transmitting the high-frequency component of electromagnetic radiation that has arisen inside the metal. The radiation observed in different directions far from the original source differs from the primary radiation in the spectral composition and shape of the emitter.

A detailed analysis of the observed phenomenon requires a particular study since the analogy between self-induced transparency, and self-emission transparency is conditional. We limit ourselves to only three remarks.

1. The emission of electrons and X-rays during the deformation of crystals and violation of the adhesive layer was first observed by B. N. Deryagin *et al*. in 1953 and C. G. Camara *et al.* in 2008 when peeling off the adhesive tape[2].

The authors of these works assumed that an electric discharge causes x-ray radiation due to deformation. The author [1.8-1.14] proceeds from the hypothesis that pores, cracks, and fractures are formed as a result of breaking the bonds between a certain number of atoms removed to such a distance that the attractive forces are insufficient to restore the previous state. The energy required to break the bond is due to the induced radiation of metastable atoms.

2. We observe dark and luminous areas in the photos, both solid and those which shape is clearly limited. We pay attention to the photos: Fig. 11, frame 27; Fig. 14 (1), frame 8; Fig. 14 (2), frames 2, 4, 6; Fig. 14 (3), frame 6; Fig. 14 (4), frames 6, 7, 8. The form of some of them completely coincides. Consequently, these photographs indicate some defects in the structure.

3. But of particular interest is the photograph of Fig. 11, frame 28, resembling a crack, as depicted in the mechanics of destruction, but most importantly, is observed in X-rays. The refraction and scattering of X-rays are widely used to detect damage (pores or cracks) in various materials. A microcrack formed in a polymer sample as a result of an impact was studied in [15] by the small-angle (about two minutes) X-ray scattering method, caused by the excitation of the *K* line of molybdenum with a voltage of 20,000 volts. Photos of these cracks A and B are shown in

[2] V.V. Karasev, N.A. Krotova and B.W. Deryagin, "*Study of electronic emission during the stripping of a layer of high polymer from glass in a vacuum*," Dokl. Akad. Nauk. SSR, 1953, **88**, 777-780; Carlos G. Camara, Juan V. Escobar, Jonathan R. Hird, Seth J. Putterman: *Correlation between nanosecond X-ray flashes and stick–slip friction in peeling tape Nature,* 2008 *455* (7216), 1089-1092.

Fig. 15 next to the photographs taken from the impact study shown in the photograph of Fig. 11 (2), frame 28 (C) and rail 40 4 (D).

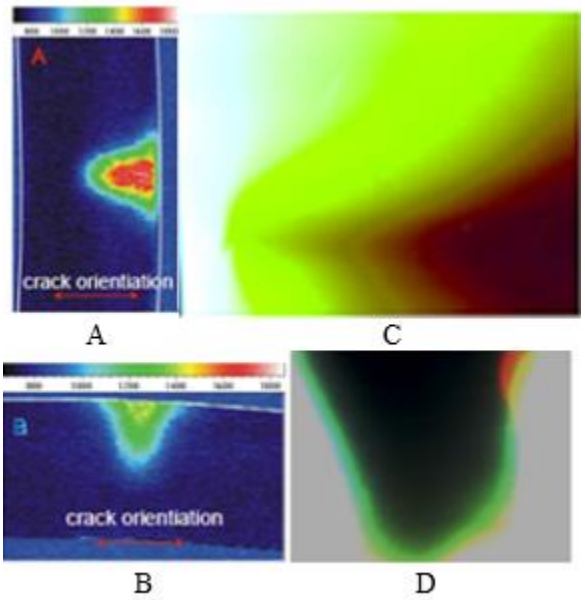


**Fig. 15**

A diagram of an experimental study of cracking with the help of X-rays from an external source is shown in Fig. 16. The coincidence of the shape of the observed defects should be considered good, taking into account that the photographs were obtained in the study of various materials at different external influences.

### 1.1.8. Single blow on the wood

A cylindrical rod of wood with a diameter of 1″ (25.4 mm) was subjected to a single blow with the tip of an ax. Fig. 17, frame 4 illustrates the p-rays caused by the impact**.**

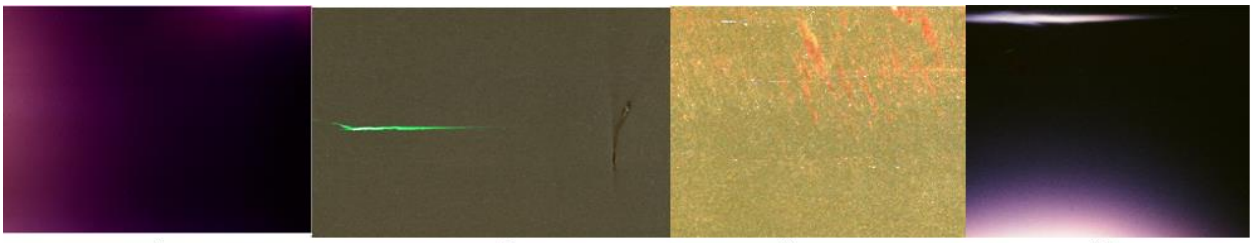


**Fig. 17**

The radiation intensity on frames 2, 3, and 5-21 is low. The color of frame 21 is changed to display the image. The photos are intended to demonstrate the effect. The line of impact shown in frame 4 is dark. Consequently, a crack has formed in this place. The intensity of the frame 22 allows us to conclude that the radiation caused by the impact is recorded on this frame. Thus, the high-frequency electromagnetic impulse is captured at a distance of 24.8 ″ (630 m) from the point of impact.

### 1.1.9. Single impact on a flagstone

A single blow with the tip of an ax was struck on a flagstone plate of 45 mm thick in the area of Fig 18, frame 2, as a result of which the plate split into two parts.

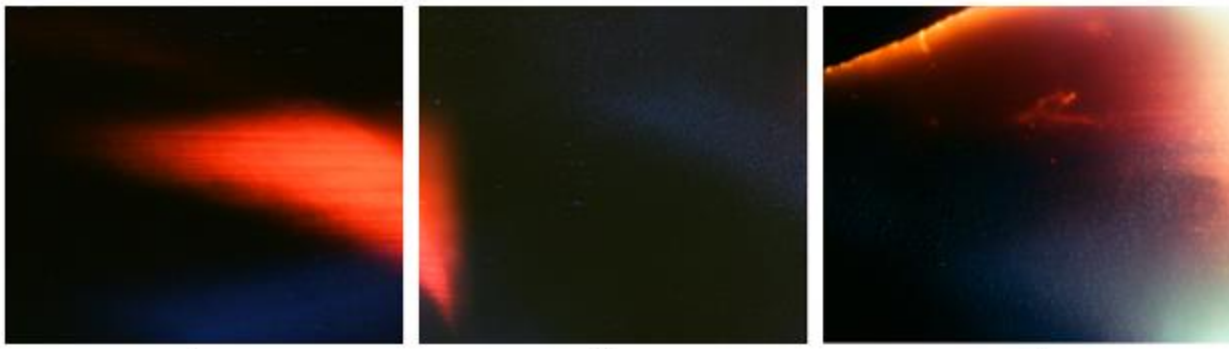

1 2 3

**Fig. 18**

Three photos are shown in Fig. 18 illustrates the effect of p-ray on photographic material. The experiment shows that no emission is observed in the region of destruction. The weak blue radiation recorded in the crack is due to the delayed radiation from the particles formed as a result of the destruction.

The photographic method does not allow to establish the sequence of processes recorded in the film. But we can assume that the intense red radiation from the fragments formed after the destruction is also delayed.

### **1.1.10**. **A single blow to the surface of the water**

A stone weighing 15 kg fell from a height of 5 m onto the surface of the water in a cylindrical container. Four plates of flagstone 45 mm thick each were located under the surface of the water inside a U-shaped container containing film.

The 16 of 27 photographs illustrating p-emission caused by an impact are shown in Fig. 19.

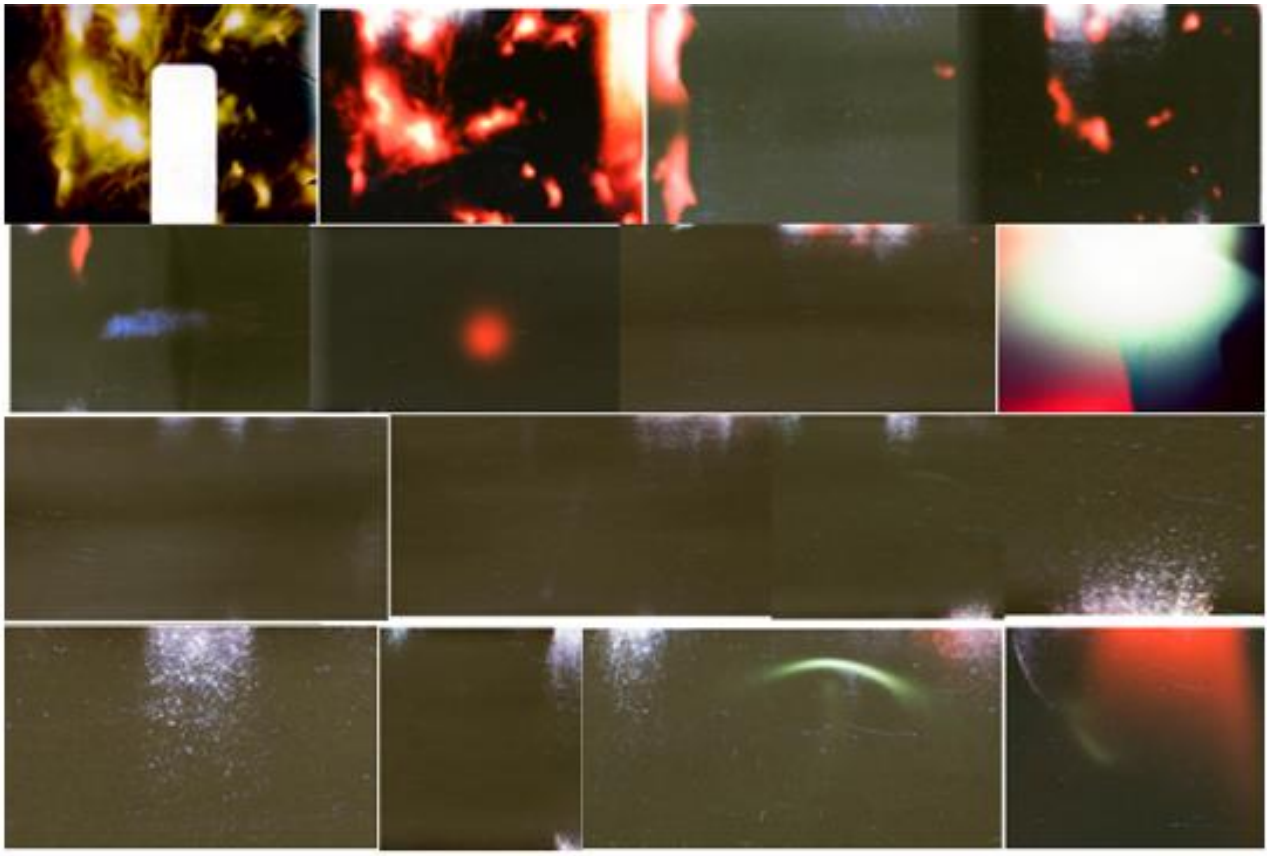

**Fig. 19**

The object, which radiation has a shape of an arc, was observed in Fig. 4, Fig.12, Fig. 14 (3), Fig.14 (4). Two luminous objects that are located next to it are shown for the first time. A characteristic feature of these objects, called fan-shaped, is that, firstly, they are formed on the edge of the photo-frame, and secondly, they appear where water is present. The second film was fixed horizontally on the outer surface of the container with water. Fig. 20 illustrates p-rays from water.

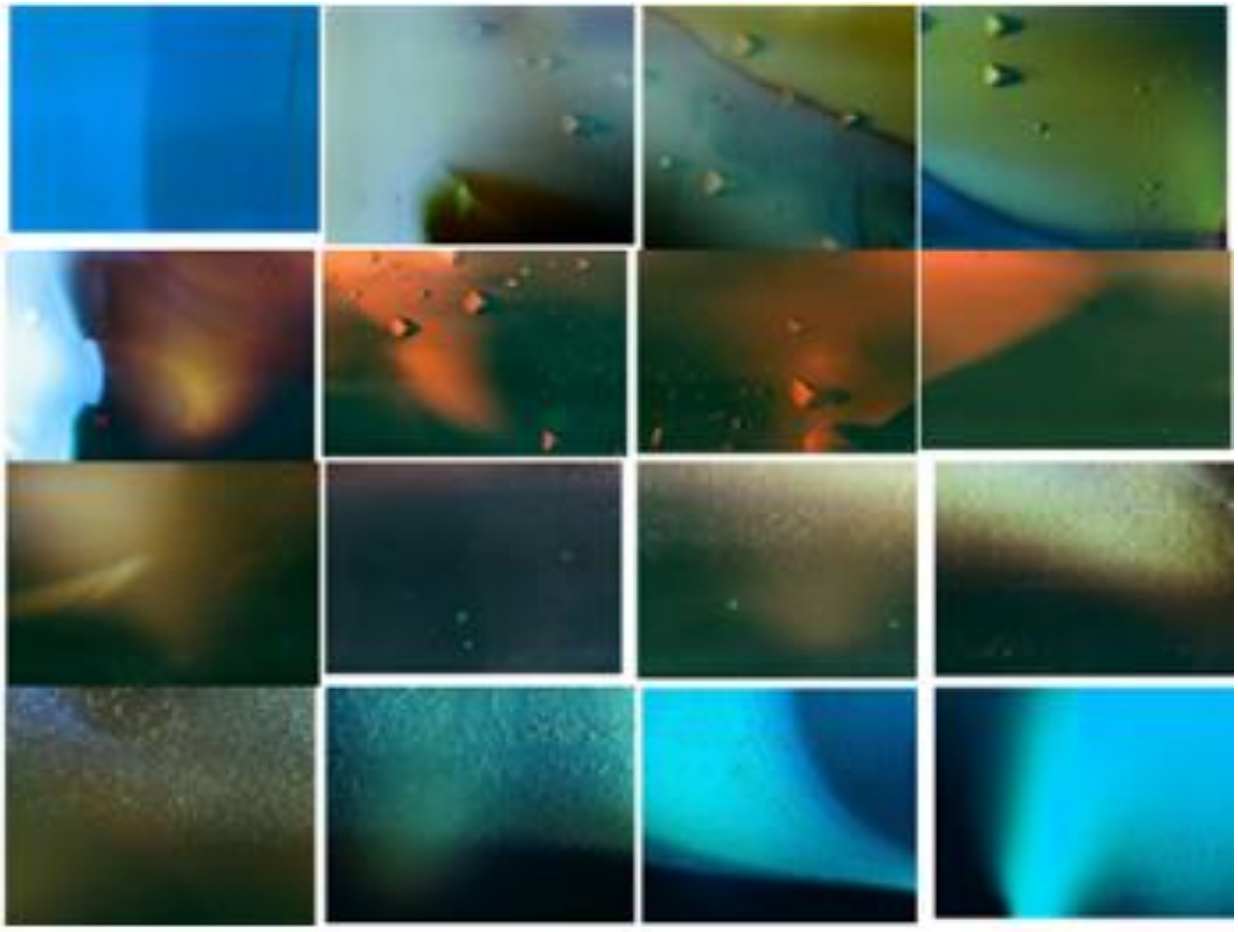

Fig. 20

### 1.1.11. Features of p-rays during shear deformation

The destruction caused by shear deformation was investigated by the contact of a solid with a rotating grinding stone, drilling holes, and friction.

A box with an aluminum bottom, loaded with stone, was dragged across the asphalt at a distance of 30 m. The p-ray radiation was recorded by a film located at the bottom.

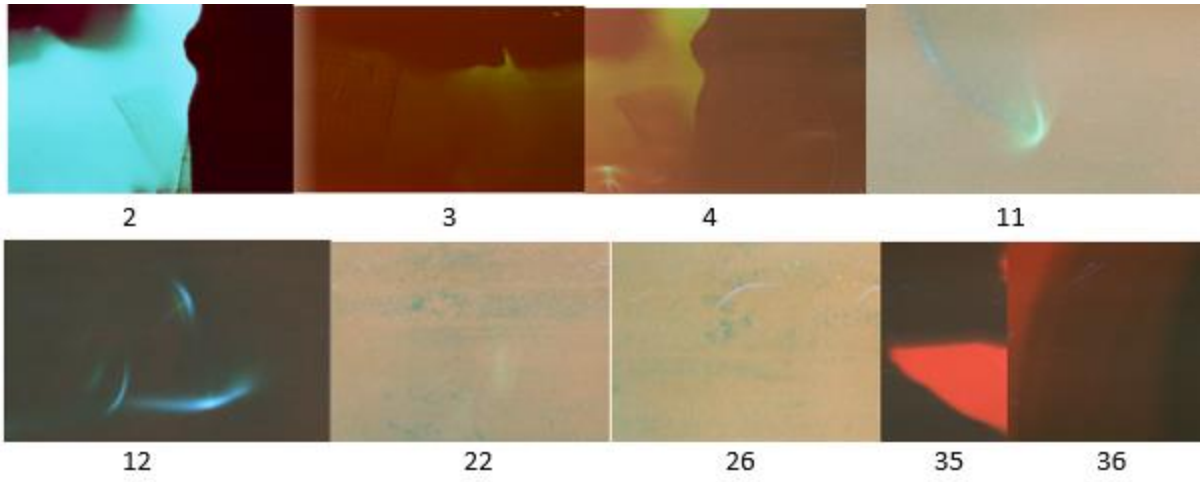


**Fig. 21**

Nine of the 36 frames shown in Fig. 21 illustrates p-ray radiation due to friction. The background on frames 22 and 26 is changed to show traces of dragging.

### 1.1.12. Features of p-rays during a rail operation

In the process of exploitation, the rails are exposed to intense influence when the locomotive and wagons move. The increase in the train's speed and the mass of the carried cargo increases the requirements for the assessment of the technical condition of the track. A characteristic feature of p- radiation is that it does not depend on the type of deformation. This allows creating a locomotive mounted device that monitors the technical condition of the track.

An experimental study of the rail track using a moving locomotive made it possible to obtain 89 photographs for the analysis of defects arising in it, which are shown in Fig. 40 1 - Fig. 40 6.

This numbering of photographs, corresponding to the protocol of experimental studies, was left in order to demonstrate the fact that the experiment was carried out on a railroad track in Northwest Railway Museum, Snoqualmie, WA.

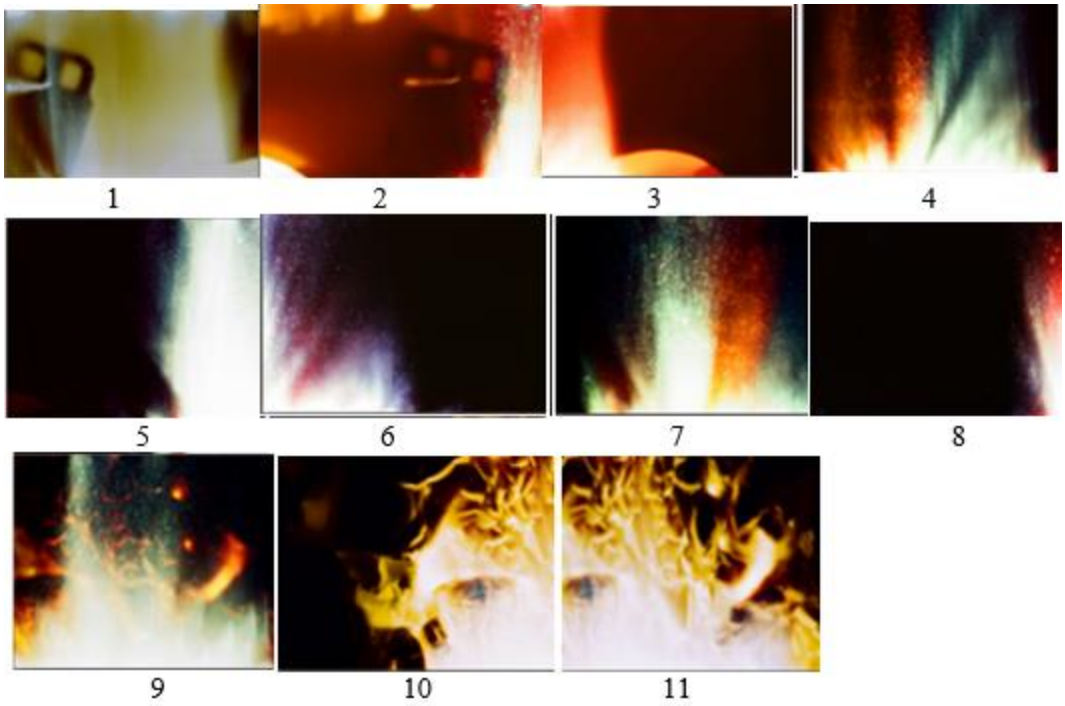


Control experiment series No. 40, test 1, performed at the Northwest Railway Museum, Snoqualmie, WA on a railroad using a locomotive

Eleven photographs were taken on a film located on the rail web in the snow. The locomotive has stopped six meters before the film.

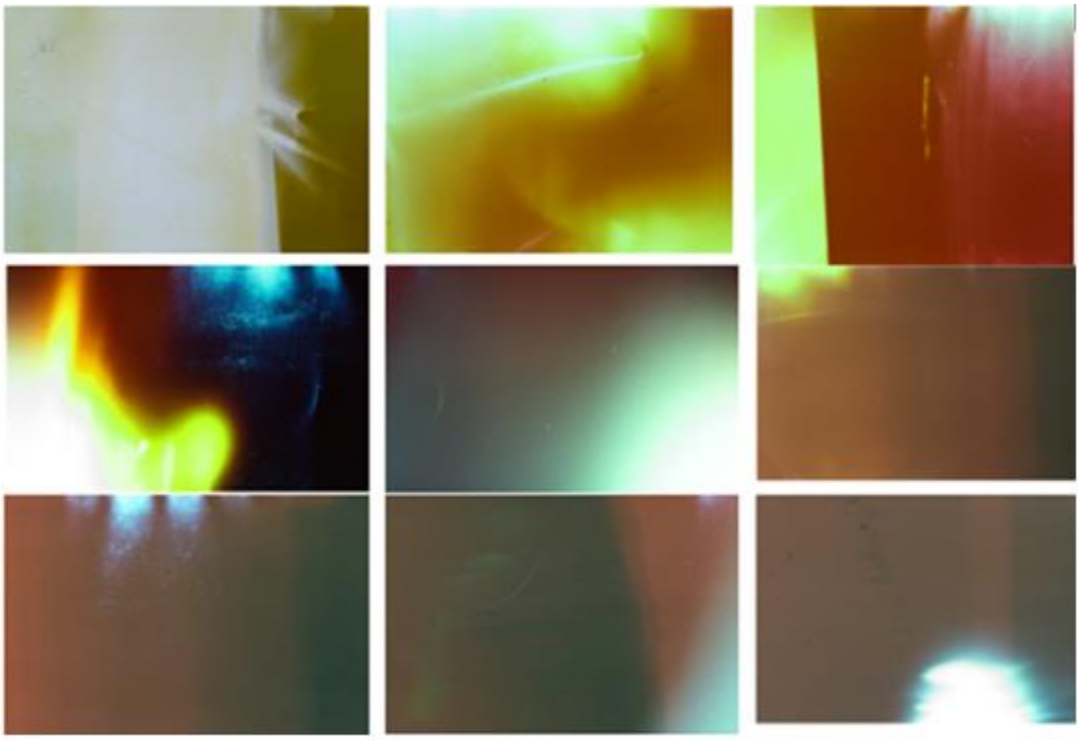

Control experiment series No. 40, test 2, performed at the Northwest Railway Museum, Snoqualmie, WA on a railroad using a locomotive

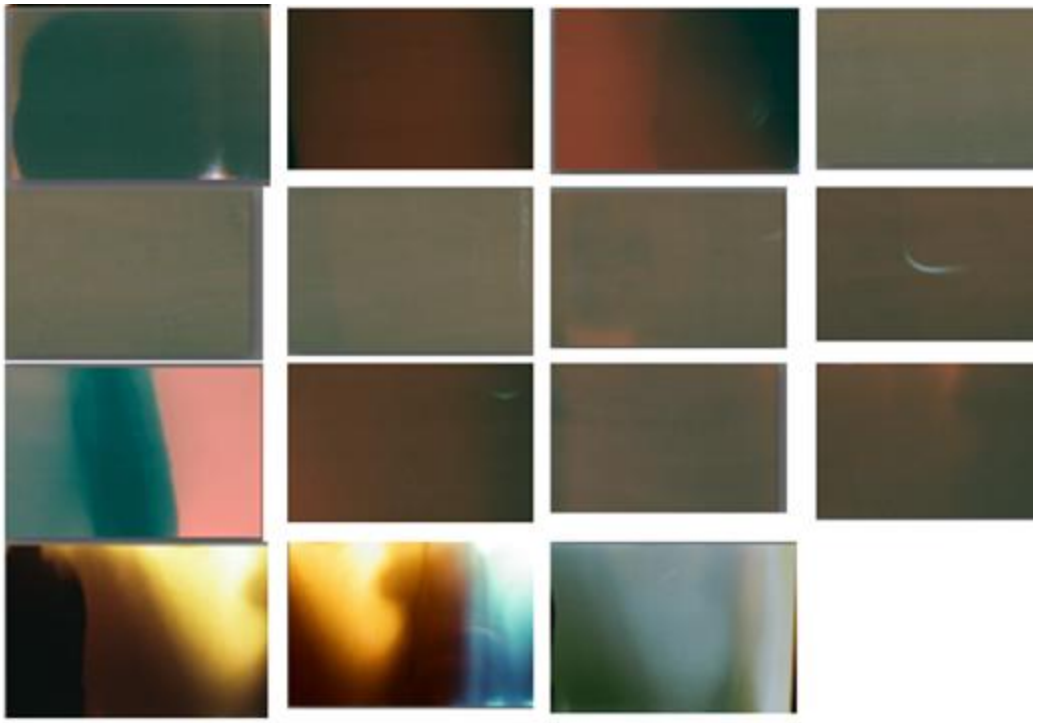

Control experiment series No. 40, test 3, performed at the Northwest Railway Museum, Snoqualmie, WA on a railroad using a locomotive

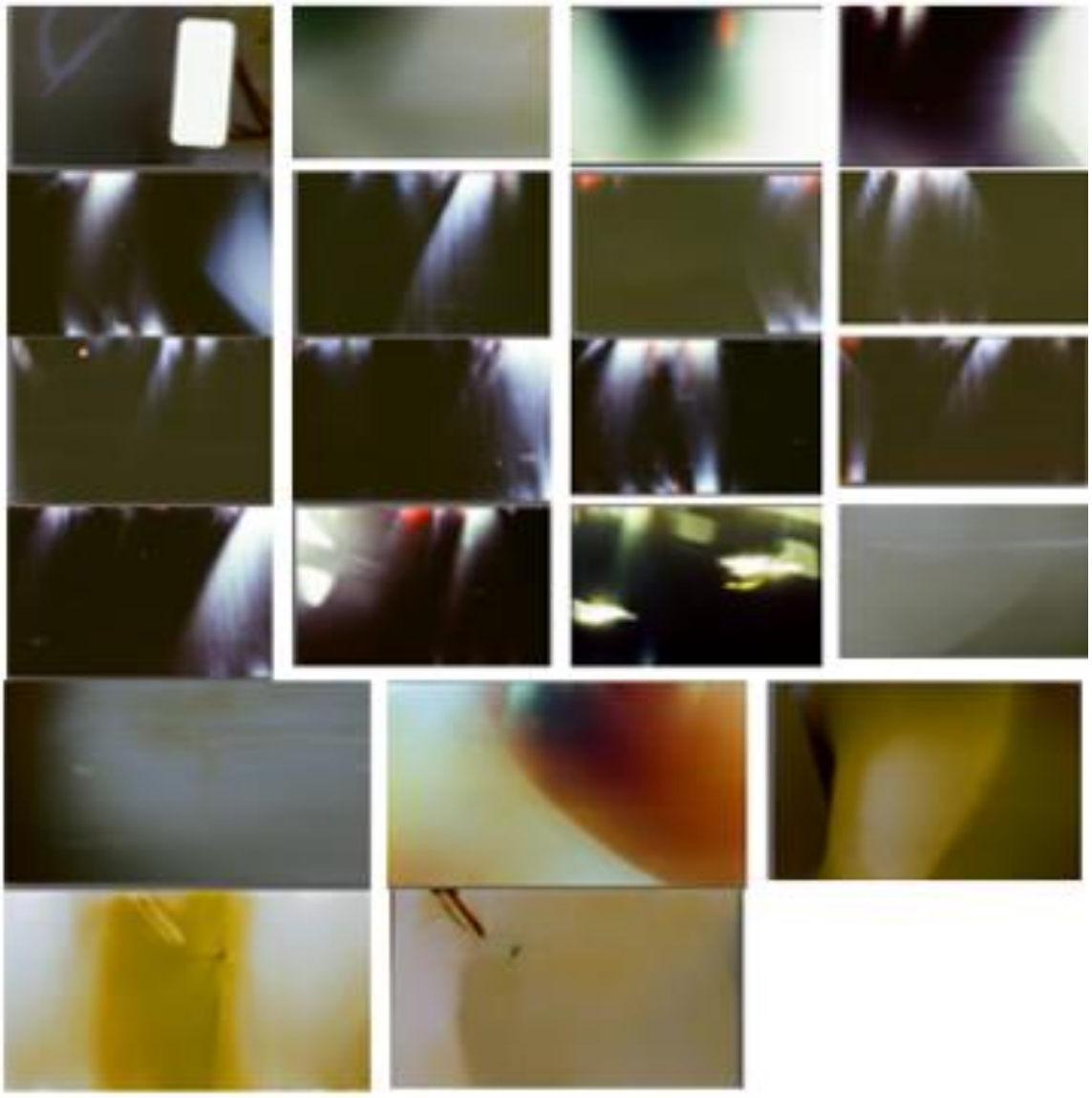

Control experiment series No. 40, test 4, performed at the Northwest Railway Museum, Snoqualmie, WA on a railroad using a locomotive

The photographic film was located on the rail web in the snow, but the locomotive has passed over it in the forward and reverses directions.

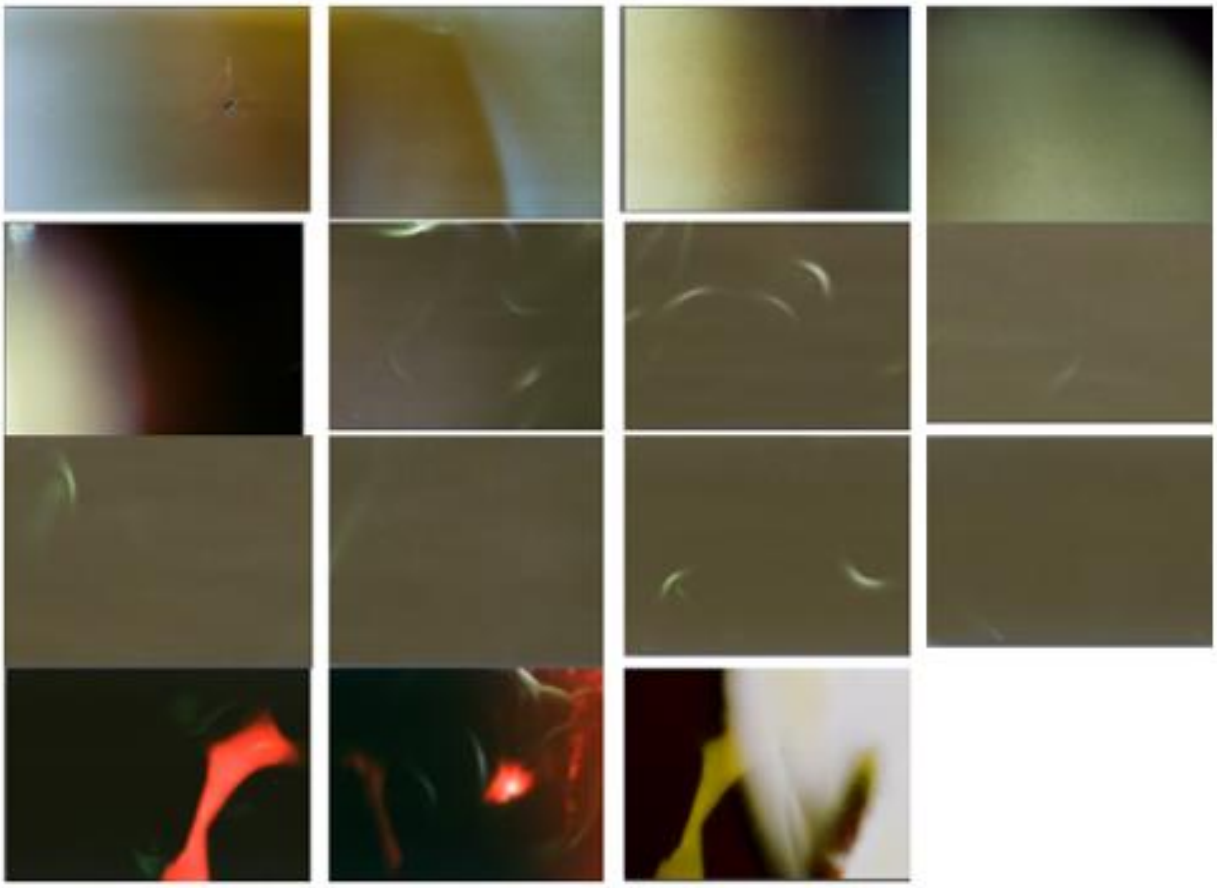

Control experiment series No. 40, test 5, performed at the Northwest Railway Museum, Snoqualmie, WA on a railroad using a locomotive

The fanlike radiation characteristic of water is observed in Fig. 40 1- Fig. 40 4.

A photographic film located on the locomotive frame revealed two identical radiating objects located in different places. They are shown on frames 13 and 15, but on frame 15, there is a defect in which energy is absorbed.

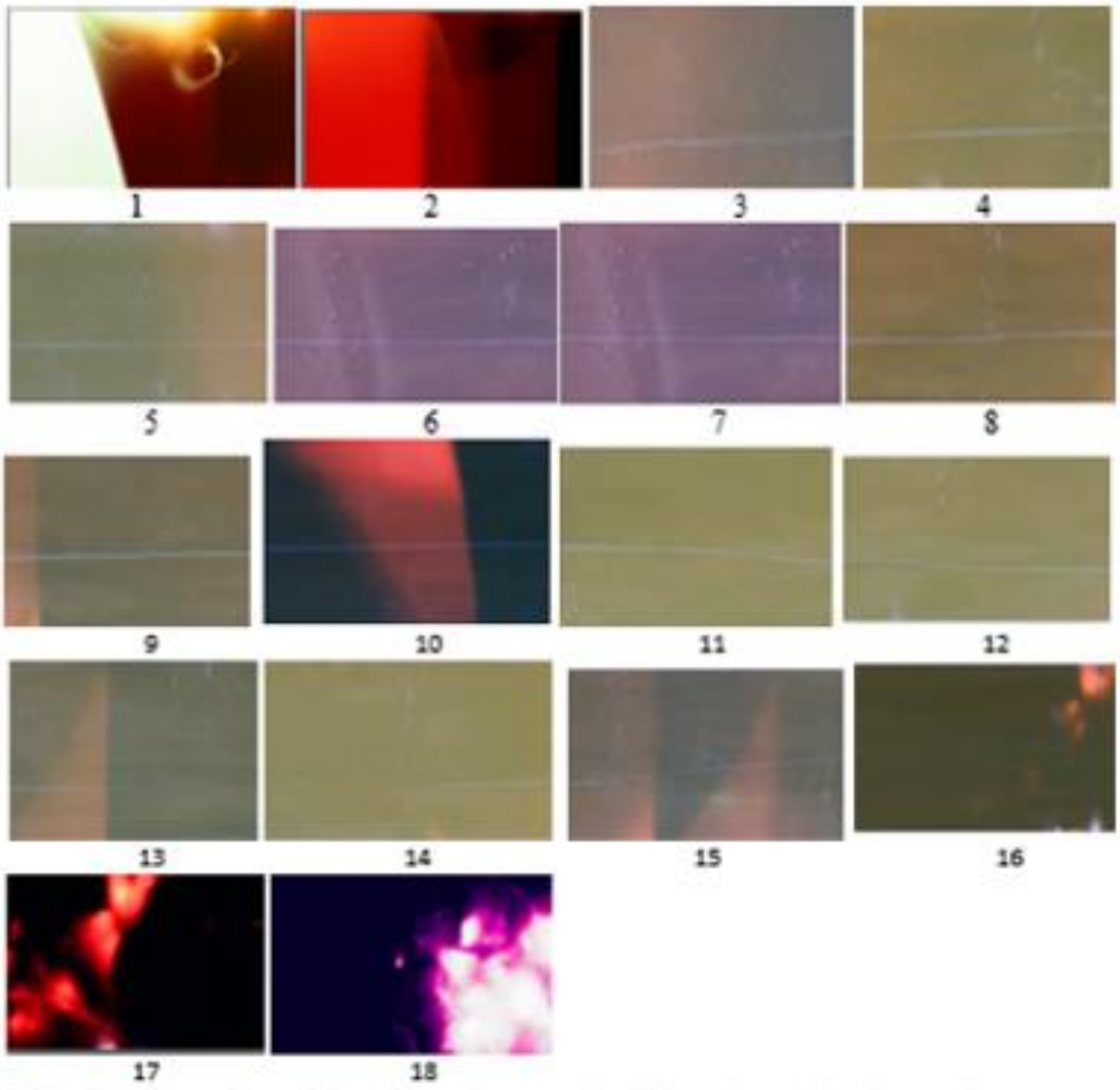


Control experiment series No. 40, test 6, performed at the Northwest Railway Museum, Snoqualmie, WA on a railroad using a locomotive. The photographs illustrate X-rays from the sleepers and the mounting rails to the sleepers.

Photos that are shown in Fig. 40 6, illustrate the p-radiation of a concrete sleeper after the locomotive passes over it. This radiation reveals a number of features that are observed only in the sleeper. First, we see a clearly defined luminous line between the rails from frame 3 to frame 16, extending from one rail attachment to another; secondly, a bright glow on frames 1, 2, 16, 17, 18 indicates an intense deformation; thirdly, the defects shown in frames 10 and 13 are identical in shape with the defect shown in frame 15, but differ in the fact that energy is radiated from them, whereas the defect shown in photo 15 is absorbed. The degree of danger of such defects can be established only on the basis of special experimental studies.

### 1.1.13. P-Rays at the phase transition

Analysis of the studies in which the efforts are being made to prevent the formation of cracks in the process of casting aluminum and its exploitation showed that in this section of the technique there had saved the paradoxical position when they search for criteria of the formation of the hot and cold cracks is carried out on the basis of erroneous hypotheses about the nature of the energy source and the mechanism of its formation.

The goals set by the authors of [1.16-1.21] can only be achieved if the methods and theory are correctly chosen. The authors of [1.18] write: “In order to investigate the effect of casting process parameters such as casting speed, billet size, and water flow rate, thermomechanical simulations were applied using ALSIM$^5$ casting simulation software. Among the studied casting process parameters, the increased billet size and high casting speed resulted in the most dramatic increase in residual stress levels. Critical crack sizes that led to catastrophic failure were also calculated and are reported against process parameters.”

The influence of the parameters of the technological process on the quality of the product is well known. However, for a mathematical program, it is necessary to establish not a statistical, but a causal relationship between all parameters of the process and the expected result.

Richard Feynman, analyzing the cause of the catastrophe shuttle "Challenger," wrote: “We went back through the report and found the analysis. It was some computer model with assumptions that were not necessarily right. You know the danger of computers, it's called GIGO: garbage in, garbage out! The analysis concluded that a little unpredictable leakage here and there could be tolerated, even though it wasn't part of the original design.”

As is known, Feynman not only revealed the cause of the catastrophe but demonstrated a physical law that was not considered when launching the spacecraft.

*Only the measured physical parameter characterizing the potential energy that can be radiated should serve as an input parameter of the computer program.*

Lalpoor [1.16], outlining the program of his research, wrote: “Therefore, the main study on this field has been confined to case studies rather than fundamental investigations. In fact, the industry preferred to solve the problem technically for the sake of production rather than performing systematic research with the aim of understanding the phenomenon. Besides being an unpredictable phenomenon, other problems have prevented the researchers from more detailed studies.”

The assumption that the problem of cracks formation and their prevention can be solved without an understanding of the physical processes is a mistake. This led to the fact that the criterion on the basis of which it is possible to predict the time, the place of appearance of a crack, to assess its danger and prevent it, was not found. The author was forced only to describe the facts which he observed. The hope that computer modeling can help solve the problem is not justified since the input parameters were not the measured physical parameters that characterize the cause of cracks formation, but the stress intensity factors, on the basis of which it is impossible to solve the problem.

This book, like my previous works, is intended to show what physical phenomenon is the cause of the destruction of the solid. The most accurate description of the phenomena of nature became possible on the basis of quantum electrodynamics, which is the most accurate physical theory.

The most accurate description of the phenomena of nature became possible on the basis of quantum electrodynamics, which is the most accurate physical theory. This theory describes the interaction of an electron and a photon, the parameters of which are determined experimentally with the maximum accuracy: the electron charge is -1.6021766208 (98) $\cdot 10^{-19}$ C, the mass of the electron is 9.10938356 (11) $\cdot 10^{-31}$ kg, the rest mass of the photon is equal to zero to within 30-31 characters, the photon charge is equal to zero to within 33 digits.

The main characteristic of the energy state of atoms is the radiation spectrum. It varies with a precision that is not available when measuring mechanical parameters. For example, the ratio of $\Delta\lambda/\lambda$ values in the range 7.5-8.5 Å is 0.00005.

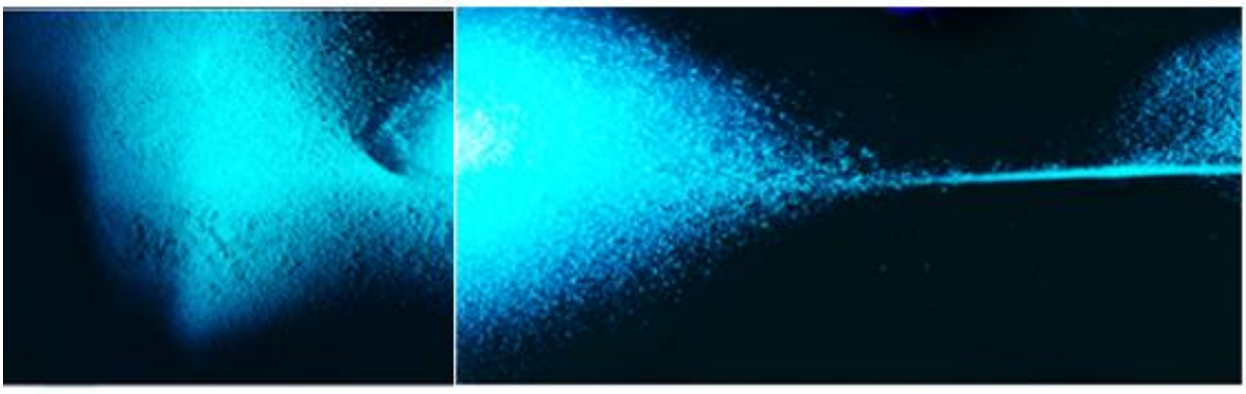

**Fig. 22**

I) Two photographs are shown in Fig. 22, illustrate the p-ray radiation of solidifying droplets of molten plastic, captured by a photographic film that was located in a container opaque to visible and ultraviolet rays.

II) The Pb-Sn alloy was melted and poured into the two lower troughs of the mold, separated by a thin partition, as shown in Fig. 23. The melt flowing down the channels to the right deeper part was cooled with water. An enlarged image obtained in p-rays is shown in Fig. 23. The left blue-green part of the photo is caused by the radiation from two melt streams. The color of the radiation of wood differs from the color shown in Fig. 10 (2) a. A clear interface between melt and wood, captured in p-rays, does not allow to make an unambiguous conclusion about whether the orange radiation is caused by the wood or a layer of paint on it.

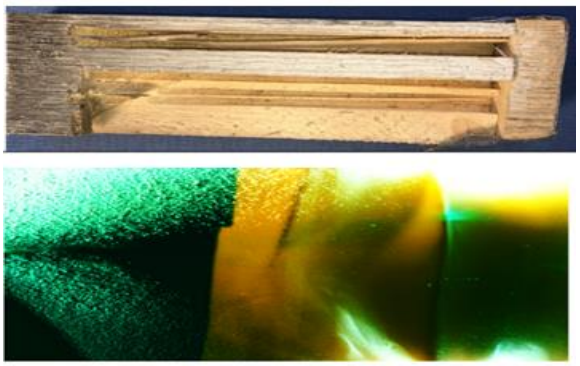

Fig. 23

**Fig. 24**

Rectangular parallelepiped of aluminum alloy 7075-T651, two ingots of cast iron, fragments of silumin, and cobblestone, shown in Fig. 24, warmed up simultaneously in the oven. The furnace temperature did not exceed 500 ° C, and the alloy was not melted. The study was limited to the rapid cooling of heated samples with water.

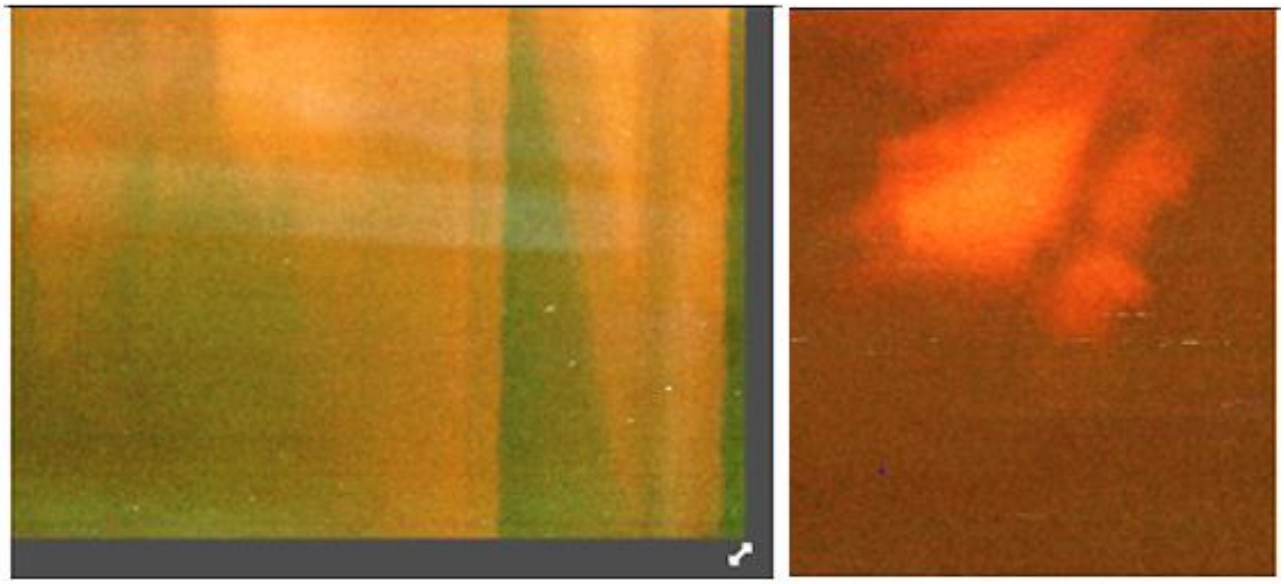

1 2

**Fig. 24 (1)**

The p-ray radiation of an aluminum alloy 7075-T651 in a wood mold is shown in Fig. 24 (1). A dark wedge-shaped area parallel to the lower and upper faces is not visually observed on the facet. The very fact of the discovery of such a defect is important, but we cannot answer the questions: what is it, where is it located, did it arise in the process of casting, machining, or heat treatment? Note that the color of the area in which the side surfaces of the mold are located differs from the color of the mold used to melt Pb-Sn. This difference is probably due to the fact that in the second case, wood is used that has been saturated with an antifungal chemical component.

Wet wood was used to cool the melt based on those amazing properties that are manifested during plant synthesis due to the absorption of photons and excitons. The rotation of the flower toward the sun is due to the conversion of photon energy into mechanical energy. There is no doubt that the rise of water from the root of a pine tree to a height of 40-50 meters is due to the additional energy that is transmitted to water molecules from the sun using photons.

The question naturally arises: do p-rays radiate when the wood is destroyed? It was answered by an experiment, the result of which is illustrated by the photos shown in Fig. 24 (2). A wooden board, 26 mm thick, was drilled 16 times over the same frame (top photo) and 10 times (bottom photo) with the aim of cumulative exposure to p-ray radiation, caused by both destruction and residual radiation from sawdust.

Fig. 25 (top view): three 13 mm holes were drilled in a sample of 7075-T651 aluminum alloy to a depth of 38.4 mm in such a way that 5 mm of metal remained above the lower surface. The holes were filled with silumin melt and cooled with water.

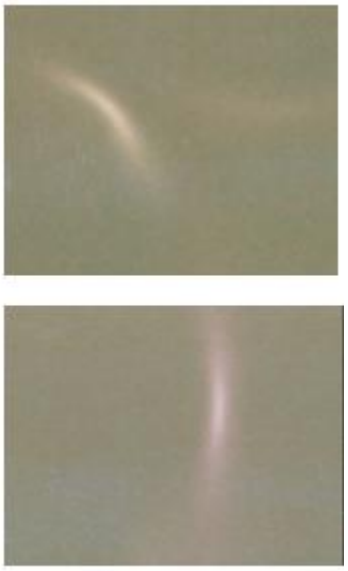

The process was captured on two adjacent frames. The experiment was performed three times.

Six photographs obtained by three repetitions are shown in Fig. 26. Note that the defects found in the experiment were repeatedly observed during other types of deformation.

Photo Fig. 24 (1) frame 2 illustrates p-ray radiation from pieces of silumin with intensive cooling. We draw attention to the fact that p-rays passed through the steel wall of the box, in which silumin is located.

Fig. 24 (2)

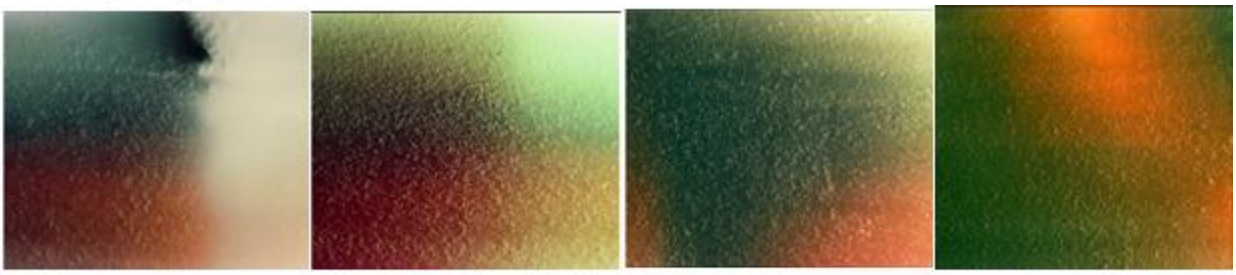

1 2 3 4

**Fig. 24 (3)**

Four photographs illustrating p-ray radiation taken at different temperature gradients are shown in Fig. 24 (3). The temperature gradient was created on two samples of aluminum alloy 7075-T651, having the shape of a right parallelepiped: 1) 2.54×3.05×6.10 $cm^3$, 2) 5.2×3.89×11.55 $cm^3$.

Samples heated to ~ 500°C were immersed with one facet on 5 mm in a wooden bath with water, the initial temperature of which was equal to 25°C. Temperature equalization started from the moment of contact with water.

Photos are shown in Fig. 24 (3), obtained with the initial gradient: 1-187, 2-156, 3-78, 4-41 degrees/cm.

It is known that the higher the temperature gradient, the higher the probability of formation of damage, including pores, cracks, and fractures due to the breaking of the bond between the atoms. The rupture of the bond between atoms occurs as a result of the absorption of photons, which is shown in the photographs by the dark region. The photo is shown in Fig. 24 (3) frame 1, obtained at the highest temperature gradient. It demonstrates the most dangerous defect.

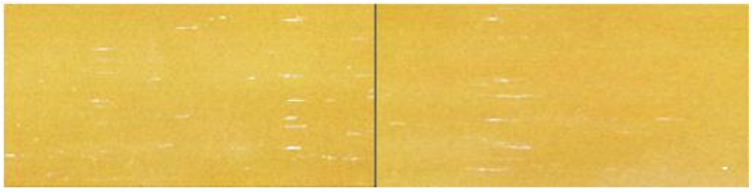

1 2

Fig. 24 (4)

Photos are shown in Fig. 24 (4), illustrate the defects found in cast iron bars during rapid cooling with water. Such defects are repeatedly recorded in a solid metal during mechanical deformation. (The color of the photos is changed to increase contrast.)

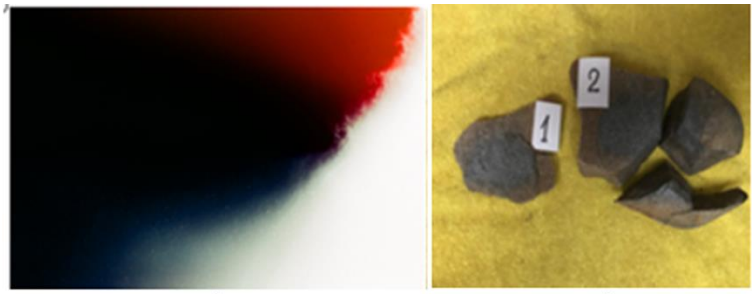


1 2

Fig. 24 (5)

A subtle crack formed in the cobblestone shown in Fig. 24, after heating to a temperature of ~ 500 ° C. The intensive cooling with water led to the separation of the stone into two fragments. Between these two fragments was a layer of unformed rock, which the crack divided into two parts, 1 and 2 (Fig. 24, frame 2).

The larger fragment collapsed into three parts after a week of exposure to sunlight, but even after this destruction continues. The formation of an uncured layer inside the stone facilitated the destruction process.

Photo Fig. 24, frame 1 is especially important for understanding the process of destruction. The red color is due to radiation from the hardened part of fragment 1; the black area is a crack; the blue area is an unhardened sand layer.

A dark area is similar to that captured in Fig. 24, frame 1, was observed in metal 16 times.

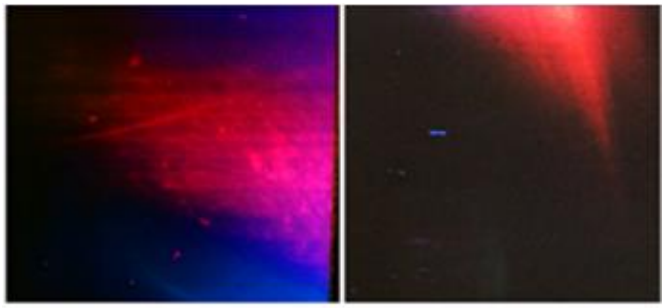

a b

**Fig. 25 (1)**

VI) Photos are shown on

Fig.25 (1), illustrate the p-ray radiation during solidification of the melt: a- silumin, b-aluminum alloy 7075-T651 in a wooden mold.

Three holes with a diameter of 13 mm, shown in Fig. 25 (2) (top view) were drilled in a sample of aluminum alloy 7075-T651 to a depth of 38.4 mm in such a way that 5 mm remained to the bottom face. The holes were filled with silumin melt and cooled with water. The process was recorded on two adjacent frames. The experiment was performed three times.

**Fig. 25 (2)**

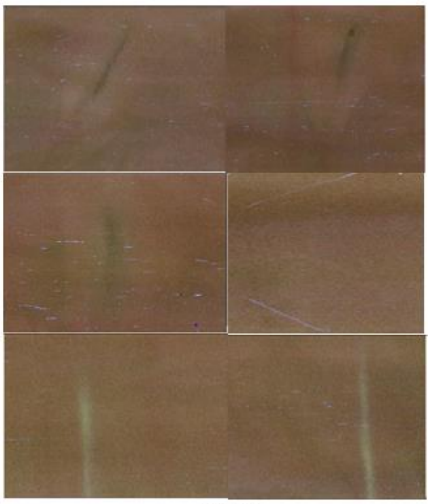

**Fig. 26**

Fig. 26 illustrates p-radiation detected during solidification. Note that the defects found in the experiment were repeatedly observed during other types of deformation.

Fig. 26 (1) illustrates the p- radiation when melting three different iron alloys: 1) a-d, 2) e-g, 3) h-i of unknown composition. The composition of the electrodes is not clear. The melting mode was not controlled**.** The pronounced white radiation recorded in the frame indicates the melting of at least three chemical elements. Monochromatic radiation recorded on the melting frames of the second alloy is characteristic of the melting of one element. A clearly defined dark area, shown on the frames h and i indicates the place where the pore was formed.

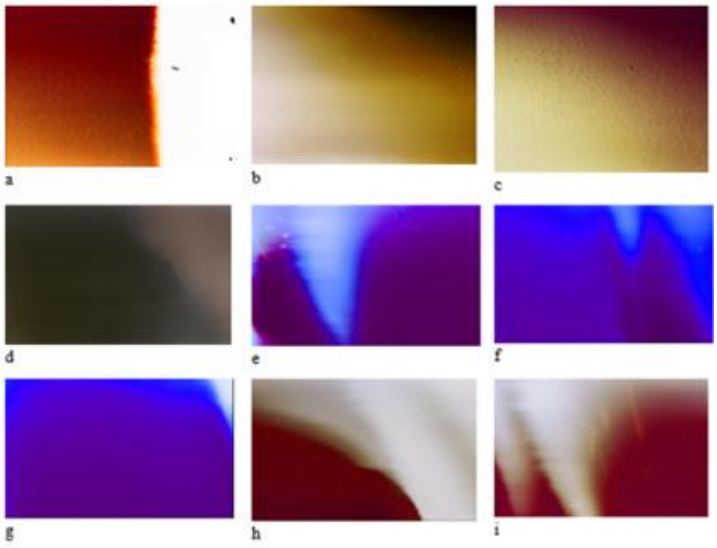


**Fig. 26 (1)**

### 1.1.14. Features of p-radiation during metal corrosion

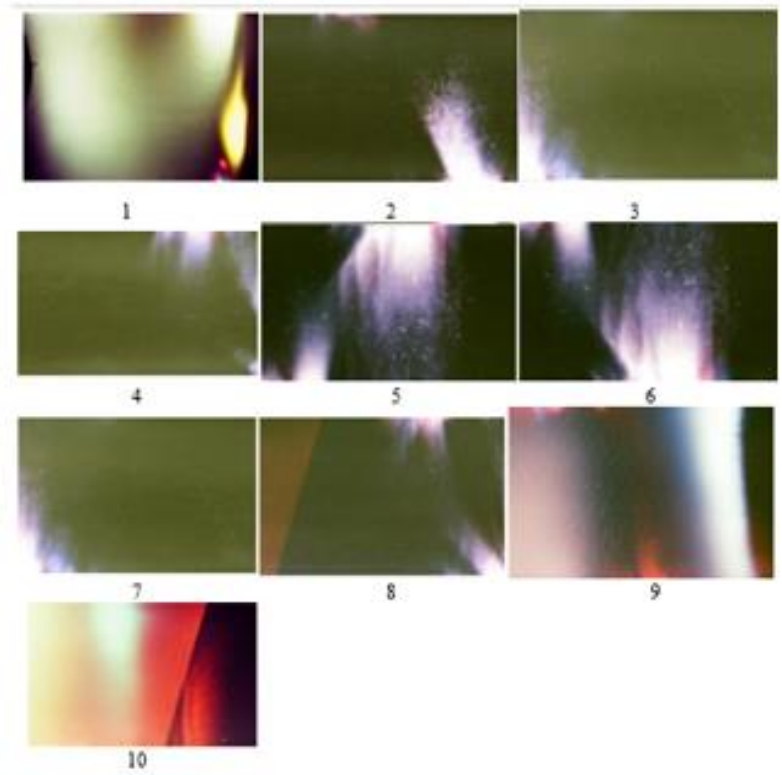


Fig. 27

A copper tube with a diameter of 25.4 mm was placed in a plastic cup with an aqueous solution of Clorox, under which there was a container with photographic film**.** Nine similar cups with a solution placed on this container were filled with thin plates of steel subjected to corrosion in varying degrees. The chemical reaction of samples 1-9 was 168 hours, including during solar irradiation. Sample 10 was not exposed to solar radiation. p-rays due to copper corrosion are illustrated in photo 1. Radiation due to steel corrosion is illustrated in photos 2-10.

### 1.1.15. P-rays due to chemical reaction

A chemical reaction is nothing more than an atomic reaction, which is caused by the exchange of atoms by photons and electrons. The emission of photons occurs as a result of the transition of an electron from a higher energy level to a lower or recombination of a positive ion with an electron. The photon energy is determined by the equation $h\nu = E_1\text{-}E_2$, where $E_1$ is the energy of the upper level, $E_2$ is the energy of the lower level. This equation is theoretical, referring to an ideal wave having one strictly specified frequency. In fact, atoms emit energy in a certain frequency range, due to the fact that energy levels form a zone whose width depends on the influence of one atom on another. The farther an electron is removed from the nucleus, the greater the influence of other atoms in the condensed matter on it, the wider the zone.

X-rays are caused by the transition of electrons to deeper energy levels, the influence of other atoms on which is significantly less than on the transitions of electrons at more distant levels, called valence ones.

An electron removed from a deep level forms, conditionally, a “hole” that fills the electron from the nearest level, causing the emission of a photon, whose frequency is less than the frequency of the absorbed photon. A new "hole" will fill the electron from a higher level. Thus, the removal of an electron from a deeper level can lead to the emission of photons with lower energy.

An analysis of the photographs above shows that with one test, both color and white emitting areas appear. The glow in such a wide area indicates that the primary Y-radiation excites atoms of various chemical elements. P-ray fluorescence analysis makes it possible to establish the qualitative composition of the areas from which the radiation originated since it does not matter for excitation whether p-rays are emitted from a p-ray tube or from material atoms.

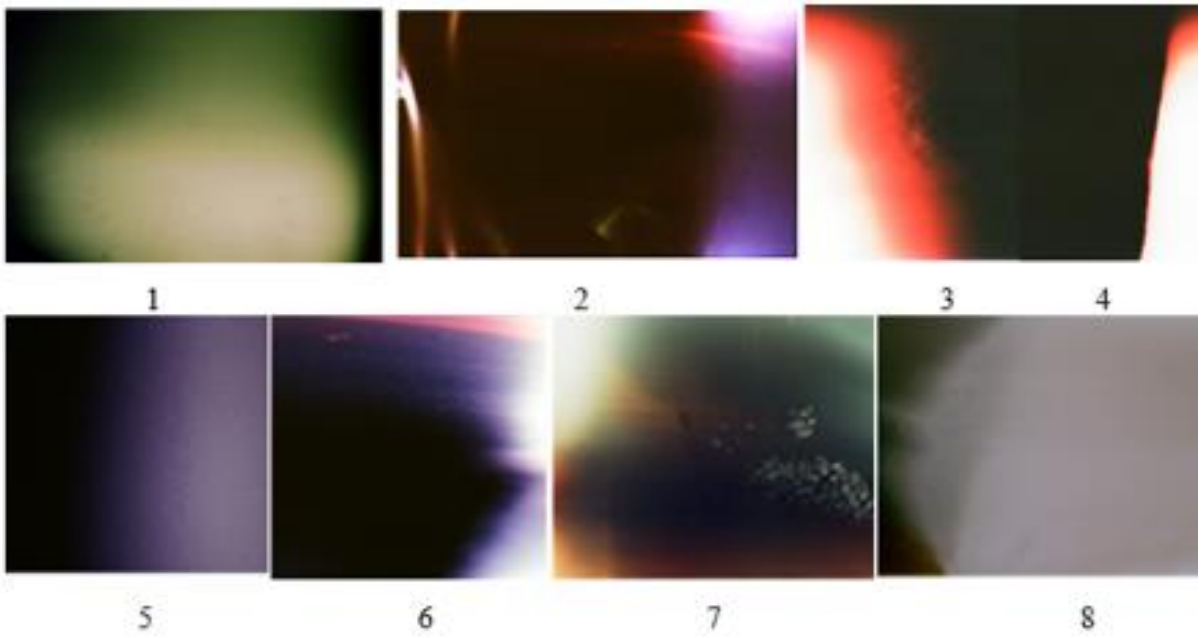


**Fig. 28**

The beaker was filled with baking soda and placed on a container with photographic film. Filling the beaker with vinegar caused a chemical reaction with the release of $CO_2$. Fig. 28. Frame 1 illustrates the p-rays emitted by this reaction; frame 2 illustrates p- radiation caused by a chemical reaction from a two sides of thin steel plate placed between the plates of a separator in a lithium battery; frame 3 illustrates p-rays emitted by dissolving powdered sugar in water; frame 4 - dissolving NaCl in water. Unfortunately, both photos were on the border of the frame. Frames 5-8

illustrate the p- radiation between the cathode (left) and the anode of the lead battery at a current of 1 ampere for 24 hours. The film was placed under the battery.

### 1.2. Maxwell's idea and experimental verification of it

D. K. Maxwell, analyzing the work of P. J. Plateau [1.22] on soap bubbles, expresses the idea of the existence of a specific region between liquid and vapor. Here it is best of all to quote from this article:

"Now we find by experiment that there is no difference between the phenomena on the part of the liquid and those in another part except in a region close to the surface and no more than a thousandth or perhaps a *millionth of a millimetre thick.* In the vapour also, everything is the same, except perhaps in a very thin stratum close to the surface. The change in the value of the energy takes place in the very narrow region between water and vapour... Hence the whole energy of the system may be divided into three parts, one proportional to the mass of liquid, one to the mass of vapour, and the third proportional to the area of the surface, which separates the liquid from the vapour ... M. van der Waals, whose academic thesis is a most valuable contribution to molecular physics, has attempted to calculate approximately the thickness of the stratum within which this continuous change of energy is accomplished, and finds it for water about 0.0000003 *millimetre*". (Italic emphasis by me).

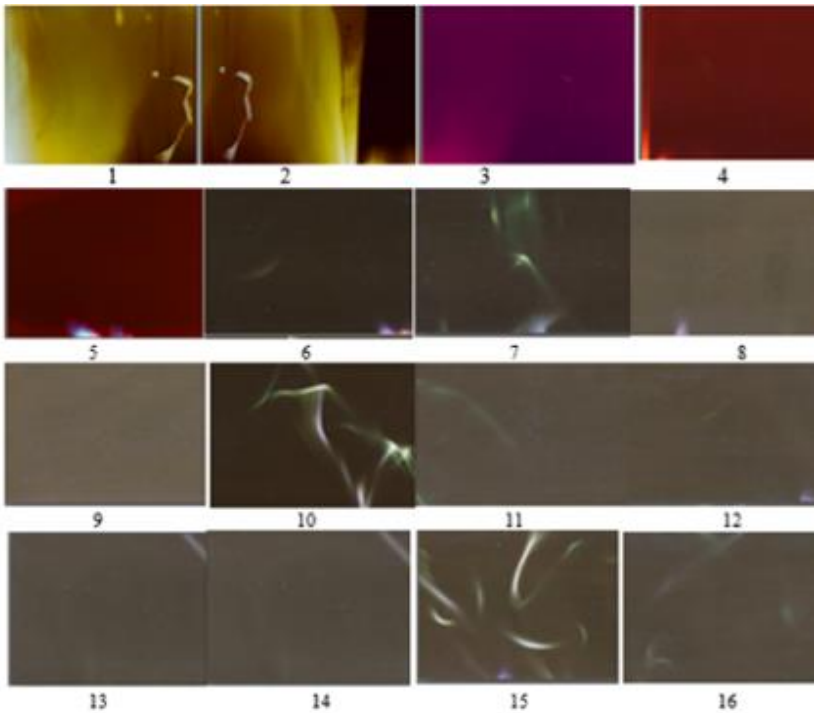


**Fig 29 (1)**

Thus, we see that Maxwell, 86 years before Feynman, drew attention to that area, which today is called nanoscale.

The role of water in human life is so great that any new information about its properties takes on special significance. The discovery of fullerene, graphene, carbon nanotubes played an important

role in modern natural science, but the region between vapor and liquid, noted by Maxwell, remained unexplored.

I) An experiment designed to test this Maxwell output was performed as follows.

A tube with a diameter of 1 cm was placed inside another plastic pipe with a diameter of 5 cm so that the axes of the pipes coincided. The space between the tubes was filled with water, which was frozen to -12 ° C. The film in a container that is opaque to visible and ultraviolet rays were wound spirally over the outer surface over a length of 18 cm.

The experiment was carried out in two stages: the first phase, the inner tube was filled with water, through which steam was passed; the second phase, the water was removed, but the steam supply intensity increased to increase the melting rate of ice

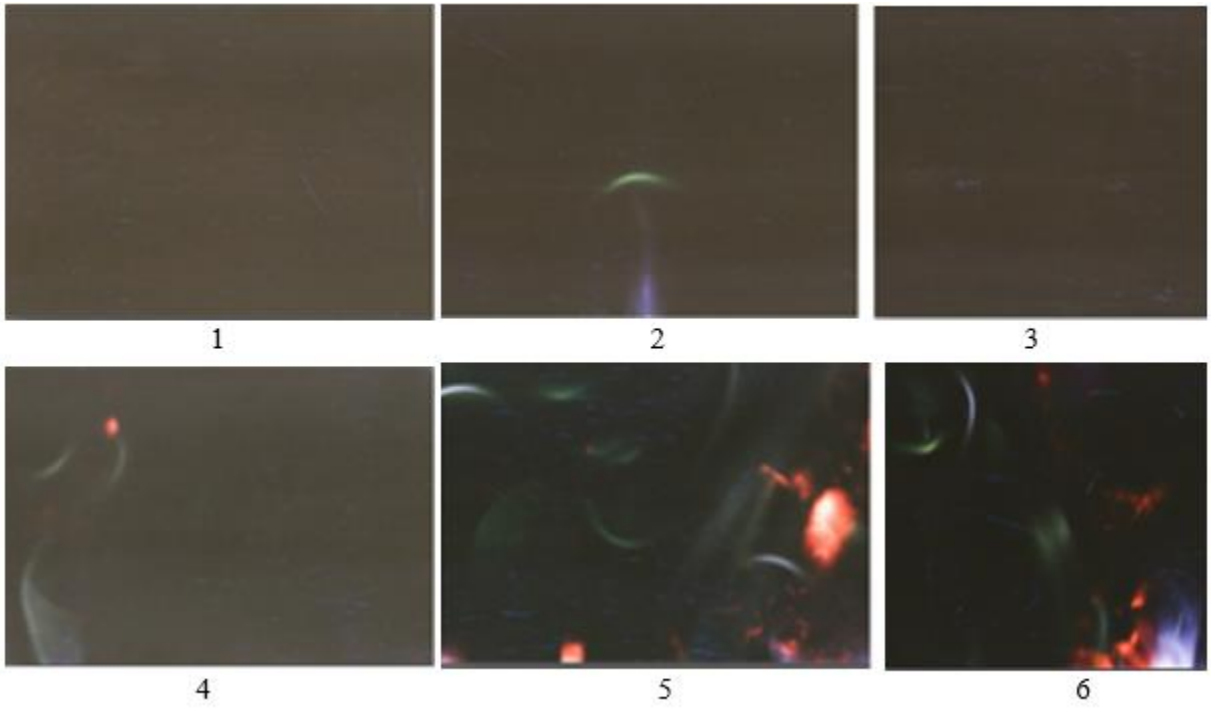


**Fig. 29 (2)**

Each stage was recorded on a separate part of the film.

Fig. 29 (1) illustrates the p-rays caused by the interaction of steam and water. This interaction occurs on the border of the bubble, captured at 16 frames. Fig. 29 (2) illustrates the p-rays caused by the interaction of water and ice. A characteristic feature of the radiation of water on the metal surface is shown in Fig. 29 (1) in the form of fan-shaped radiation, which is recorded only on the edge of the film: frames 2, 4 5-8, 12, 15; 29 (2), frames 2, 6. The arc-shaped figures shown in Fig. 29 (1), frames 10 and 15; 29 (2) frames 2, 4, 5 6, are observed many times during the deformation of various materials.

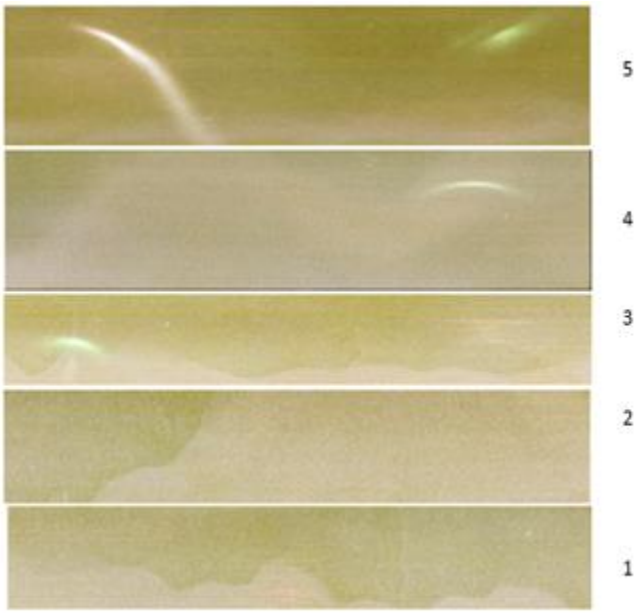


**Fig. 30**

II) A container with the photographic film was placed on the outer surface of a glass cylinder with water at the bottom, below which the heater was located.

Fig. 30 illustrates the p-radiation caused by the formation of bubbles in water, which is captured at an exposure time of 15 minutes boiling. Frames are located at different distances from the bottom, which was not recorded.

### 1.3. Destruction of the stone, the ocean floor, and the Earth's surface

Investigation of the causes and mechanisms of solid body destruction in nature is the subject of physical geology. However, the study of sparks, the use of wood as a mold, and the study of the process of breaking stone to understand the mechanism of cracking in metals are due to two factors. First, these phenomena occur in accordance with the laws of nature, which can be disclosed, and secondly, it excludes the influence of the human factor.

The spark caused by the impact of metal on the stone was used by a man thousands of years ago. However, electromagnetic radiation in the p-ray range has been investigated for the first time. Wet wood was used to cool the melt on the basis of those amazing properties that manifest themselves in the synthesis of plants due to the interaction of photons and excitons. The turn of the flower to the sun is caused by the transformation of photon energy into mechanical energy. There is no doubt that the rise of water from the root of the pine to a height of 40-50 meters is due to the additional energy that is transferred to the molecules of water from the sun by means of photons.

Alloys of metals, composite materials consist of various chemical elements that form compounds. The formation of such compounds is accompanied by the release of energy. For example, the enthalpy of formation one molecule of titanium nitride is 3.49 eV, of aluminum dioxide, which is 17.36 eV. The mechanical and thermodynamic properties of these compounds differ from the properties of titanium and aluminum, respectively. The formation of such compounds in the main

matrix is accompanied by the formation of a boundary whose structure changes as a result of heat absorption. The generation of cracks often occurs at the boundary of the inhomogeneity, as shown in Fig.31.

A photograph of a crack formed at the feldspar and quartz boundary, obtained with a scanning electron microscope [1.23], is shown in Fig. 31.

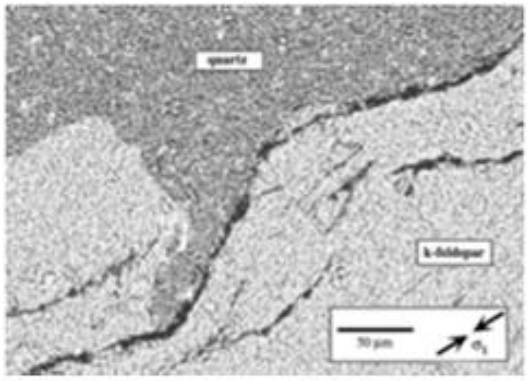

**Fig. 31**

Similar photos, as noted above, were observed in the metal, but they differ in that they demonstrate a defect that was formed not only on the surface but also inside the sample. The experiments described above showed that Y-ray photons are emitted from atoms, regardless of their location in the solid.

Multi-kilometer cracks growing towards each other were repeatedly observed in nature. It has been established that the ridges on the ocean floor move towards each other, forming cracks.

The simulation of these processes on a scale of 1: 2,000,000 was performed in [1.24]. The formation of cracks was carried out under the action of centrifugal forces. The result of the experiment for two types of opposing cracks is shown in Fig. 32.

P-radiation caused by the formation of a 30 $cm^2$ crack is shown in Fig. 18. We can imagine the energy and power of the radiation that accompanies the motion of the ocean floor ridges.

*This means that the motion of the ocean ridges can be monitored with the help of sensors of Y-radiation and spacecraft.*

Simulation of mechanical processes occurring at the bottom of the ocean is justified by the fact that the reaction to the external action is due to the transition of electrons not in the valence band, but from the energy levels located below it. In this case, the photon energy does not depend on what other atoms surrounding the atom that emitted it.

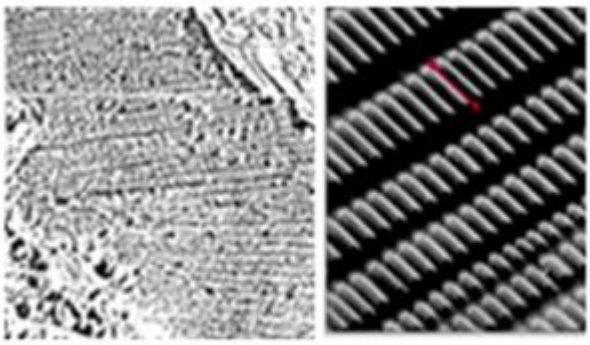

**Fig. 33 a** **Fig. 33 b**

Modeling of ocean-bottom deformation processes, Fig. 33 a, caused by the motion of the continent, was performed in [1.25]. Platinum film 4 nm thick was deposited on the surface of the polymer film. The stretching of the polymer film by 100%, as

indicated by the arrow, led to the rupture of the platinum film into fragments, as shown in Fig. 33 b, similar to the breaks on the ocean floor.

The rupture of the platinum film in a direction that is perpendicular to the applied force disproves the models adopted in fracture mechanics.

Earthquakes, landslides, tsunamis are the most dangerous natural phenomena that a person cannot prevent. The warning of danger remains the only possibility for salvation. Tsunami hazard assessment is carried out on the basis of seismic waves, the radiation of which is due to ground motion, the change in the intensity of the magnetic field and the electrical conductivity of the rocks. *The fact that any deformation is accompanied by P-radiation before the appearance of cracks allows us to use this fact for earlier forecasting of earthquakes and tsunamis by placing X-ray sensors, as is done for measuring other signals.*

Modeling of the earthquake prediction process is demonstrated by the example of the destruction of marble, granite, and flagstone.

**Fig. 34**

The sample of flagstone shown in Fig. 34, 52 mm thick, was deformed using a 25-ton press. Five fragments were obtained as a result of four experiments. All fragments have a clear cut, which indicates the crystalline state of the sample.

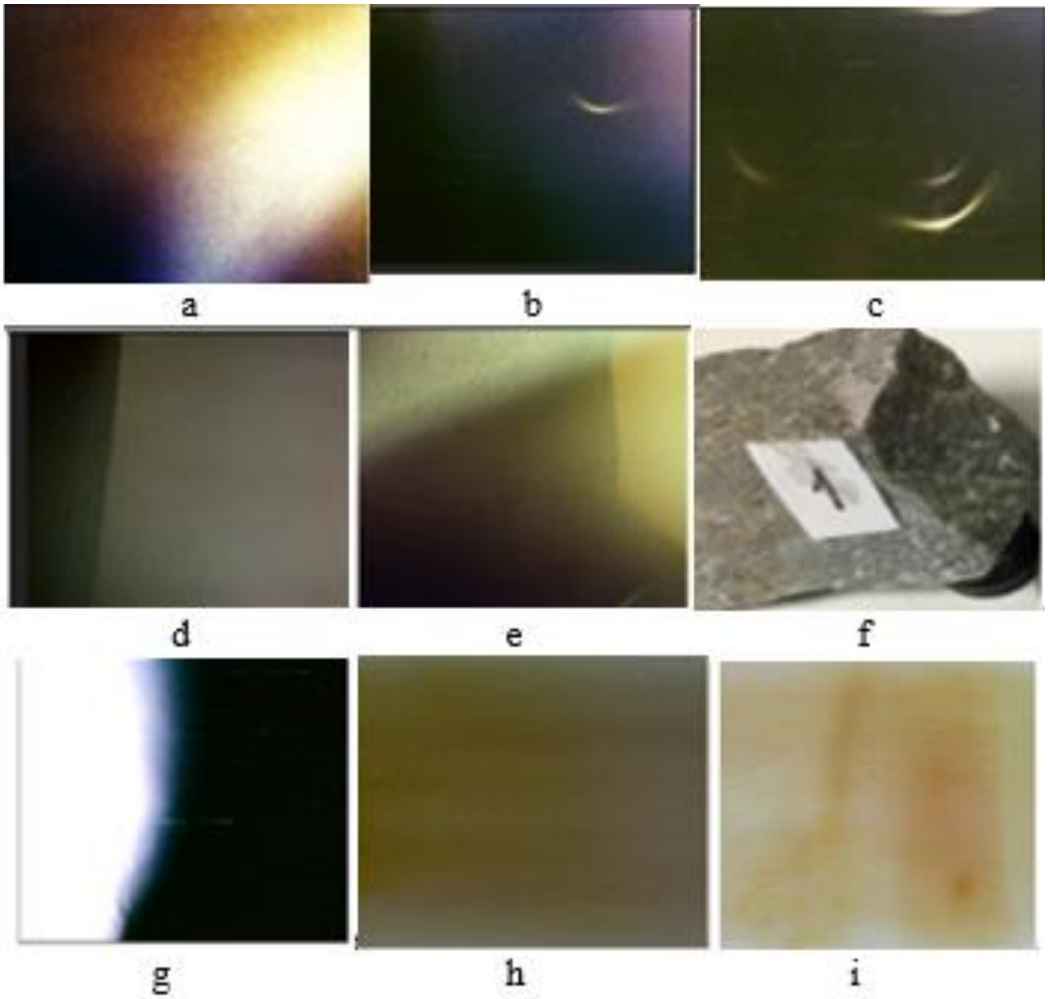


**Fig. 34 (1)**

All the experiments in this study are designed to demonstrate the possibility of using in the industry electromagnetic radiation accompanying deformation. Detailed analysis of the processes of stone destruction as a building material is the subject of a special study. We, in this regard, confine ourselves to a brief analysis of the most important aspects. The film recorded 12 frames of cracks forming in the flagstone, 9 of which are shown in Fig. 34 (1). Frame f illustrates the crack surface shown in frame e. The crack in the photographs is a dark area since, in it, the energy is absorbed by the atoms, between which the bond breaks. Such dark areas are captured earlier. These areas are captured in photographs a, b, d, e, g. Each of the photographs demonstrates the features of crack formation. The glow, as noted earlier, is captured both before the formation of the crack and after that, but we cannot differentiate this fact in the photographs a, b, e, g.

The photograph g is of particular interest due to the fact that it illustrates the foreign inclusion region shown in Fig. 34 (1) c, formed during crystal growth. The crack divided this area into two

parts. Fig. 34 (1) g shows that one of the parts, bordering on the crack, is shining. This luminescence is due to the delayed radiation from the atoms of the energy source.

Photo Fig. 34 (1) c demonstrates another foreign region, the brown color, which was fixed on the photocell in Fig. 34 (1) h and Fig. 34 (1) i, but visually became visible only after a week of storage in air. This transformation is typical for the corrosion of a metal.

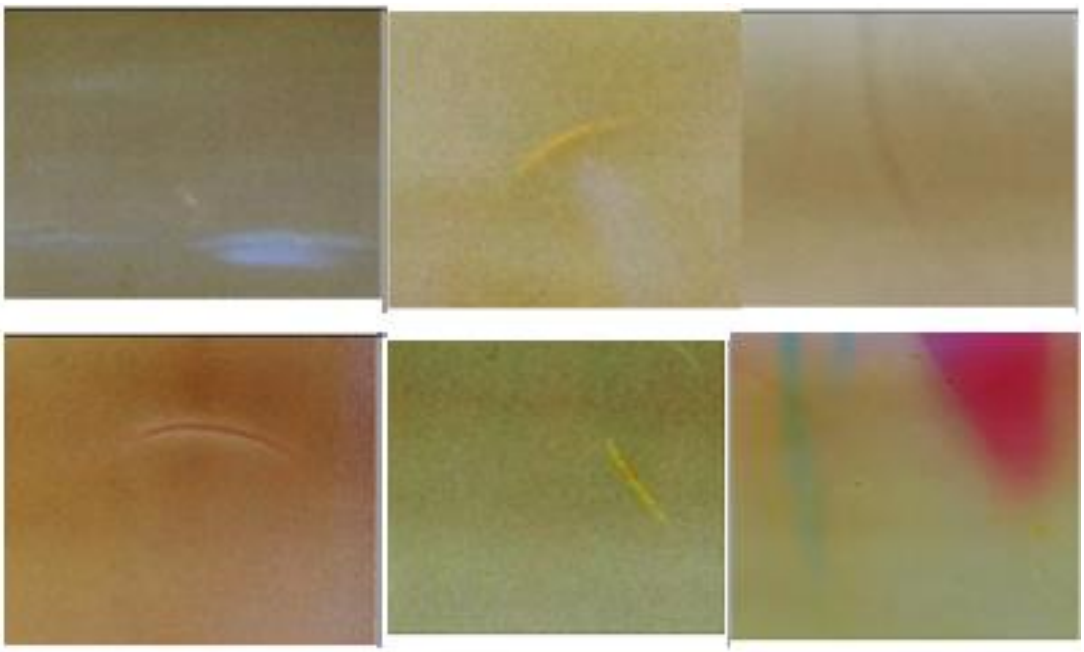

**Fig 34 (2)**

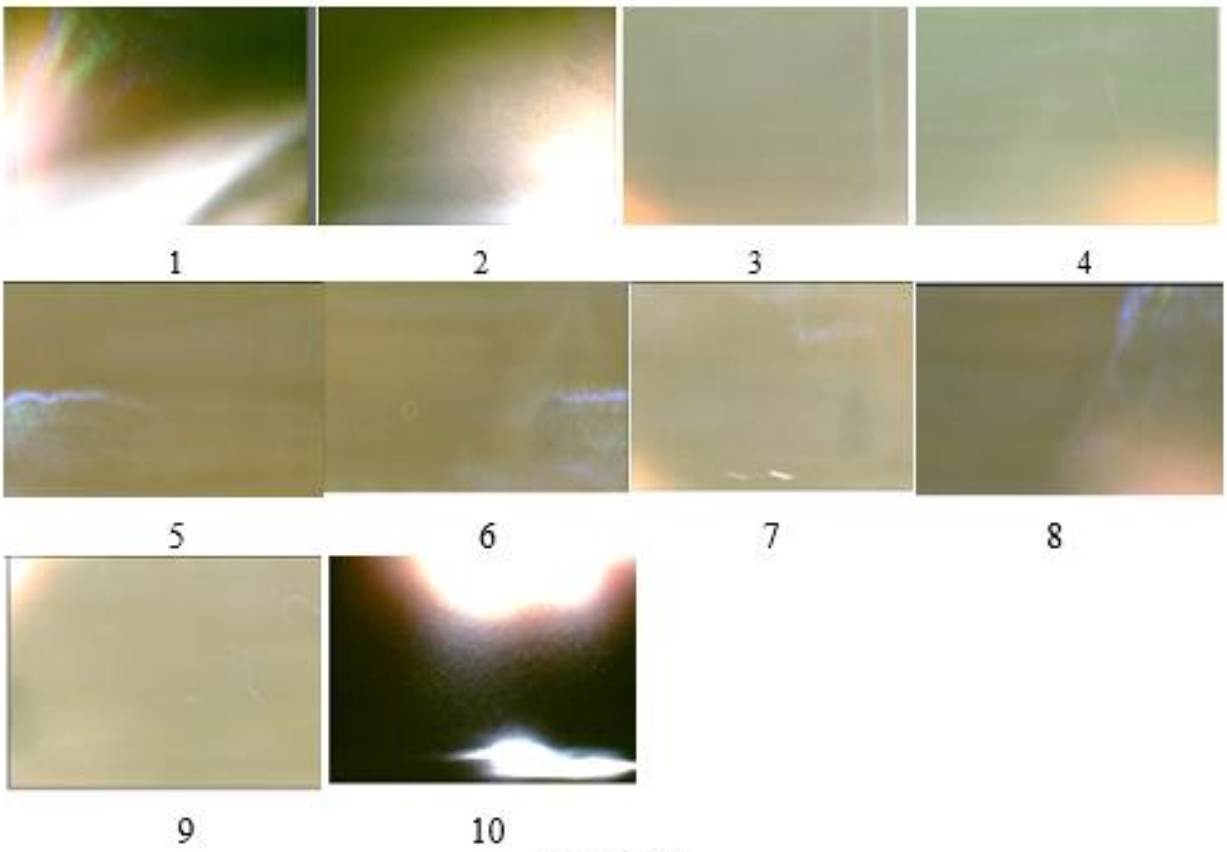


**Fig. 34 (3)**

Arc-shaped glowing defects, captured in Fig. 34 (1) b, c, and have been observed repeatedly and are shown in Fig. 25 (spiral), frames 5, 16, 18; Fig. 28 (3), frames 3.1, 3.13; Fig. 28 (4), frames 4.4 and 1.10.

The six photographs are shown in Fig. 34 (2), illustrate the defects that have arisen in the marble plate outside the cracks, but the photographic method does not allow determining when the radiation occurred before or after failure. The spectral composition of the defects is due to the atoms of the chemical elements that form it, but the clearly limited form remains unsolved.

The granite plate, 10 mm thick, and 300×300 $mm^2$ were destroyed at a higher strain rate than a marble plate of the same size. The direction of cracks in marble and granite without prior attenuation is unpredictable, like the formation of cracks in the glass.

The area of the film is no more than 12% of the sample area. This led to the fact that a crack over the surface of the film was formed only in one case, which is captured on the frame 10, as shown in Fig. 34 (3).

The second sample of the flagstone of the same thickness and area as the first collapsed at a higher loading speed.

14 15 16 17

**Fig. 34 (4)**

The crystal structure of the second sample of the flagstone was different from the structure of the first one in that the faces had the shape of a rectangle, as in the first, the shape of a parallelepiped with dihedral angles of 80 ° and 100°. Cracks in the second sample of the flagstone were recorded on nine frames out of ten, shown in Fig. 34 (4) and Fig. 34 (5). The change in the shape of the crack from frame 15 to frame 23 is due to the impulsive character of its formation. Frames 19-22 indicate the formation of a clearly defined crack boundary.

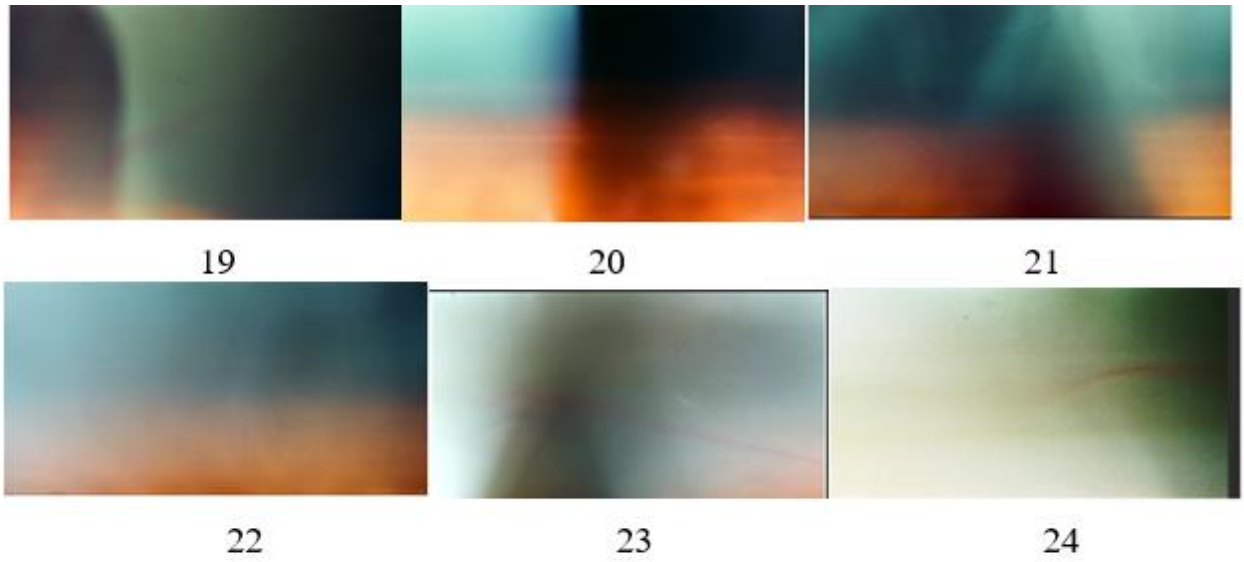

19 20 21

22 23 24

**Fig. 34 (5)**

The projection of a luminous defect in the form of a pink string is observed on frames 18, 19, 23, 24. The length of this projection on the *xy* plane is ~ 140 mm.

It is known that on the surface of the crack, there are hills and valleys, strata. The above pictures show how the surface of cracks forms.

*Thus, it has been experimentally confirmed that the processes of p-ray sources formation in materials forming mountains are not different from processes in other solids. Continuous monitoring of electromagnetic, including p-radiation from seismically dangerous areas of the*

*earth's surface and the ocean floor, makes it possible to diagnose earthquakes at an early stage and to warn about the possibility of a tsunami.*

### 1.4. P-ray-luminescence of metals

Photons emitted during the destruction of a solid are intensely absorbed by metals, causing luminescence, including in the Y-ray range. The excitation of atoms was carried out by photons emitted by the particles formed upon the destruction of alloys and glass, as shown in Fig. 7 b, c, d, e, and Fig. 35. Alloys of lead and tin, aluminum, iron, copper, were used as screens.

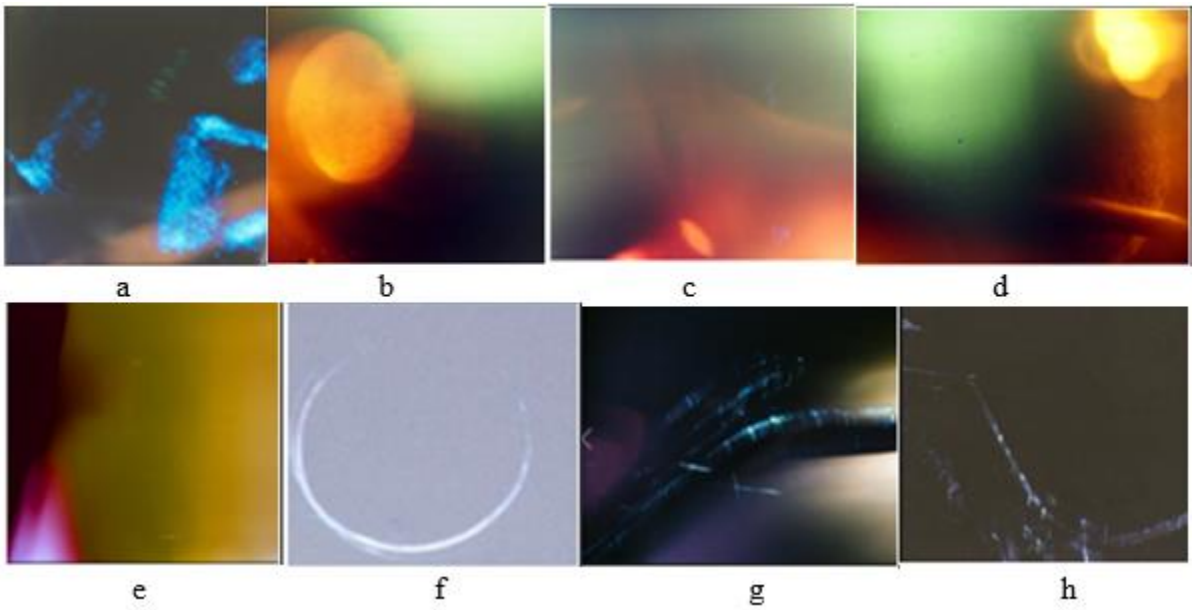


**Fig. 35**

Photos are shown in Fig. 35, obtained under the following conditions:

a) aluminum foil in one, four and eight layers, located on the surface of the container, was irradiated with Y-rays emitted from iron alloy particles; b) a steel washer located on the surface of the container was irradiated with Y-rays emitted from copper alloy particles; c) the same washer was irradiated at twice the exposure and d) in tripled exposure to fix the position of the Pb-Sn alloy wire located inside the container (g-photograph of the same wire upon irradiation from steel particles, h-from glass particles); e-aluminum foil, located on the surface of the container (shown at the bottom left), was irradiated with p-rays emitted from copper particles formed after destruction; f - steel lock washer was irradiated with radiation from particles of steel.

The use of screens has made it possible to estimate the energy of p-ray photons by transmission, which is at least 50 keV.

The absorption of photons causes luminescence of metals, including p-ray luminescence, a spectrum that depends on both the frequency of the radiation source and the absorber. The photographs have shown that the number of radiation source-absorber combinations is unlimited.

A wide spectrum of radiation and luminescence, to some extent associated with destruction, predetermines the possibility of predicting changes in the wear and tear of a solid during its operation, if its mechanism is understood.

### 1.5. Control experiments

Investigation of the spectrum of electromagnetic radiation of atoms is the only possibility for an objective assessment of their energy state and its change in the process of manufacturing the element of the structure or device and its operation.

The use of electromagnetic radiation to detect defects occurring during the manufacturing process is demonstrated by the example of drilling holes and installing rivets.

### 1.5.1. Weld quality control

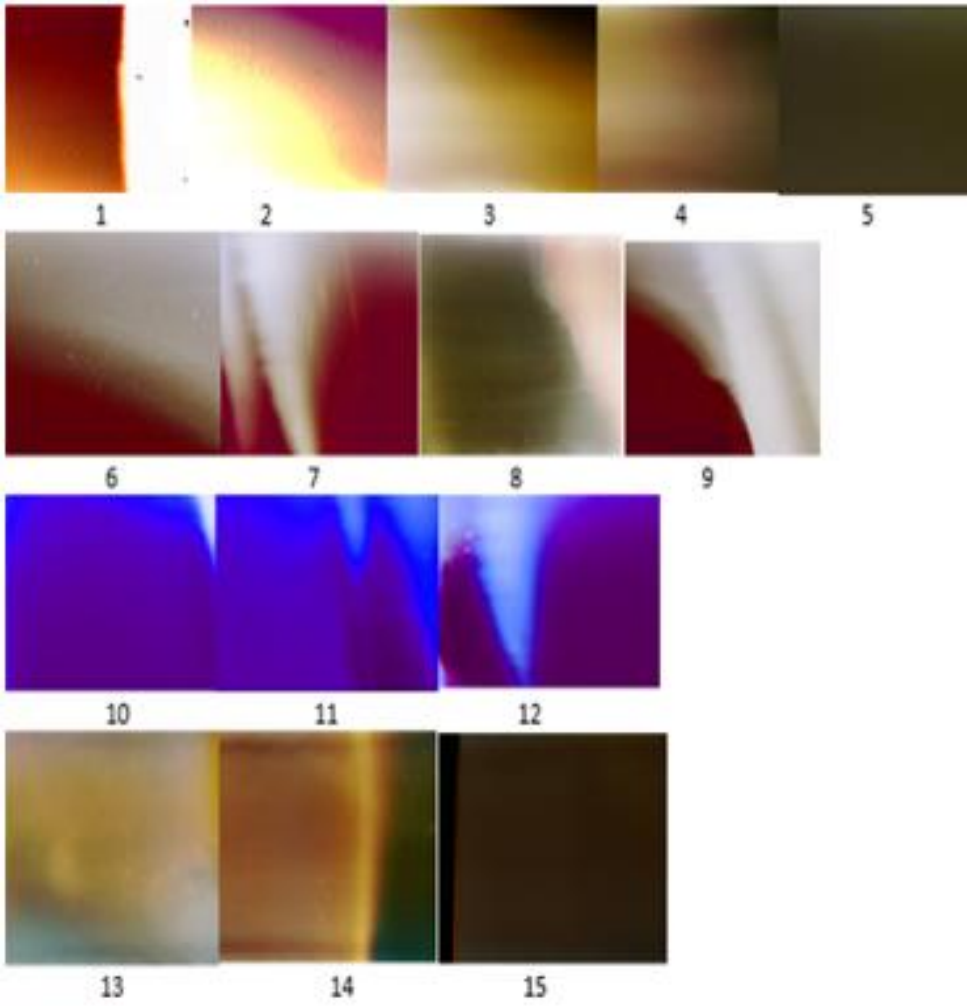


**Fig. 36**

Fig. 36 illustrates p-radiation during the melting of four different iron alloys: 1) 1-5, 2) 6-9, 3) 10-12, 4) 13-15 of unknown composition. The composition of the electrodes was not established. The melting mode was not controlled. The structure of defects and their danger is determined on the basis of special laboratory studies that were not carried out in this work.

The research results allow only preliminary conclusions to be made. The pronounced white radiation recorded on frame 1 indicates the melting of at least three chemical elements.

### 1.5.2. Rivet quality control

An experimental study of the control of the creation of a riveted overlap joint was carried out on two plates of an aluminum alloy, 1.1 mm thick each, tightly pressed together to each other by clamps. Drilling was carried out with a drill with a diameter of 4 mm at a speed of 0.2 m/s on the testing machine. On the surface of the container was placed a plastic plate 2 mm thick, protecting the container from damage.

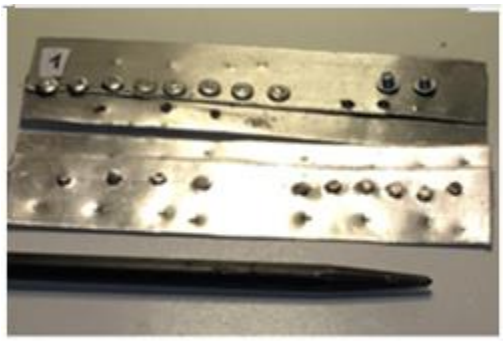

**Fig. 37**

Twenty holes were made, as it is shown in Fig. 37.

p-ray radiation was recorded using FUJIFILM SUPERIA X-TRA 800 film at 14 frames, 9 of which are shown in Fig. 38 (1). We cannot assess the danger posed by the defects found during the drilling of holes, which are shown in Fig. 38 (1). But the fact that they are all directed from one rivet hole to another is alarming since it has been experimentally established that in a riveted joint, there are defects called hidden cracks, the number of which exceeds 80%. Indeed, these defects, which are detected by p-ray radiation, constitute 70% of all the holes. They manifest themselves not only during drilling but also during riveting, as seen in frame 18 (Fig. 38).

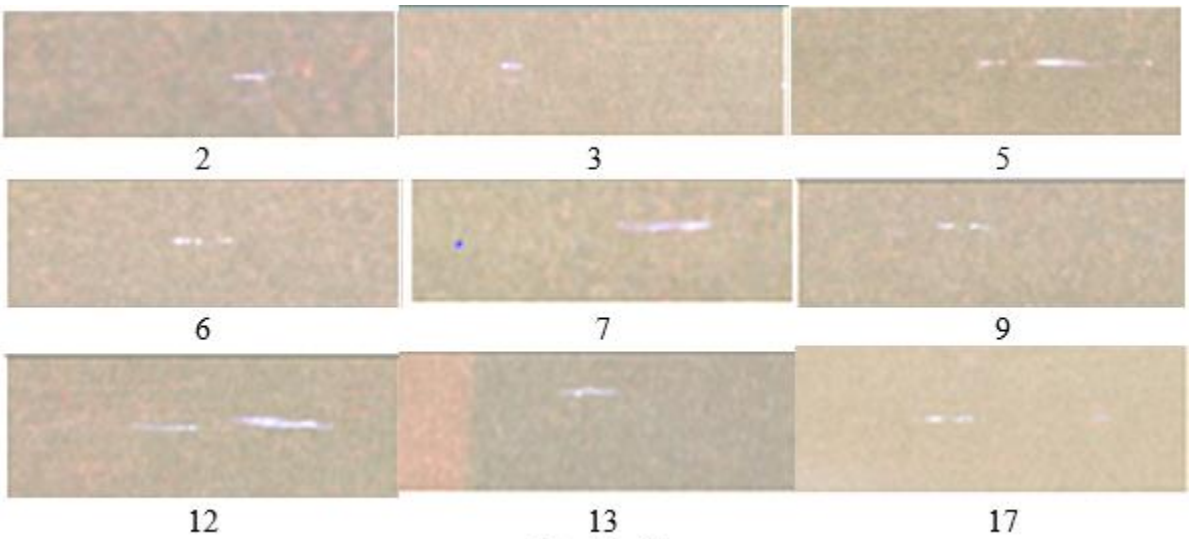


**Fig. 38 (1)**

The nature of the radiation while drilling the holes in metal is significantly different from that observed during glass (Fig. 5a, 5b) and concrete (Fig. 6a) drilling.

The position of the holes is shown in Fig. 31. One of the holes (Fig. 31, 1) was drilled in such a way that one edge of the plates will be damaged during the rivet installation.

The plates were joined by hollow aluminum rivets with an aluminum core with a diameter of 3.5 mm; the length of the rivet is 4 mm. The container with the film was located on a flat steel anvil. A plate made of glass, 5 mm thick, was fastened with clamps to the surface of the container. The deformation of the rivets was carried out using a pointed punch (Fig. 31) to increase the number of damages.

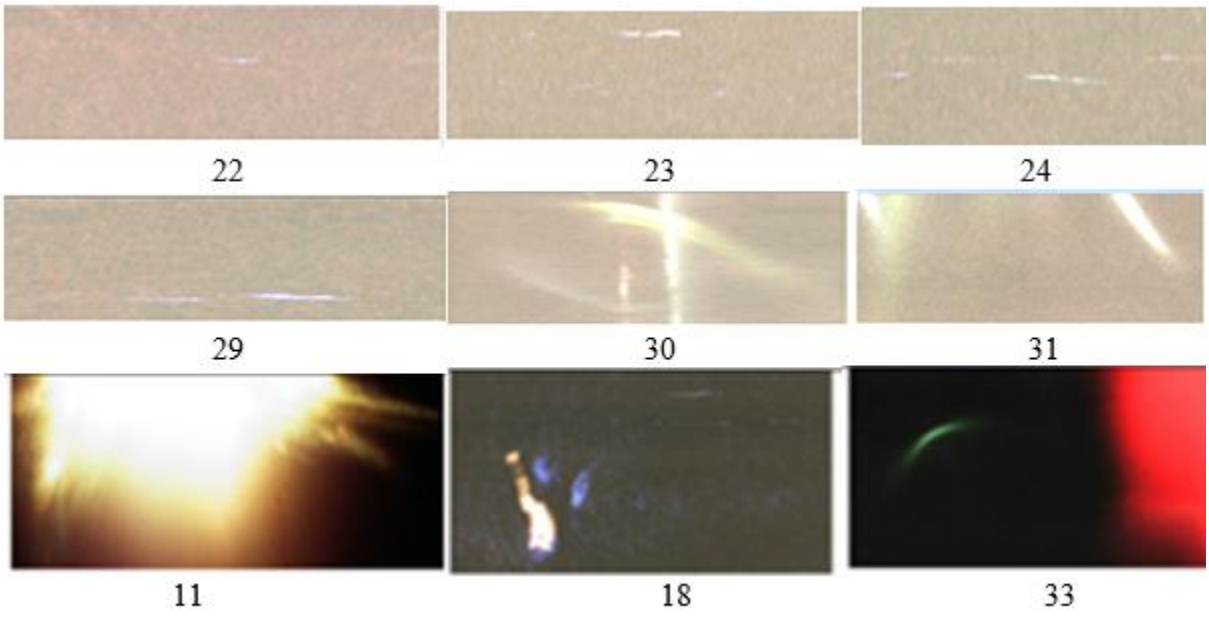


**Fig. 38 (2)**

The results of the study are shown in Fig. 32.

Let's pay attention to frames 18 and 19, which are identical to the photos shown in Fig. 3c, Fig. 4c, Fig. 4 e, obtained at the break. A bright defect captured on frame 18 is caused, most likely, by damage to the glass on which the riveting was performed.

The intense radiation of the glass upon its damage is observed on frames 30, 31, and 33.

Defects are shown in Fig. 34 were formed during the installation of rivets. Similar defects were observed in all impact interactions.

Control of self-emission transparency of the ground

The self-emission transparency of wood (Fig. 17) and railway sleepers (40 6) allows us to conclude that such a phenomenon should be observed in the ground. Experimental verification of this hypothesis was carried out near the railroad track, on which the train passed.

### 1.5.3. Experimental verification of the possibility of using self-emission transparency

The self-emission transparency of wood (Fig. 17) and railway sleepers (40 6) allows us to conclude that such a phenomenon should be observed in the ground. Experimental verification of this hypothesis was performed near the railway track.

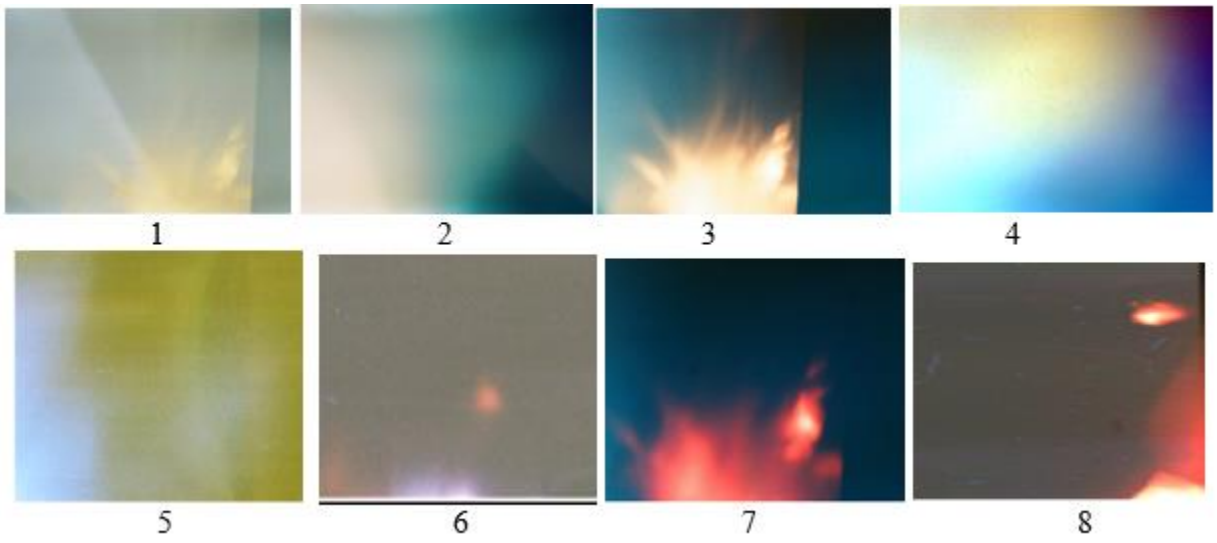


**Fig. 39 (1)**

Fig. 39 (1) illustrates the p-rays captured on a photographic film located on one of the large stones that strengthen the embankment of the railway track located three meters from the rails. The freight train of two locomotives and 113 platforms passed completely past the container. Frames 1 and 3 illustrate luminous areas similar in shape to those observed in the photographs of series 40, test 1, frames 9-11. Frame 6 illustrates the radiation characteristic of water; frames 7 and 8 illustrate the radiation characteristic of fastening rails and sleepers, similar to what is observed in photographs of series No. 40, test 6, frames 16 and 17. Such coincidences cannot be accidental.

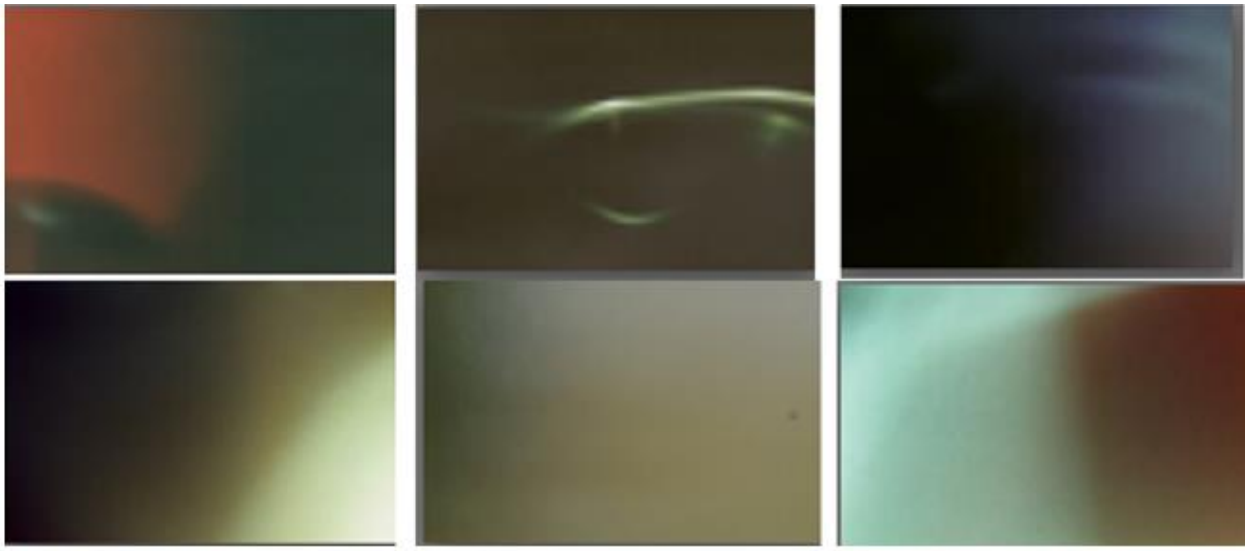

**Fig. 39 (2)**

The six photographs are shown in Fig. 39 (2), illustrate the p-radiation caused by a passing train and recorded on a film located in soft soil at a depth of 2.5 cm at a distance of three meters from the rails**.**

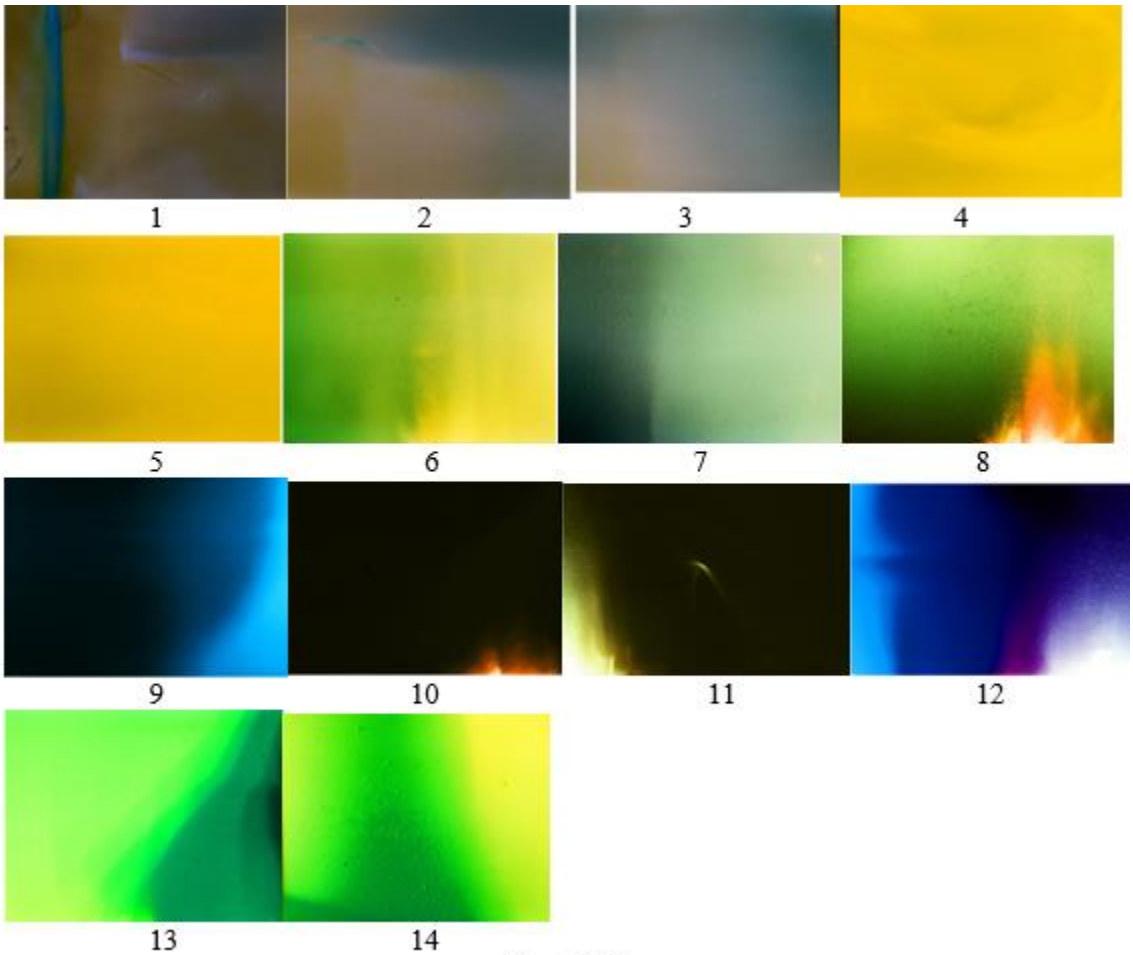


**Fig. 39 (3)**

The 14 frames shown in Fig. 39 (3) are recorded on the film located in the same place as the film Fig. 39 (1), but it recorded a p-radiation caused by the movement of the train at a distance of more than a mile from the film. Frames 6, 8-11 illustrate areas in which radiation is similar to areas previously observed. Frames 13 and 14 illustrate some defects, like cracks.

Photos are shown in Fig. 19, 20, 29 (1), 29 (2), 30, and where water is present, it can be concluded that water is also the medium in which self-emission transparency takes place. An experiment, the result of which is shown in Fig. 39 (4), confirmed this assumption.

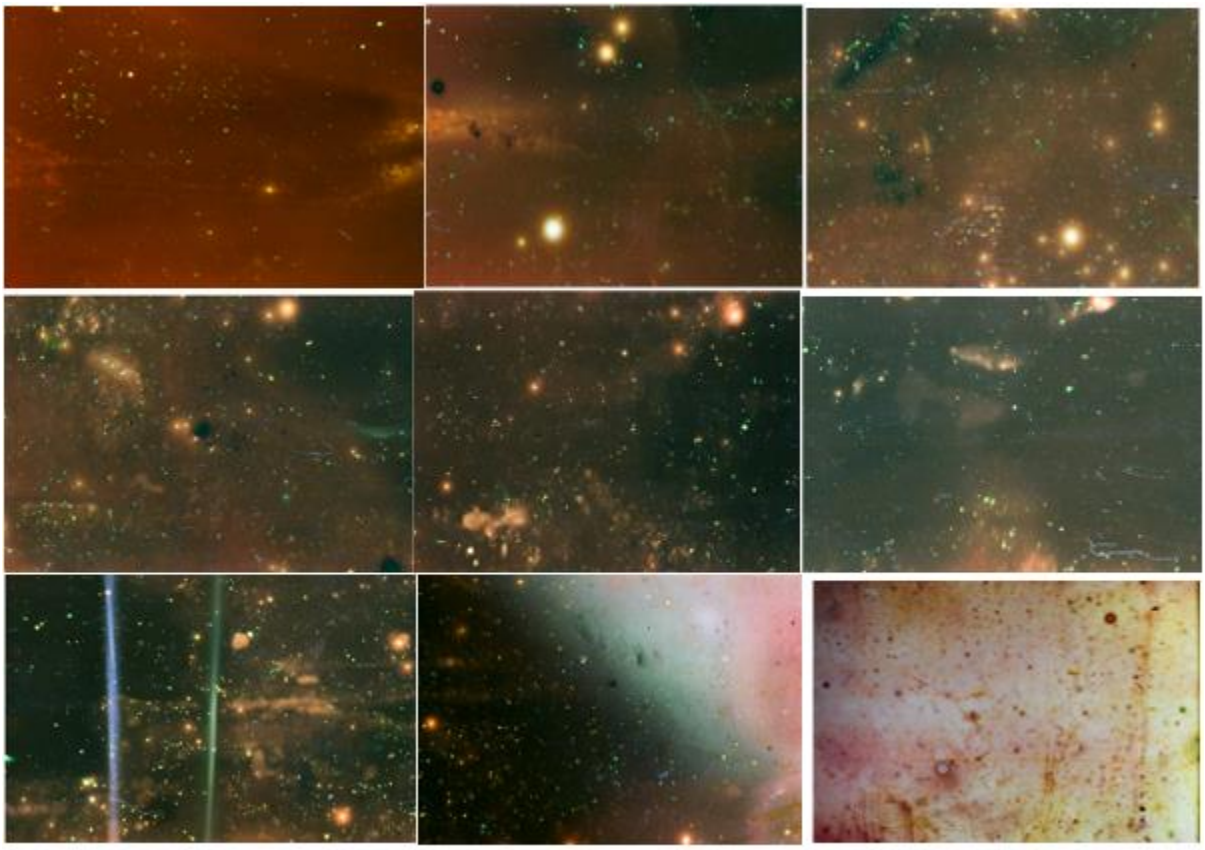

**Fig. 39 (4)**

Photographic film floated on the surface of the bay, a hundred meters from the ferry, which moored at the pier. The container was waterproof and opaque to visible and ultraviolet rays. The depth of the bay was 30-40 cm. The nine frames are shown in Fig. 39 (4), illustrate the p-radiation, but the photographs do not allow an unambiguous answer, which determines the observed picture, which differs from that shown in Fig. 19 and Fig. 20.

### 1.5.4. Demonstration of the use of self-emission transparency for monitoring rail track damage

Experimental series No. 43 contains eight tests, the results of which are illustrated by 84 photographs. A control experiment was performed at the Northwest Railway Museum, Snoqualmie, WA, the USA, on a railroad using a locomotive.

The location of the films for the study of p-radiation caused by the movement of the locomotive is shown in this photo.

Four studies were performed when removing the locomotive from 20′ (6 m), 412′ (150 m), 1320′ (403 m), and braking before 2623′ (800 m).

The plan for the experiment.

1. The first experiment (test 7 and 8). Film containers are located on the head and foot of the rail. The locomotive, located on the right at a distance of 6 m, begins to move to the right. After 20 seconds, the films are removed.

2. The locomotive is approaching the 150 m mark. Films No. 1 and No. 4 take the place of films No. 7 and No. 8 and are removed after 20 seconds.

3. The locomotive approaches 400 m. Films No. 5 and No. 6 take the place of films No. 1 and No. 4 and are removed after 20 seconds.

4. The signal for the start of emergency braking is given by the driver in the interval of 400-800 m so that films No. 2 and No. 3 are placed on the rail. The experiment is over.

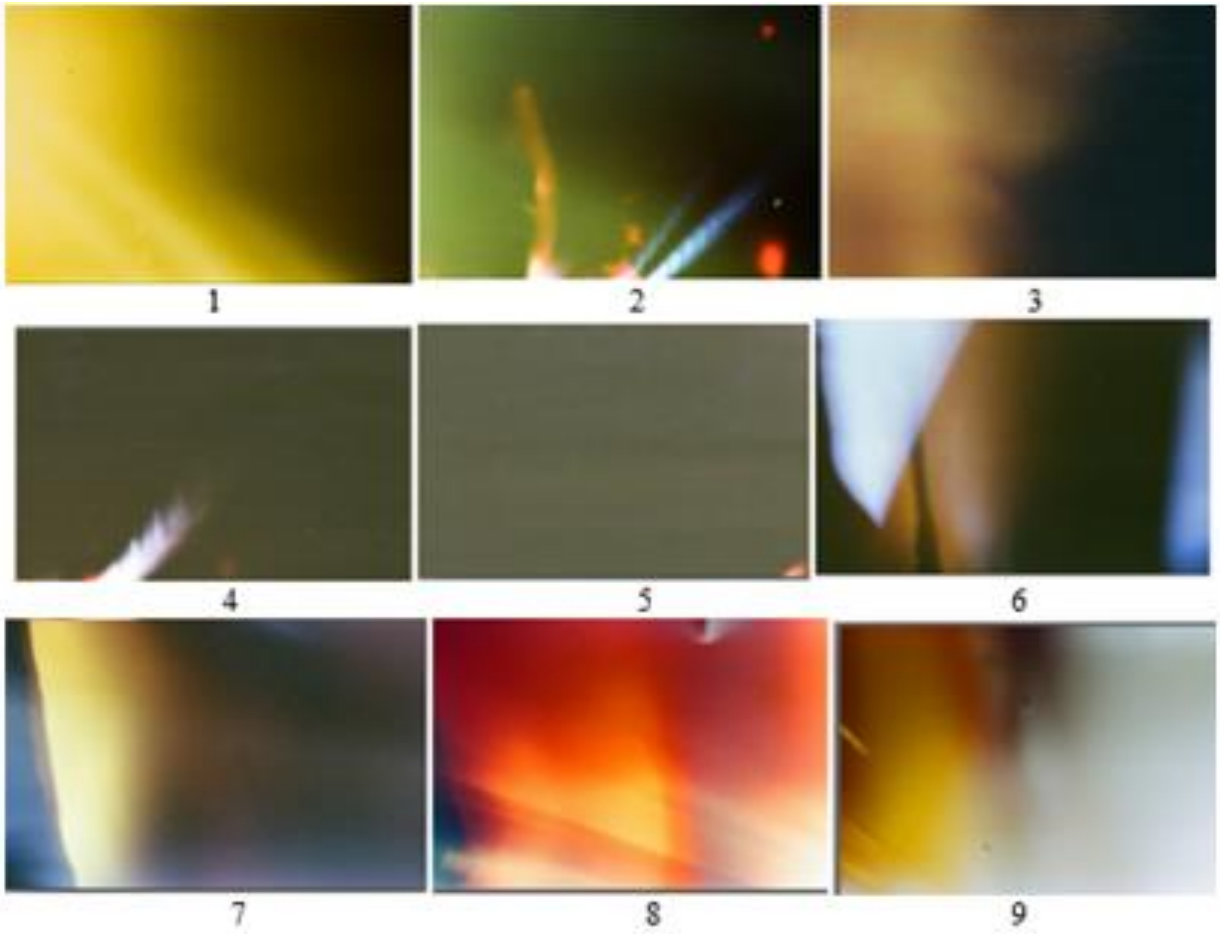


Experimental series No. 43, test 7. Control experiment performed on Northwest Railway Museum, Snoqualmie, WA on railway using a locomotive. Photos obtained at a distance of 20′ (6 m) from the locomotive.

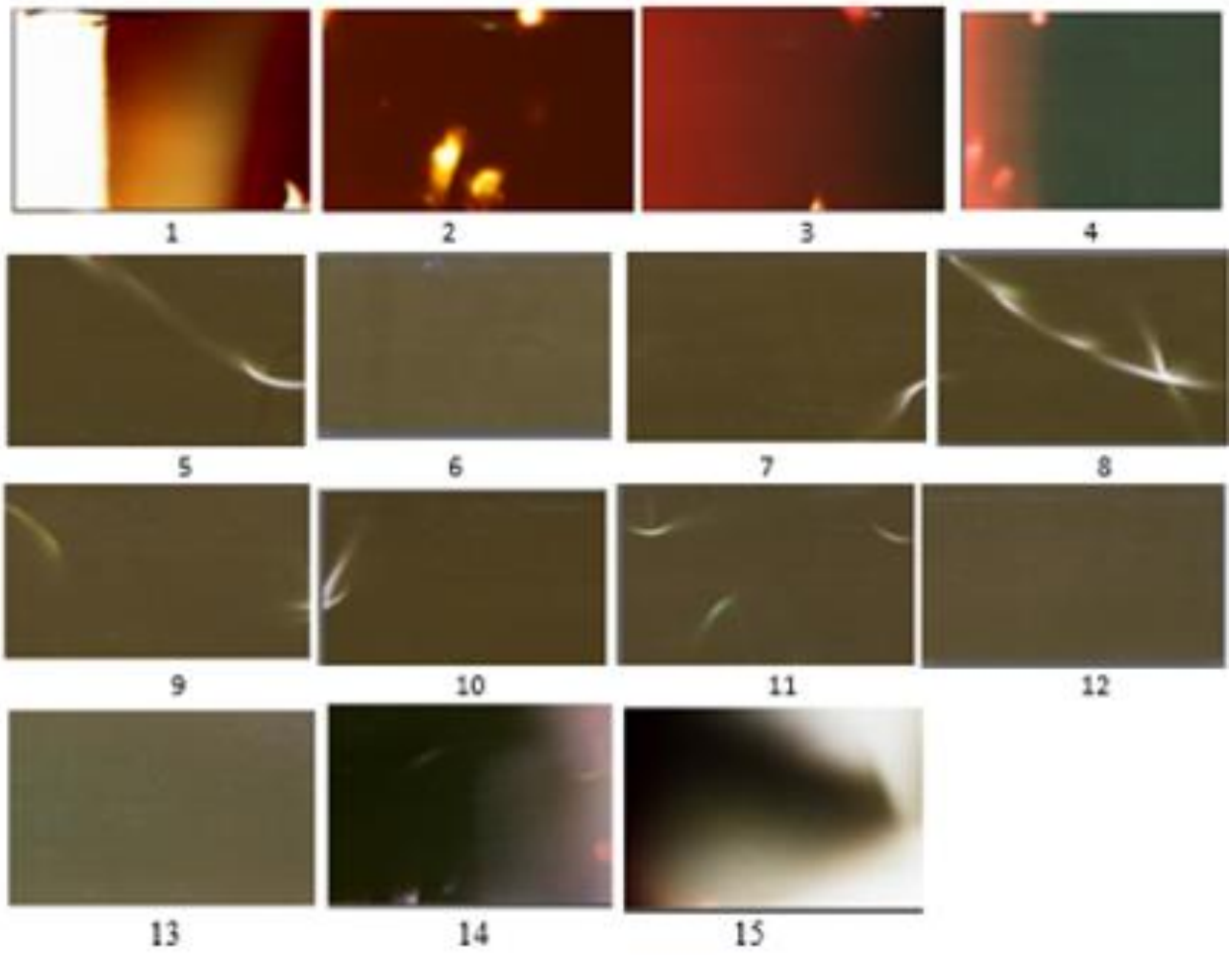


Experimental series No. 43, test 8. Control experiment performed on Northwest Railway Museum, Snoqualmie, WA on railway using a locomotive. Photos obtained at a distance of 20′ (6 m) from the locomotive.

Note. 1) Locomotive began to move away from the films from this distance. 2) Pay attention to the white radiation recorded in frames 2 and 4. Such fan-shaped luminous objects were observed repeatedly.

Note. 3) Tests 7 and 8 were performed simultaneously on different parts of the rail. 4) Luminous objects do not represent danger. The danger area is represented by dark objects in which atoms absorb energy radiated by a local group of metastable atoms. Such a dark region, similar to a crack, is captured on frame 15. We can assume that the region radiating energy is captured on frame 14 and partially on frame 15.

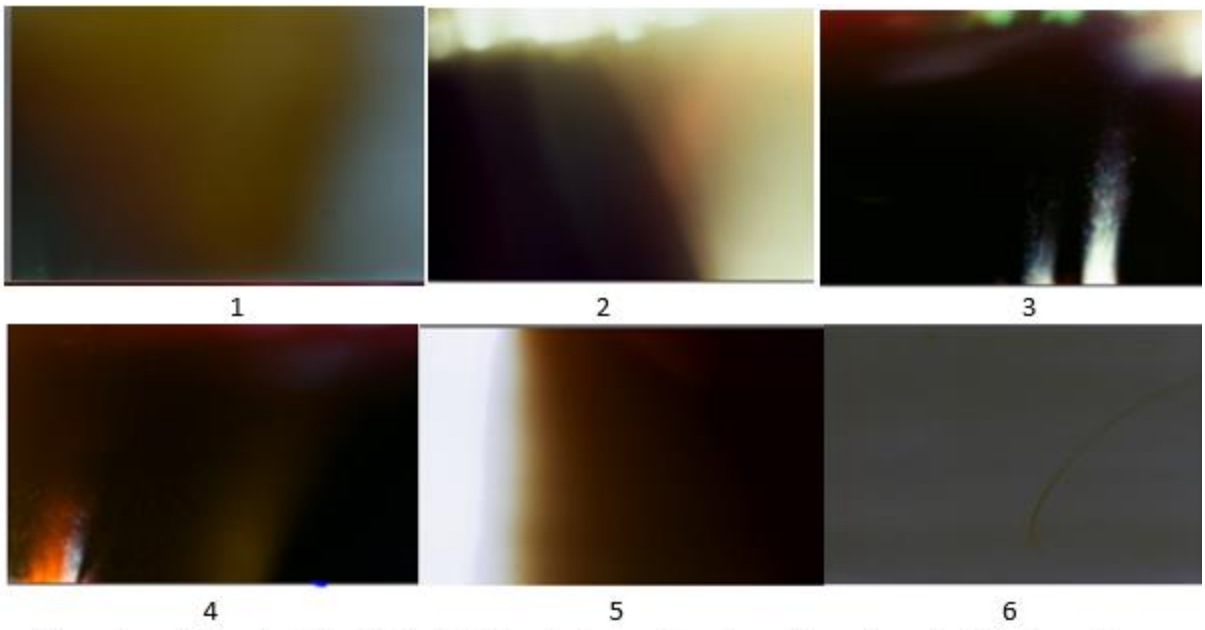


Experimental series No. 43, test 1. Control experiment performed on the Northwest Railway Museum, Snoqualmie, WA on railway using a locomotive. Photos obtained at a distance of 492′ (150 m) from the locomotive.

Note. Pay attention to the white radiation recorded in frames 3 and 4. Such fan-shaped luminous objects were observed repeatedly.

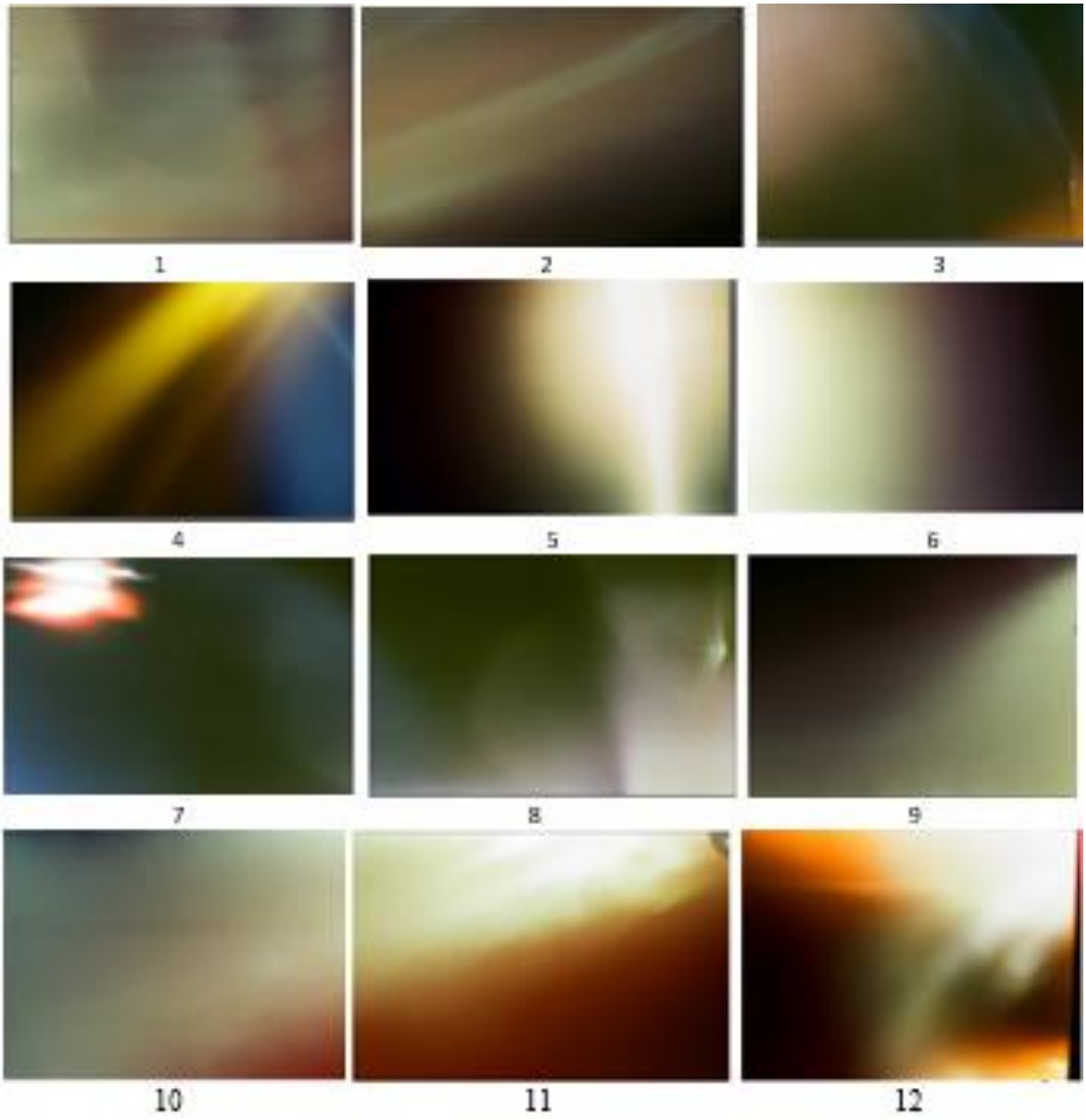


Experimental series No. 43, test 4 Control experiment performed on the Northwest Railway Museum, Snoqualmie, WA on railway using a locomotive. Photos obtained at a distance of 492' (150 m) from the locomotive.

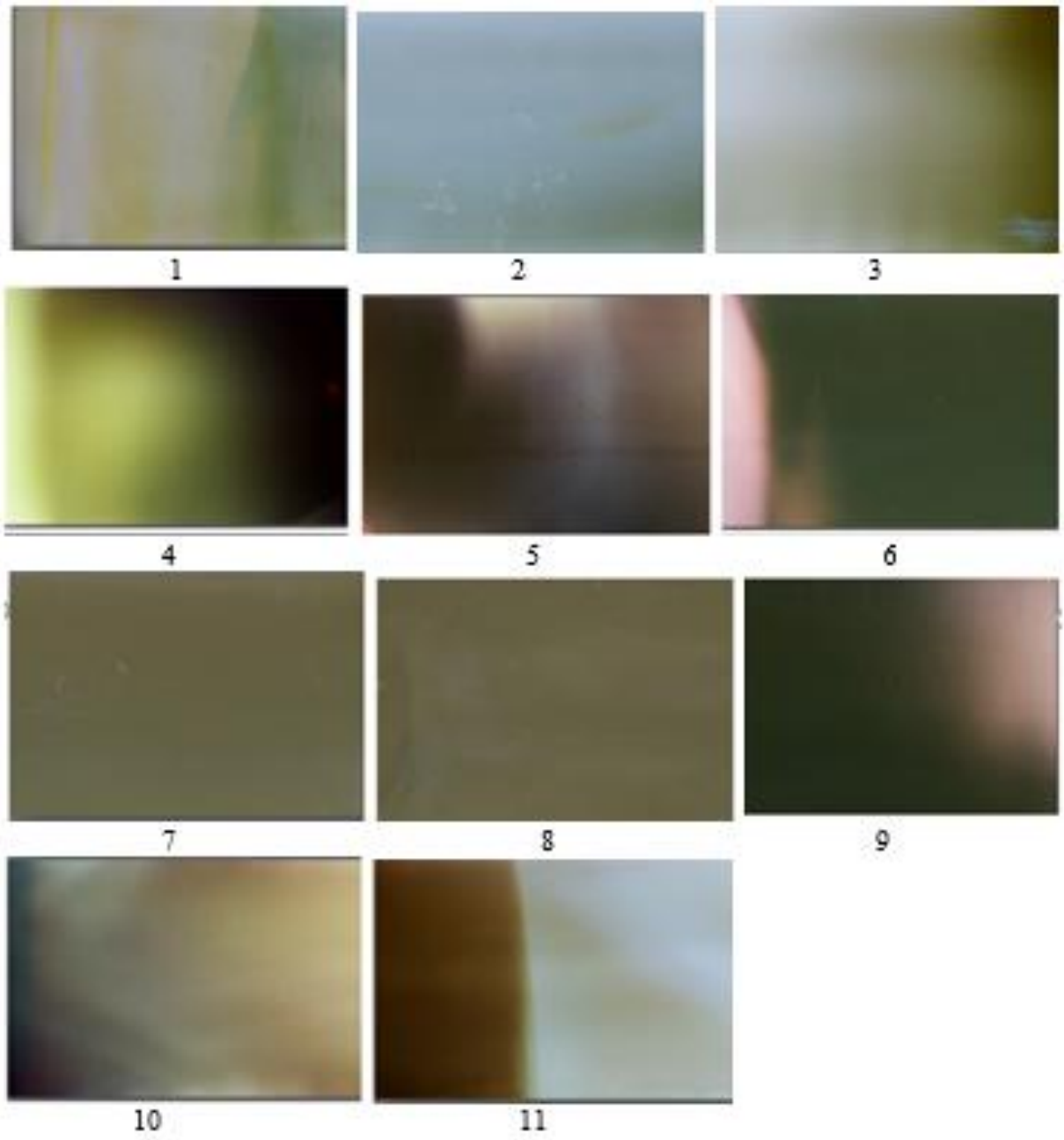


Experimental series No. 43, test 5 Control experiment performed on the Northwest Railway Museum, Snoqualmie, WA on railway using a locomotive. Photos obtained at a distance of 1320' (403 m) from the locomotive.

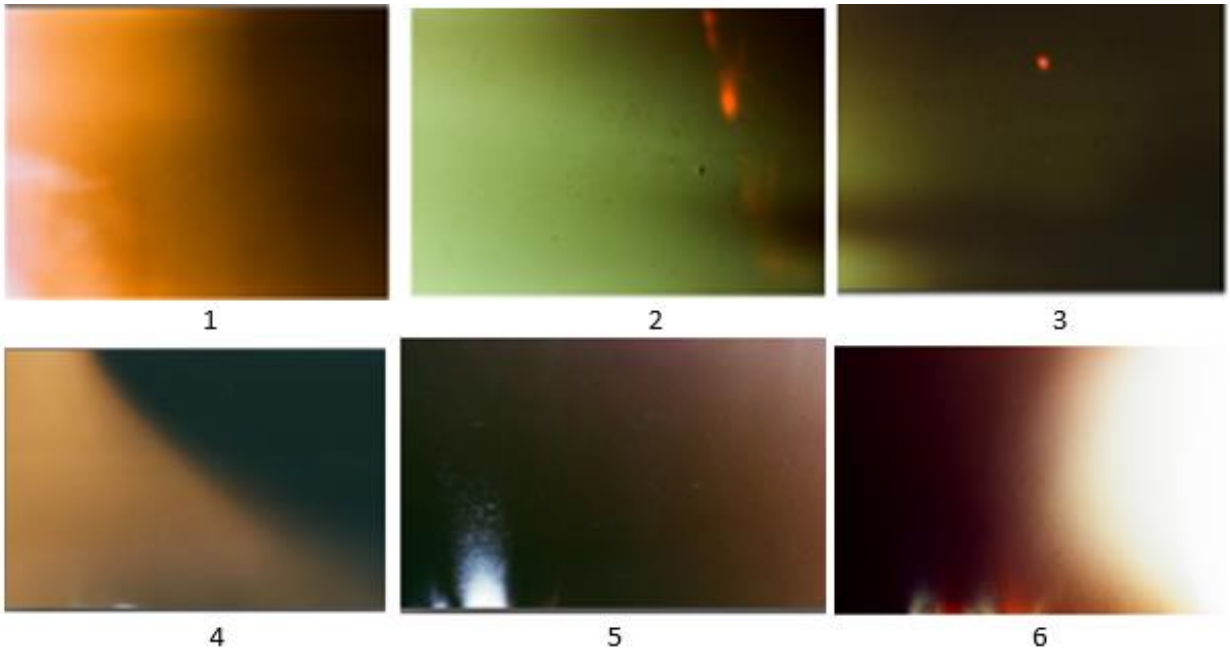


Experimental series No. 43, test 6 Control experiment performed on the Northwest Railway Museum, Snoqualmie, WA on railway using a locomotive. Photos obtained at a distance of 1320′ (403 m) from the locomotive.

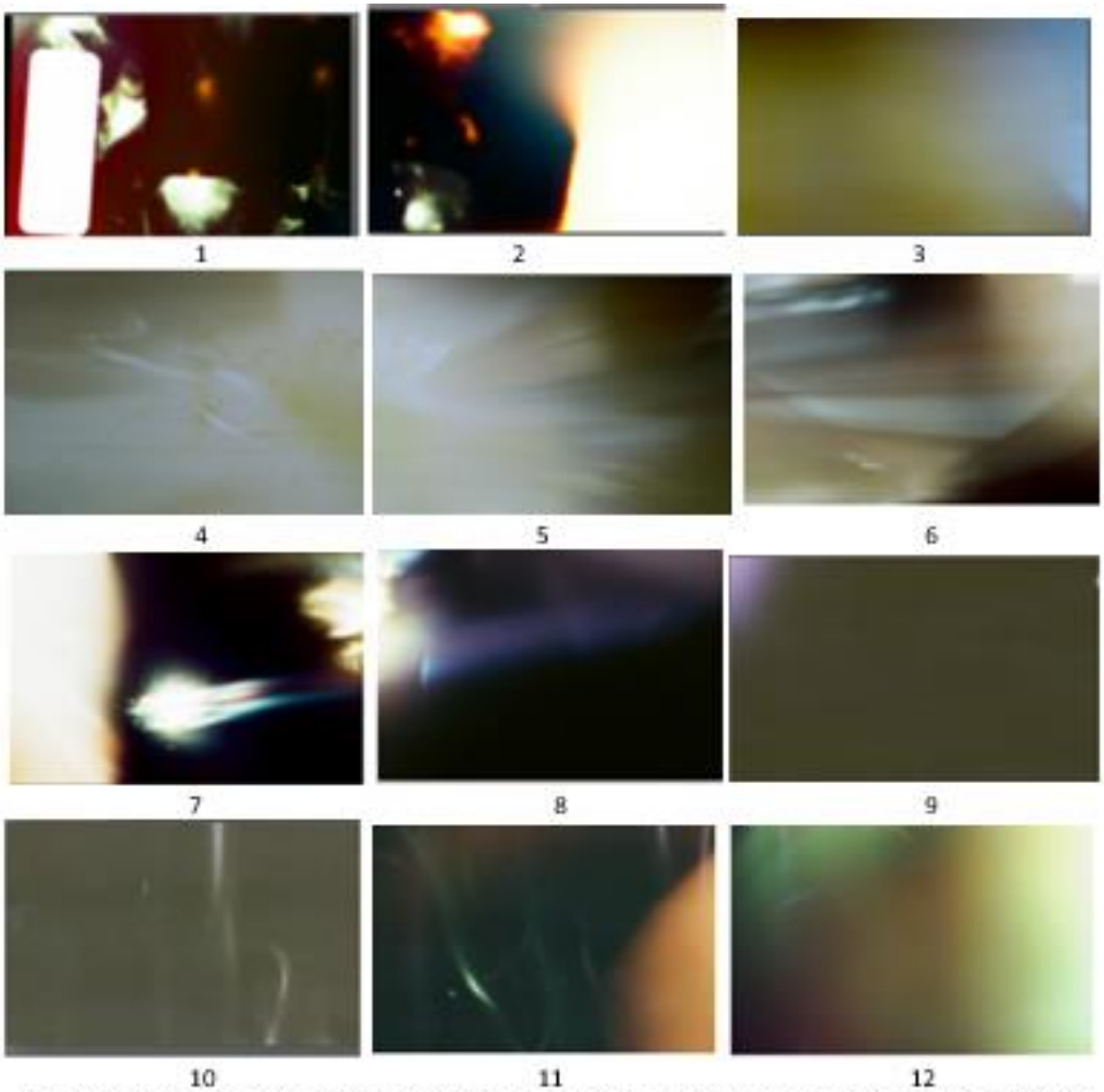

Experimental series No. 43, test 2. Control experiment performed on the Northwest Railway Museum, Snoqualmie, WA on railway using a locomotive. Photos obtained at a distance of 2623′ (800 m) from the locomotive.

Note. Photos were taken during the emergency braking of the locomotive at a distance of ½ mile from the place of braking. Pay attention to frames 4-8 caused, probably, by friction.

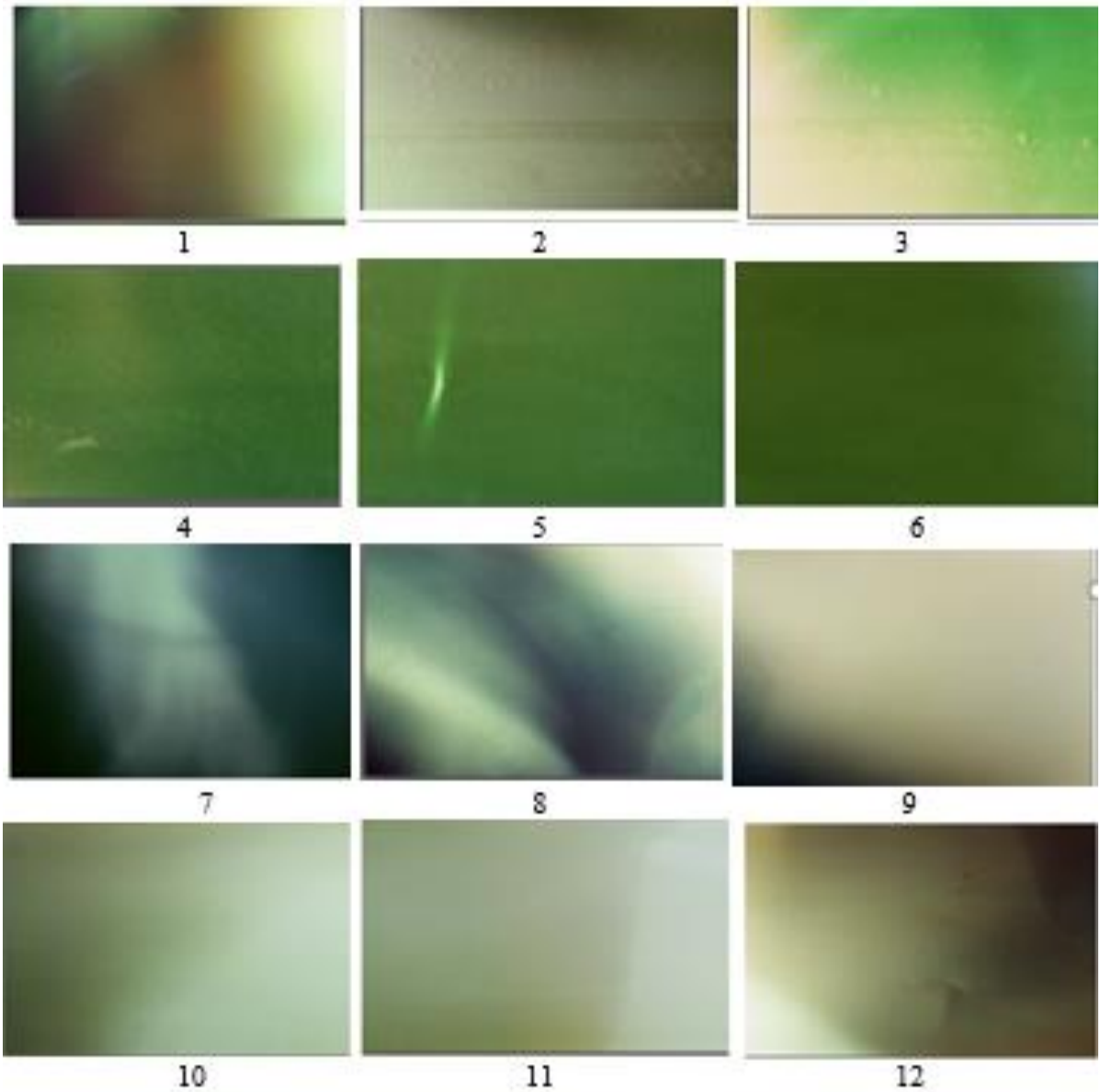


Experimental series No. 43, test 3Control experiment performed on the Northwest Railway Museum, Snoqualmie, WA on railway using a locomotive. Photos obtained at a distance of 2623′ (800 m) from the locomotive.

Note. 1) Control experiment series №40 at the North-West Railway Museum, Snoqualmie, WA on the railway using the locomotive was performed before the series number 43.

2) Photos in the experimental series No.40 tests 2-4 and 6 recorded p-radiation caused by the deformation by the locomotive passing over them.

## Conclusions

**1.** *This book is intended for those professionals and organizations that must ensure the safety of the design and operation of the facilities on which people live and work.* ***The 537 photographs given in this chapter are used as a necessary and sufficient condition to refute all theories of strength and fracture that do not take into account the energy of electromagnetic radiation***.

**2.** *The proof of the fact that the destruction of a solid is caused by atomic reactions when the influence of nuclear reactions can be neglected is the main conclusion that follows from an experimental study. The fact that atomic reactions are accompanied by electromagnetic radiation, the spectrum of which extends into the area called the X-ray, is of particular importance. Any effect on a substance is accompanied by an atomic reaction in which photons with energy of 50-100 keV are emitted.*

**3.** *Presented a discovery of p-rays, i.e., p-radiation and its difference from X-rays. p-rays is a region of high-frequency electromagnetic radiation accompanies*

**4.** *The simplicity of the experiment and its absolute reliability testifies to the fact that atomic reactions occur in accordance with a natural phenomenon stipulated by a law that can only be formulated on the basis of quantum mechanics.*

**5.** *The theoretical justification of the observed phenomenon is given in the third chapter of the book; however, focused research on this phenomenon is necessary, using the entire arsenal of modern experimental methods.*

**6.** *P-radiation arising in solids allows us to classify defects by color and shape, but the color of the defect does not mean that the defect emits electromagnetic waves, which frequency corresponds to a given spectral range. The color of the defect is the result of the photochemical reaction of the photographic material and its processing method.*

**7.** *The invariable coincidence of the destruction and the appearance of a dark region on the film suggests that the absorption of photons became the cause of the destruction.*

**8.** *Electromagnetic radiation, including p-radiation, is observed for all types of external influences in all materials, regardless of shape, composition, structure.*

**9.** *P-radiation during deformation of a solid is observed both before destruction and after it from fragments formed as a result of destruction. At the time of destruction, radiation is not observed, since it is absorbed.*

**10.** *The effect of p-rays on alloys and glass causes luminescence in a wide spectral range, including X-ray.*

**11.** *The electromagnetic response of all solids, regardless of composition and structure to nonlinear deformation, indicates a widespread natural phenomenon called internal triboluminescence.*

**12.** *Now since the cause of man-made disasters has been established, the nature and mechanism of catastrophic destruction are revealed and described from the standpoint of quantum mechanics; disregard of the quantum mechanical mechanism during the operation of structures and devices leads to a catastrophe, which is a crime.*

## References to Chapter I


**1.1.** J. C. Maxwell, III. *On the Equilibrium of Elastic Solids*, pp.31-74, The Scientific Papers of James Clerk Maxwell, Edited by W. D. NIVEN, M.A., F.R.S.

**1.2.** J. C Maxwell, *Letter to William Thomson*, 18 December 1856, The Scientific Le*tters & Papers of James Clerk Maxwell, v.1, 1846-1862, 487-491.*

**1.3.** S. P. Timoshenko**,** *History of Strength of Materials: with a Brief Account of the History of Theory of Elasticity and Theory of Structures*, McGrow-Hill Company, Inc. NY, pp 438, (1953).

**1.4.** R. Mises, *Mechanik der festen Körper in plastisch-deformablen Zustand, Nachr. d. Kgl. Ges. Wiss. Göttingen, Math. -phys. Klasse 4, 582-592, (1913).*

**1.5.** *Columbia Accident Investigation Board*, Subsequent Printing and Distribution by the National Aeronautics and Space Administration and the Government Printing, (2003).

**1.6.** T. E Bell and K. Esch, *The Challenger Disaster: A Case of Subjective Engineering*, IEEE Spectrum, (2016), https://spectrum.ieee.org/tech-history/heroic-failures/the-space-shuttle-a-case-of-subjective-engineering.

**1.7.** S Post, *Space Shuttle Case Studies: Challenger and Columbia*, 121 st ASSE Annual Conference, Indianapolis, IN, (2014).

**1.8.** V. P. Rombakh, *Atom Parameters, and Metal Properties*. Logistics Capital Inc., Edmonds, WA, P. 311 (2008).

**1.9.** V. P. Rombakh, *Introduction to the physics of destruction,* P. 259 2014, http://catastrophepreventing.com/.

**1.10.** V.P. Rombakh, *Railway Catastrophic Deformations: Nature and Mechanism of Formation of Specific Defects*, International Crashworthiness Conference, San Francisco, USA, July 12-16, (2004).

**1.11.** V.P. Rombakh, *Catastrophic deformation of the rail,* Metal technology (Moscow), **7**, 23-28; **8,** 15-19**; 10,** 12-14, **(**2004).

**1.12.** V. P. Rombakh, *Damage of metals: atomic nature,* International Conference on Fatigue Damage of Structural Materials V, Hyannis, MA, USA, September 19-24, (2004).

**1.13.** V. P. Rombakh, *Two interpretations of Maxwell's solid mechanics*
Edmonds, WA USA P. 78 (2016),

**1.14.** V. P. Rombakh, *Potential Energy of Distortion and its Assessment, VII International Conference Deformation and destruction of materials and nanomaterials,* Sbornic_DFMN, 246-247, (2017).

**1.15.** J. Schors, K.-W. Harbich, M. P. Henschek, and A. Lange, *Non-Destructive Micro Crack Detection in Modern Materials,* ECNDT - We.2.2.2, Federal Institute for Materials Research and Testing (BAM), Germany (2006).

**1.16.** M. Lalpoor, *Study of Cold Cracking during DC-casting of High Strength Aluminum Alloys,* Ph.D. thesis. The Delft University of Technology, P. 150 (2010).

**1.17.** M. Lalpoor, D.G. Eskin, and L. Kargerman, *Cold Cracking Development in AA7050 Direct Chill–Cast Billets under Various Casting Conditions*, Metallurgical and Materials Transactions A, **41**, 2425-2434 (2010).

**1.18.** D. G. Eskin, L. Katgerman, Dr. Suyito, J. F. Mooney, *Contraction of aluminum alloys during and after solidification*, Metallurgical and Materials Transactions A, **35**, 1325–1335 (2004).

**1.19.** M.Lalpoor, D. G. Eskin, D. Ruvalcaba, H.G. Fjær, A.Ten Cate, N.Ontijt, L.Katgerman, *Cold cracking in DC-cast high strength aluminum alloy ingots: An intrinsic problem intensified by casting process parameters,* Materials Science and Engineering: A **528**, 2831-2842, (2011).

**1.20.** L. Zhang, D. G. Eskin, A. Miroux, T. Subroto, and L. Katgerman, *Effect of inlet geometry on macrosegregation during the direct chill casting of 7050 alloy billets: experiments and computer modeling,* IOP Conf. Series: Materials Science and Engineering **33,** 012019, (2012).

**1.21.** T. A. Subroto, *Connection between hot tearing and cold cracking in DC-casting of AA7050: Experiments and computer simulations,* Thesis, Delf University of Technology, (2014), pp 186.

**1.22.** J. C. Maxwell, Plateau on Soap-Bubbles. *The Scientific Papers of James Clerk* Maxwell, Volume II. pp 393-399.

**1.23.** E. Eberhardt, B. Stimpson, and D. Stead, *Effects of Grain Size on the Initiation and Propagation Thresholds of Stress-induced Brittle Fractures*, Rock Mech. Rock Engng. **32** (2), 81-99. (1999)

**1.24.** T. Tentler, *Analogue modeling of tension fracture pattern in relation to mid-ocean ridge propagation*, Geophysical Research Letter, **30**, No. 6, 1268, doi:10.1029/2002GL015741, pp.4 (2003)

**1.25.** L. Volynskii and S.L. S.L Bazhenov: *Folding instabilities and of the thin coating on a soft polymer substrate as a model of oceanic crust*. Geofisika Internationale, 40, No 2, 87-95, (2001).

## CHAPTER II. DEMONSTRATION OF P-RADIATION FROM PLANT CELLS AND LIVING ORGANISMS

*Experimental work should be questioned until the facts force us to abandon all doubt.*

L. Pasteur

### 2.1. Examples of experimental research

Success, technology, chemistry, biology, and medicine at each stage of development are provided by the discovery of the laws of nature and the use of equipment created on the basis of these laws. The discovery of L. Galvani laid the foundation for the study of electromagnetic (in modern interpretation) signals in the organs of animals and humans. The use of nuclear magnetic tomography characterizes the path that humanity has traveled in 250 years.

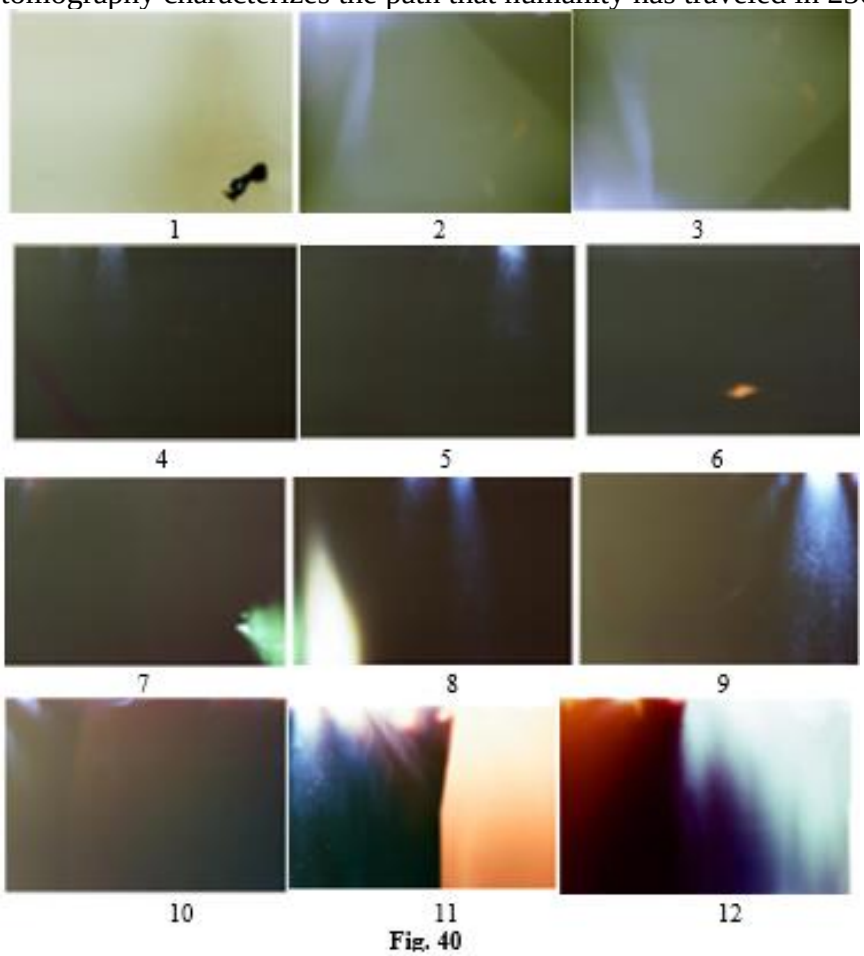

Fig. 40

Non-invasive methods for analyzing the functioning of the brain and cells of other organs of animals and humans have been used since the end of the 19th century. A study of the region in which atomic reactions are accompanied by electromagnetic radiation with an energy of 50-100 keV, but without the potential difference accelerating electrons, is demonstrated in the first chapter by numerous examples. Similar examples are given in this chapter.

**Example No. 1.**

A container with a film was placed on the author's head in a circle in the frontal part. The exposure time was 36 hours. Twelve photographs are shown in Fig. 40 illustrate the result of an experiment. Repeated repetition of fan-shaped radiation, which is observed in the presence of water, allows us to conclude that frames 2-5 and 7-12 illustrate the same effect. Frame 1 illustrates the hearing aid that plays the role of the screen. Pay attention to the glow of the battery, similar to that shown in Fig. 28, frames 5-8.

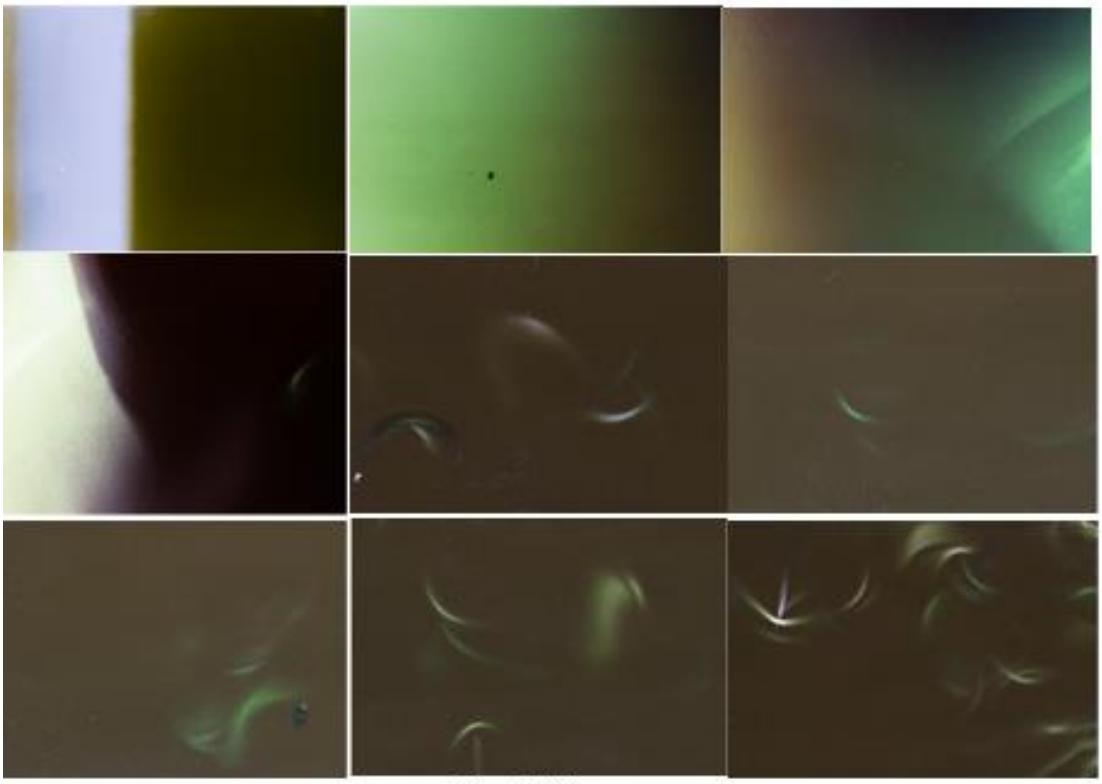

Fig. 41 (1)

**Example No. 2.**

A container with the film was placed on the chest of the author in a circle at the level of the heart. The exposure time was 36 hours.

Nine of the 13 photographs shown in Fig. 41 (1) illustrate electromagnetic radiation from an area located to the left of the heart.

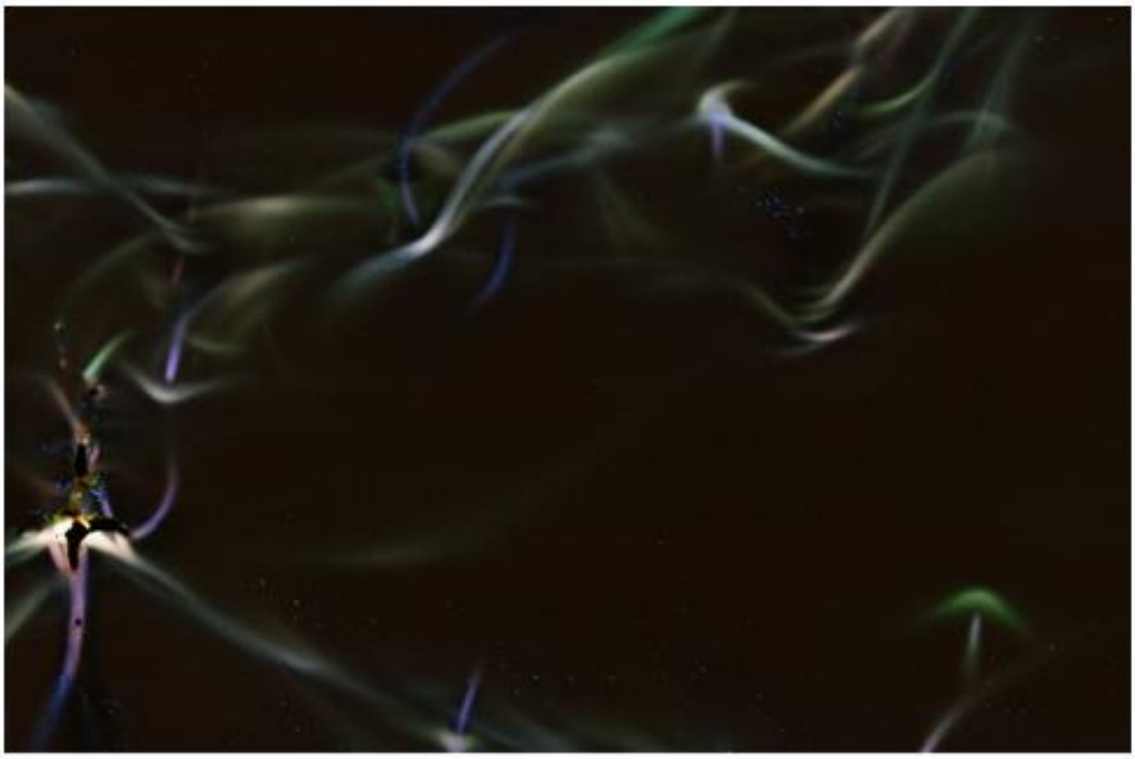

Fig. 41 (2)

**Example No. 3**.

Photo Fig. 41 (2) illustrates electromagnetic radiation in the region of the heart. The author underwent the installation of three stents and bypass surgery.

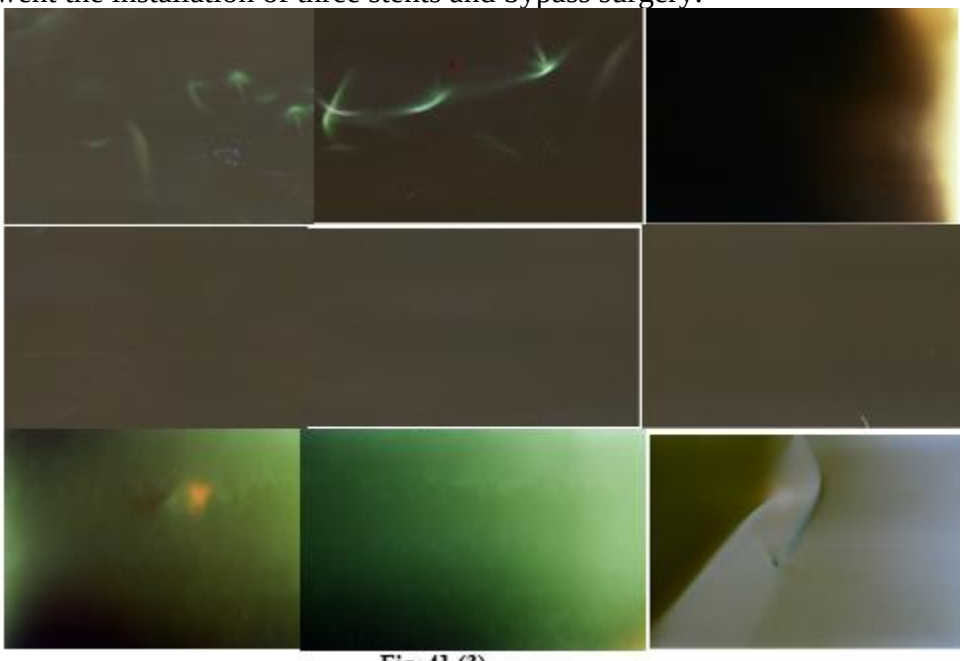

Fig. 41 (3)

**Example No.4**.

Nine of the 14 photographs shown in Fig. 41 (3) illustrates electromagnetic radiation in the area to the right of the heart.

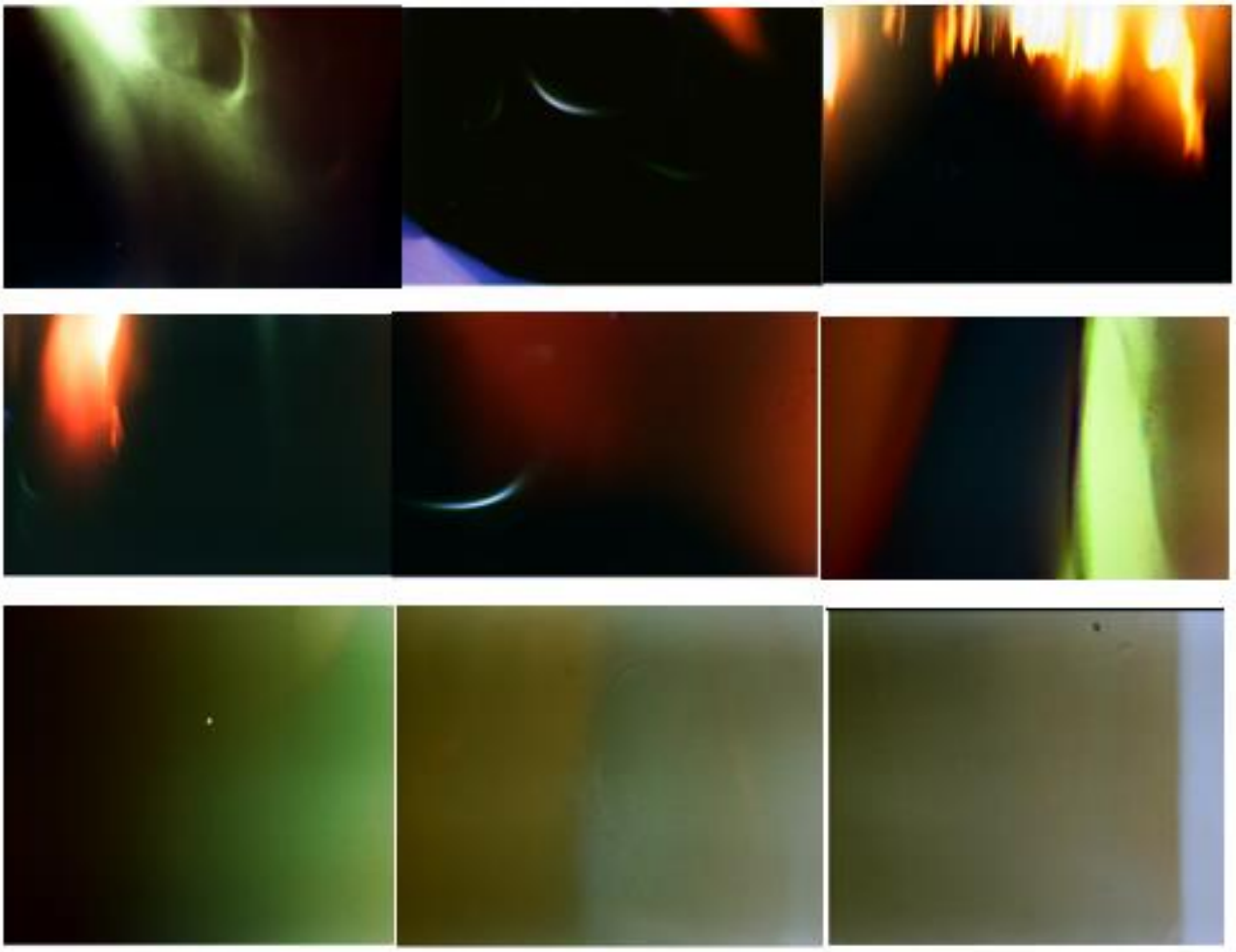

Fig. 42

**Example No. 5.**

Nine photographs are shown in Fig. 42 illustrate electromagnetic radiation from the lower back of the author. The author went through a spinal traction cycle to reduce the pain caused by a pinched nerve between the 4 and 5 vertebrae of the lower back. The hanging foot of his right leg remains an unresolved problem for him.

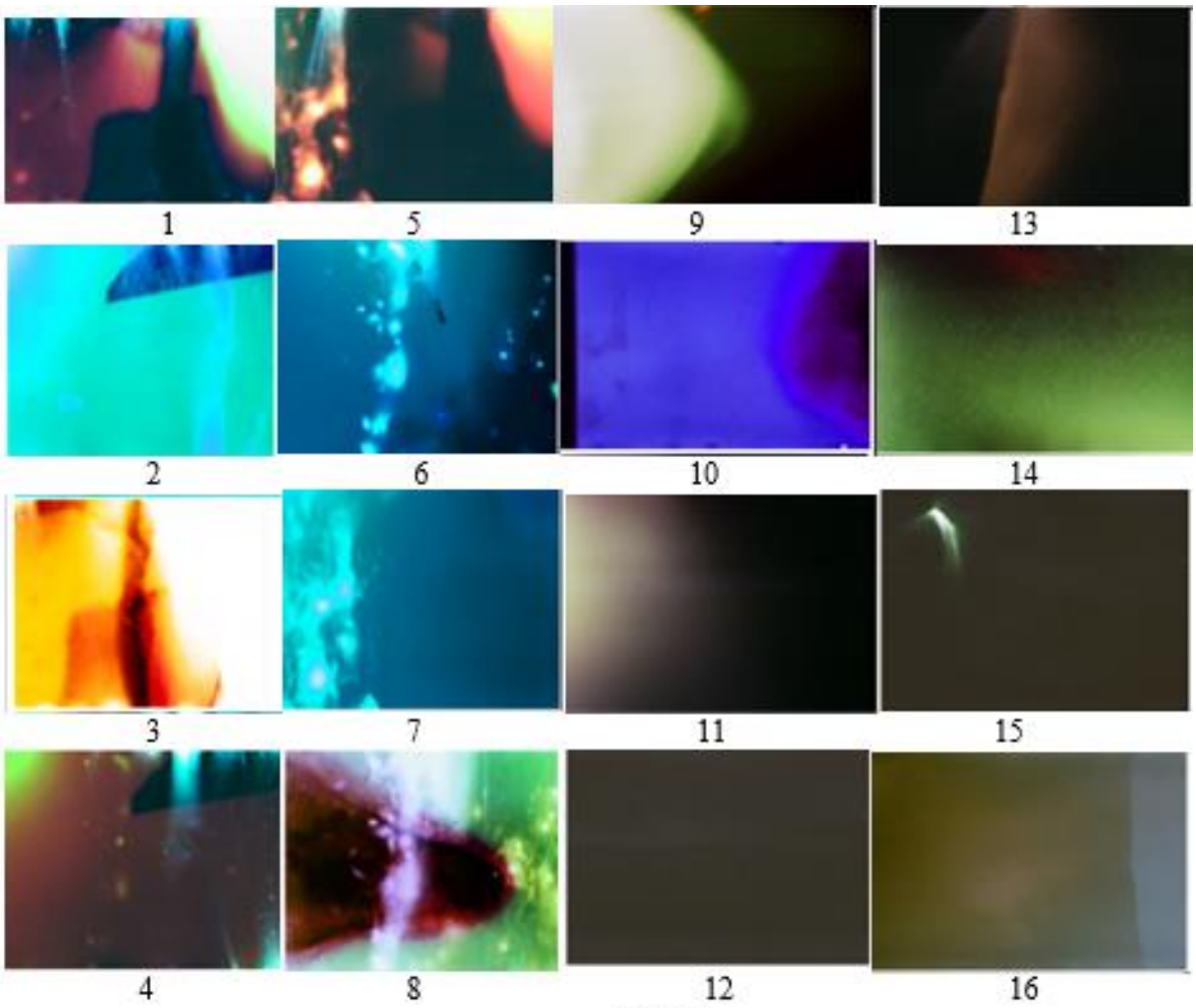


**Fig. 43**

**Example No. 6**.

Fig. 43. 16 photographs from 28 illustrate fragments of the author's spine. Frames illustrating electromagnetic radiation from individual regions of the spine from the cervical vertebrae to the coccyx are located in a rare order of increasing number.

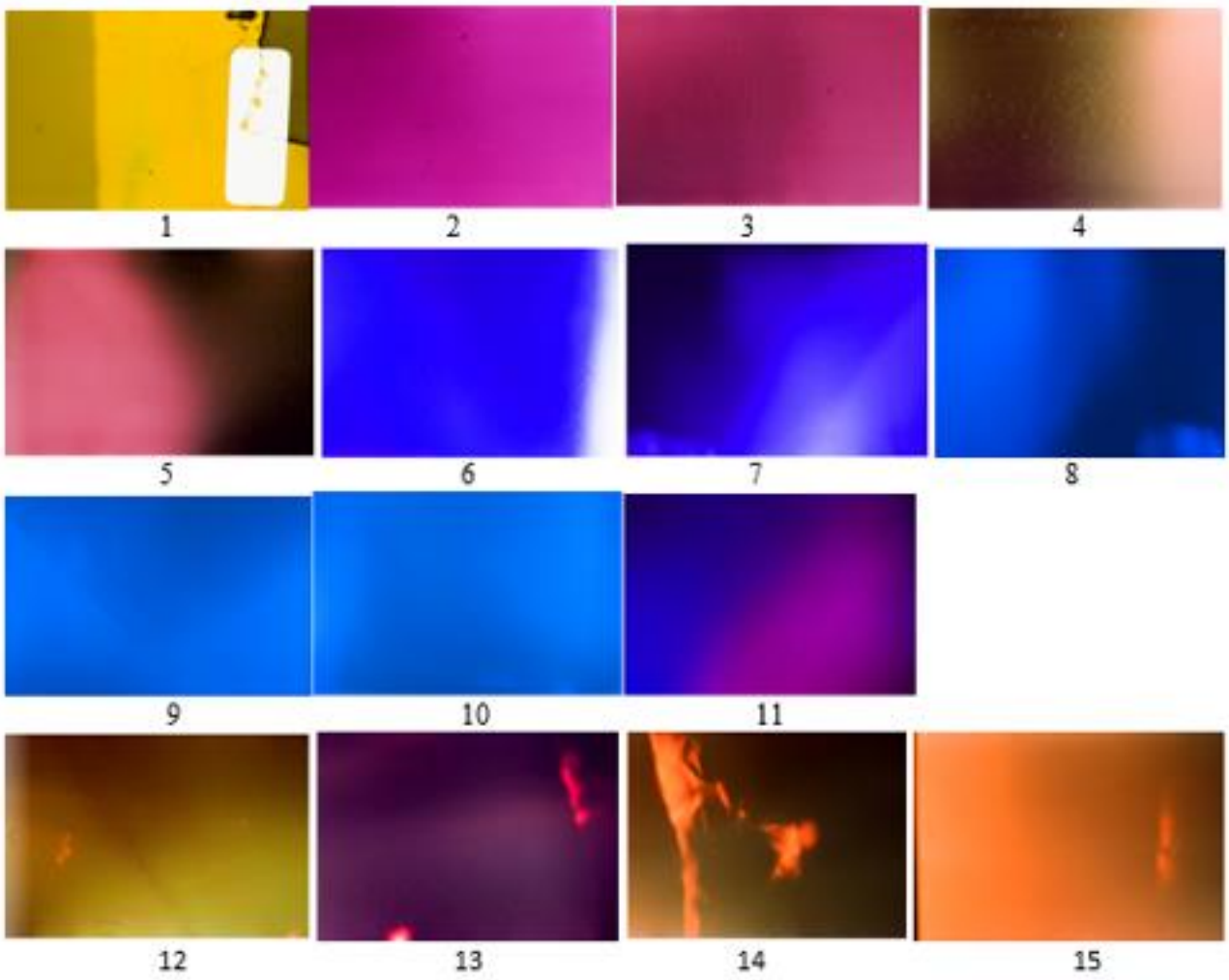


**Fig. 44**

**Example No. 7.**

15 photographs illustrate electromagnetic radiation from the author's left foot from the knee joint (frame 1) to the hip joint (frame 14), frame 15, probably the edge of the ilium. The hip joint of the author is prone to osteopenia.

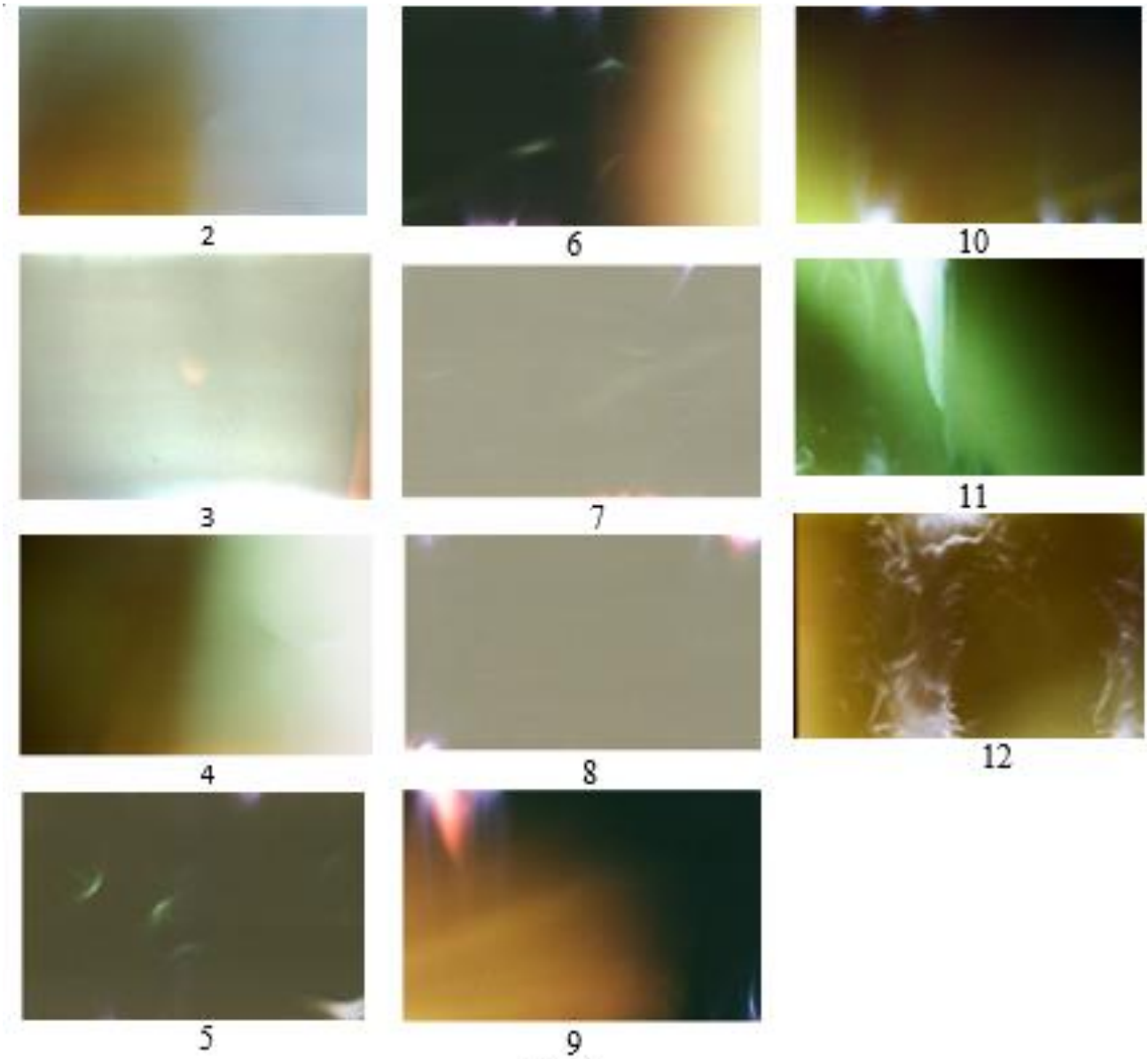


**Fig 45**

**Example No. 8**.

11 photographs illustrate electromagnetic radiation from the author's right leg from a point above the knee joint (frame 2) to the hip joint (frame 11) and probably the ilium (frame 12).

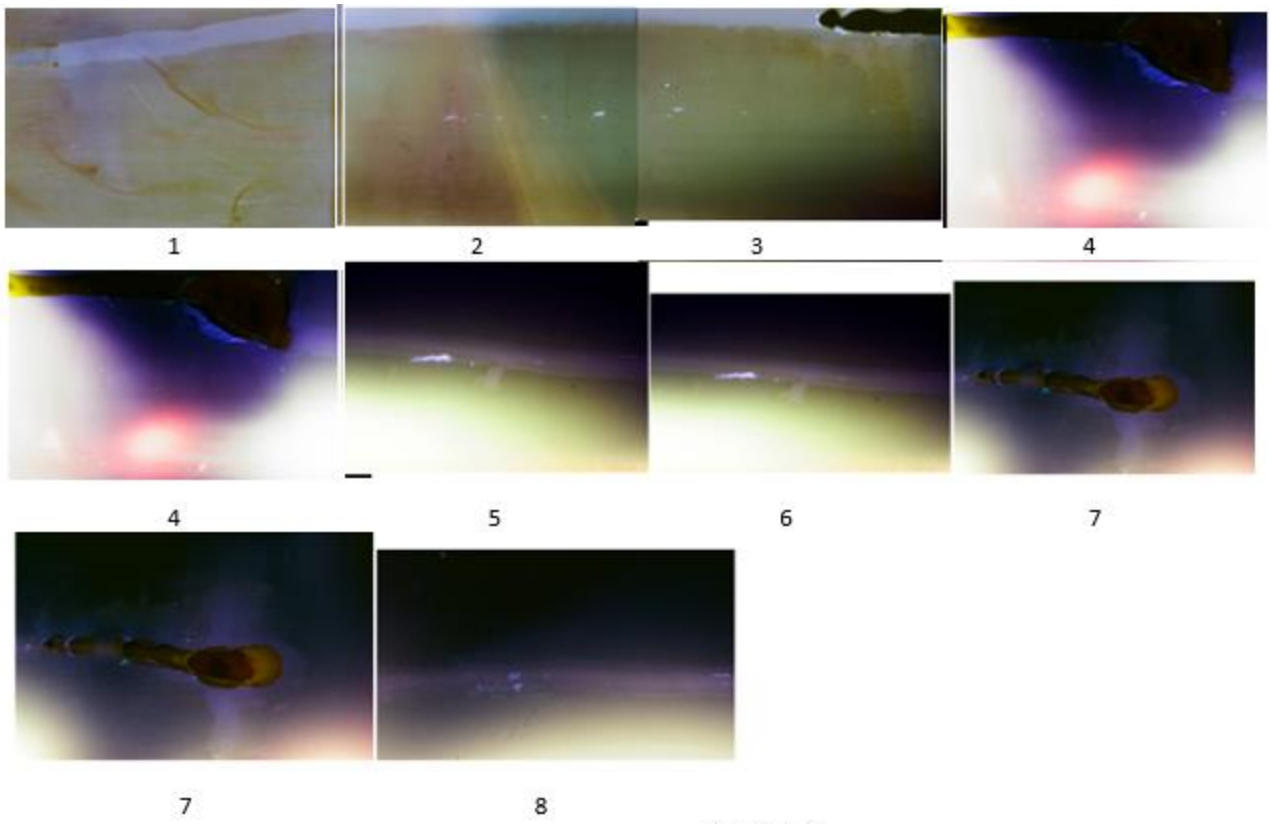


**Fig 46 (1)**

**Example No. 9**.

Fig. 46 (1) illustrates electromagnetic radiation during the genesis and development of greenfly larvae (Calliphoridae) in fish. Frames 4 and 7 are used twice for demonstration.

**Fig. 46 (2)**

**Example No. 10.**

Fig. 46 (2) illustrates electromagnetic radiation during the genesis and development of greenfly larvae (Calliphoridae) in a chicken egg.

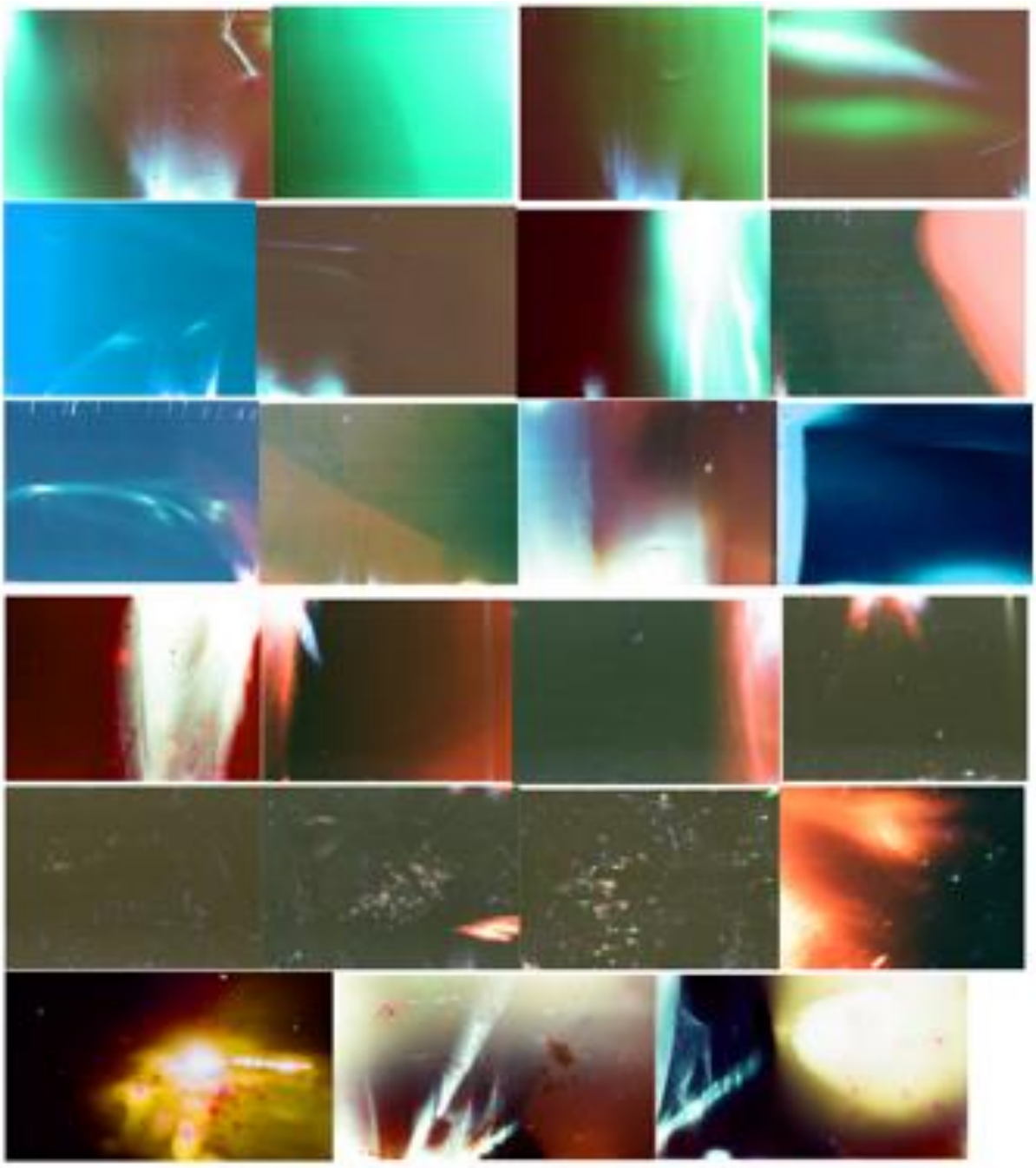

Fig. 47

**Example No. 11.**
Fig. 46 (1) illustrates electromagnetic radiation during the growth of strawberry roots.
The exposure was 168 hours.

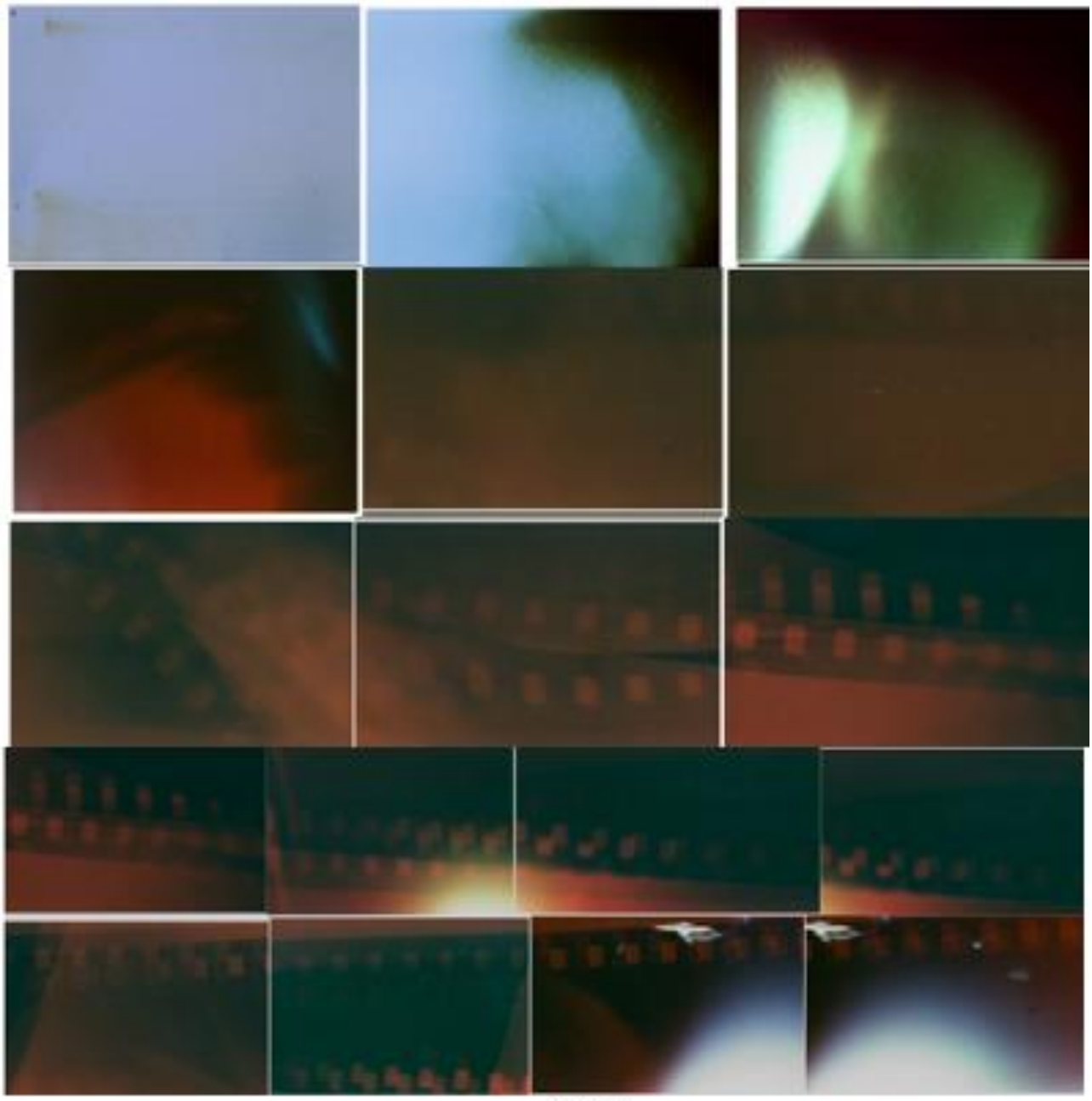

Fig. 48

**Example No. 12**.
Fig. 48 illustrates the electromagnetic radiation of a growing pine. A container with the film was placed around the barrel at a slight angle to the horizon. The exposure was 168 hours. The film shift is due to pine growth

.

**2.2. A brief analysis of the results of the experimental study**

The 537 photographs are given in the first chapter, and 135 are shown in the second chapter to understand the reason for the similarities and differences between the response of inorganic material to external influences with radiation from plant cells and living organisms under the influence of only solar radiation and gravity. Frame 1, Fig. 40 is shown in this chapter, not by

chance, as well as the human brain. The electromagnetic signals of the brain and heart have been studied for many years. There is no doubt that a comparison of encephalograms, cardiograms, and p-radiation signals will help to understand the information that they carry. There are no fundamental obstacles to the implementation of a non-invasive method for studying the spectral composition and intensity of p- radiation.

In this regard, the result of such a study will be called a protonogram. Frame 1 indicates that the material of the hearing aid has absorbed the p-rays. Consequently, metals absorb it more intensely. The experiment confirms this conclusion. But special experimental studies are needed to find out whether this is due to insufficient signal intensity or a change in frequency.

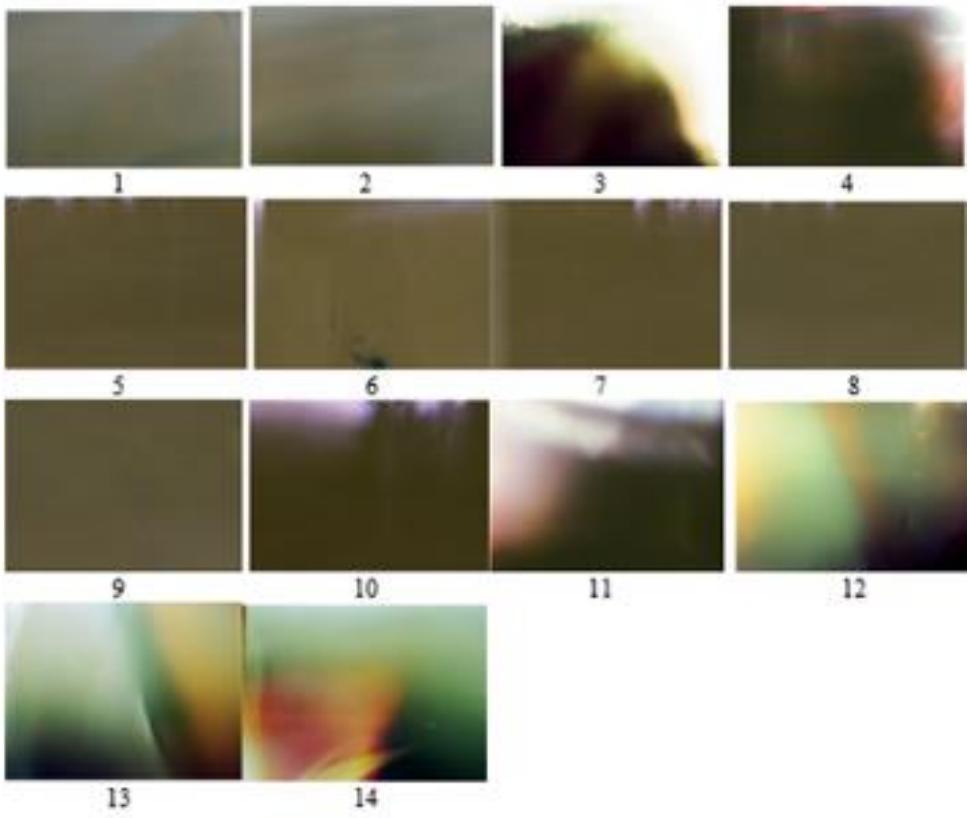


**Fig. 49 (1)**

Fig. 49 (1) illustrates electromagnetic radiation when examining the author's spine, similar to that shown in Fig. 43, but in this experiment, screens of lead, iron, and aluminum foil were placed on the container. Screens made of lead and iron completely absorbed the radiation, which is partially observed at the edge of the screens. The absorption of radiation by aluminum is shown in frame 3. Frames 11-14 illustrate the radiation when the screen is absent.

This study is only a demonstration and does not claim to be a detailed analysis of the observed phenomenon. But these photos allow us to draw certain conclusions.

It is known that the bulk of the human body is water. The fan-shaped radiation illustrates its manifestation. The use of screens made it possible to observe the manifestation of water reactions in almost all frames, Fig. 49, whereas in Fig. 43, it is observed only on frames 1, 2, 4, and 5.

An important role in redox reactions is played by iron ions. The $Fe^{2+} \rightarrow Fe^{3+}$ transition is possible only upon the absorption of a photon, while the $Fe^{3+} \rightarrow Fe^{2+}$ transition is accompanied by photon emission. Photos Fig. 41 (1), Fig. 41 (2), Fig. 41 (3) show how the brightness of blood vessels changes when approaching the heart, indicating the emission of energy. The brain performs other functions in the body than the heart. A researcher will observe a different kind of nimargram to compare it with an encephalogram, because other atomic reactions are realized in the brain, as photographs show.

The emission spectra of the atoms of each chemical element are strictly individual. Photos characterize the color change of an element in the process of functioning of the cells of the body. It is established that the color of the same area changes. For example, frames 12, 13, 14, captured in Fig. 49 are not observed in Fig. 43.

The color characteristic of the emergence of fly larvae changes, as shown in Fig. 46 (1), and depends on the environment in which this occurs, Fig. 46 (2).

Photographs from an examination of the left leg, Fig. 44 differ from the photographs obtained by examining the right leg, Fig. 45.

Fan-shaped figures characteristic of water are observed in both organic and inorganic materials. The arched shapes characteristic of blood vessels shown in Fig. 41 (1), Fig. 41 (2), Fig. 41 (3) are observed in photographs during the destruction of the stone Fig. 39 (1), frames b and c; at steam-water contact, Fig. 29 (1), frames 10 and 15; Experimental series No. 43, test 8.

*This allows us to conclude that the source of such radiation is iron and hydrogen ions.*

New methods proposed on the basis of the discovery by physicists of a natural phenomenon are applied in biology and medicine.

One hundred percent reliability of the proposed method has been demonstrated in this chapter guarantees the success of using protonogram.

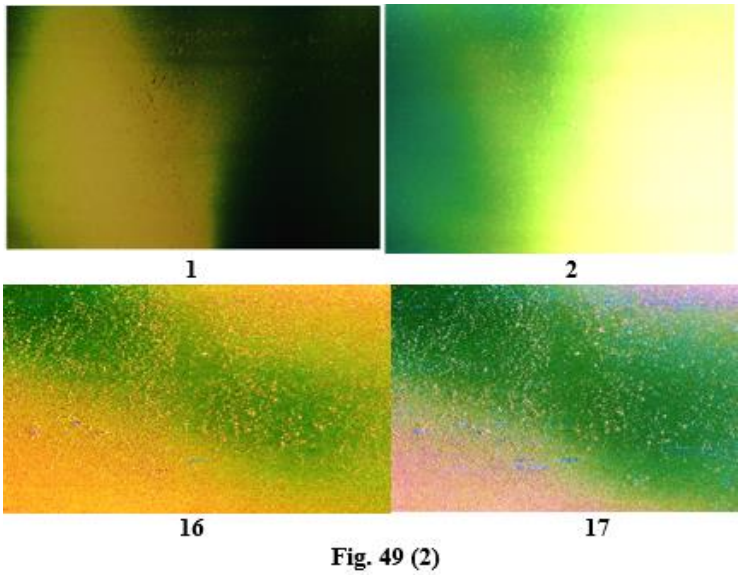

Fig. 49 (2)

Photos Fig. 40- Fig. 48 shows that the p-radiation intensity of plant cells and living organisms is sufficient to study and control the processes occurring in them. Fig. 49 (1) indicates that metals intensely absorb this radiation.

ig. 49 (2), frame 1 illustrates the results of a study of the transparency of the author's left hand for p-radiation, which is caused by a current in a conductor located above it. The current was created by a short circuit at the terminals of the battery, which was far from the film to minimize the effect of the spark. The position of the two strands of the conductor is visible on frame 1.

A feature of this experiment is that the film was located in a container on the surface of a steel plate, as shown in Fig. 1 c.

Fig. 49 (2), frame 2 illustrates a mirror-symmetric image of the author's left hand. This conclusion seems fantastic, but mirror symmetry is observed on such a number of luminous and dark frames that we are obliged to consider this fact proven, especially since this natural phenomenon is not uncommon.

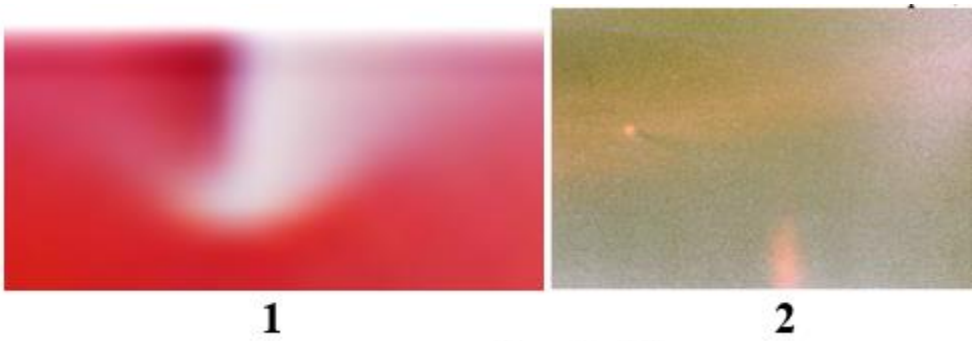

**Fig. 49 (3)**

The frequency of occurrence of various luminous or dark objects is different. One such purpose is showing in Fig. 49 (3), frame 1. It is recording in three photographs out of 1026 obtained in an experimental study.

The finger of the author's son was located between the container with film and a massive steel ingot. The hammer hit the surface of the metal. Frames 16 and 17 illustrate the absorption of p-radiation with a finger. A metal strike reveals some numerous point objects that are fixed at a considerable distance from the place of impact, as has been observed repeatedly. This effect was recorded on all 27 frames, including frames 1 and 2 in this experiment.

The study of currents passing through the human organs is essential to identify the damage to which they lead. A copper wire 0.02 mm thick and 4 cm long exploded during a short circuit in the battery. Fig. 49 (3), frame 2 illustrates the nature of the explosion. The tabular data allow us to estimate the mass of the wire ($M=112.2\cdot10^{-6}$ g) the energy (A=0.56 J) needed for evaporation and the power ($W\approx1\cdot10^{10}$W).

Studies of human life showed that human brainpower is ~ 12 watts, and energy consumption is 10.8 kcal/h, which is 20% of the total energy consumption. The photographs in this chapter show the high brightness of p-radiation. The sensitivity of screens and photo material can be increasing tens of times. It means that p-radiation can be used in biology and medicine.

## CHAPTER III. QUANTUM-MECHANICAL INTERPRETATION OF EXPERIMENTAL RESULTS

*We must put forward laws that apply to uncharted areas, to ensure that science does not turn into empty protocols about experiments.*

R. Feynman

### 3.1. Emission caused by protons

The history of physics indicates that plausible hypotheses are not immediately confirmed experimentally, and erroneous hypotheses are not immediately refuted by them. Experimental confirmation or refutation is late for years, centuries, or even millennia, as happened with the atomic hypothesis. The time between the confirmation or refutation of the hypothesis is reduced today due to the modern experimental base and the increase in the number of people who are engaged in scientific research.

The fate of the experimental discovery is different, but it can also wait a long time for recognition and application. Heron's steam spinner turned into a steam engine only two millennia later.

The mathematical expression of Newton's second law $F=ma$ can be represented in form $a=\frac{1}{m}F$ here $a$ is the acceleration of the body, $m$ is its mass, $F$ is the force acting on the body. The formula is obtained on the basis of an experiment in which mass and force were measured; acceleration was calculated based on distance and time measurements. Newton understood that for different time intervals, the acceleration could be different.

He used the differential calculus developed by him, and G. Leibniz to study functions in a small interval of changing the argument. Newton's second law for one-dimensional motion can be written as the equation

$$a=\frac{dv}{dt}=\frac{d^2s}{dt^2}=\frac{1}{m}F \quad (1),$$

where $v$ is the instantaneous velocity, $s$ is the path traveled by the body during this time interval.

Newton postulated that body mass does not change during movement, but Einstein theoretically showed after 218 years that body mass depends on its speed and is related to energy

by the equation $E = mc^2$, where $c$ is the speed of light. Einstein's predictions were fully confirmed and form the basis of modern physics and technology, including nuclear.

But the advances in physics in the theory of strength and fracture of a solid are ignored.

Example No. 1. A crack 4.8 m long formed in the API 5L X46 oil pipeline (Argentina) formed after 20 years of operation []. Theoretical analysis of experimental results is based on the use of the Paris-Erdogan formula

$$\frac{da}{dN} = C\Delta K^m \quad (2)$$

where $a$ is the crack length ($m$), $N$ is the number of exposure cycles, $C$ is the proportionality coefficient (m/cycle), $m$ is the exponent, $\Delta K = K_{max} — K_{min}$ is the change in the stress intensity factor.

As a result of the calculations, the following values were obtained: $m$ = 6, $C = 3.818 \cdot 10^{-15}$ m/cycle.

Formula (2), proposed 300 years after Newton's publications, is identical to formula (1), but it contains gross errors.

1. The left-hand side of the $\frac{da}{dN}$ equation, called the crack growth rate, cannot be considered as a derivative, so N → 1, but not to zero.

2. The dimension $\frac{da}{dN}$ coincides with the dimension of the proportionality coefficient C. Therefore, the second factor is dimensionless, but it has a dimension by definition. Such a formula is devoid of physical meaning. This is enough to acknowledge that such a formula cannot be used, but other errors must be pointed out.

3. The formula contains five members, of which only the length of the crack is measured, the number of cycles is calculated. There is no experimental evidence of the functional dependence of the crack growth rate on the stress intensity factor. All experiments refute such a relationship.

4. The proportionality coefficient $C$ is meaningless, since it is based on a simple division of some numbers because the obtained value is comparable with the size of the atomic nucleus; length measurements accurate to the billionth of a nanometer the authors could not perform length measurements accurate to the billionth of a nanometer since there are no such devices and attempts to create are meaningless since the laws of mechanics cannot be used in this area.

Example No. 2 Equation NASGRO

$$\frac{da}{dN} = C\left[\left(\frac{1-f}{1-R}\right)\Delta K\right]^n \frac{\left(1-\frac{\Delta K_{th}}{\Delta K}\right)^p}{\left(1-\frac{K_{\max}}{K_c}\right)^q}$$

it is widely used to analyze the results of an experimental study of the technical state of structures and devices, but in all modifications and variants, it is identical to the Paris or Paris-Erdogan equation, because all expressions in parentheses do not have a dimension. This means that the NASGRO equation differs from the Paris Erdogan equation only in a numerical factor, but it contains all the same errors of the equations consists of the numerical value of the proportionality coefficient.

5. Newton formulated the law of attraction of bodies on the basis of a comparison of the acceleration of the Moon, the acceleration of gravity on Earth, the radius of the Earth, and the distance between the Earth and the Moon. The laws of Kepler, which formulated them on the basis of the Tycho Brahe protocols recorded as a result of many years of research on planetary motion, were important for Newton. Kepler's laws helped Newton understand the role of the center of gravity. But Newton's formula $F \sim \frac{M_1 M_2}{r^2}$ needed experimental verification. Only 111 years later Cavendish

experimentally determined the coefficient of proportionality and had the right to write

$$F = G\frac{M_1 M_2}{r^2}.$$

Here $M_1$ and $M_2$ are the mass of interacting bodies, r is the distance between them.

But only after 158 years, the planet Neptune was discovered "on a feather". The universality of Newton's law was recognized, and it became known as the law of universal gravitation.

The theoretical prediction of electromagnetic waves made by Maxwell and G. Hertz confirmed experimentally after 22 years.

The special theory of relativity, the theory of gravity, the theory of spontaneous and stimulated emission, proposed by Einstein, formed the basis of modern physics, space exploration, atomic nucleus energy, and the creation of lasers.

The brilliant prediction of the ability to control individual atoms, formulated by R. Feynman, was confirmed experimentally after 24 years.

These examples are given to show that Newton, Maxwell, Einstein, Feynman, and other theoretical physicists used the mathematical apparatus, deeply understanding, sometimes intuitively, the laws of nature. Mathematical extrapolation and interpolation are permissible only within the scope of the law of nature.

*Mathematical extrapolation and interpolation are permissible only within the scope of this law of nature. Stress intensity factors, Paris-Erdogan, and NASGRO equations, their modifications are offered without experimental verification and understanding of the laws of nature. Moreover, experiments refute the legitimacy of their use*.

The wording of the law established on the basis of small experimental data or prediction stimulates the search for broad experimental confirmation.

Only four photographs were taken by the author in the first experiment, but at the final stage, their number could be increased infinitely both for inorganic materials and for plant cells and living organisms. This indicates that atomic reactions are caused by the interaction of not only valence electrons, but also ions formed as a result of the removal of electrons from deeper energy levels.

The glow of blood vessels in the lungs and heart shown in Fig. 41 (1), Fig. 41 (2), Fig. 41 (3), due to the transition $Fe^{3+} \rightarrow Fe^{2+}$, is not accompanied by a fan-like study characteristic of water. Consequently, the water molecule dissociated into hydrogen and oxygen atoms before it.

*This allows us to conclude that the source of such radiation is iron and hydrogen ions.*

The high penetrating ability of an electromagnetic pulse, described in the first chapter, indicates the discovery of another effect in which electromagnetic radiation pulses are generated with a duration shorter than the relaxation time for resonant transitions in various media. This fact can be explained by that the energy of p-radiation caused by deformation is 50-100 keV, which corresponds to a frequency of $10^{18}$-$10^{19}$ Hz, which is four orders of magnitude higher than the frequency of a femtosecond laser, with which self-induced transparency is observed.

The energy of X-rays is due to the potential difference, accelerating the electrons to such an energy that is enough to remove electrons from levels close to the nucleus. The absence of a potential accelerating difference in the experiments demonstrated above poses us with the problem of detecting an energy source that can replace an electrostatic generator.

*An analysis of the results of an experimental study convinces us that atomic reactions in a substance containing hydrogen occur with the participation of protons since hydrogen atoms are ionized earlier than atoms of other elements.*

Hydrogen embrittlement of steel, grinding of palladium upon saturation with hydrogen are caused by the transformation of a hydrogen molecule into a proton particle devoid of electrons, which is an integral part of atomic nuclei. The idea of the participation of protons in reactions occurring in the cells of a living organism was expressed in the works of G. N. Petrakovich [3.2]. However, he was mistaken that a proton in a metal can travel a considerable distance due to its low

mass. A proton, like an electron, has a charge. The directed motion of a charged particle in an electron-ion plasma is possible only under the influence of an external electric field, but even in this case, the speed of the directed motion is very low due to proton collisions with electrons and ions. The total electric current in the substance, due to the conduction current and the bias current, is set along the conductor or dielectric with the speed of electromagnetic waves.

### 3.2. P-radiation in electric and magnetic fields

#### 3.2.1. P-radiation due to electric current

The results of the experimental verification of this hypothesis are demonstrated below.

P-radiation, which was observed during a chemical reaction (Fig. 28) and corrosion (Fig. 27), which is also the result of a chemical reaction, suggests that it should be observed during electrolysis and electric current in metals.

The results of the experimental verification of this hypothesis are demonstrated below.

**Experiment No**. 1.


**Fig. 50**

Photos shown in Fig. 50 illustrate p-radiation caused by the movement of ions in a lead battery between the cathode (frame 4), the anode (frame 1), and in the region between them (frames 2 and 3). Current strength 1 A, exposure 18 hours. The container was located under the battery.

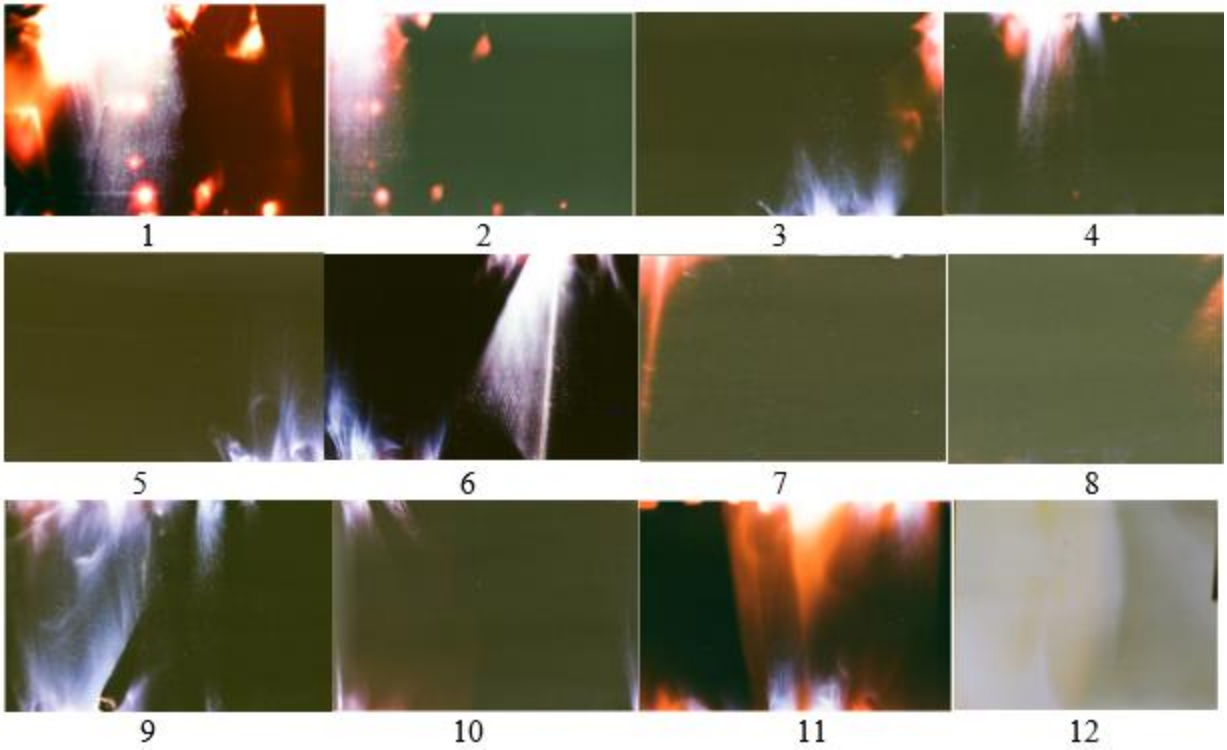


**Fig. 50 (1)**

**Experiment No. 2**

Two copper wires leading to the lightbulb were located on the surface of the container with the photographic film along with it. The light bulb with two spirals was located above the container covered with aluminum foil to reflect light at the height of 6 cm. Lead plates were located under the light bulb on the surface of the container. This eliminated the heating of the container. Current from the battery, with a power of 1 A, was passed for 18 hours. Photos shown in Fig. 50 (1) illustrate radiation recorded on photographic film. Fan-shaped radiation is recorded at eleven out of twelve frames.

The ordered arrangement of the luminous areas on frames 1 and 2 coincides with the shape of the spirals in the lightbulb and their attachment points. Such a coincidence cannot be accidental.

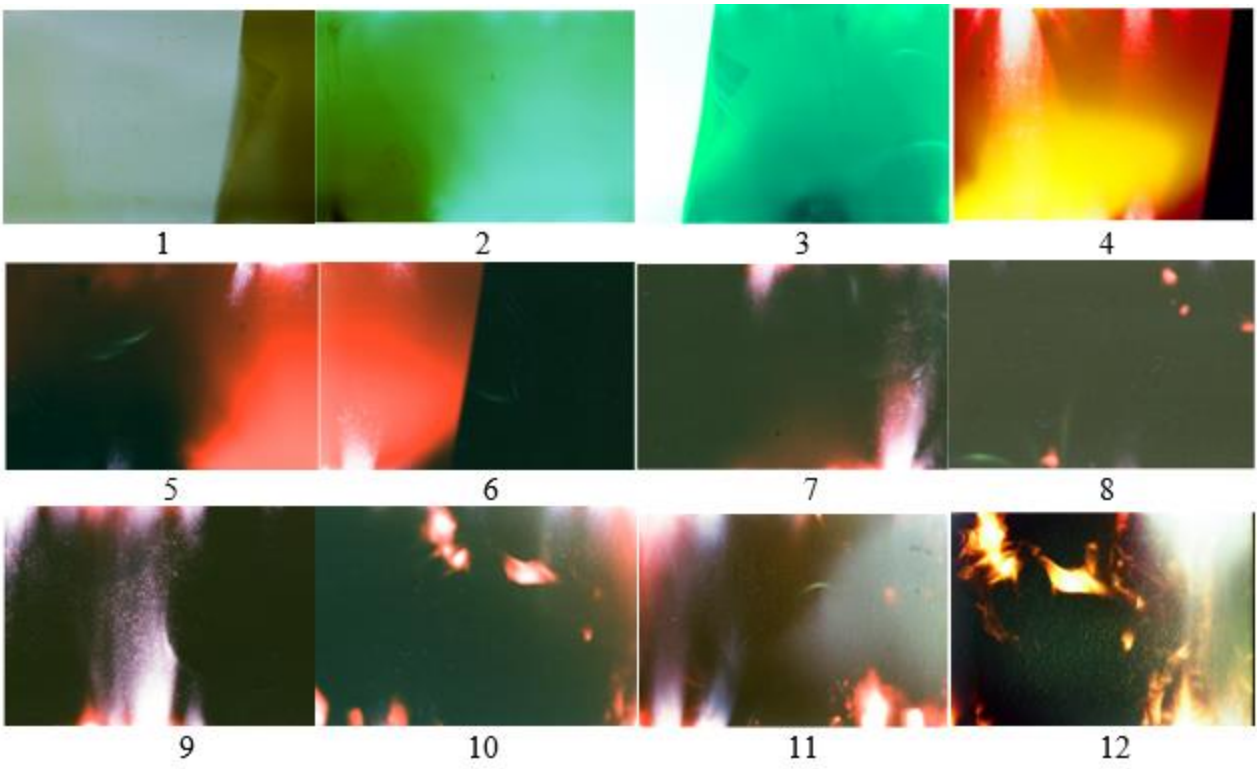


**Fig. 50 (2)**

**Experiment No. 3**

Photos shown in Fig. 50 (2) illustrate p-radiation that has arisen in a conductor through which an alternating current has passed. Fan-shaped radiation is recorded at ten out of twelve frames.

The photos obtained to confirm the fact that the electric current through the metal is accompanied by electromagnetic p-radiation, the mechanism of which must be explained. Note that the current in the conductors passed in the opposite direction.

The totality of facts allows us to conclude that the hypothesis about the participation of protons in the formation of the energy spectrum recorded in all the photographs given in the book is the most plausible.

*However, the proposed hypothesis needs confirmation, which can only be obtained on the basis of experimental studies by modern methods with changes in temperature, magnetic and electric fields, the use of tritium, resonance methods, etc.*

The speed of the chaotic motion of the proton is so high that the proton energy is sufficient to remove the electron from deeper energy levels. The experiment indicates that the direction of the p-radiation of the photon formed after recombination and its phase are random. Therefore, such photons can form a point defect, but not a pore or crack.

### 3.2.2. The effect of a magnetic field on p-radiation

**Experiment No. 4.**

A copper wire, through which a direct current of 1 A was passed, was located on the surface of the container with a photographic film having a length of 580 mm, under which in the center of the container was a steel plate with a length of 216 mm. A permanent magnet with a diameter of 76 mm was placed above the container, attracting the plate. Photographs illustrating the electromagnetic radiation recorded after eighteen hours of exposure are shown in Fig. 50 (3).

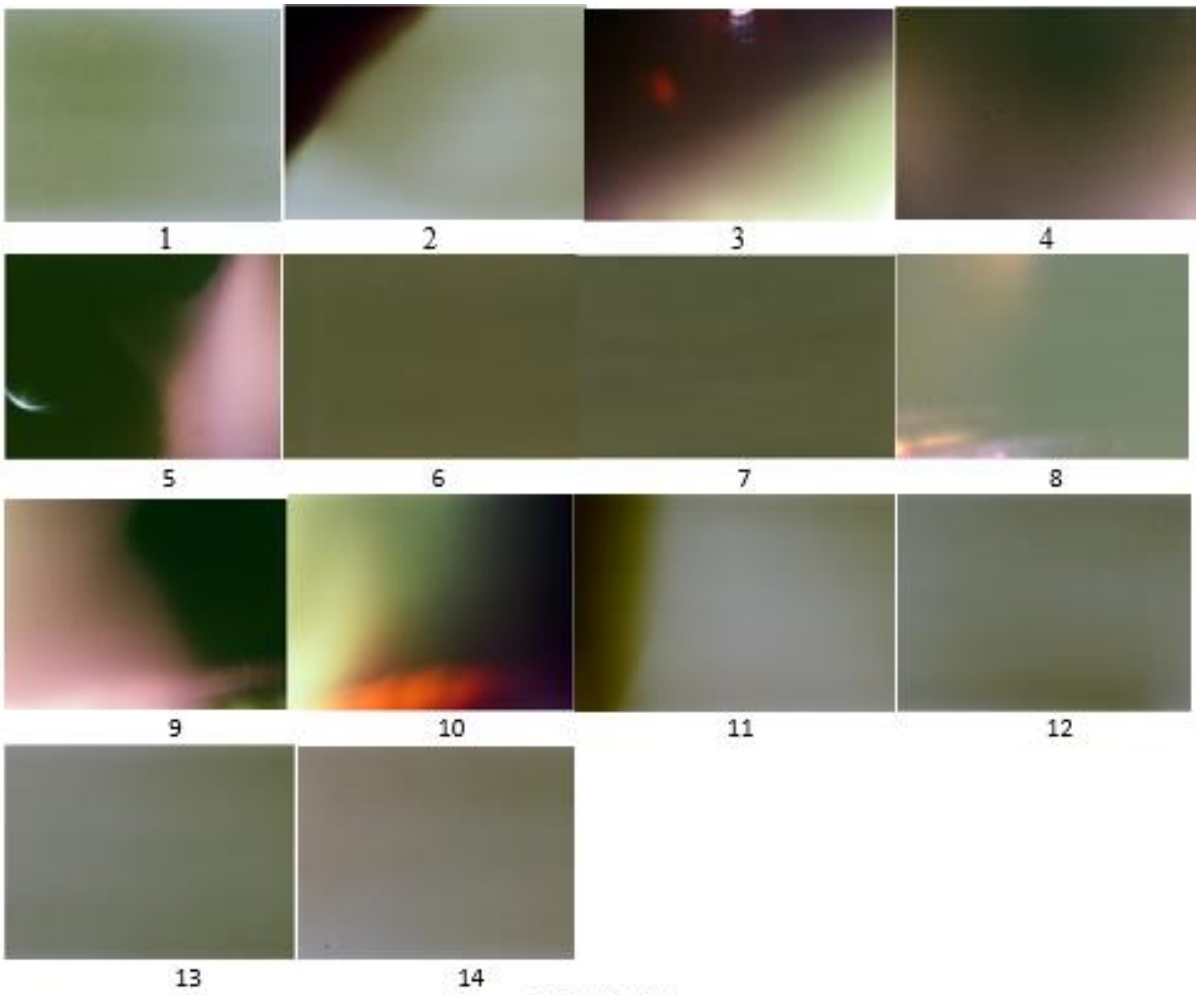


**Fig. 50 (3)**

The photographs show that the fan-shaped radiation disappeared completely where an external magnetic field was applied to the magnetic field of the current. It is observed only in frame 3, located outside the field of the permanent magnet.

Electromagnetic waves in metal create an electric current caused by the movement of electrons.

It is known that a conductor in which current flows in a magnetic field is subjected to an Ampere force. The trajectory of a charged particle moving in a magnetic field changes under the action of the Lorentz force.

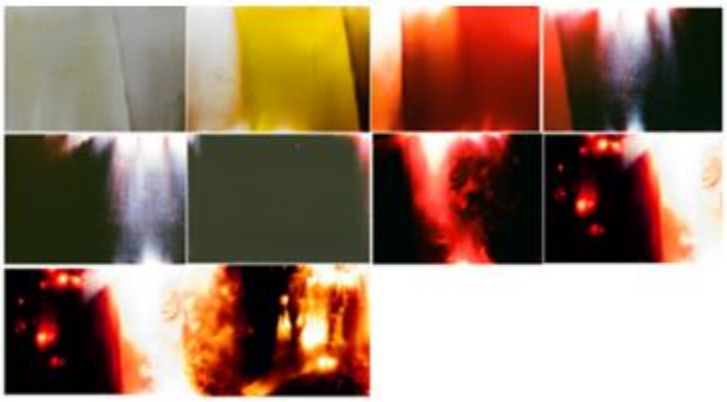

Fig. 51 (1)

**Experiment No. 5** demonstrates the possibility of detecting signals at a distance from the radiating surface, which can be used to analyze damage in places where the installation of sensors is impossible. The experimental results are given below**.** The container with the film was placed at two points on the vertical surface of this corner part of the car trailer so that the central part of the container was separated by 21 mm from it. An ax hit the butt of the corner p-radiation is recorded in Fig. 51 (1).

Fan-shaped radiation is observed in eight frames out of ten.

**Experiment No.6.**

Fig. 51 (2)

The container with the film was placed at two points on the vertical surface of this corner part of the car trailer so that the central part of the container was separated by 21 mm from it. An ax blow was made on the butt of the steel plate. The p-radiation placed on the film is shown in Fig. 51 (2). Fan-shaped radiation is observed in six frames out of twelve.

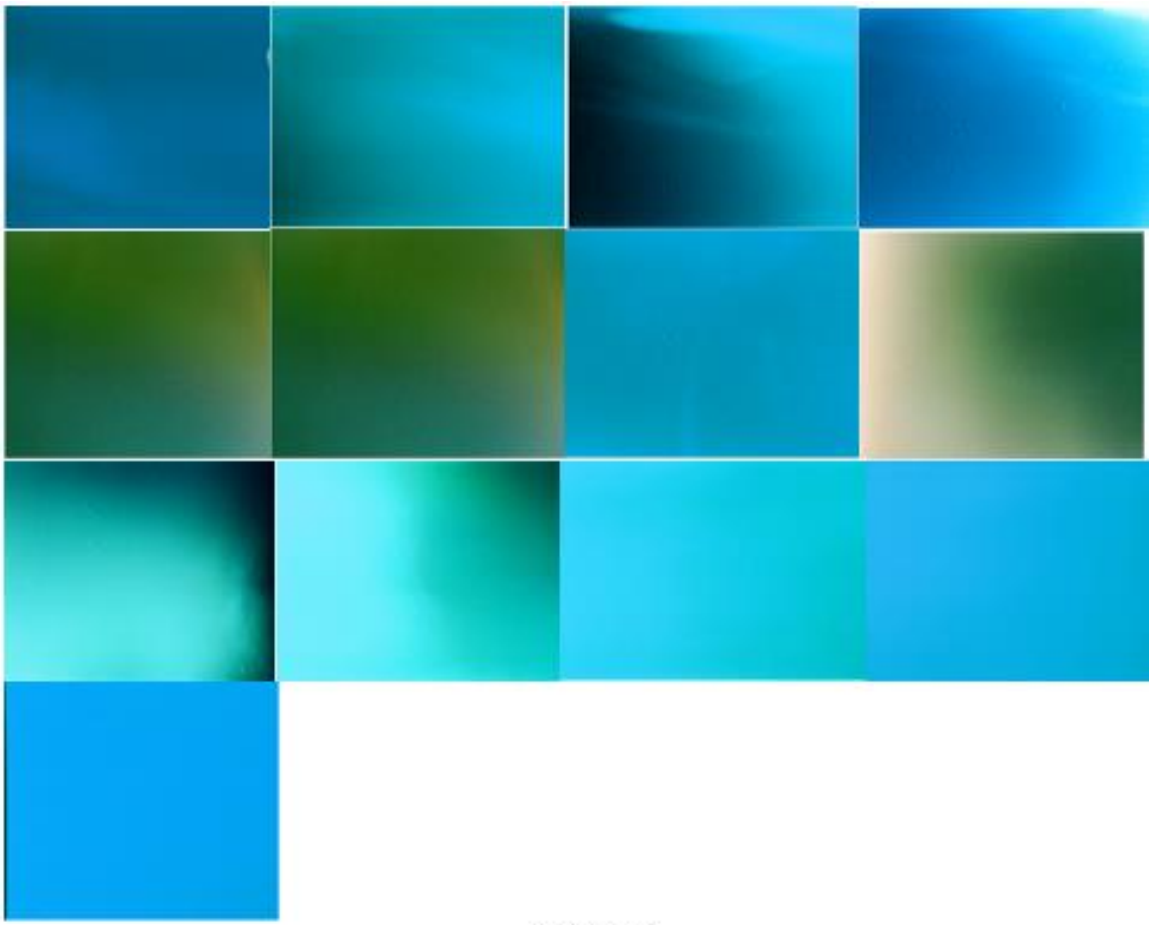

Fig. 51 (3)

**Experiment No.7**

A container with the film was attached to the vertical surface (*xz*) of this corner part of the car trailer at all points. A permanent magnet with a diameter of 76 mm was attracted by metal from the side of the container in its central part. An ax blow was made on the butt of the steel plate (surface *xy*) outside the container to the right and the left. The p-radiation recorded on the film is shown in Fig. 51 (3). Fan-shaped radiation is not recorded in any of the eleven frames.

**Note.** The magnetic field vector is perpendicular to the ax velocity vector.

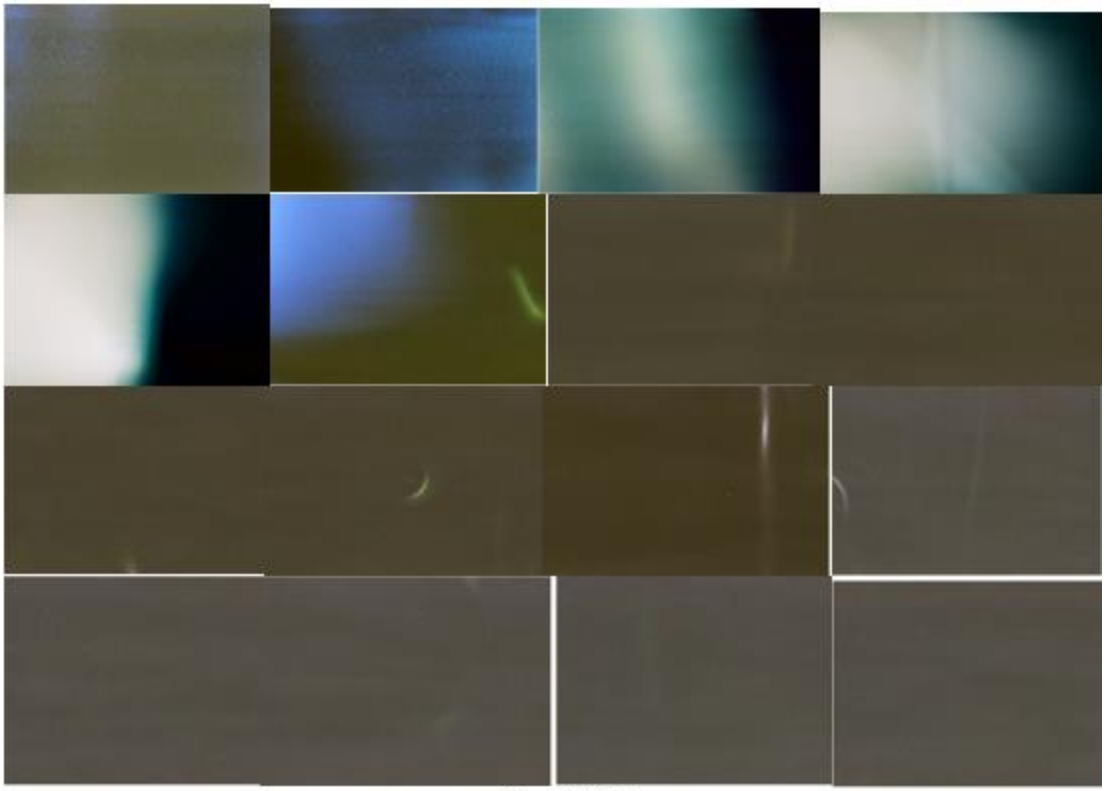

Fig. 52 (1)

**Experiment No.8.**

Two containers with a photographic film were located on both sides of the steel plate (surface *xz*), each of which was pressed to the surface with adhesive tape and a magnet. The area of the two magnets was 26% of the container area. The ax hits were on the surface *xy* outside the container on the right and left. Twenty-seven frames recorded on one of the films are shown in Fig. 52 (1) and Fig. 52 (2).

Twenty-seven frames recorded on a second film are shown in Fig. 53 (1) and Fig. 53 (2).

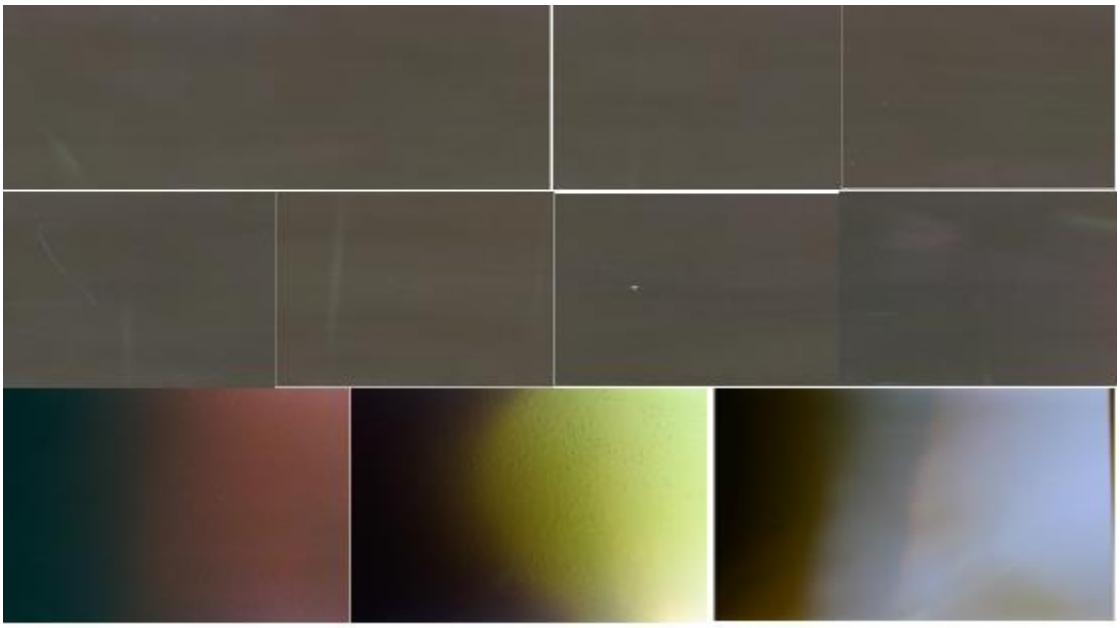

**Fig. 52 (2)**

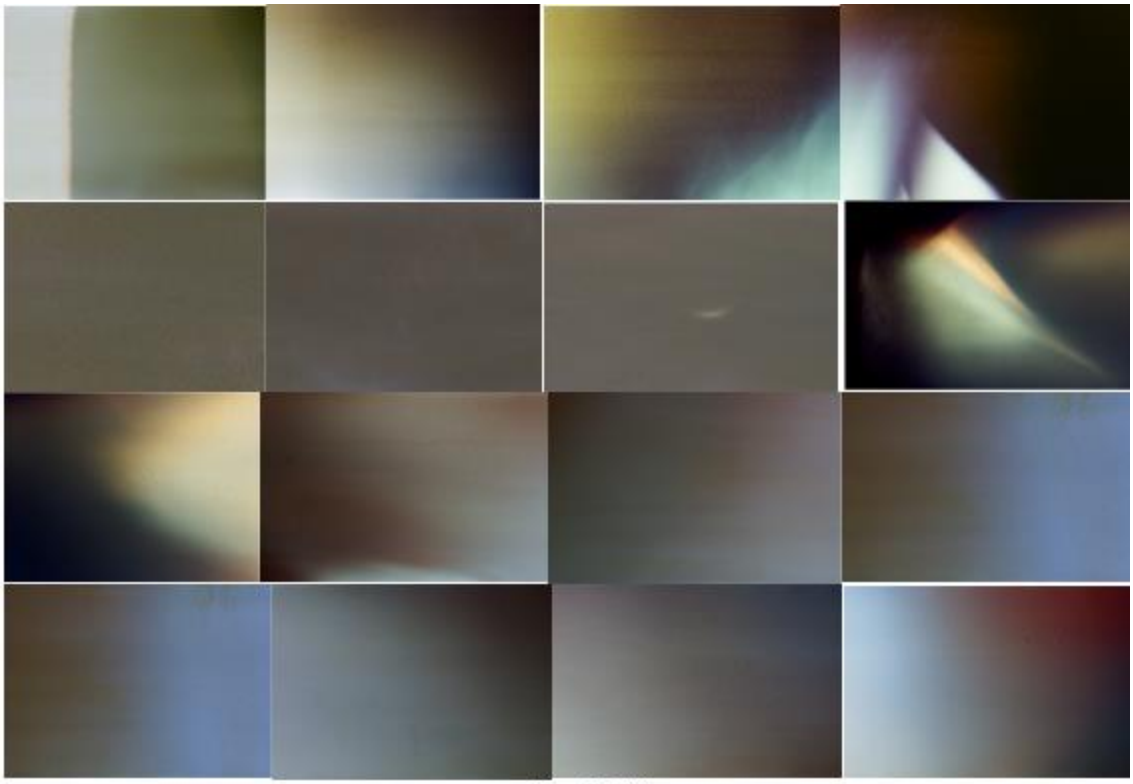

**Fig. 53 (1)**

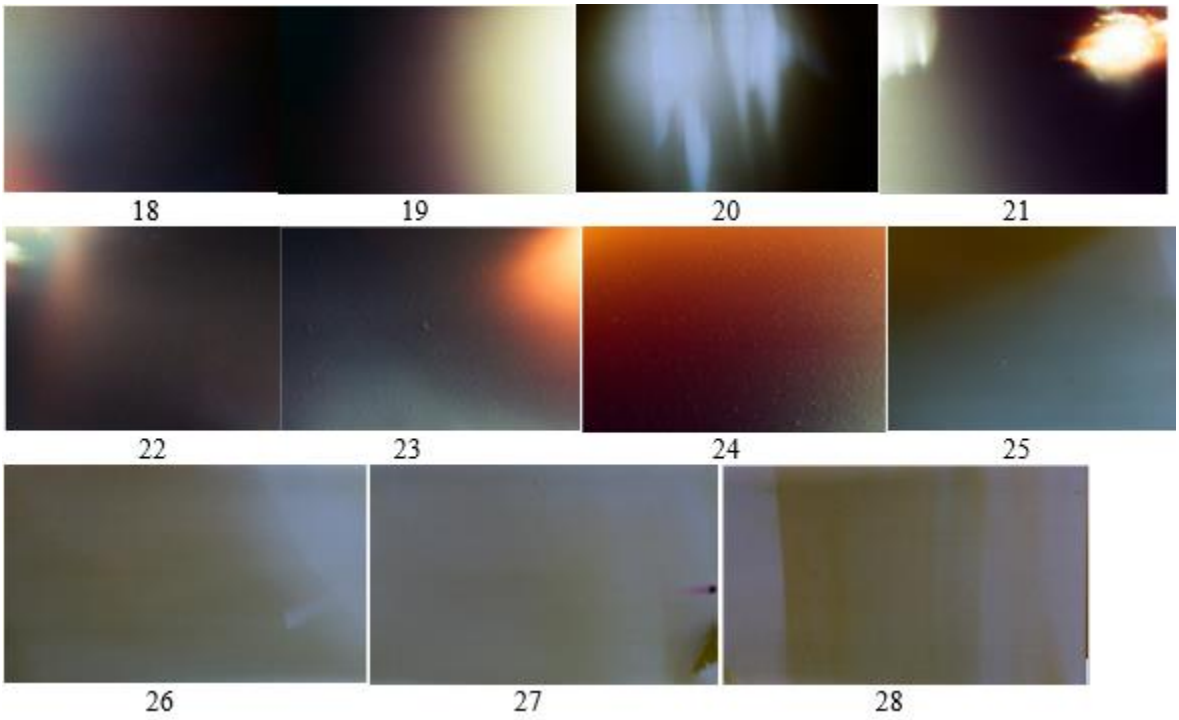


**Fig. 53 (2)**

The magnetic field in experiments No. 7 and No. 8, directed perpendicular to the direction of the fan-shaped radiation, inhibited the reaction of its radiation. A magnetic field, changing the direction of a charged particle, does not change the magnitude of the velocity.

**Experiment number No. 9**

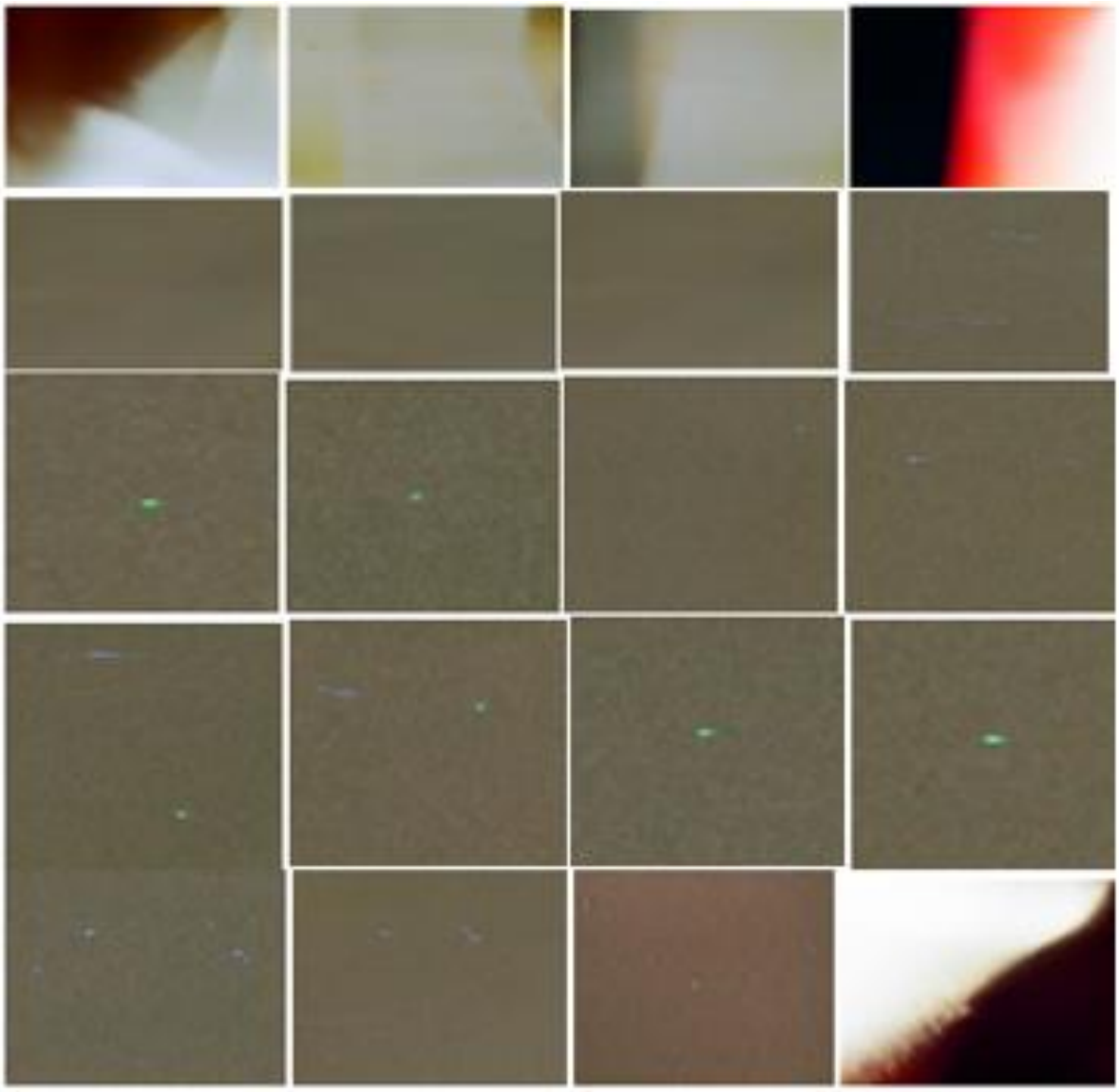

Fig. 54 (1)

A container with a photo film was placed on the surface *xy* of an aluminum alloy beam. The impact by ax tip was made on the right and left of the container in the direction of the *z*-axis. Fig. 54 (1) illustrates p-radiation recorded at 20 frames. The reaction of aluminum alloy to impact is significantly different from the reaction of steel. Color photographs are observed only in five frames near the place of impact. Point luminous objects or objects in the form of strokes are recorded on most frames. Such objects were previously observed during drilling of an aluminum alloy, as shown in Fig. 38 (1) and Fig. 38 (2).

**Experiment No. 10.**

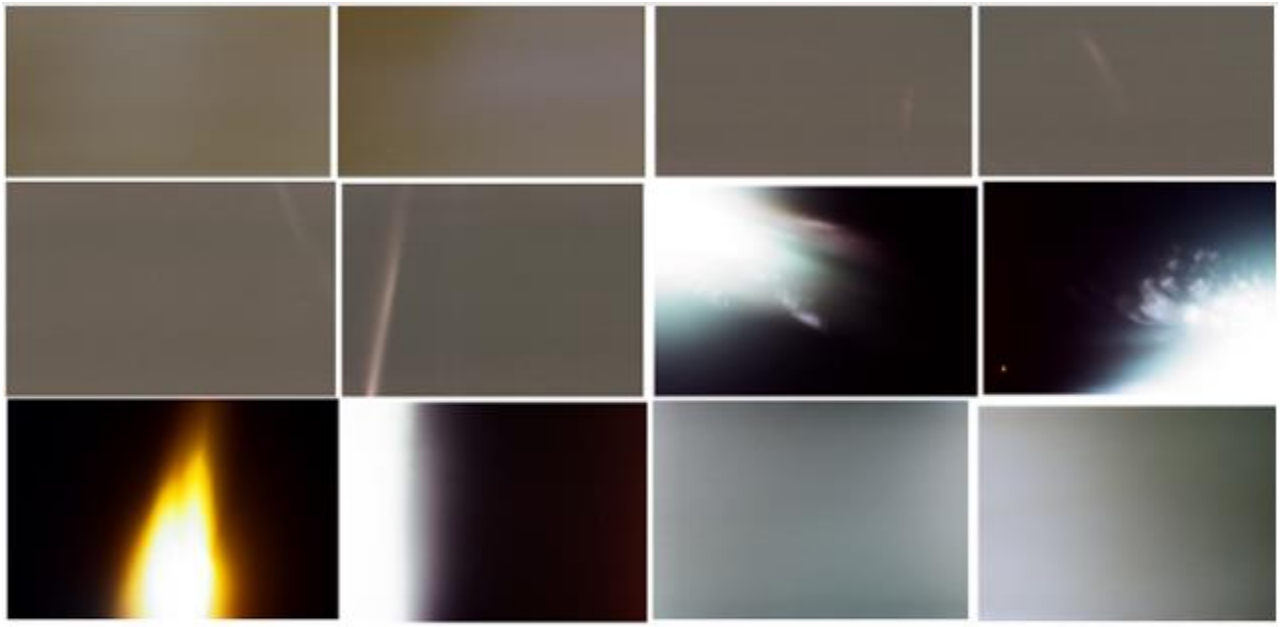

Fig. 55

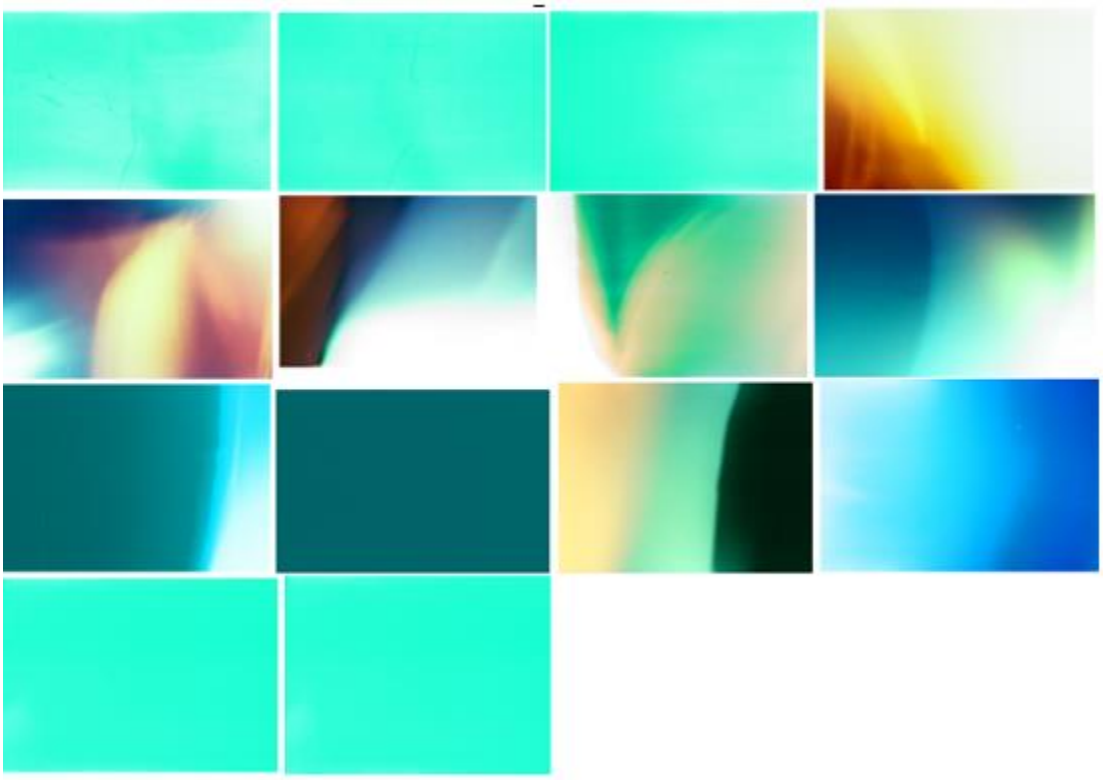

Fig. 56

Photos shown in Fig. 55 and Fig. 56, obtained by arranging a container with a film on the surface *xz* of an aluminum alloy beam. The impact was applied on the *xy* surface in the direction of the *z*-axis. Fig. 55 illustrates a shock response without a magnetic field; Fig. 56 illustrates the response to a shock with a magnetic field.

### 3.2.3. Analysis of the results of an additional experimental study

An additional experimental study was carried out to answer the questions that arose in the analysis process. The photographs obtained as a result of the experiment allow us to draw the following conclusions.

1. An external magnetic field changes the character of p-radiation in the iron alloy, caused by both electric current and shock. Exposure to a magnetic field led to a decrease in the surface radiation density (luminosity) due to an increase in the radiation area. Using this effect can reduce the probability of bond breaking between atoms, which leads to erosion, peeling, cracking.

2. The distribution of energy in an aluminum alloy under external influence leading to self-emission transparency differs from the distribution of energy in an iron alloy. Maximum radiation is observed in the impact region. This is particularly clearly shown in Fig. 54 (2).

3. The impact causes the charge to shift in the direction of the impact. The nature of the effect of the magnetic field depends on the direction of the magnetic field with respect to the direction of impact (the movement of charged particles). Of particular interest is the comparative analysis of the photographs shown in Fig. 51 (3) and Fig. 56, illustrating the fact that the frequency of a photon causing a glow from an aluminum alloy and an iron alloy is the same. Such a coincidence cannot be accidental.

4. The influence of a magnetic field on the character of self-emission transparency indicates that the analysis of atomic reactions should be carried out, taking into account the magnetic quantum number.

5. The experiment is intended to prove the necessity of abandoning methods of analysis of the processes of hardening and fracture of a solid based on classical mechanics. Each photograph serves as evidence that the response of individual atoms and their combination to an external action is due to electromagnetic interaction.

6. The whole variety of discovered effects can be used in practice.

## 3.3. Theoretical Foundations of Strength and Fracture of Materials

Ertl's main research [3.1] is devoted to the problem of catalysis, in which the surface plays an important role. He said: “The atoms in the surface layer of a solid have fewer neighbors than those in bulk and are hence chemically unsaturated and may form new bonds (=chemisorption) with suitable molecules impinging from the adjacent gas or liquid phase. By this step, existing bonds will be modified or may even be broken (=dissociative chemisorption). The surface species formed may jump from one site to neighboring ones, then may react with others, and the formed produced molecules eventually leave the surface (=desorption). If operated in a flow reactor, the catalyst can, in this way, continuously operate without being consumed”.

The use of modern experimental technology provided an opportunity to understand the interatomic interaction processes leading to an acceleration of the chemical reaction and the production of the final product, for example, fertilizers.

A photograph of the platinum surface [3.1] obtained by catalytic oxidation of CO using photoemission microscopy and shown in Fig. 56 illustrates spiral waves in the 500 μm region. Such waves are characteristic of Belousov-Zhabotinsky vibrational reactions.

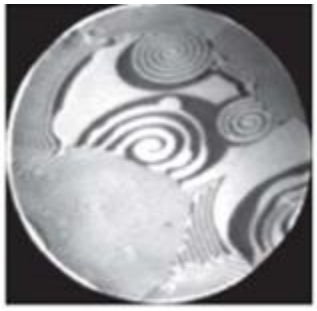

**Fig. 56**

Colored and white figures of various shapes with clearly defined boundaries, given in the book, indicate the existence of local groups of atoms that emit energy at the same frequency. Such radiation is possible only for atoms of the same chemical element.

Small red or red and white shapes that have a distinct circle shape, similar to those shown in Fig. 50 (1) frames 1 and 2, or Fig. 50 (2) frames 8 and 10 were observed repeatedly in the presence of water. Fan-shaped radiation is observed repeatedly during rail deformation, metal corrosion, metal solidification, etc. Analysis of photographs shows that simultaneously with white radiation, radiation with a lower frequency appears, indicating that in p-radiation transitions of electrons to valence, energy levels are realized.

Advances in the study of nano-materials and their surfaces are due to the use of electron microscopy. But the electron microscope is not applicable to living organisms, large objects; black and white image does not allow to determine the frequency characteristics of the studied object. The energy of electrons accelerated by a potential difference of 20 keV is 4600 times higher than the binding energy of iron atoms in a crystal. Therefore, the method is destructive.

***The photographs shown in the second chapter, and especially in Fig. 46 (1) and Fig. 46 (2), indicate that pathological changes in the cells of plants and living organs will be displayed on***

***the nimargram. This will distinguish a malignant tumor from a benign one and analyze the processes leading to aging.***

P-radiation caused by deformation in one direction propagates in different directions, as shown in many photographs. Thus, self-emission transparency is due to the fact that a change in the electric field that has arisen in a certain region propagates in the form of electromagnetic waves.

The theoretical basis for the strength and destruction of materials is quantum electrodynamics.

It may seem strange that we are talking about quantum electrodynamics, but not about quantum mechanics. Understanding the mathematical apparatus of quantum electrodynamics, like quantum mechanics, requires serious training, but we do not need it, because we restrict ourselves to the fact that, firstly, quantum electrodynamics is a theory that describes the interaction of photons with charged particles, in particular, electrons; secondly, this is the most accurate physical theory; thirdly, it gives quantitative forecasts that can be verified experimentally with extremely high accuracy.

Quantum theory is based on experimental facts that are considered impossible from the standpoint of classical mechanics. The rest mass of the photon and its charge are equal to zero. This fact is established with high accuracy, which is not available to mechanical measurement methods. But a photon can turn into a particle and an antiparticle, the rest mass and charge of which are not equal to zero. A particle, such as an electron, has wave properties; particles can interfere and diffract. Energy, momentum, and angular momentum are quantized.

Quantum mechanics and quantum electrodynamics are created on the basis of axioms, postulates, and laws that differ from classical ones. We will consider the hypothesis to be an axiom, which is based on an experiment and there are no experiments that refute it. This will create a quantum theory of strength, which is not yet available.

**3.3.1. Axioms, postulates, and the law of destruction**

**Axiom 1**. *All* things are made of atoms—little particles that move around in perpetual motion, *attracting each other when they are a little distance apart, but repelling upon being squeezed into one another.* (R. Feynman).

**Axiom 2**. Atoms of one chemical element having a different configuration of the electron shell can be simultaneously present in the material. (Author).

**Axiom 3**. The energy state of an atom is determined by the number of electrons and their location around the nucleus.

**Axiom 4**. The integrity of a solid is due to the electromagnetic interaction that holds the atoms in dynamic equilibrium. The main physical parameter characterizing the equilibrium is the binding energy of atoms. By bond, energy is meant the energy that is needed to separate a solid into separate neutral atoms at 0ºK. Bond energy is measured in eV/atom. 1 eV=$1.60218 \cdot 10^{-19}$J.

**Postulate 1.** All processes in the matter in the absence of nuclear reactions occur as a result of atomic reactions due to electromagnetic interaction. (According to E. Noether's theorem).

**Postulate 2.** The external influence energy is distributed unevenly in the material due to electromagnetic wave interference caused by reflection at the boundaries of the inhomogeneity. This leads to the formation of standing waves, as a result of the absorption of which the structure of local regions changes. (Author).

**Postulate 3.** The potential energy of a deformed body is equal to the sum of the bond energy of atoms and the sum of energy of metastable atoms of local regions. (Author).

**Definitions**:

- A solid consists of atoms of various chemical elements in a certain quantitative ratio, which is called composition.
- The change of a structure is not only a change in the mutual arrangement of atoms but also the configuration of their electron shell.
- The anatomic reaction is a process in which an atom absorbs photons or electrons; emits photons or electrons. The atomic reaction is recorded with the help of characters, taking into account the law of conservation of energy and the law of conservation of charge.

**The law of destruction of solid**

The analysis of numerous experimental facts made it possible to formulate the law of destruction of a solid.

*The formation of pores, cracks, and the destruction of a solid is the result of a break in the bond between a finite number of atoms that absorb photons emitted stimulated by metastable atoms of local groups resulting from the conversion of mechanical energy into electromagnetic energy, in which the excitation of atoms occurs upon absorption of photons and/or the action of protons formed as a result of ionization of hydrogen atoms*.

This formulation of the law characterizes the necessary conditions for destruction and sufficient arguments for describing the mechanism of the natural phenomenon. It clarifies the understanding of the term p-radiation, indicating that the excitation of atoms during an atomic

reaction occurs both by photons and protons. The predominance of a particular type of excitation should be established in a focused experimental and theoretical study.

The law based on the experiment is proposed as the most probable hypothesis or postulate, which can be refuted only by experiment.

*The law of destruction predetermines that the reliability and durability of the material are determined by the ratio of the rate of accumulation energy in local groups of atoms called the domain of destruction to the rate of its dissipation, but not by strength.*

The conducted experiment refutes the postulates of von Mises and the model of Irvine, which underlie modern ideas about the source of energy and physical processes leading to destruction.

The theoretical basis for describing the processes of destruction is the quantum-mechanical interpretation of Maxwell's ideas, which he outlined in the totality of articles, reports, and letters.

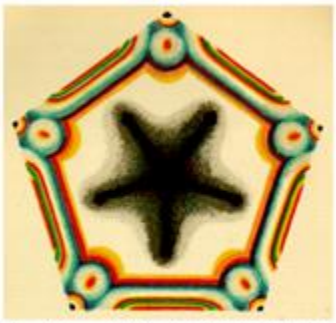

Plate III a: CHROMATIC EFFECTS OF A PENTAGON OF UNANNEALED GLASS IN POLARIZED LIGHT

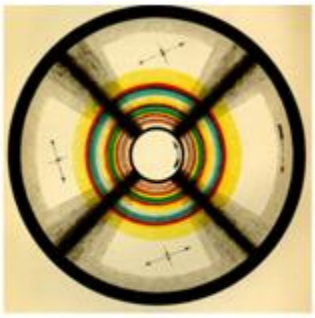

Plate IV: DIAGRAM SHEWING THE COLOURS EXHIBITED BY A PLATE OF GELATINE WHEN EXPOSED TO A TORSIONAL SHEAR

The study of Maxwell's work on mechanics cannot be limited to one letter to Thomson [1], as Timoshenko did. Maxwell predicts a special area, which we now call nanoscale, in one article; proposes a method similar to the finite element method, but based on bending, in another article; opens the phenomenon, which is called the Maxwell effect; investigates mechanical phenomena through the interference of polarized beams and demonstrates in the lecture the figures shown in Fig. Plate III и Plate IV.

The idea of bias currents, the reality of which was confirmed experimentally, will help us understand the mechanism of the transformation of mechanical energy into an electromagnetic one. Maxwell suggested that the formation of the potential energy of distortion is due to the displacement, but not the stress, which is caused, as is customary in modern theories. The analysis of Maxwell's works on mechanics was considered in [1.13].

### 3.3.2. Quantum-mechanical interpretation of Maxwell's equation

Quantum mechanics allows us to estimate the energy state of an atom or group of atoms in the local region of materials theoretically, and modern experimental methods allow us to verify this estimate.

Therefore, we will consider all atoms (ions) at which the property of the material does not change, regardless of what their energy state is, normal, signifying *AN*. A change in the properties of a material means that the energy state of a group of atoms has changed. Such atoms are called morbid (painful, pathological), denoting *AM*. This simplifies the description of processes without violating scientific rigor. We can describe all the changes that occur in the material of structures and devices using five atomic reactions occurring as a result of the exchange of atoms by electrons e- and photons hν, where h is the Planck constant, ν is the photon frequency, and hν is its energy.

1. $AN + h\nu \rightarrow AN^* = AM$ (I). The transition of an electron to an excited metastable level.

2. $AN + h\nu_1 \rightarrow AM^+ + e^-$ (II). Forced additional ionization.

3. $AN + e^- \rightarrow AM^- + h\nu_2$ (III). Recombination of an ion and an electron.

4. $AN^* - h\nu_3 \rightarrow AN$ (IV). The spontaneous or stimulated transition of an excited atom with the emission of energy.

5. $AM^+ + e^- \rightarrow AN + h\nu_4$ (V). Recombination of a morbid atom and an electron.

Here $AM^+$ is a morbid atom (ion) whose charge has grown; $AM^-$ Morbid atom (ion), the charge of which decreased.

Using the concepts of normal and morbid atoms allows you to interpret the Maxwell's equation

$$U = U_1 + U_2 \quad (1)$$

from the standpoint of quantum mechanics.

The total energy of the atoms of the element at the initial moment $t = 0$ is due to the energy state of normal atoms

$$U_1(0) = \sum_{i,j} \varepsilon_i N_{n,j}(0) \quad (2),$$

where $\varepsilon_i$ - is the energy of a normal atom of the *i* type, $N_{i,j}$ is the number of atoms of this sort. The energy of morbid atoms is neglected. At time $t = t_c$, the total energy

$$U(t_c) = \sum_{i,j} \varepsilon_i N_{n,j}(t_c) + \sum_{k,l} \varepsilon_k N_{m,l}(t_c) \quad (3),$$

$$U_2(t_c) = \sum_{k,l} \varepsilon_k N_{m,l}(t_c) \quad (4)$$

$\varepsilon_k$ -the energy of *k*-type morbid atoms, $N_{m,j}$ -their number. Restricting ourselves to one type of normal and one type of morbid atoms, we write:

$$U(t_c) = \varepsilon_i N_n(t_c) + \varepsilon_k N_m(t_c) \quad (5).$$

The experimental confirmation of the Zhukov's formula in the study of various crystalline and amorphous materials allows us to conclude that the number of morbid atoms increases exponentially:

$$N_m(t_c) = N_m(0)e^{\Gamma} = N_m(0)e^{\frac{A}{Dk_BT}} \quad (6),$$

$$\text{where } \Gamma = A/Dk_BT \quad (7)$$

wear rate equal to the ratio of the energy storage rate in the destruction domain

$$A = U_2/t \quad (8)$$

to the speed of her dissipation

$$B=Dk_BT \quad (9).$$

Here, the parameter *D* is similar to the Einstein coefficients in the theory of spontaneous and induced radiation, $k_B$ is the Boltzmann constant, and *T* is Kelvin temperature.

The parameter $\Gamma$ has no analogs in classical mechanics. Its introduction is due to the Heisenberg uncertainty relation $\Delta E \cdot \Delta t \geq \frac{\hbar}{2}$, where $\hbar$ is the Dirac constant, since the accumulation of energy is due to the emission and absorption of photons, while the dissipation of energy is due to spontaneous and thermal radiation.

### 3.3.3. Mechanism of formation domains of destruction

The problem of the energy source is the cornerstone of any physical theory. The experiment described above not only confirmed the hypothesis of a real energy source, the radiation of which leads to the formation of cracks and destruction but also indicates the ways in which a natural phenomenon called internal triboluminescence can be used to more accurately predict the wear of the elements of structure and devices to prevent catastrophic destruction. The experiment refutes the hypothesis that the source of energy is elastic energy accumulated in stress concentrators. The energy of a p-ray photon is millions of times higher than the energy of an atom in stress concentrators, and the speed of a photon is 50,000 times higher than the speed of a phonon (a quantum of acoustic waves).

This fact is so significant that neglecting is unacceptable.

The hypothesis of the formation of a destruction domain was formulated in [1.8]. A detailed analysis of the processes leading to the destruction of a solid is performed in [1.9].

The emission of electrons upon the destruction of a solid was repeatedly observed, but this fact cannot be confirmed or refuted in this experiment since the distance from the radiator to the film was 2-5 cm. This layer of air and the rubber layer completely absorb electrons if they are radiated. The radiation of X-rays in the stratification of tape was discussed in the monograph [1.9]. However, these effects were associated with an electrical discharge between the separating bodies.

Discharge in the air (dielectric breakdown) is accompanied by electromagnetic radiation. The photons' frequency and energy depend on the potential difference. X-ray radiation is possible when electrons emerge in the discharge channel, are capable of removing an electron not from the valence shell of the atom but from deeper energy levels.

Such photons arise in the lightning, which arises at a potential difference of millions of volts. However, the high-frequency discharge in gases (the Tesla experiment) is accompanied by the emission of photons whose energy is many times lower than the energy of the X-ray photons.

The frequency of radiation in modern microwave ovens is 2.45 GHz. Consequently, the photon energy is $1 \cdot 10^{-5}$ eV, which corresponds to the energy of the thermal vibrations of the atoms. Photons of this range are absorbed by atoms on the metal surface.

This means that in the experimental study described above, a completely different physical phenomenon is observed, due to the emission of photons whose energy is sufficient to break the bonds of a large number of atoms.

This means that in the experimental study described above, a completely different physical phenomenon is observed, due to the emission of photons whose energy is sufficient to break the bonds of a large number of atoms.

Numerous experimental studies of the processes of destruction of nano-, meso- and macro objects allow us to formulate the fundamentals of the physics of destruction.

This formulation of the natural law contains all the necessary and sufficient information in order to use it to prevent the catastrophic destruction of structures and devices elements.

To do this, we need:

1. understand the mechanism of energy generation processes, the radiation of which is sufficient to form defects that prevent the further operation of an element of structure or device.

2. experimentally find those local areas, called destruction domains, in which the accumulation of energy takes place;

3. determine the potential energy, the rate of energy accumulation and the rate of its dissipation;

4. to find non-destructive methods of constant monitoring of the domain of destruction;

5. find methods to reduce the velocity of energy accumulation and increase the velocity of its dissipation in order to prolong the time of safe operation.

### 3.4. X-ray radiation of celestial objects and p-radiation

The experiment showed that the loss of integrity of a solid body and its destruction is caused by the absorption of photons, i.e., by quanta of electromagnetic radiation of atoms, including in the X-ray range, due to the participation of *ions*.

The justification of such a conclusion is possible only from the standpoint of quantum mechanics, a brief summary of which is given.

The formation of molecules, compounds, and a solid from atoms is due to the chemical bond between them, which is established as a result of the attraction of electrons and nuclei of atoms and the repulsion of electrons from electrons and nuclei from each other. The positive charge of the nucleus, equal to the number of protons, corresponds to the serial number of the element in the periodic table. The number of electrons of a neutral atom is equal to the number of protons in the nucleus.

The arrangement of electrons in the electron shell is characterized by four quantum numbers in accordance with two rules: 1) the electrons are arranged in the order that determines the minimum energy; 2) each electron in an atom differs from the others in at least one quantum number. We restrict ourselves to the main quantum number, which denotes the period in the periodic table, and orbital, which denotes the shell. Period No. 1 contains two elements. The first shell is denoted by the letter s. It can have no more than two electrons. Thus, two elements: $1s^1$ - hydrogen, $1s^2$- helium. Period 2 contains eight elements from number three (Li, electronic structure $1s^22s^1$) to number 10 (Ne, electronic structure $1s^22s^22p^6$). Thus, helium and neon have completely filled shells. Atoms of these elements do not enter into a chemical reaction.

Atoms of these elements do not enter into a chemical reaction.

Period No. 3 contains eight elements from number 11 (Na, electronic structure [Ne] $3s^1$) to number 18 (Ar, electronic structure $1s^22s^22p^63s^23p^6$).

Table 1

Electron Configuration

The ground state electron configurations of octavalent elements

| Name | Symbol | Electron configuration | Name | Symbol | Electron configuration |
|---|---|---|---|---|---|
| Iron | Fe | $[Ar]3d^6 4s^2$ | Ruthenium | Ru | $[Kr]4d^7\ 5s^1$ |
| Cobalt | Co | $[Ar]3d^7 4s^2$ | Rhodium | Rh | $[Kr]4d^8\ 5s^1$ |
| Nickel | Ni | $[Ar]3d^8 4s^2$ | Palladium | Pd | $[Kr]4d^{10}\ 5s^0$ |

Of particular interest to us are the atoms of iron, cobalt, and nickel located in period No. 4, the maximum valency of which is 8. The maximum valency of 8 is rhodium, ruthenium, and palladium, located in period No. 5.

The electronic structure of the atoms of these elements is shown in Table 1. A characteristic feature of the atoms of these elements is that in Fe, Co, and Ni 4*s*, the level is completely filled, while 3*d* is only partially filled; in Ru and Rh 4d 5*s* are partially filled; level 5*s* of palladium is not filled, while 4*d* is completely filled.

The fourteen elements shown in table 2, called lanthanides, have valence shells partially filled.

Table 2

Electron Configuration

The ground state electron configurations of the lanthanides

| Name | Symbol | Electron configuration | Name | Symbol | Electron configuration |
|---|---|---|---|---|---|
| Cerium | Ce | $[Xe]4f^1\ 5d^1\ 6s^2$ | Terbium | Tb | $[Xe]4f^9\ 6s^2$ |
| Praseodymium | Pr | $[Xe]4f^3\ 6s^2$ | Dysprosium | Dy | $[Xe]4f^{10}\ 6s^2$ |
| Neodymium | Nd | $[Xe]4f^4\ 6s^2$ | Holmium | Ho | $[Xe]4f^{11}\ 6s^2$ |
| Promethium | Pm | $[Xe]4f^5\ 6s^2$ | Erbium | Er | $(Xe]4f^{12}\ 6s^2$ |
| Samarium | Sm | $[Xe]4f^6\ 6s^2$ | Thulium | Tm | $[Xe]4f^{13}\ 6s^2$ |
| Europium | Eu | $[Xe]4f^7\ 6s^2$ | Ytterbium | Yb | $[Xe]4f^{14}\ 6s^2$ |
| Gadolinium | Gd | $[Xe]4f^7 5d^1 6s^0$ | Lutetium | Lu | $[Xe]4f^{14}\ 5d^1\ 6s^2$ |

The chemical bond between atoms is due to the exchange of electrons from these energy levels. However, the electron should be considered not only as a particle but also as a wave that does not have clear boundaries. Quantum chemistry uses the term orbital. The orbital is often depicted as a three-dimensional region in which there is a 95 percent probability of electron detection. Four types

of orbitals *s, p, d,* and *f* are used in the tables. Orbitals may overlap. This overlap is called hybridization, which is most often observed for *s* and *p* orbitals.

The property of neutral atoms to attract an electron from another atom was called L. Pauling electronegativity. The maximum value of electronegativity is 4.0 on the scale proposed by Pauling for a fluorine atom, and the minimum is 0.7 for France atoms.

Photon radiation occurs when an electron returns to the energy level from which it was removed as a result of ionization. The energy required to remove electrons, called the ionization potentials, is measured with the utmost possible accuracy, especially for those metals that are used to produce X-rays.

The maximum energy (maximum radiation frequency) is achieved when the electrons are removed from 1s of the orbital. The ionization potential of the first I (1s1) and second I (1s2) electron for five elements is shown in table 3.

Ionization Potential

Table 3

| Element | I ($1s^1$) eV | I($1s^0$) eV |
|---|---|---|
| Fe | 8828 | 9277.69 |
| Co | 9544.1 | 10012.12 |
| Ni | 10288.8 | 1015.40 |
| Cu | 11062.38 | 11567.617 |

The approach of the sodium and chlorine atoms leads to the atomic reaction of the formation of the $Na^+Cl^-$ molecule, at which energy of 4.26 eV is emitted.

*NaCl* molecules in water form a solution, the evaporation of which is accompanied by crystallization and radiation of energy equal to 0.75 eV/molecule.

The dissolution of the salt is accompanied by p-radiation, as shown in Fig. 28, frame 4.·

Such photon energy is insufficient to pass through the container. The ionization potential of the first and second electrons from the 1s orbital of the four elements is shown in Table 3. This energy is insufficient to pass through the web of the I 4·9.5 beams of 101.6 mm, as shown in Fig. 14 (3), frame 7.

This conclusion follows if the blow stimulates X-ray radiation. We can assume that in this case, multiphoton absorption is realized due to nonlinearity. But such photons should be directed in one direction, while the radiation is chaotic.

The hypothesis of the participation of protons in the ionization of atoms seems to be preferable, given the success of X-ray astronomy.

The success of X-ray astronomy, which studies space objects by their X-ray radiation with photon energies from 0.1 to 100 keV, has become possible in connection with space exploration, because the Earth's atmosphere absorbs X-rays at an altitude of 100-30 km. An X-ray source was

discovered in the constellation Scorpio in 1962. It is a neutron star whose x-ray power exceeds the total solar radiation power by 60,000 times.

A neutron star, called Scorpio X 1, which has a huge mass, "sucks" out of an adjacent star, the mass of which is smaller, the substance (mainly hydrogen, helium, carbon) that form it. This phenomenon is called accretion. Ions accelerated by attraction reach the neutron star with great speed and cause intense X-ray radiation.

The use of space vehicles made it possible to study the X-ray radiation of not only stars (energy sources at high temperatures) but also planets of the solar system, their satellites, comets, and asteroids whose temperature does not exceed 10 K (-263 ° C).

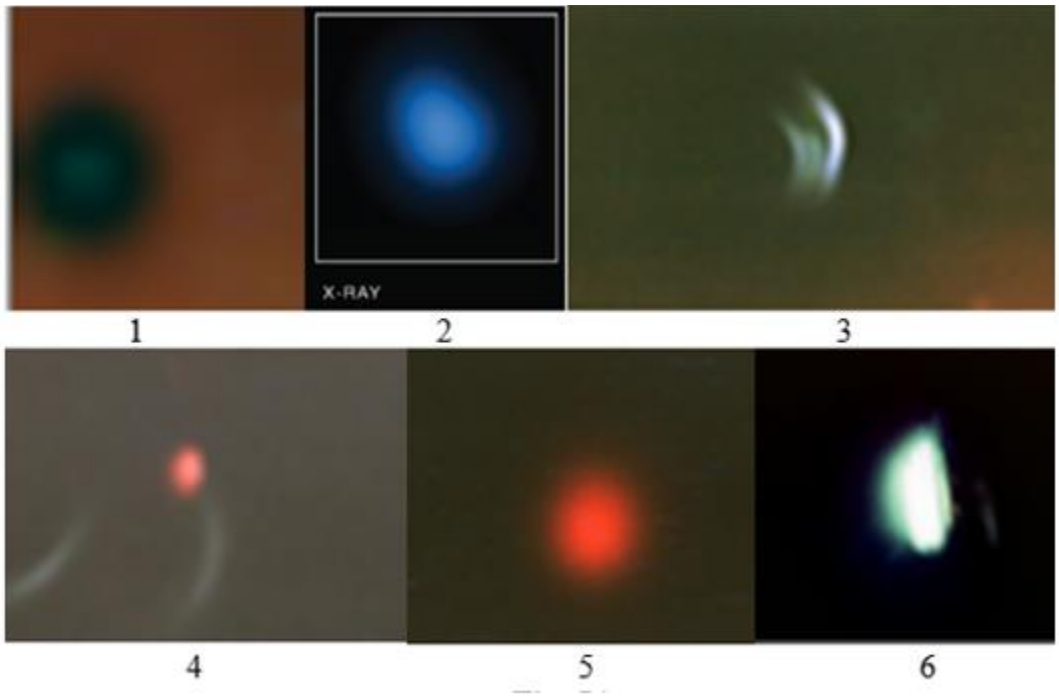


**Fig. 57**

Radiation of an X-ray photon is the result of the recombination of an ion and an electron in which the electron has been removed from the internal orbital. The ionization potential of 1*s* electrons of multielectron atoms is independent of the influence of other atoms.

Fig. 57 is shown to show that there is no fundamental difference between X-ray photographs obtained from celestial objects, especially from the dust cloud and comet ice given in [3.4–3.9], from photographs obtained in the experimental study, the results of which are given above.

The frames illustrate 1) one of the fragments of p-radiation of the bottom of the bay, shown in Fig. 39 (4); 2) X-ray radiation of the planet Pluto [Pluto: A dwarf planet in the outer regions of the Solar System. (Credit: X-ray: NASA / CXC / JHUAPL / R. McNutt et al; Optical: NASA / JHUAPL)]; 3- p-radiation from a steel beam, recorded on a film located on the *xz* surface in the direction of the *y*-axis (Fig. 12 (Spiral)), caused by an impact on the upper surface *xy* in the direction of the *z*-axis; 4) p-radiation detected during ice melting (Fig.29 (2)); 5) p-radiation from water caused by the impact of a falling body on a horizontal surface (Fig. 19); 6) p - radiation from the same steel beam, recorded simultaneously with frame 3, but on a different film located on the lower surface *xy* (Fig. 12).

Three containers with the photographic film were placed on the asphalt near the house to study p-radiation from the Earth and / or the Sun. Exposure time 72 hours. Mechanical stress was excluded.

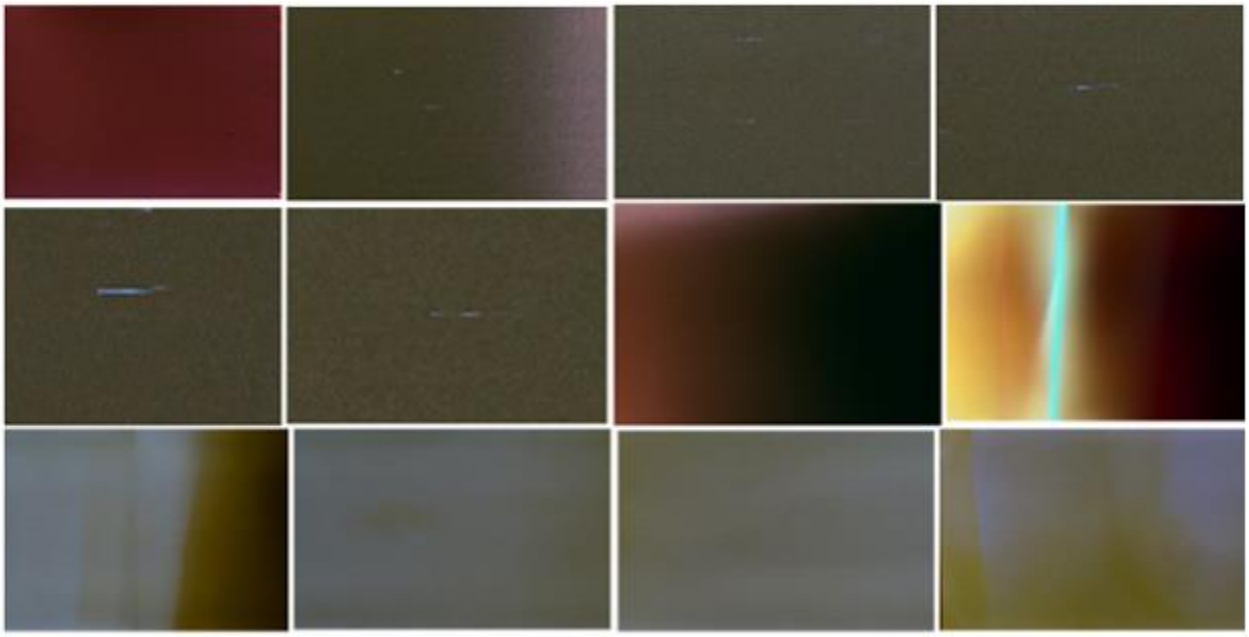

**Fig. 58 (1)**

Fig. 58 (1) illustrates p-radiation recorded on a photographic film located in the shade on the surface of which a methane tank was placed. The days were sunny. The radiation intensity allowed us not to change the contrast and color of the photographs. The picture located in the upper left corner was taken when the film remained in a metal cassette. Luminous lines, similar to those observed in the metal during deformation, are visible in five frames. The bright flash shown in one of the frames was not previously observed.

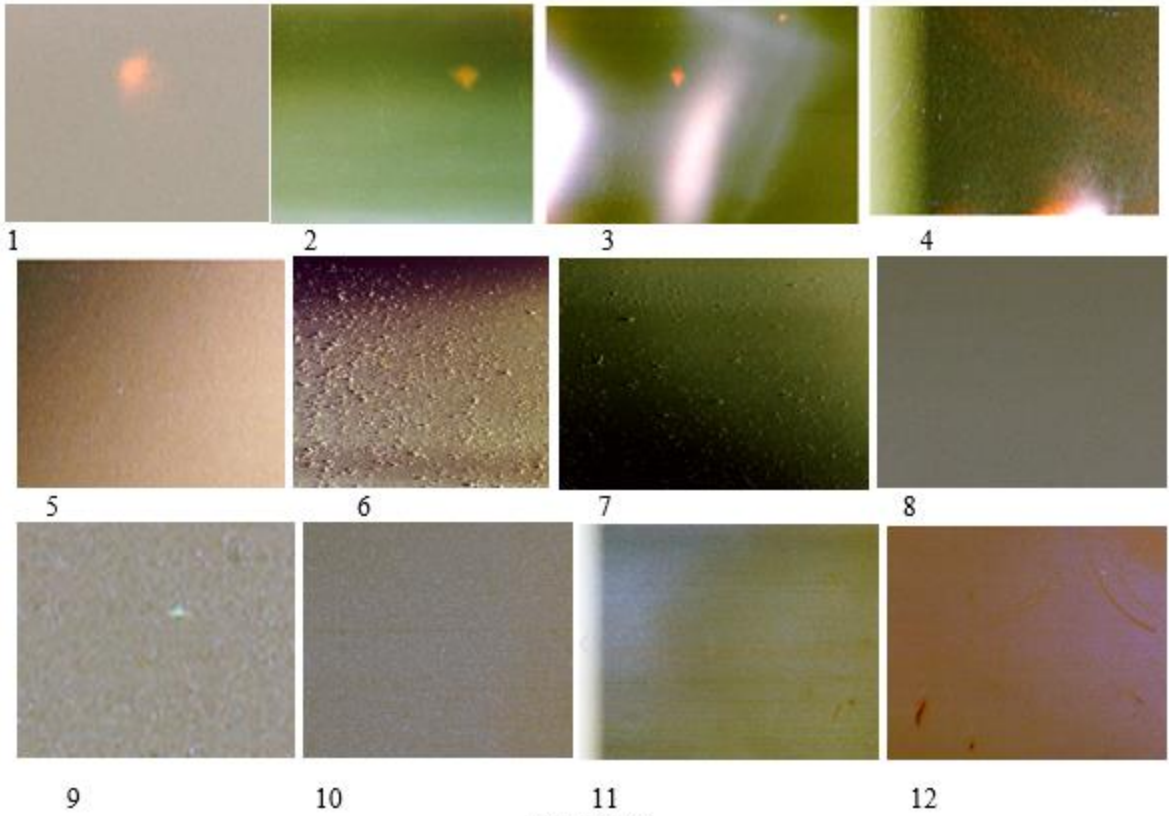


**Fig. 58 (2)**

Fig. 58 (2) illustrates p-radiation recorded on a photographic film located on asphalt under a stone, on the surface of which a third container was placed at a distance of 30 cm. The days were cloudy. Once it was raining, but a direct hit of water on the containers was excluded. Photos illustrate the part of the frame that demonstrates the most characteristic objects. Increased contrast has led to a color change.

Please pay attention to frames 1-4, identical to frames, which are illustrated in all other photographs, when water is present on the surface of the container. Frames 6 and 7 are characteristic of the emission of metals.

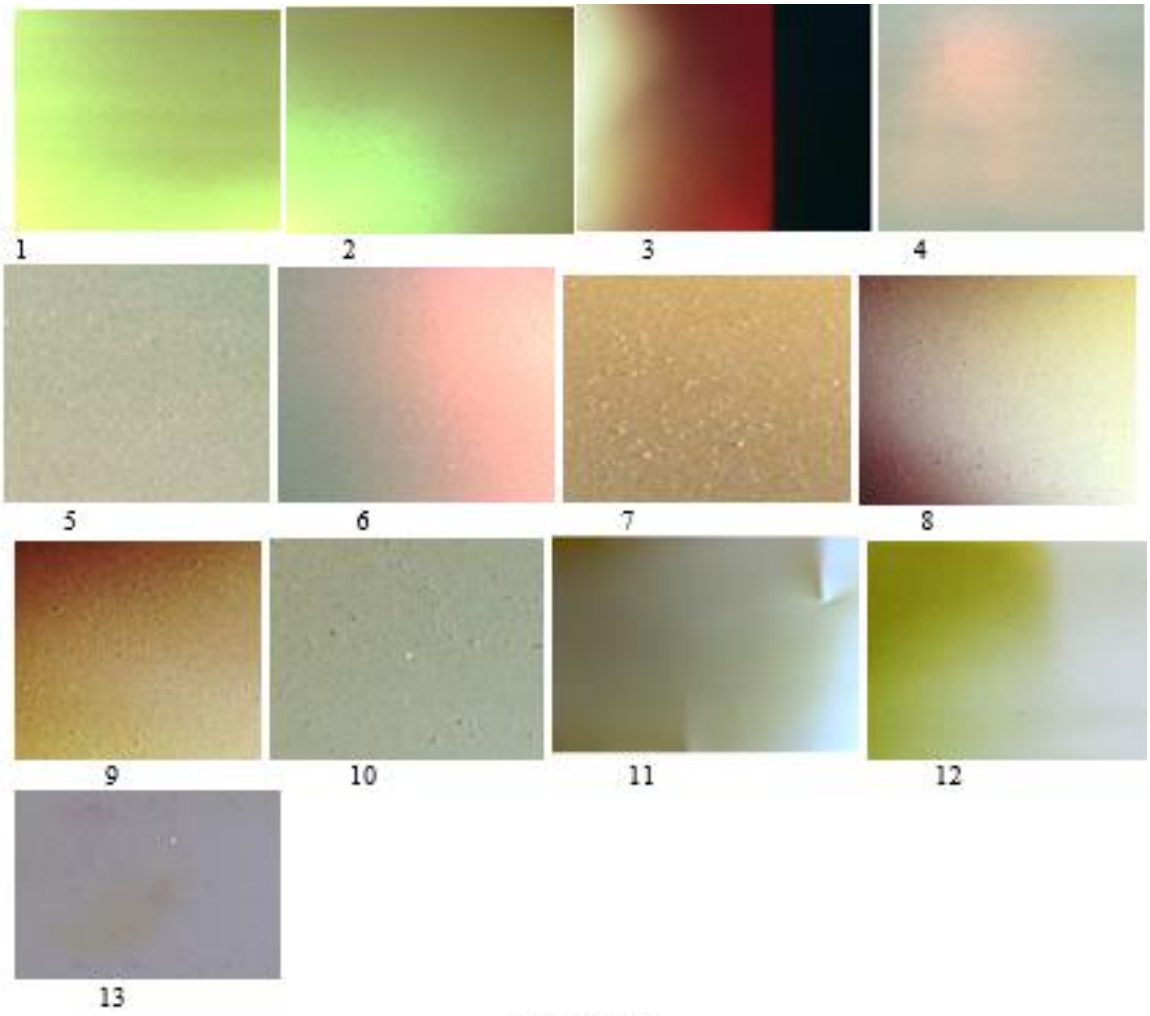


**Fig. 58 (3)**

Fig. 58 (3) illustrates p-radiation recorded on a photographic film located at a distance of 30 cm from the surface of the Earth but connected with it through a stone. Frame color changed with increasing contrast. Of particular interest is the photograph shown in frame 11.

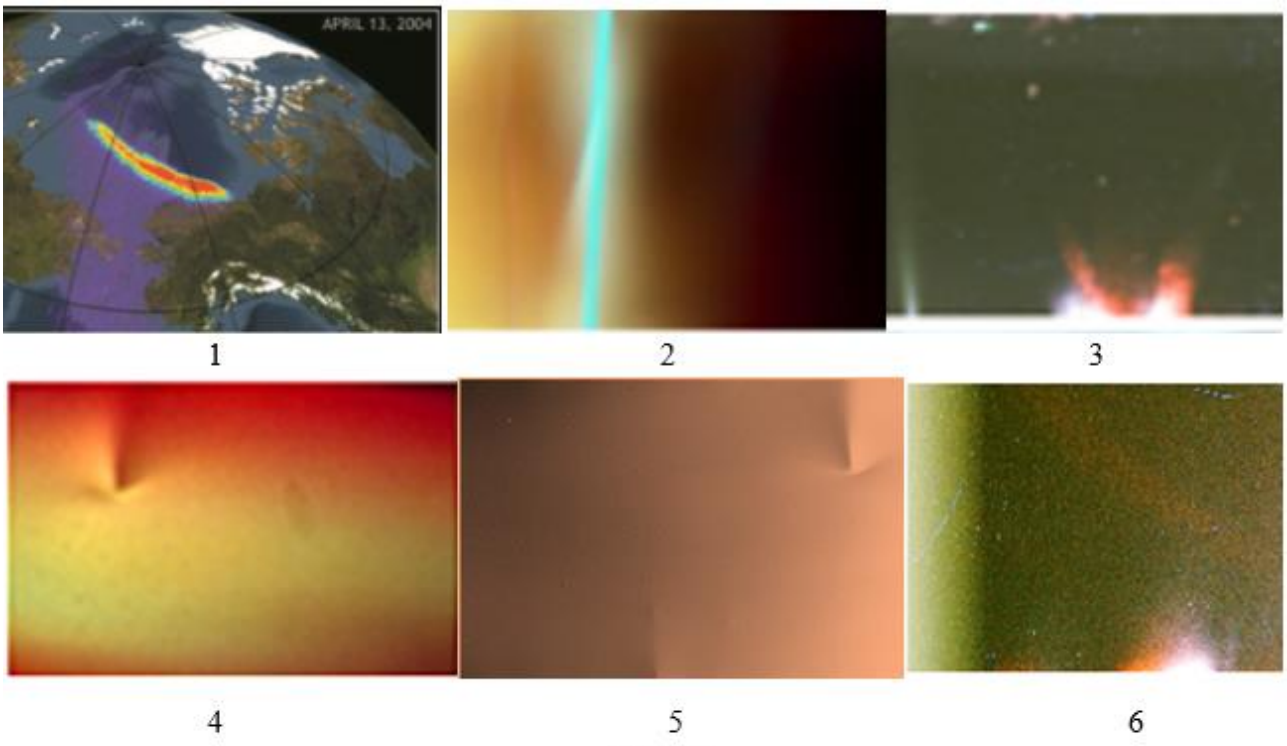


**Fig. 59**

Fig. 59, frame 1 shows a photograph of the Earth's radiation obtained with the Chandra HRC-1 telescope [3.9] near the north pole. The authors note photon energy changes from 0.1 to 100 keV.

Flashes of intensity were observed in individual regions. There is no doubt that the nature of the flash shown in frame 2 and its mechanism are identical to the formation of radiation, which was recorded by the telescope. *It is especially important to note that it is directed from east to west.*

The identity of the nature and mechanism of the radiation shown in frames 3 and 6 is also not in doubt, but frame 3 is caused by the deformation of the metal, while the radiation recorded on frame 6 is caused by atomic processes in the Earth and /or on the Sun. The photograph (frame 4) was obtained upon impact on metal, while a photograph (frame 5) was obtained upon emission from the Earth and/or the Sun. The identity of the figures is not in doubt, but each of them is a mirror image of the other. Such an effect is observed in some crystals or molecules.

A detailed analysis of the X-ray radiation of celestial objects is beyond the scope of this study, but focused research is needed to answer questions that arise using a phenomenon called p-radiation. The identity of the photographs is not in doubt, despite the fact that the sizes of the areas emitting energy differ by billions of times.

The identity of the photographs is not in doubt, despite the fact that the sizes of the areas emitting energy differ by billions of times.

Conclusion

*The experimental results allow us to conclude that the emission of X-ray photons in the absence of a voltage accelerating electrons is due to the excitation of atoms by protons, which before other atoms are converted into an atomic nucleus.*

This allows you to study the processes of electromagnetic radiation of celestial objects in the x-ray region, simulating them on the Earth, similar to how it is shown in Fig.31 a and Fig. 31b. The evaluation of the usefulness of using this method should be decided by those who are interested.

**3.5. The conversion of mechanical energy into electromagnetic**

The experiment confirmed the hypothesis that an energy source is a group of atoms whose energy storage is due to the transition of atoms to higher metastable energy levels, including from levels located below the valence band. Such transitions are realized only when the atom absorbed a photon whose energy is sufficient for this.

The origin of such photons is due to mechanical action. The transition of mechanical energy to electrical was first demonstrated by Faraday when the magnet moves in the coil. Magnetic field changing created a changing electric field.

Maxwell formulates the hypothesis that a changing electric field creates a changing magnetic field in a conductor and a dielectric.

Two of these fields propagate in space in the form of an electromagnetic wave at the speed of light. This hypothesis was confirmed experimentally and became the basis of classical electrodynamics.

Planck comes to a conclusion about the quantum properties of light. Particle light photon and the nuclear-electronic structure of atoms became the basis of quantum mechanics, and the interaction of electrons and photons is the basis of quantum electrodynamics.

Quantum mechanics makes it possible to explain the mechanism of excitation of p-ray photons in a solid, but it must be remembered that the laws of classical mechanics can not be applied to atoms, because other physical laws operate in the nano-world.

The basis of quantum mechanics is the experimentally established fact that electromagnetic waves are simultaneously particles that have a mass, but only when moving. Such a particle, called a photon, is produced in an atom upon the transition of electrons from one energy level to the other. But there are no photons in atoms. Experimental evidence suggests that electrons, ions and other particles, whose rest mass are different from zero, exhibit wave properties, that is, interfere. The wavelength of the particles can be calculated from the de Broglie formula, $\lambda = \frac{h}{mv}$ where $h$ is the Planck constant, $m$ is the mass of the particle, and $v$ is its velocity. This hypothesis was confirmed

experimentally and forms the basis for the creation of an electron and atomic force microscopes, neutron diffraction.

Atoms in molecules and solids are attracted and repelled, but the *nature of the forces is electromagnetic*. Gravitational attraction is 40 orders of magnitude weaker than electromagnetic one; it can be neglected.

The bond between atoms is established as a result of the exchange of atoms by photons and electrons.

*The breaking of bonds between atoms is the result of an atomic reaction caused by an electron-photon exchange. These reactions can be described only by the methods of quantum mechanics. But the question arises: how do mechanical forces break the bond between atoms?*

*There is only one answer: mechanical energy must transform into the electromagnetic one.*

*There are no other ways in nature.*

*But now this path is indicated by the law of destruction, using which the mechanism of loss of integrity and destruction of a solid body is revealed.*

We will first consider the physical processes through which the energy of mechanical deformation is transformed into electromagnetic radiation.

A cloud of free electrons, up to 2 nm in thickness, is formed above the surface of a solid or its parts, for example, above the surface of grains. The density of the cloud is due to the work function and the temperature. The existence of such a cloud is confirmed experimentally. It is used in vacuum photocells and solid-state photodiodes. The laws of the photoelectric effect, established experimentally, were explained by Einstein on the basis of the quantum nature of light.

The contact between the two bodies begins when the two clouds interact. Each cloud is held by the positive charge of the body from which the electrons were emitted.

For example, in a solid one electron passed from the grain located above to the grain located below. This led to the lower charge of the lower grain, while the charge of the upper grain increased, and a contact potential difference arose. The shift of the upper grain relative to the lower grain is accompanied by the emission of electromagnetic waves, which is caused by a change in the electric field, which causes a change in the magnetic field.

Two varying fields form an electromagnet wave, which propagates in the gap between the grains, forming a waveguide and partially penetrates into the grain. The absorption of photons by atoms of grains is accompanied by an increase in temperature and luminescence.

Internal friction, internal photoelectric effect, internal contact potential difference, segregation of impurities, internal corrosion determine the possibility of a phenomenon called internal triboluminescence due to relative displacement of grains, twins, or phases separated by boundaries from which electromagnetic waves are reflected.

Of course, this mechanical model, described by the mechanism of the formation of energy, the radiation of which leads to destruction, does not reflect the processes caused by the interaction of electrons and photons. But every time we stroke a cat and create a spark, we do not think about the destructive energy of this small discharge. A spark of 1 mm in dry air occurs at a potential difference of 300-450 volts. The kinetic energy of the aluminum atom at the melting point is 0.04 electron volts per atom, which is 7-10 thousand times less than the electromagnetic energy in this simple case.

Molecules of water vapor rise from the surface of the heated earth. The cooling water vapor condenses and forms water droplets. Water droplets were freezing turn into ice crystals. The impact of two small ice crystals leads to the fact that a part of electrons passes from one of them to the other. A crystal that has lost electrons is positively charged, while another crystal is charged negatively.

Airstreams carry crystals with minimal density and minimal mass into the upper part of the cloud. The potential difference between charged clouds or a positively charged cloud and Earth reaches millions of volts. The air in some channel turns out to be highly electrified, having a high conductivity, in which recombination begins. The flow of photons (electromagnetic waves) initiates recombination (lightning), in which the accumulated energy is emitted in a few nanoseconds. The current in the lightning is millions of amperes.

Thus, the movement of ice crystals (mechanical energy) creates electromagnetic waves (photons). The photons absorbed by atoms, ionize the air between the clouds, forms a conductive channel through which there is a discharge of enormous power, creating areas of high air pressure and acoustic waves (thunder roars). Electromagnetic energy was transformed into mechanical.

N. Tesla showed that the formation of thunderclouds occurs as a result of standing electromagnetic waves. The formation of low-frequency standing electromagnetic waves in the Earth's atmosphere is called the Schumann resonance.

It was experimentally established that lightning occurs outside the atmosphere of the Earth, where there are no ice crystals. Consequently, the mechanism of such lightning formation differs from the mechanism of the formation of lightning in the atmosphere, but nature remains the same.

Another type of lightning is created in nature. It is called ball lightning. This phenomenon demonstrates the possibility of long-living a local gaseous region existence, in which

electromagnetic energy is accumulated. The formation of galaxies from stars, liquid, solid from atoms, and living organisms from molecules is due to this natural phenomenon. The emergence, development, and long-term existence of a region, the potential energy of which is higher than the minimum, is possible only in the case when the lifetime of the collection exceeds the lifetime of the individual.

The mechanism for implementing this phenomenon was formulated by R. Feynman in the first lecture on physics for students. Paragraph 1-2, called "Mater is made of atoms," begins with the words:

“If, in some cataclysm, all of scientific knowledge were to be destroyed, and only sentence passed on to the next generations of creatures, what statement would contain the most information in the fewest words? I believe it is the atomic hypothesis (or atomic fact, or whatever you wish to call it) that all things are made of atoms, little particles that move around in perpetual motion, attracting each other when they are a little distance apart, but repelling upon being squeezed into one another.
In that one sentence you will see an enormous amount of information about the world, if just a little imagination and thinking are applied.”

If we consider the fact that Feynman was already the Nobel Prize laureate for the creation of quantum electrodynamics, then this Feynman formulation should be recognized as the first postulate of any physical theory, including the quantum theory of destruction.

### 3.5.1. The mechanism of destruction of a solid

P. L. Kapitsa Nobel Prize laureate in the lecture “The Recollection of Lord Rutherford” notes that: "Moving forward our knowledge of nature occurs when between theory and experience a contradiction arise. These contradictions give the key to a broader understanding of nature; they force us to develop our theory. The larger these contradictions, the more fundamental the restructuring of the laws by which we explain the processes are occurring in nature and on the basis of which we use nature for our cultural development."

This contradiction between the theory of destruction and experiment persists today.

The experiment shows that this contradiction can be eliminated only on the basis of an understanding of those natural phenomena that result in the transformation of the mechanical energy of deformation into electromagnetic and electromagnetic energy into mechanical energy of destruction.

An analysis of the experimental facts allows us to conclude that the electron cloud plays an important role above the surface of a solid. The pyroelectric effect is described three hundred years BC, the contact potential difference at the contact of solids was discovered by A. Volta in the early

19th century, the piezoelectric and photoelectric effects were discovered in the second half of the 19th century. The man became acquainted with electrification by friction and struck a spark by striking iron from flint several thousand years BC.

B. Franklin showed that the sparks arising from the discharge of charged bodies, and lightning in the clouds have a common nature, and invented a lightning conductor.

The experiment showed that p-ray radiation is observed during deformation and from fragments after fracture, confirming the mechanism of formation of the energy source based on the following reasoning.

Two solid dielectrics, above the surface of which are a cloud of electrons, approach each other at a distance of 2 nanometers. A contact potential difference arises between the bodies. The displacement of one body relative to another is accompanied by a change in the electric field. A changing electric field causes a change in the magnetic field, which in turn causes a change in the electric field. This is how an electromagnet wave is born. If, as a result of the displacement of the body are separated, they are charged. If, after the separation of the body to bring together, then a spark forms between them. Visible radiation is caused by the fact that electrons, when flying through the air, ionize the gas molecules. Positively charged ions and electrons recombine, causing luminescence. Electrons that reach a positively charged body also produce a glow. This phenomenon is called triboluminescence.

Sparks formed by the friction of steel on flint, are particles of metal. They were the first object that was explored by me, as shown in Fig.1. Sparks did not melt a thin polymer film, did not ignite vapors of alcohol, gasoline, and methane if the metal was not heated by friction to red color. This fact was known in the 19th century and was used by miners to illuminate before Davy invented the lamp named after him. He is described in the first lecture of Faraday on the chemical history of a candle.

This lecture M. Faraday begins with a warning: “And, before proceeding, let me say this also: that, though our subject be so great, and our intention that of treating it honestly, seriously, and philosophically, yet I mean to pass away from all those who are seniors among us. I claim the privilege of speaking to juveniles as a juvenile myself.”

After 80 years, M. Planck has to admit that: “Scientific truth does not triumph, convincing its opponents and forcing them to see the light, but rather because its opponents eventually die, and the new generation grows up being familiar with it.”

J. B. Lamarck wrote: "No matter how great the difficulties were with the discovery of new truths in the study of nature, but even greater difficulties stand in the way of their recognition."

These quotes by great scientists characterize the role of the human factor in science, the thousand-year history of the development of which shows that technological progress is due to the use of new discoveries. A scientist who hides these discoveries commits a crime against the younger generation.

Crimes become especially serious when they try to hide new methods aimed at ensuring the safe operation of structures, confirmed by experiments.

### 3.5.2. The mechanism of the pore, cracks formation and destruction

All experiments presented above refute the hypothesis that dynamic processes between atoms can be explained without taking into account electromagnetic interaction. The integrity of a solid is due to the dynamic balance of the forces of attraction and repulsion between atoms, which can be disturbed by external influences. Each atom in the Universe can only be exposed to another atom through a photon or electron emitted by other atoms.

The law of destruction was formulated on the basis of the analysis of the experimental study, which made it possible to establish the initial postulates.

1. *The only force acting on an atom is an electromagnetic field when gravitational attraction can be neglected.*

*2. The relationship between atoms is due to the attraction of electrons to the nuclei and the repulsion of electrons from electrons and nuclei from nuclei.*

*3. Any atomic reaction is caused only by a change in the electron shell of atoms.*

*4. A bond break occurs as a result of an increase in repulsive forces due to the ionization of atoms generated by an electromagnetic pulse, the source of which is a local group of metastable atoms.*

*5. The number of broken bonds (the character of the damage) is due to the energy accumulated by the atoms of the local group and absorbed by other atoms.*

The nature and mechanism of damage and destruction of a solid, proposed on the basis of the experiment, is fundamentally different from the one used so far. The speed of formation of a line or region of broken bonds is due to the speed of electromagnetic waves, while a signal of a change in structure propagates with the speed of acoustic waves, similar to that with lightning and thunder.

### 3.5.3. Experimental facts confirming the mechanism of transformation of mechanical energy into the electromagnetic

The experiment showed that any deformation of a solid is accompanied by electromagnetic radiation, which is caused by the relative displacement of the components separated by the heterogeneity boundary. Such boundaries are formed between grains, twins, foreign inclusions such as fish-eye, chemical compounds formed in a solid, at the interface, for example, martensite-residual austenite, etc.

### 3.5.4. The movement of grains, twins and macroscopic layers of material

The production of the first high-entropy alloys (HEA) stimulated experimental studies on their creation and the study of properties. The number of possible combinations of alloys based on the five elements is almost borderless.

Analysis of reviews devoted to the technology of obtaining and studying the properties of these materials shows that the number of synthesized alloys increases by tens every year.

Experimental studies, the results of which are analyzed, are performed at the modern level using X-ray diffraction analysis, scanning electron, atomic force microscopes, field ion microscope, neutron diffraction, and X-ray fluorography. Modern methods allow us to investigate changes in the position of individual atoms. However, the analysis of properties is based on the use of previous theoretical models.

We confine ourselves to a brief comparative analysis of the research results presented in this article with those given in chapter I. The main interest in this analysis is represented not only by phase transformations but by changes in the position of the grains during the aging process.

Let us pay attention, first of all, to the difference between both the experimental research method compiled by the author of the book and the authors of the article and the evaluation of the research results.

The experiments described in the book were carried out on macroscopic samples; the direct radiation of X-rays caused by the deformation of the samples was fixed on the film. Photos illustrate the result of a photochemical reaction due to the frequency and intensity of radiation.

The experimental methods used by the authors of the article need clarification since the creation of such methods has become possible based on an understanding of the processes occurring in the area that is today called nanoscale. A region is called nanoscale if at least one of its dimensions is less than 100 nm.

The processes occurring in this area can only be described from the standpoint of quantum mechanics. The thickness of the samples used in the article corresponds to that size. It is known that an object can be distinguished only when the wavelength is less than the size of this object. Louis de Broglie in 1924 formulated the hypothesis that the particles have wave properties and proposed the equation $\lambda=h/mv$, connecting the wavelength λ with Planck's constant *h*, the particle mass *m*, and its velocity *v*, which was confirmed experimentally.

It was found that electrons interfere and diffract. This phenomenon forms the basis of quantum mechanics, the creation and use of electron microscopes, field ion microscope, electron diffraction, neutron spectroscopy, and neutron diffraction.

A detailed analysis of these methods, which ensured the intensive development of materials science, is necessary for research laboratories, but they are not applicable for continuous monitoring of the technical condition of structures and devices. First, they are performed on specially prepared nano-sized samples; secondly, the electrons probing the sample are accelerated by high voltage, at which the probing electrons interact with the atoms of the sample, changing its properties; thirdly, all processes are performed in a vacuum.

In this regard, we confine ourselves to analyzing the results of research obtained with the integrated use of nanomaterials using modern, highly sensitive equipment.

For example, the authors of the review [3.10] associate mechanical properties only with stress or with dislocations, but note: "In terms of hardness/strength, the most critical factors are: (1) Hardness/strength of each composing phase in the alloy; (2) Relative volume ratio of each composing phase; (3) Morphology/distribution of the composing." The same factors as the main ones are noted in the review [3.11].

We consider only three experimental work performed using modern technology.

A wide study of phase transformations in the high-entropy alloy Fe-30Mn-10Co-10Cr-0.5C was carried out in [3.13].

Investigation of changes in the mechanical properties of the Co20Cr26Fe20Mn20Ni14 alloy caused by tensile and torsional deformation at a pressure of 5 GPa and a temperature of 77 and 300 K has been made in [3.12].

The aim of this work is to unravel the *mechanisms* of phase transformation and twinning in a model interstitial high-entropy alloys and their effects on strain hardening.

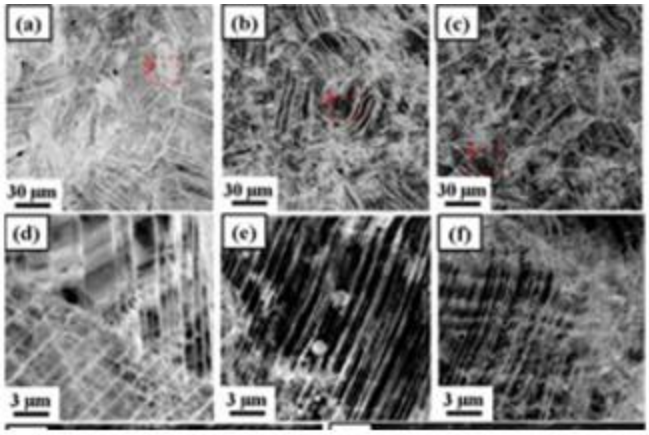


**Fig. 60**

Fig. 60 shows photographs of an alloy obtained by the backscattering of electrons in a scanning electron microscope during torsion strain. Turns of ~ 2-15° and higher were carried out at temperatures of 77 and 300 K in several stages at different time intervals to study the aging process, in which the formation of twins was observed. Material studied after two hours and two weeks of natural aging following cryo-HPT processing were entirely different. A change in the structure during a single rotation is shown in Fig.60 frames (**a d**); three times (**b e**); fivefold (**c f**). The shift was accompanied by a decrease in grain size and the formation of twins.

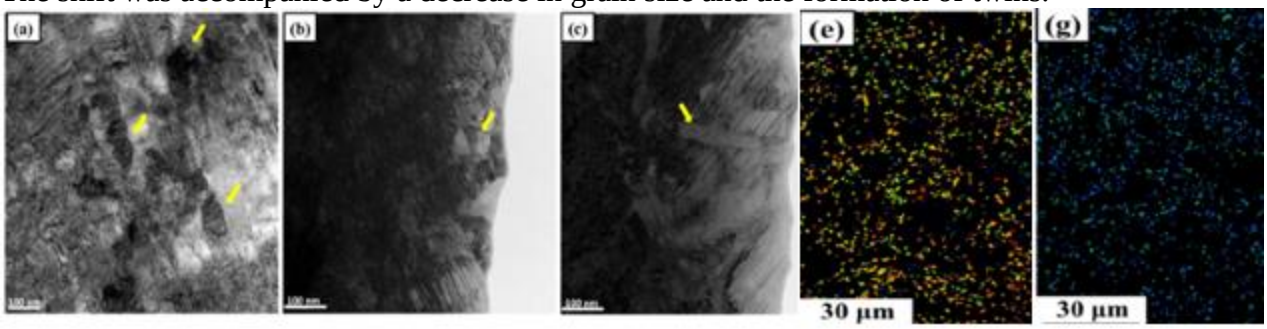


**Fig. 61**

Photos 61 (**a**), (**b**), and (**c**) in [3.12] illustrate nanoscale grains, lamellar twin structures, and coplanar slip traces in the $Co_{20}Cr_{26}Fe_{20}Mn_{20}Ni_{14}$ alloy after 5 rotational displacements. The results of this study are of undoubted scientific interest, but we use the above results only for comparison with those photographs obtained in the study of macroscopic samples.

The performed study is of undoubted scientific interest, but we use the above results only for comparison with those photographs obtained in the study of macroscopic samples. Analysis of the photographs shown in Fig. 61, allows us to draw conclusions that are based on the fact that the processes leading to a change in a structure are due to atomic reactions, both at the macroscopic and nanoscale levels.

1. The authors of [3.12] used samples (**a**), (**b**), (**c**) for research that had not previously undergone deformation.

2. The first displacement (**a d**) of the grains was accompanied by the formation of a twin, the layered structure of which is similar to the formation of mountains. A triple shift (**b e**)

led to a decrease in the thickness of the layers, probably caused by a decrease in grain size. A five-fold shift **(c f)** led to the partial destruction of single crystals. 3. Each experiment was accompanied by a change in properties, the control of which is very important during operation. Non-destructive testing is possible using p-radiation.

4. Photographs of the granular structure (g) and (e) shown in Fig. 61 are identical to those that have been repeatedly observed with p-radiation.

5. Photos (a), (b), (c) shown in Fig. 61 indicate that the crystalline layered structure is maintained at the nanoscale.

The main goal of the book is to demonstrate the practical application of p-radiation, discovered on the basis of experiment.

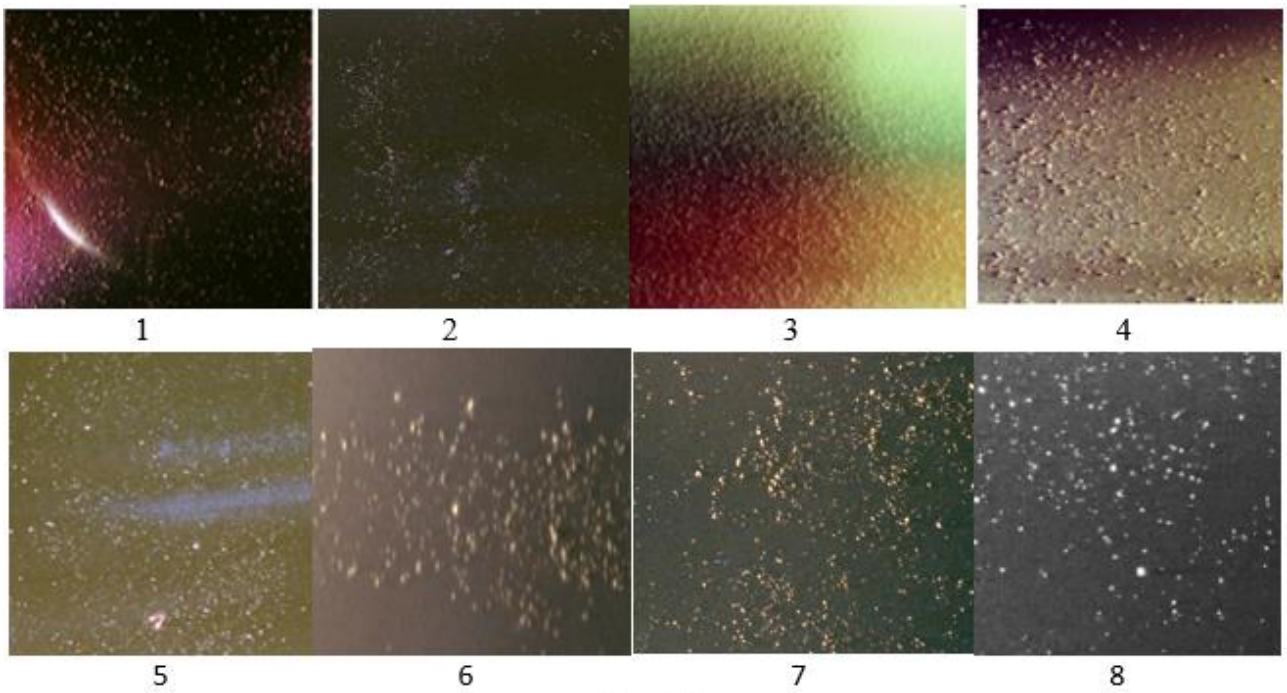


**Fig. 62**

Fig. 62 once again demonstrates such an opportunity. Areas were similar to those shown in Fig. 61 (g) and Fig 61 (e) were repeatedly observed in an experimental study, including five times on the surface of the Earth {See Fig. 58 (2) and Fig. 58 (3))}. Frame 3 was shown in Fig 24 (3); the remaining frames were obtained upon impact on the metal. Photo Fig 62, frame 5, was taken at a distance of 560 mm from the point of impact; photo Fig 62, frame 8- at a distance of 665 mm.

A study of the twinning process of the high-entropy alloy Fe-30Mn-10Co-10Cr-0.5C (at. %) was performed in [3.13]. Samples with a grain size of 3–7.8 μm underwent tensile deformation, during which nucleation and a change in the shape of twins were observed, as shown in Fig. 63.

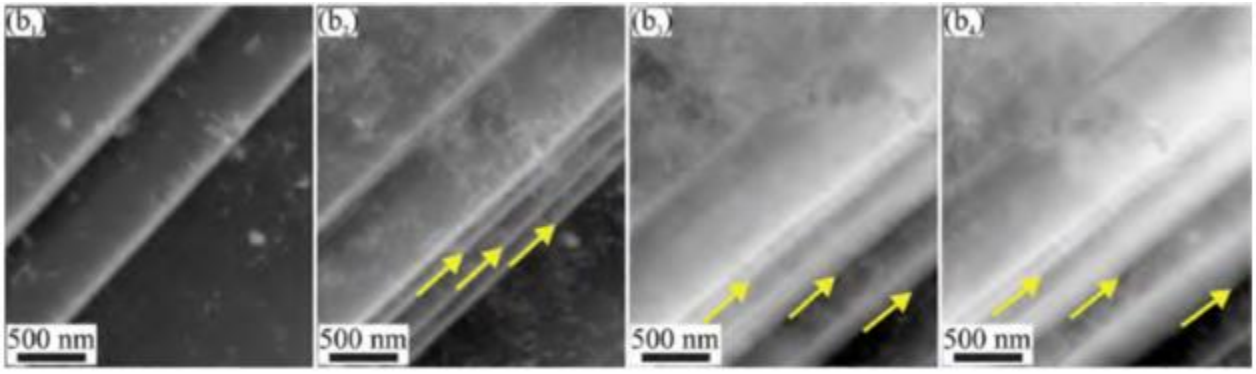


**Fig. 63**

The authors note that an increase in the width of the twins arising at a pressure of ~ 736 MPa (b1) occurred when the voltage changed by 6.7% (**b**$_2$), 10.1% (**b**$_3$), 12% (**b**$_4$).

The hardness of the material is considered in materials science as one of the most important parameters that determine its reliability and longevity, more than three hundred years. The methods for its determination are diverse and numerous. They are also used to study nanomaterials.

However, this is a fallacy. Reliability and durability are due to the ratio of the rate of energy storage to the rate of its dissipation. The larger the ratio, the shorter the safe life. Numerous experiments have proved the fallacy of the hypothesis that the potential energy of a deformed body is stored in stress concentrators.

### 3.5.5. Dislocation model failure

The hypothesis of dislocation as a defect in the crystal structure was formulated in the early thirties of the last century almost simultaneously with the birth of matrix and wave quantum mechanics. The successes of quantum mechanics at each of its stages forced proponents of the existence of this defect to give it more and more new properties, recognizing that the dislocation contains atoms with dangling bonds, i.e., ions. But covalent, ionic, and metallic bonds are due to ionization of atoms. Therefore, we must recognize that the metal is a continuous dislocation.

It is assumed that the dislocation is formed by atoms at the edge of the half-plane, but there is no experimental evidence that the photon emitted by such an ion, when recombined with an electron, differs from the photon emitted by recombination with the same ion located elsewhere.

The theoretical interpretation of the effects observed in the study of materials may be different, but the fact that the birth and change of dislocations are caused by atomic reactions, the description of which is possible only by quantum mechanics, remains unchanged. The term dislocation density is widely used in modern theories. Dislocation density is a measure of the

number of dislocations per unit volume of crystalline material. In one of the methods, the total length of the dislocation line in a unit volume is measured and divided by the volume. Parameter $m^{-2}$ is devoid of physical meaning if it is not indicated what is distributed over the area, but, as we see, a measurement of the broadening of the spectral line is used to estimate it, which is due to the fact that the frequency of radiation of atoms in the studied region is different.

A dislocation, by definition, is a group of atoms having dangling bonds, i.e., a group of ions in a metastable state. Such a local group is considered in this metal model as a destruction domain, the radiation from which occurs as a result of the recombination of an ion (a component of a dislocation) with an electron. Such an act is considered in the theory of dislocations as the movement of dislocations or during plastic deformation, as the healing of cracks. In fact, there are two acts in which one ion recombines, and the other ionizes. The position of the maximum is due to the maximum probability of radiation with a given frequency. However, a comparative analysis is possible only if the reader understands the difference between the descriptions of the same phenomena by the authors of this article and the author of the book. First of all, let us pay attention to the difference between both the experimental research method performed by the author of the book and the authors of works performed on high-precision modern equipment, including in the nano-region and the description of the research results.

The experiments were carried out by me on macroscopic samples, the direct radiation of p-rays from which, caused by the deformation of the samples, was recorded on photographic film. The photographs illustrate the result of a photochemical reaction due to the frequency and intensity of the radiation.

The experimental methods used by the authors of the article need clarification since the creation of such methods has become possible based on an understanding of the processes occurring in the area that is now called nanoscale. An area is called nanoscale if at least one of its dimensions (mostly thickness) is less than 100 nm. The thickness of the samples used in the articles corresponds to this size if they are examined using electron microscopes, ion projectors, electron diffraction.

A detailed analysis of these methods, which provided an intensive development of materials science, is necessary for research laboratories, but they are not applicable for continuous monitoring of the technical condition of structures and devices. First, they are performed on specially prepared nanosized samples; secondly, the electrons probing the sample are accelerated by a high voltage at which the probing electrons interact with the atoms of the sample, changing its properties; thirdly, all processes are performed in a vacuum.

Any local group of atoms of one chemical element located in a solid can be called a cluster, dislocation, or domain, but all the dynamic processes in it are caused by nuclear, electromagnetic, and gravitational interactions. Neglect of gravitational and nuclear interactions is possible outside the stars. Using a dislocation model outside of quantum mechanics is meaningless since the processes occurring between atoms cannot be described without taking into account the interaction of atoms. The experimental facts presented above indicate that the response form of local groups of atoms to external action, with all its diversity, is limited.

## References to Chapter III


3.1. M.D. Chapetti, J.L. Otegui, j. Motylici: *Fatigue Assessment of an Electrical Resistance Welded Pipeline*, Int. J. of Fatigue, 2002, **24**, 21-28.6

3.2. Г.Н. Петракович. *Биополе без тайн*. Сборник научных работ. - 2009.- 306 с. - ISBN 5-85617-010-5. Десятый том «Энциклопедии Русской Мысли»

3.3. A. Bhardwaj, R. F. Elsner, G. Gladstone, T. E. Cravens, C. M. Lisse, K. Dennerl, G. Branduardi-Raymont, B. J. Wargelin, J. Waite, Jr, I. Robertson, N. Østgaard, P. Beiersdorfer, S. L. Snowden, V. Kharchenko, *X-rays from Solar System Objects, Planetary and Space Science*, vol.55 (2007) pp.1135–1189.

3.5. A. Bhardwaj, G. R. Gladstone, R. F. Elsner, J. H. Waite, Jr., D. Grodent, T. E. Cravens, R. R. Howell, A. E. Metzger, N. Ostgaard, A. N. Maurellis, R. E. Johnson, M. C. Weisskopf, T. Majeed, P. G. Ford, A. F. Tennant, J. T. Clarke, W. S. Lewis, K. C. Hurley, F. J. Crary, E. D. Feigelson, G. P. Garmire, D. T. Young, M. K. Dougherty, S. A. Espinosa, J.-M. Jahn, A. Bhardwaj(1), G. R. Gladstone, R. F. Elsner, J. H. Waite, Jr., D. Grodent, T. E. Cravens, R. R. Howell, A. E. Metzger, N. Ostgaard, A. N. Maurellis, R. E. Johnson, M. C. Weisskopf, T. Majeed, P. G. Ford, A. F. Tennant, J. T. Clarke, W. S. Lewis, K. C. Hurley, F. J. Crary, E. D. Feigelson, G. P. Garmire, D. T. Young, M. K. Dougherty, S. A. Espinosa, J.-M. Jahn, *X-rays from Solar System Objects Planetary and Space Science*, vol.55 (2007) pp.1135–1189.

3.6. T. E. Cravens, *X-ray Emission from Comets*, REVIEW: PLANETARY SCIENCE, 2002, **206,** 1042-1045.

3.7. C. M. Lisse, T. E. Cravens, K. Dennerl, *X-Ray and Extreme Ultraviolet Emission from Comets* https://www.lpi.usra.edu/books/CometsII/7014.pdf, 631-642.

3.8. K. Dennerl, C. M. Lisse, A. Bhardwaj, V. Burwitz, J. Englhauser, H. Gunel, M. Holmström, F. Jansen, V. Kharchenko and P. M. Rodríguez-Pascual, *First observation of Mars with XMM-*

*Newton, High-resolution X-ray spectroscopy with RGS*, Astronomy, Astrophysics, 2006, 451, 709-722.

3.9. Bhardwaj, M. Lisse, *X-Rays in the Solar System*, Encyclopedia of the Solar System, 2007, 637-658.

3.10 M.-H. Tsaia and J.-W. Yeh, *High-Entropy Alloys: A Critical Review*, Mater. Res. Lett., 2014 Vol.2, No.3, 107–123, http://dx.doi.org/10.1080/21663831.2014.912690/

3.11. S. Kumar, S. Kumar, V. Singh, J. J. Kumar, High-Entropy Alloys, a Review, International Research Journal of Engineering and Technology (IRJET) V. 03 1563-1566 (2016).

3.12. J. Moon, Y. Qi, E. Tabachnikova, Y. Estrin, W.-M. Choi, S.-H. Jo, B.-J. Lee, A. Podolskiy, M. Tikhonovsky, and H. S. Kim, *Microstructure and Mechanical Properties of High-Entropy Alloy $Co_{20}Cr_{26}Fe_{20}Mn_{20}Ni_{14}$ Processed by High-Pressure Torsion at 77 K and 300 K*, Sci Rep. 2018; 8: 11074. Published online 2018 Jul 23. doi:10.1038/s41598-018-29446-y/3.13.3.1

3.13. M. Wang, Z. Li, Dierk Raabe, *In-situ SEM observation of phase transformation and twinning mechanisms in an interstitial high-entropy alloy*, 2018, Acta Materialia **147**:236-246.

## CHAPTER IV. PRACTICAL USE OF P-RADIATION

*Science is a collective creation and cannot be anything else; it is like a monumental building, which needs to be built for centuries, where everyone has to bring his own stone, and this stone often costs him all lifetime*.

A. Poincare

This book is intended to implement the method proposed for non-invasive monitoring of atomic reactions and their application. It is published six months after the registration of a patent application. New experiments were performed by me in order to better understand the nature and mechanism of the observed phenomenon. The results of experimental studies of great scientific and practical interest were published, but the authors remained in the position of classical mechanics, trying to explain the phenomenon that they are observing.

The simplicity of the experiment, its absolute reliability, allowed a small team to carry out an experiment at minimal cost, which demonstrates the possibility of using the method in almost all branches of technology and medicine. But for this, it is necessary to agree with the author or propose a method that is superior to the one that was proposed by me.

### 4.1. Method name

When I started the study, I was convinced that X-ray radiation is not only a consequence of deformation and degradation but also its cause. The method was called MAPED, which meant Method for Assessing the Potential Energy of Distortion. The experimenter was convinced that the radiation was not X-ray, the nature of which was unknown, and it was called Y-radiation, just as K. Roentgen called the radiation that he discovered with X-rays. The search for the cause of radiation has led to the fact that the excitation of atoms, at which the photon energy exceeds 50 keV, is possible only with the participation of protons. Photons of this range are called n-rays. The experiment showed that p-radiation occurs during all observed atomic reactions. This allows me to call the method *nimar* (non-invasive monitoring of atomic reactions), just like the laser was named.

### 4.2. Material research

The proposed method does not exclude the possibility of using other experimental methods for studying the properties of materials. It supplements them with the need for experimental determination of the accumulated energy A, the accumulation rate, and dissipation B. These

parameters are estimated based on measurements of the intensity of spontaneous electromagnetic radiation and the establishment of a functional relationship between energy and radiation intensity. The well-known method of constructing *S-N* curves is replaced by the method of *A-N* curves. The use of *A – N* curves in a number of examples is shown in [1.9, 1.13] and described in the appendix. We will consider the results of experimental studies of new materials produced in the last decade.

1. The authors of [3.13] used the electron-channel contrast image under controlled diffraction conditions (cECCI) to observe crystalline defects, especially dislocations, stacking faults, and nano-twins, near the surface of bulk samples. The aim of the study is to understand in more detail the formation of the defects below and next to the indent and to contribute in this way to a better understanding of the pattern formation process.

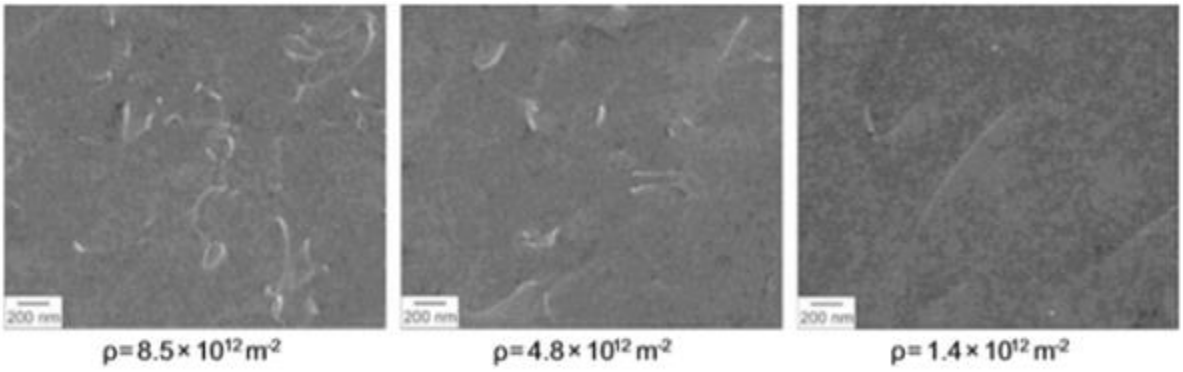


**Fig. 64**

Fig. 64 illustrates examples of a defective state of a test sample for different grains before nanoindentation observed by electron diffraction. The authors believe that photographs indicate a high heterogeneity of the density of dislocations in this material. Figure a shows high, b medium, and low defect rate. Calculations show that the average dislocation density is ~ ~3,5·$10^{12}$ м $^{-2}$ $m^{-2}$.

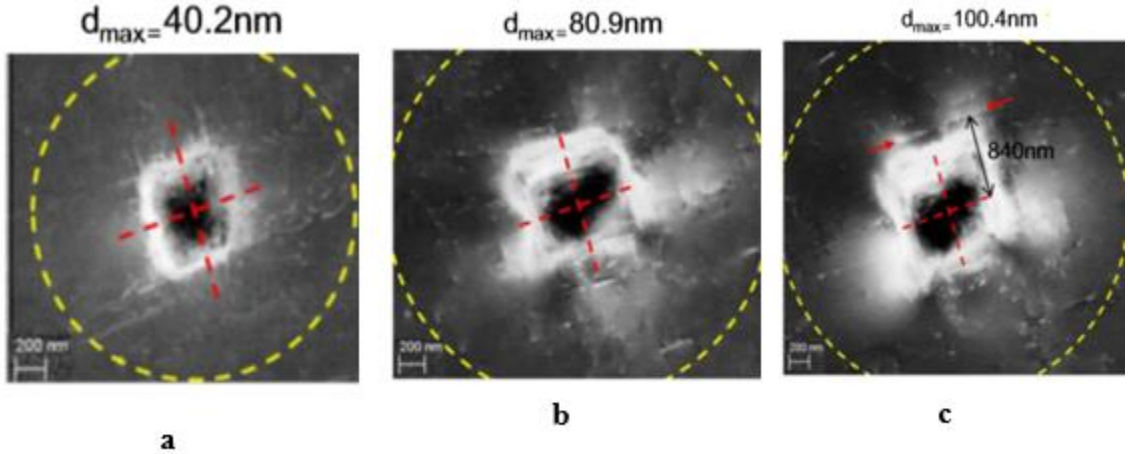


**Fig. 44**

Fig.44 shows three photographs of an imprint obtained after immersion of the indenter to a depth of $d_{max}$ = 40.2 nm, $d_{max}$ = 80.9 nm, and $d_{max}$ = 100.4 nm. The zone of plastic deformation, which including all detected defects, is limited by yellow circles.

The authors suggested that within the circle, there are dislocations the density of which can be calculated and used for a deeper understanding of the formation of defects by applying the simulation of discrete dislocation dynamics (DDD) using the parallel dislocation simulation code (ParaDiS).

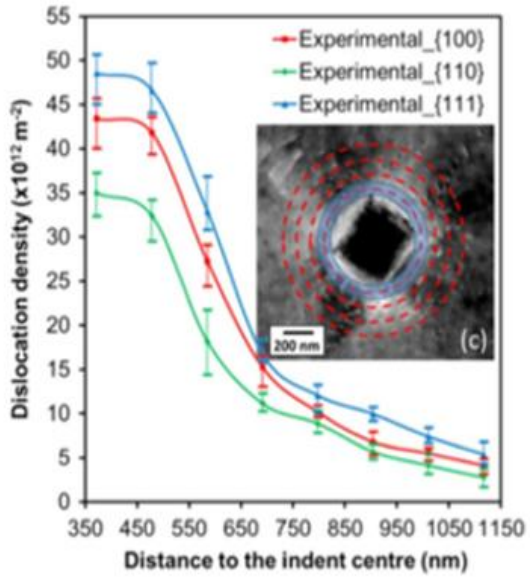


**Fig. 66**

Fig. 66 illustrates a method for calculating the number of dislocations. The principle of measuring the density of dislocations is shown in the example (001): red circles indicate distances of 350, 450, 550, and 650 nm. The number of dislocations inside each ring is calculated and divided by its area. The maximum dislocation density is $3.5 \cdot 10^{13} m^{-2}$.

The fact that the method proposed for the study did not give the expected results is noted by the authors themselves. They write, "However, detailed information on how these patterns are actually formed in terms of the underlying dislocation activities was not provided. In addition, the variation of hardness and/or elastic modulus with indentation depth, the so-called indentation size effect, raises a lot of *difficulties with obtaining real values of the mechanical properties*." (Emphasis added)

Note that the main difficulty is due to the fact that not only the indenter affects the atoms, but also the electrons accelerated by the potential difference of 30 kV. The speed of electrons is such that they not only diffract but also cause cathodoluminescence, X-ray radiation, and additional ionization of atoms. The study of the properties of materials using indentation and carbon loss from a diamond indenter was considered in the author's paper [1.9].

An experiment performed by me allows us to analyze the results of the indentation of materials using p-radiation, supplementing the measuring device with a detector for measuring the intensity of electromagnetic radiation.

### 4.2.1. The formation of Lüders bands and their role

Samples of the Al-6.15% Mg-0.65% Mn-0.25% Si-0.2% Fe-0.1% Cu, wt.% alloy 0.5 mm thick, having the shape of double-sided blades with a working part size of 0.5 × 3 × 6 mm, were subjected

to tensile strain to break, [ 4.2]. An incision of 30–40 μm deep was made on the lateral surface of the working part of the sample, which was about 1% of the width of the sample, which was considered as a stress concentrator.

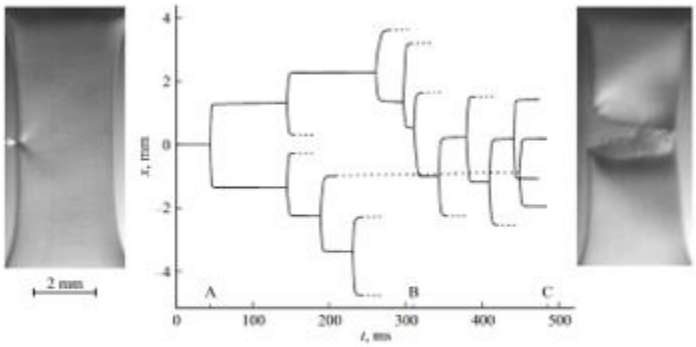


**Fig. 67**

The dynamics of deformation macrobands and cracks were investigated in situ using a FASTCAM Mini UX100 (Photron) high-speed digital video camera filming a surface of a deformable metal in oblique lighting. Video filming rates ranged from 500 to 20,000 frames/s depending on the objectives of the study: the dynamics and morphology of the Lüders band, the dynamics of the Porteven–Le Chatelier bands, and the kinetics of the development of the main crack.

Video processing consisted of subtracting sequential digital images using a computer program.

One of the diagrams given in [4.2] is shown in Fig. 67. Her description is cited: “The correlation diagram x (t), which shows the spatiotemporal evolution of the boundaries of the strain bands at the last strain jump with a break in the sample. A — moment of nucleation of the primary deformation band from the geometric stress concentrator; AB is the temporary stage of cascade propagation of strips; BC is the stage of localization of plastic deformation near the section through which the crack passes, C is the start time of the main crack. "

**Fig. 68**

The conclusions made in work show that the study of the metal surface in the process of deformation in reflected light does not allow obtaining information about the nucleation mechanism and changes in the Lüders bands. The hypothesis about the main role of stress concentrators in the notch region in fracture processes is erroneous. A deeper cut was made by me to study the radiation of an aluminum plate under tension. The photograph shown in Fig. 3, the

frame indicates that the destruction occurred at the place of attachment of the plate, but not in the area of the notch.

Fig. 68 illustrates an enlarged photograph shown in Fig. 4, frame c. Fig. 68 (1) illustrates fragments at a further twofold magnification. We can call luminous bands an analog of the Lüders bands, but not in form, but in the energy state of groups of atoms. We observe a rare case in which not only radiation from metal atoms is recorded, but also “linear discharges” between the expanding fragments. The emission of photons indicates that the deformation was accompanied by ionization of atoms and subsequent recombination. The luminescence along the stem cannot be explained either by stress concentration or by dislocation density.

The results of experimental research are of undoubted scientific interest. They are described in detail and allow us to draw conclusions about the mechanism of occurrence, but the authors try to explain the phenomenon from the standpoint of the dislocation model. They write, “The discussion thus suggests that one dominant factor governing discontinuous yielding in austenite-ferrite duplex medium Mn steels is the grain size, which needs to be small enough to provide a large interface area, thus providing a *high density of dislocation sources*.” (Emphasis added). So, we see that the model of dislocations uses the term density of sources that form dislocations. If the source means a stress concentrator, then its energy is not enough for the formation of a material object.
We observe a rare case in which not only radiation from metal atoms is recorded, but also “linear discharges” between flying away fragments.

*Photons can emit only atoms of particles formed during a break, or air atoms ionized by radiation*. The emission of photons indicates that the deformation was accompanied by ionization of atoms and subsequent recombination. *The luminescence along the stem cannot be explained either by stress concentration or by dislocation density*.

### 4.2.3. Martensitic transformation

Martensitic transformation (phase transition) occupies a special place in materials science. Interest in this phenomenon is growing due to the ability to use modern high-precision and highly sensitive experimental equipment. An analysis of the works devoted to solving this problem showed that research teams with modern equipment, performing empirical research at the highest level, unsuccessfully try to explain the results of their research. We confine ourselves to demonstrating this paradoxical situation using the analysis of publications on this issue as an example. The results

of experimental studies acquire unique scientific value and practical value. The main goal for the author of this book remained the rationale for the practical use of the phenomenon described in it.

The results of an experimental study [4.3] are of undoubted scientific interest. They are described in detail and allow us to conclude the mechanism of the phenomenon, but the authors try to explain the event from the standpoint of the dislocation model. They believe that one of the dominant factors determining intermittent deformation in austenitic-ferrite duplex media of Mn steel is the grain size, which should be small enough to provide a large interface surface area, which ensures a high density of dislocation sources.

So, we see that the dislocation model uses the term density of sources that form dislocations.

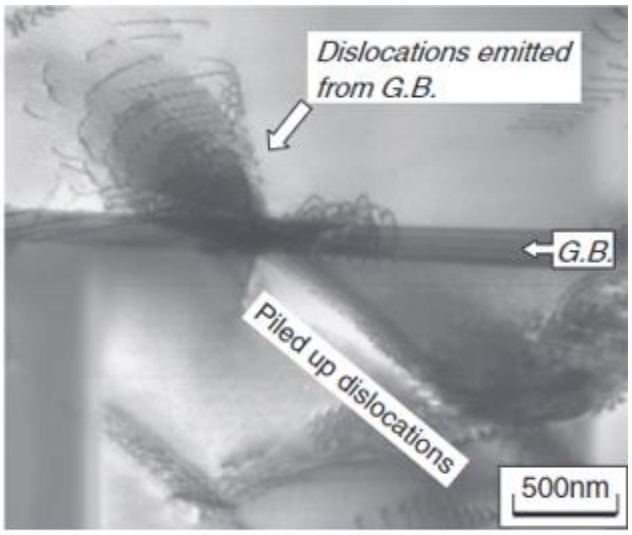

**Fig. 69**

If a source means a stress concentrator, then its energy is insufficient for the formation of a material object. However, the authors consider various models, including those related to the dislocation velocity, $v = \left(\frac{\sigma}{\sigma_0}\right)^n$, which is just the ratio of the applied voltage σ to the reference voltage $\sigma_0$, where n is a constant. It makes no sense in a scientific work to call a parameter that does not have a dimension speed, but we will not attach serious significance to this**.**

The photograph Fig.69 taken from [4.4] inspires confidence among supporters of the dislocation model that dislocations are emitted from the grain boundary, but this is a fallacy. Firstly, radiation occurred between two grains whose surfaces form an angle (the boundary of the second grain is visible in the upper left corner); secondly, the radiation is periodic in nature and is directed from the source perpendicular to the surface of another grain; thirdly, it differs from the radiation shown in Fig. 68 and Fig. 68 (1) only higher resolution; fourthly, such radiation is demonstrated in this book in numerous photographs; fifth, additional sources are observed to the right of the main source, which must be taken into account in order to understand the mechanism of atomic reactions in a solid. Fig.70, taken from [4.5], illustrates the formation of twins. A detailed description of the experiment and its results does not require additional explanation. It is well known that the most important result of such a study is the discovery of the mechanism of the austenite-martensite phase

transition, which lasts ten-millionths of a second. Authors write the starting article, "TRIP steels possess a microstructure consisting of austenite with sufficient thermodynamic instability such that transformation to martensite is achieved during loading or deformation. Many automotive TRIP steels possess retained austenite within a ferrite matrix, which may also contain hard phases like bainite and martensite. In the case of these alloys, the high silicon and carbon content of TRIP steels results in significant volume fractions of retained austenite in the final microstructure.

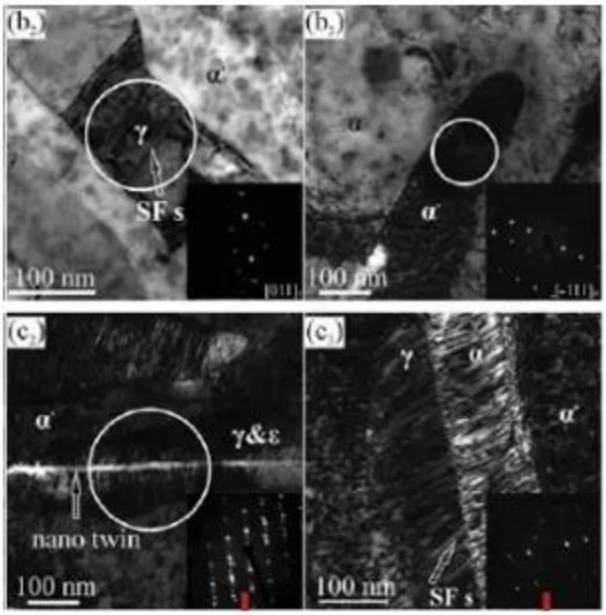


Fig. 70

The title of the article "Smaller is less stable: Size effects ..." indicates that the item is devoted to problems related to the Hall-Petch effect. The Hall-Petch equation characterizes the relationship between grain size and yield strength. It is assuming that grain boundaries inhibit dislocations. But in nanomaterials, the opposite effect is observed. This experimental fact proves that the extrapolation of the laws of mechanics into the nanoscale is unacceptable. It should be recalled that the dislocation model was presented at the beginning of the thirties of the last century in order to explain why the experimental value of the shear energy turned out to be an order of magnitude less than the theoretical value.

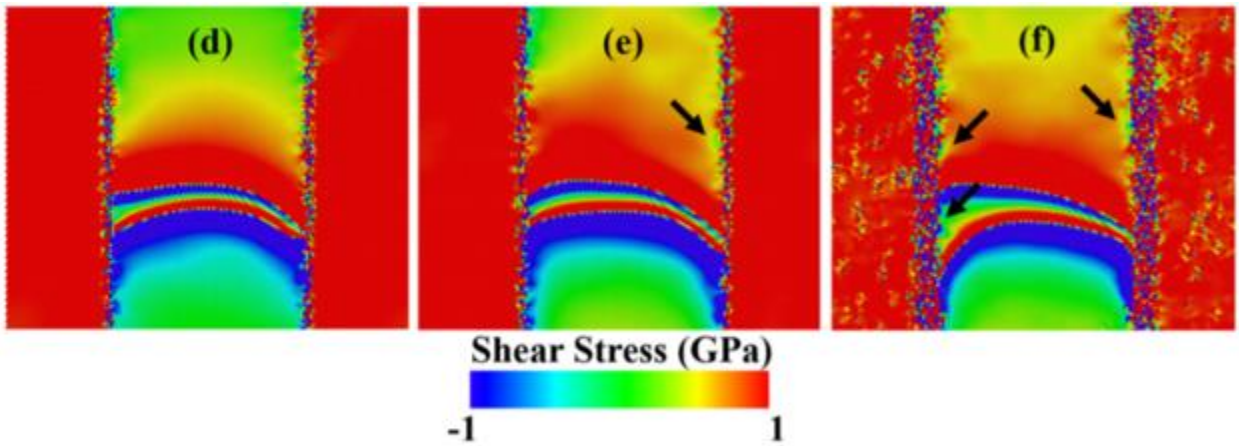


Fig. 71

The authors of [4.6], simulating atomic processes, demonstrate them using color drawings, some of which are shown in Fig. 71. They, explaining the little girl, write, "Local atomic structure

and (d), (e), (f) atomic shear stress distribution during dislocation propagation simulations at 3% applied shear strain. Black arrows denote local regions of low stress."

This model is erroneous. It is refuted by numerous experiments performed at the macro level. Photos of nano-objects confirm them. Fig. 72 illustrates the results of studies of the formation of cracks in a thin film of copper on the surface of flint under tensile strain and temperature change, performed in [4.7], using a transmission electron microscope. The authors note that photograph (a) illustrates the fatigue dislocations in a 3.0 μm film after $5\times10^3$ cycles, while photograph (b) shows a crack in a 0.2 μm film after $2\times10^4$ cycles. We see in the photo (a) grains separated by gaps. It is difficult to understand on what basis this conclusion made about the existence of the dislocations and what caused fatigue. The authors claim that the photograph shown in Fig. 72 (1), illustrates the "parallel glide" of dislocations and thinning along boundaries.
We pay attention to the fact that the area designated as Damage along TBs passes between the grains, originates, bends, and ends at the junction of three grains. The formation of such cracks is repeatedly observing, but we will limit ourselves to one example.

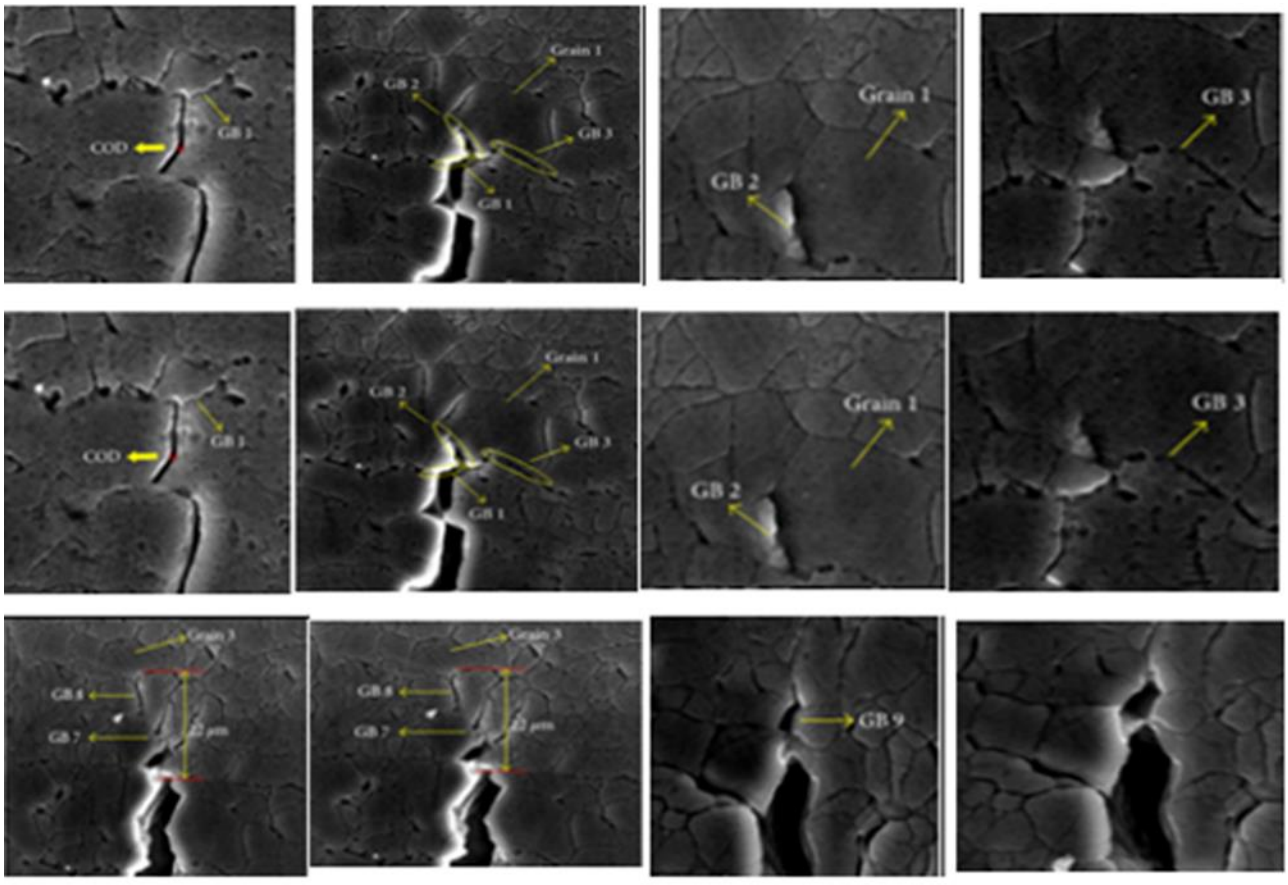


**Fig. 73**

Twelve of the twenty-nine photographs cited in [4.8] are showing in Fig.73. They illustrate the process of forming cracks along grain boundaries and changing the color of grain boundaries. A 7050-T7451 aluminum alloy dumbbell sample is subjecting to tensile strain. The crack formation has been examined using a scanning electron microscope, a photograph of one of which is shown in Fig. 74 (d). It "stuck" at the grain boundary, as approached it at an angle of 90 °.

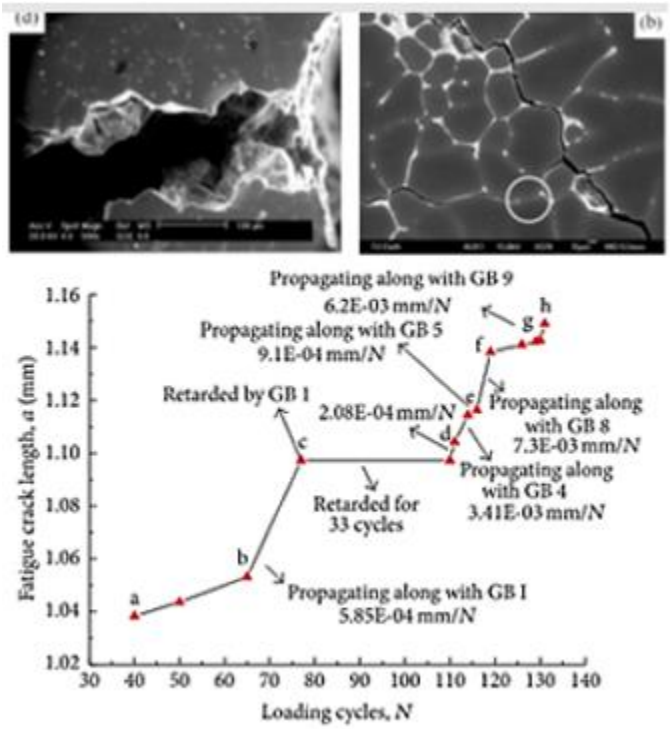


**Fig. 74**

A crack enveloping nine grains are showing in Fig. 74 (b); The final graph compiled by the authors allows us to trace the spasmodic nature of the crack growth. The spasmodic crack growth indicates the accumulation of energy and its pulsed radiation. The atomic structure of the metal makes it possible to estimate the energy needed to break the bond during the abrupt growth of a crack, taking the alloy for pure aluminum, the wight of which is $h$ =0.8 mm. The distance between aluminum atoms is $r$=2.86·10$^{-10}$ m, the binding energy of atoms is $\varepsilon_b$ =3.34 eV, the maximal energy has been accumulated before the jump g → h, which is necessary for breaking the bond over a length of $l$=6.2·10$^{-6}$ m. The pulse energy $A$ is estimated using the formula: $U_2 = \frac{lh\varepsilon_b}{a^2}$.

*Such processes are realizing in stars, a laser, and, as we see, in a solid, but they can only be describing using quantum mechanics.*

However, an analysis of the works published from 2004 to December 2019 shows that the authors are trying to find an explanation of the observed effects using dislocations and models proposed by Taylor, Orowan, Cottrell, Olson, and Cohen, which are refuted by the results of the experiments described in the book.

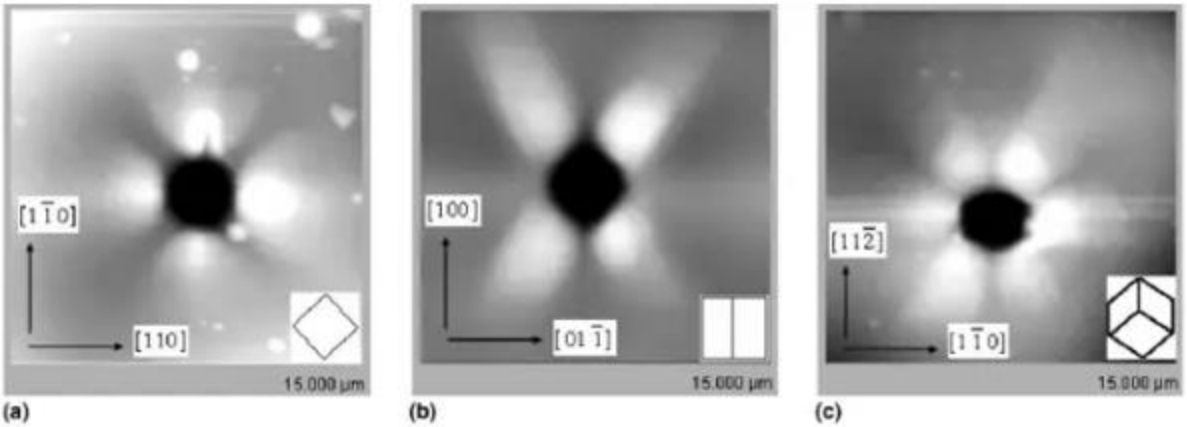


**Fig.75**

Three photographs of copper nanoindentation shown in Fig. 75 were published in [4.9] 15 years before the publication of [4.3], but the authors did not interpret the observed phenomenon from the position of dislocations, remaining in the area of classical mechanics.

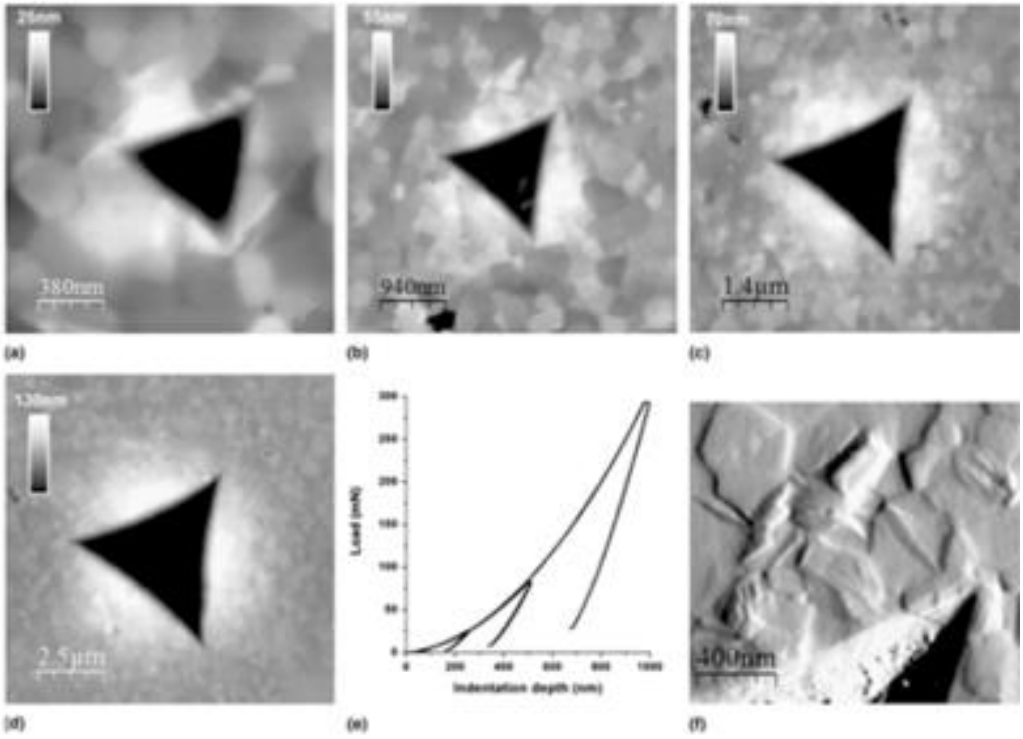


**Fig. 76 (1)**

Fig. 76 illustrates the result of the nanoindentation of polycrystalline and single crystals of yttrium-doped zirconium oxide with tetragonal and cubic phases. Analysis of the mechanisms of deformation is carried out using atomic force microscopy (AFM), as well as using micro-Raman spectroscopy [4.10]. The use of the Raman effect to study the processes occurring in nanoobjects radically changes the interpretation of the observed phenomenon.

The Raman effect is that a photon absorbed by a molecule in a gas, liquid, and solid is partially absorbed by it, "taking" the energy of the molecule. An increase or decrease in energy causes the photon frequency to increase or decrease. Mechanical methods cannot explain this phenomenon. But micro-Raman spectroscopy provides complete information about the processes in nanomaterials, including carbon.

The areas around the indenter shown in Fig. 75 and Fig. 76 (1) excludes the possibility of isolating any dislocation. But the authors of [4.10] write, “So, if the dislocation remains at the border of the residual imprint, the pile-up observed around the indentation can be explained by the deformation field induced by all the pile-up of dislocations present under the residual imprint.”

The authors describe photo (b) as follows, “In Fig. 76 (2b), dislocation slip lines, with a curved shape, characteristic of zirconia cubic crystals, are clearly observed inside the imprint. Furthermore, the comparison of the derivative and the topographic AFM measurements clearly show that the slip lines stop when they reach the border of the residual imprint**.”**

However, we see that strict patterns are manifested in four different directions, two of which are characteristic of twins. At the same time, dark and light lines are observed. All this indicates the manifestation of anisotropy of atomic reactions during the formation of the imprint. The layered construction of the nano-region is similar to the construction of the mountains. Such repeated coincidences cannot be called random, and it is impossible to explain using dislocations**.**

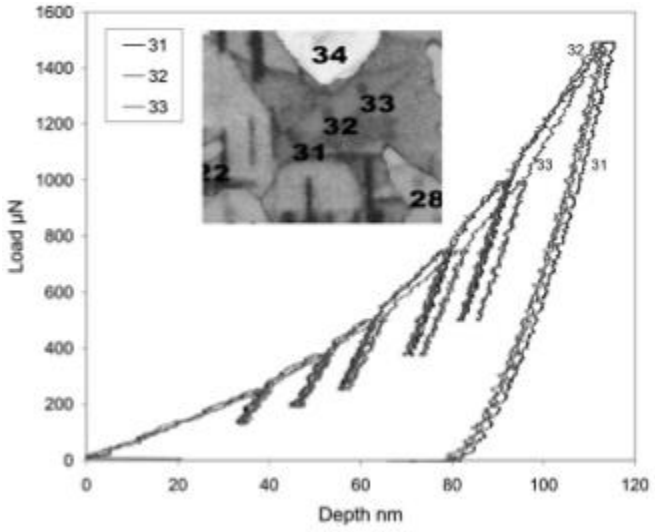


**Fig. 77**

The graph is shown in Fig. 76 (1) e, acquires special significance when indentation is carried out on one grain.

The hexagonal (α) phase of the Ti-5Al-5Mo-5V-3Cr-0.5Fe alloy was studied by the nano-identification method in [4.11]. The result of the three measurements is shown in Fig. 77. It indicates that the breaking of bonds between atoms was spasmodic, indicating the accumulation of energy and its simulated radiation.

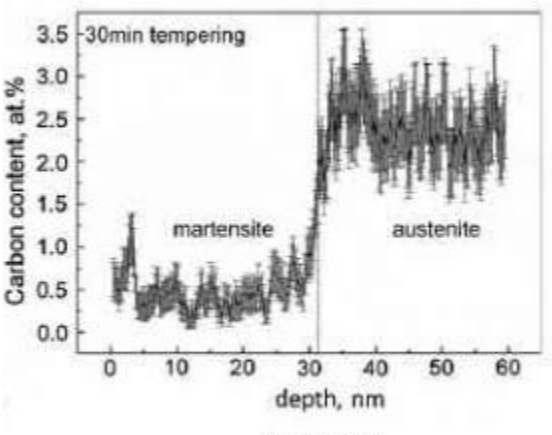


Fig.78 (1)

### 4.3. Carbon segregation

The segregation of carbon atoms (ions) has repeatedly been observing. First of all, it is necessary to note the experimental studies performed at the Max-Planck Institut für Eisenforschung, Germany, at a high level, which present the results of *discoveries* that require explanation.The high strength of fullerene and carbon nanotubes stimulated the hypothesis that their introduction into the alloy will increase the performance of the material. The experiments, [4.11], showed that fullerene is localized between grains and did not significantly affect the phase transition. However, carbon segregation in $10^{-7}$ seconds of the essence changes the property of one phase compared to another one.

Changing the properties at such a rate occurs as a result of an atomic reaction, at the phase boundary of which a transition layer is forming, graphically shown in Fig. 78 (1), characterizing the distribution of carbon in martensite and austenite [4.12].

The ratio of elements in the alloy is showing in table 1 given in this work.

Table 1
Chemical composition of material used for the investigation (1.4034, X44Cr13, AISI 420).

| | C | Cr | Mn | Ni | Si | N | Fe |
|---|---|---|---|---|---|---|---|
| wt.% | 0.437 | 13.6 | 0.53 | 0.16 | 0.284 | 0.0205 | Bal. |
| at.% | 1.97 | 14.19 | 0.52 | 0.15 | 0.55 | 0.079 | Bal. |

The 0.23C – 1.23Si – 1.50Mn, wt.% alloy with a higher carbon content was investigating in [4.13]. The carbon distribution is showing in Fig. 78 (2). It can be concluded, that the martensite / residual austenite (α′ / γ) transition occurred in a layer of the order of one nanometer.

It has been experimentally established that segregation of bismuth from a Cu-Bi alloy leads to embrittlement even with a monoatomic bismuth layer. The question naturally arises: why do bismuth atoms, whose atomic mass is 3.29 times higher than the atomic mass of copper, easily diffuse in the alloy? The segregation of a bismuth atom becomes possible when it is ionized. The ionic radius of $Bi^{3+}$ is 0.117 nm, $Bi^{5+}$ is 0.09 nm, while the length of the Cu – Cu bond is 0.29 nm.

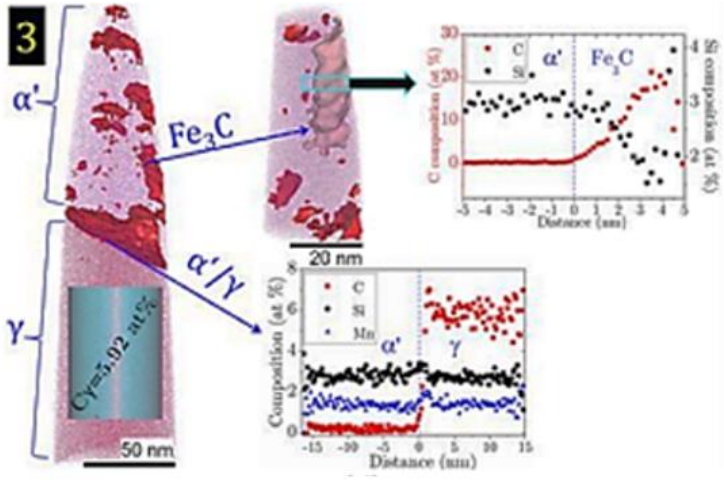


Fig. 78 (2)

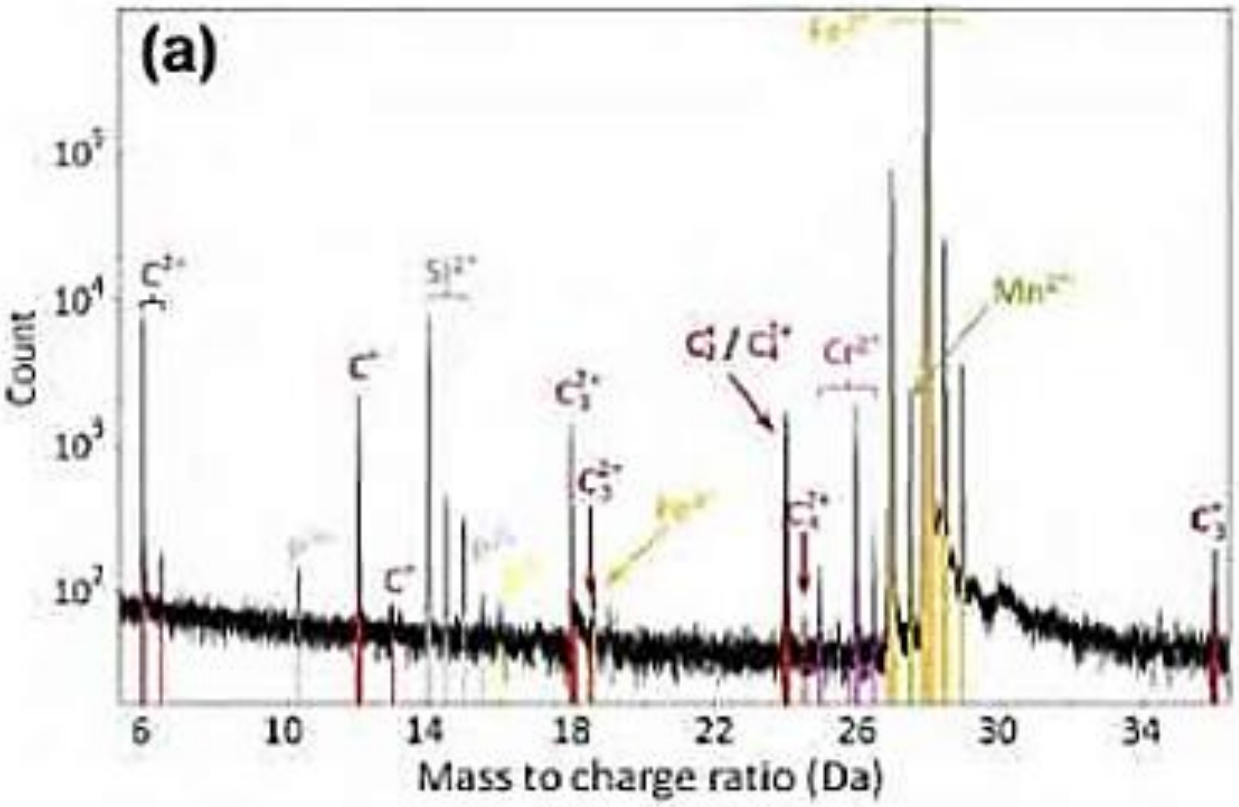


Fig. 78 (3)

The radius of the $C^{1+}$ ions is 0.04 nm; of the $C^{4+}$ ion is 0.03 nm; the C-C bond length is 0.125 nm, the C = C bond is 0.133 nm. The results of mass spectrometric studies performed in [4.14], shown in Fig. 78 (3) indicate the formation of atomic ions and ions of the $C_4^{2+}$.molecule.

*This fact allows us to conclude that graphene is formed at the martensite – austenite interface, which substantially changes the phase property.*

The validity of the hypothesis can be verified using micro-Raman spectroscopy or other methods.

### 4.4. Hydrogen embrittlement

Hydrogen embrittlement of steels is well known. The creation of highly entropic alloys stimulated the search for a composition with maximum time and a maximum volume of hydrogen storage, but the problem of the effect of hydrogen on the strength properties of the material remains no less important. The method of monitoring atomic reactions allows you to perform research quickly and without high costs. Palladium is the most promising metal for the experiment.

### 4.5. Tin Plague

The conversion of white tin to gray (β-Sn → α-Sn phase transition) is causing by a change in the electron shell of atoms from $Sn^{4+}$ to $Sn^{2+}$ with decreasing temperature.

The bond weakening occurs when the electron shell of atoms is measured. For example, white tin (β-Sn) at a temperature of -13.2º C turns into the gray tin (α-Sn) and crumbles. The reason for this

phase transformation is that ion recombination occurs in which Sn4+ ions have an ionic radius of 0. 68 Å are converting to $Sn^{2+}$ ions with a radius of 1.02 Å. This leads to the fact that the specific volume increases by 25%, and the metal turns into powder.

This phase transition can be investigated in detail using the method proposed by me. Pure tin emits acoustic waves during bending (crackling is heard) due to internal friction. Such deformation will be accompanied by p-radiation.

### 4.6. Metal welding

Melting of metals during welding is accompanying by the formation of specific defects that differ from defects due to deformation and corrosion. The process of energy storage and destruction of such a defect may differ from procedures in solid metal. Consequently, n-radiation is also different. This fact requires individual studies both during the formation of the seam and during its operation.

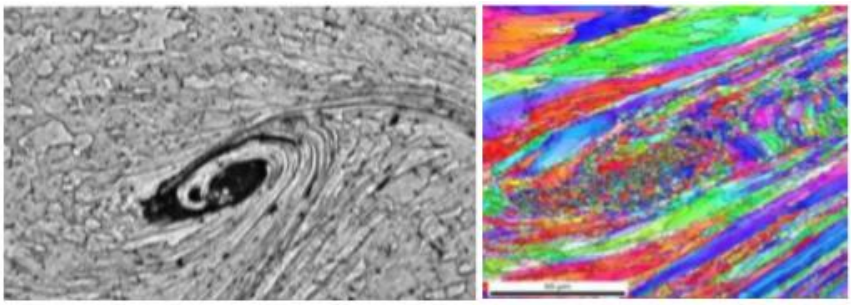

**Fig. 79**

This difference is due to that p-radiation characterizes the region in which the atoms were excited and transferred to the normal state. All other methods describe the object by transmission or reflection. Only taking all factors into account allows us to give an objective assessment of the danger of a particular defect during the operation of an element of a structure or device. Fig. 79 illustrates the vortex zone of the aluminum – aluminum joint formed during explosion welding and the map of the vortex zone obtained by EBSD analysis [4.16]. P-radiation, characterizing the weld, has not been previously used. But it is necessary to find the correspondence between the defect and its image, so using the method becomes possible. The advantage of the proposed method is that a color image appears on the bright screen, characterizing not only the shape but also the distribution of chemical elements, which will differ from what it was before melting. The photograph is showing in Fig. 79 indicates that mixing has occurred as a result of the formation of the vortex. The mechanism of this phenomenon is not disclosing. It may be due to the Coriolis force, whose action is related to the daily rotation of the Earth and the direction of the melt by rotation, choosing which you can reduce the Coriolis force to zero. A weld defect, for example, in a pipeline, often causes catastrophic failure. Prediction of cracks in it requires taking

into account all the features of atomic melting and solidification reactions. But such a statement is possible only with the use of quantum mechanics.

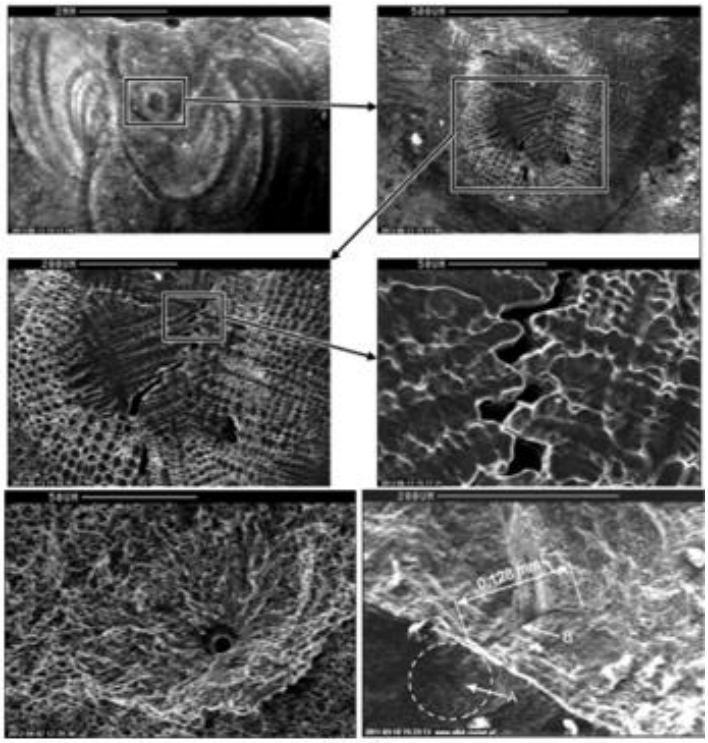

Fig.80

The weld of a pipeline made of the 7CrMoVTiB10-10 alloy was studied using a scanning electron microscope in [4.17]. Fig. 80 illustrates photographs of a defect found during the examination. Electron microscopic study of the weld, the results of which are showing in Fig. 79, and Fig. 80 are of undoubted scientific interest, indicating the possibility of the formation of vortices, craters, and cracks that have arisen near them. However, the microscope cannot be used to control the pipeline during its operation. Therefore, p-radiation should be used instead of a microscope and an x-ray source, but it does not exclude the possibility of a detailed study using other methods. The deformation of a solid is accompanying by electromagnetic radiation in a wide range: from radio to Hexa-frequencies. Studies performed in each field provide various information on the behavior of atoms.

### 4.7. Infrared radiation

A dumbbell-shaped sample of s45c alloy has been subjecting to tensile deformation in [4.18]. The infrared radiation of the sample was studied simultaneously with the construction of the *S-N* curve. It means that the authors investigated that part of the strain energy, which was transforming into heat.

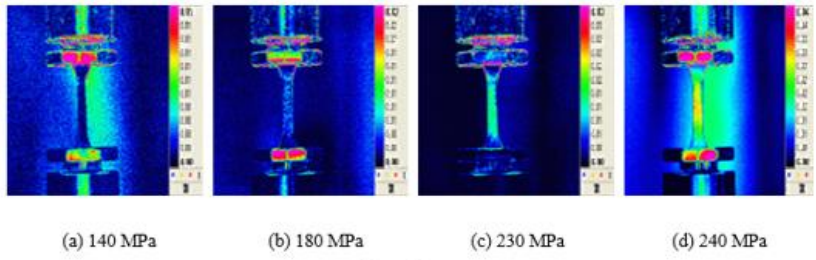

(a) 140 MPa (b) 180 MPa (c) 230 MPa (d) 240 MPa

Fig. 81

This work aimed to evaluate stress distributions using the thermographic method in an adiabatic system. Changes in infrared radiation caused by changes in load shown in Fig. 81. We draw attention to the fact that Maxwell, in a letter to Thomson (1856), excluded heating losses from consideration. But we, using the theory of heat capacity, can estimate the energy of the vibrational motion of atoms at a given temperature. For a bit, we take it equal to $\varepsilon = 3k_B T$, where $k_B$ is the Boltzmann constant, T is the absolute temperature.

Changing the temperature of one kelvin will be $\Delta\varepsilon = 2.58 \cdot 10^{-4}$ эВ$/K$, which we can neglect in comparison with the photon energy of p-radiation.

### 4.8. Search for defect-free alloys

A broad search for new technologies for producing high-strength defect-free alloys made by D. G. Eskin *et al*. They used all the achievements of modern experimental technology.

We confine ourselves to only a small part, [4.19-4.24], of published works, the purpose of which was best the authors formulated.

I. 1) "The final objective of this work was to apply the fracture mechanics to determine the critical crack/void size that may lead to the catastrophic failure of the billets. This may not only provide us with the failure probability during the DC-casting process, but it also gives us an idea of what void/crack sizes may trigger the failure. The comparison of such crack/void sizes with the actual void size in DC-cast billets may reveal what kind of voids are the most critical." 2) "In this study, we scrutinized the cold cracking phenomenon with the aim to establish a criterion that predicts cold cracking during DC-casting." [4.19].

II. "In our previous article, we used the constitutive parameters and plane strain fracture toughness ($K_{Ic}$) values of the genuine as-cast material for simulation of residual stresses in the DC-cast billet. The next step taken in the current article is to study the influence of casting variables on the magnitude and distribution of residual thermal stresses in DC-cast billets." [4.20].

**"A**t the moment, we have a numerical process simulator to simulate the aluminum DC-casting process, called ALSIM[3]. Although, at its current version, ALSIM 6 has criteria to estimate the susceptibility for both HT and CC, it was reported that ALSIM's crack prediction capability has not yet reached its full potential. Therefore, the main goal of this study is four-fold: (1) Verify the connection between HT and CC experimentally. (2) Complete ALSIM materials database for AA7050 for a better crack prediction accuracy. (3) Analyze ALSIM model sensitivity with respect to different DC casting parameters and materials database. (4) Propose a concept of a new crack prediction criterion so that ALSIM could capture the connection between HT and CC quantitatively." [4.21**].**

The experimental base, which the researchers had, made it possible to research the highest level, and significant results obtained, which are described and presented in books, dissertations, and articles. However, the analysis of the research results was performed by the methods of fracture mechanics, based on the theories of Griffiths, Orowan, and the Irwin model. Fracture toughness and impact toughness are estimated based on stress intensity factors following standards, including E399. So, we see that the laboratories of Germany, Great Britain, Russia, and China do not use new theories of physics.

We will consider one more example.

[3] ALSIM is a casting-simulation software developed by the Norwegian Institute for Energy Technology (IFE), Kjeller, Norway ALSIM.

**5. The formation of cracks in the fuselage of aircraft**

The catastrophic destruction of the Boeing 737-297 fuselage, which occurred in April 1988, showed that the control methods existing at that time, which should ensure the safe operation of aircraft, are imperfect.

US President Signs PUBLIC LAW 100-591 — NOV. 3, 1988 "RESEARCH PLAN AND REPORTS," which includes the essential tasks:

1. "...the Administrator necessary to ensure the continued capacity, safety, and efficiency of aviation in the United States, considering emerging technologies and forecasted needs of civil aeronautics, and provide the highest degree of safety in air travel.
2. Administrator considers to be necessary to ensure that aviation safety will be given the highest priority..."

However, more than thirty years have passed. However, the control methods that should ensure aviation security have not fundamentally changed since they are still basing on the hypotheses that the experiment throws down. I examined the mechanism of cracking in the fuselage of an airplane in [1.9]. In this book, we will examine additional evidence of the need to abandon such hypotheses.

The term metal fatigue is using for almost 150 years, but there are still no units of measure. A method for numerically assessing fatigue is absent. The absence of a quantitative criterion in the formation of cracks excluded the possibility of forecasting even in the case when two cracks appeared simultaneously. A catastrophe in which the rail exploded into 300 fragments (Hatfield. UK. 2000) occurred after an ultrasound study the day before did not reveal any dangerous defects. Such disasters have occurred repeatedly. On April 1, 2011, a crack of 59″·9″ (1498.6·226 $mm^{2)}$ formed in the Boeing 737-300. The plane flew in only 48,748 hours. They managed to plant it, but this incident did not change the methods for studying the causes of the formation of such cracks.

The nine panels of the Boeing 727 fuselage, which had a flight time of 66412, were experimentally investigated following the FAA FASTER (the Full-Scale Aircraft Structural Test Evaluation and Research) program at the Federal Aviation Administration William J. Hughes Technical Center).

One of the panels was investigating in [4.24]. Cracks called fatigue were discovered in the vicinity of several riveted holes, of which we will consider one. The A40 AFT crack was found to the left of the A40 rivet hole earlier than the A40 FWD crack on the right. The growth rate of the A40 AFT crack exceeded the crack growth rate of A40 FWD.

The results of measuring crack lengths were used in the NASGRO equation, in the solution of which the same parameters of this equation for two different cracks were obtained. If we agree with Irwin's hypothesis, then the critical value, first of all, will reach the one that was born earlier, grows faster, that is, the length of which is more significant. This follows from the NASGRO equation. But experiments indicate that destruction is due to the energy that will be accumulated, radiated, and will work to break bonds. The energy calculation $\Delta U_2=F(\frac{\Delta l}{\Delta N})$, performed for the crack A40 FWD is shown graphically in Fig. 28 as a function of the number of cycles. Of particular interest is the deep minimum at $N$ = 141229. The remaining changes $\Delta U_2$ against the background of this minimum are leveled.

The A40 AFT crack was found to the left of the A40 rivet hole earlier than the A40 FWD crack on the right. The growth rate of the A40 AFT crack exceeded the crack growth rate of A40 FWD. The results of measuring crack lengths were used in the NASGRO equation, in the solution of which the same parameters of this equation for two different cracks were obtained. If we agree with Irwin's hypothesis, then the critical value, first of all, will reach the one that was born earlier, grows faster, that is, the length of which is greater. This follows from the NASGRO equation. But experiments indicate that destruction is due to the energy that will be accumulated, radiated, and will work to break bonds. The energy ΔU2 required to expand the crack Δl when changing the number of cycles of external action ΔN is calculated by the equation

$$\Delta U_2 = \frac{h\varepsilon_b}{a^2} \cdot \frac{\Delta l}{\Delta N},$$

where $a$ is the lattice constant of aluminum, $h$ is its thickness, $\varepsilon_b$ is the binding energy.

Please pay attention to the fact that the proposed equation is fundamentally different from the equations of mechanics since the crack growth rate is an argument, not a function.

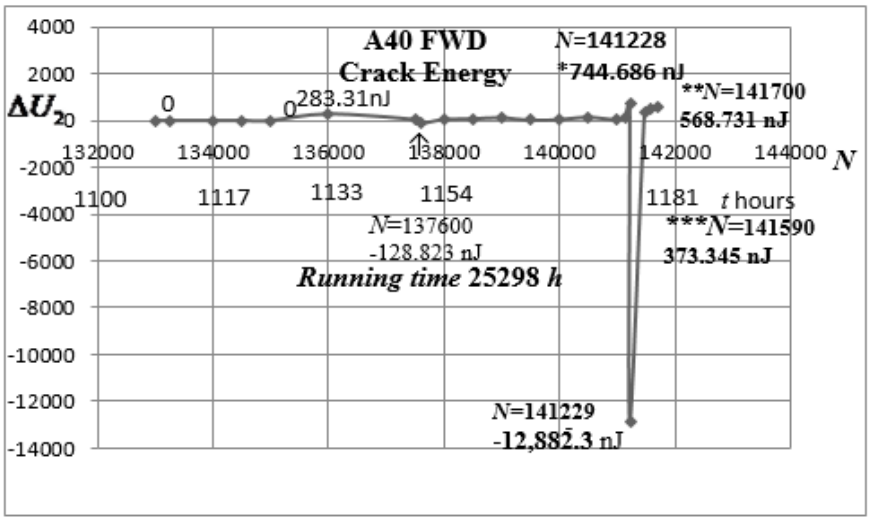


**Fig. 82 (1)**

The numerical values for aluminum studied in [4.24] are as follows: $h$ = 1.6·10$^{-3}$ m, $a$=4.05·10$^{-10}$ m, $\varepsilon_b$= 5.34·10$^{-19}$ J. Fig. 82 (1) illustrates the energy generation of the formation of two cracks. The deep minimum energy is reduced by a factor of 100 to demonstrate the entire range of values on this scale.

Consequently, $\Delta U_2 = \frac{1.6\cdot10^{-3}\cdot5.34\cdot10^{-19}}{4.05^2\cdot10^{-20}} \cdot \frac{\Delta l}{\Delta N} = 5.219 \cdot 10^{-4} \frac{\Delta l}{\Delta N}$

Graphically, the function $\Delta U_2 = F\left(\frac{\Delta l}{\Delta N}\right)$ is shown in Fig. 82 (1) along the ordinate axis; the number of tests ($N$) and the time of one test cycle ($t$) were used as the abscissa. Of particular interest are the two minimums of the potential strain energy, one of which is denoted by the arrow ↑. The energy accumulated in this minimum is small and did not significantly affect the processes. But the energy accumulated at $N$ = 141229 is 12882.3 nJ. Subsequent tests at *$N$ = 141228, ** $N$ = 141590, and *** $N$ = 141700 are accompanied by the absorption of energy, which is spent on breaking bonds and elongation of the crack.

The total consumption is equal to 1704.762 nJ, which is ~ 13% of the accumulated energy.

*Consequently, the accumulated energy can be radiated, forming a catastrophic crack. Indeed, in one of the tests in this area, a crack of* 11.8 *inches was formed.*

Fig. 82 (2) illustrates the energetics of the formation of two cracks. The energy of the deep minimum decreases 100 times to demonstrate the full range of values on this scale.

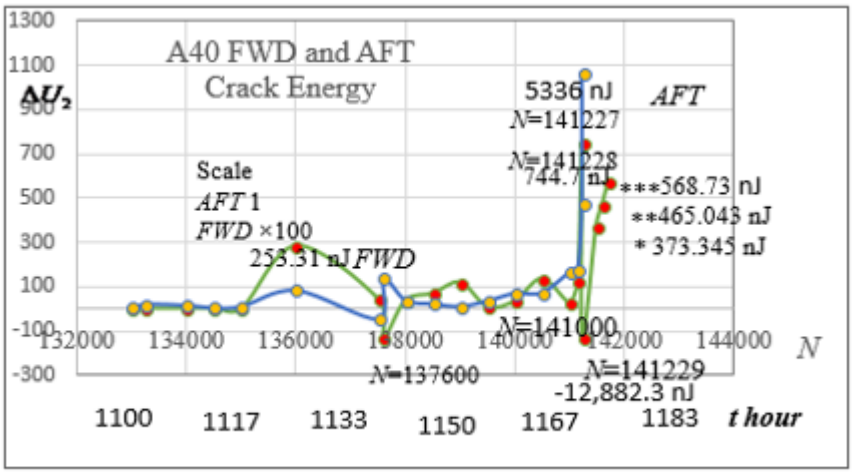


**Fig. 82 (2)**

However, this is not the only drawback of the experimental study that is using still. One test lasts 25-30 seconds. The experiment continues 25,298 hours. The crack is forming during a millionth of a second. Thus, it is impossible to establish at what point this happened. The method is destructive and cannot be used in practice.

*So, we see that the theoretical analysis of experimental results from the position of mechanics, based on erroneous hypotheses, distorts the real results of research processes.*

However, this is not the only drawback of the experimental study that is using still. One test lasts 25-30 seconds. The investigating time was 25298 hours. The duration from one measurement of the crack length to the next was hundreds of hours. This time did not allow researchers to determine the moment when the destruction occurred. The method is destructive and can no more be used in practice.

### 6.1. Repulsion and attraction cracks

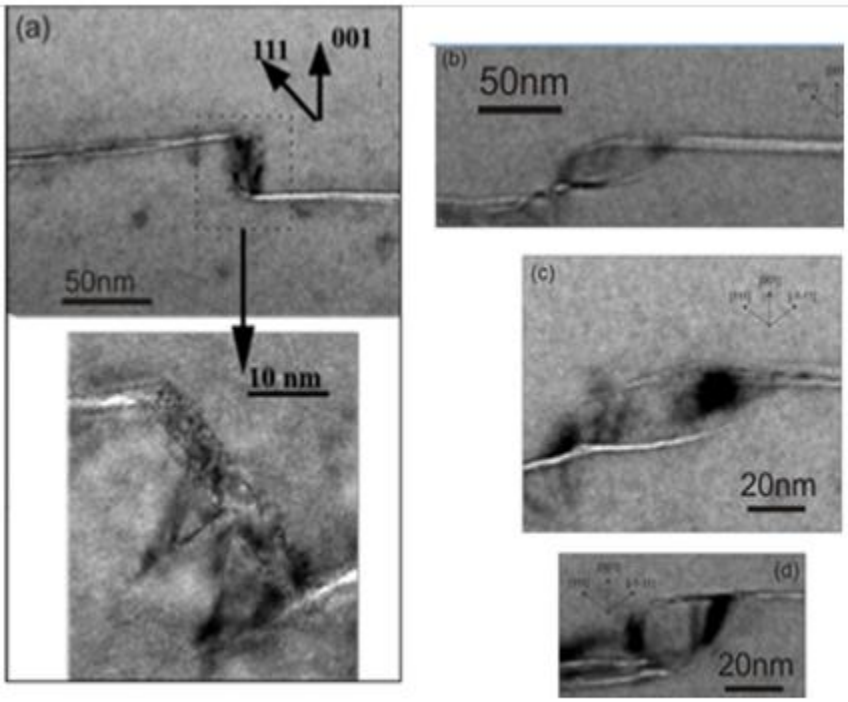


**Fig. 83**

Of particular interest are parallel cracks growing towards each other, as shown in Fig. 83 for a silicon nanoplate irradiated with hydrogen and helium ions [4.25]; the riveted joint of the fuselage panel during bending deformation and tension [4.26], shown in Fig 84; upon deformation of the Earth's surface, Fig 85 (1) [4.27]; tensile polymers, Fig 85 (2), [4.28] and Fig 85 (3), [4.29]. A distinctive feature of such cracks is that each of the cracks, not reaching the meeting point, bends and bends around it. Such cracks are called repulsion and attraction.

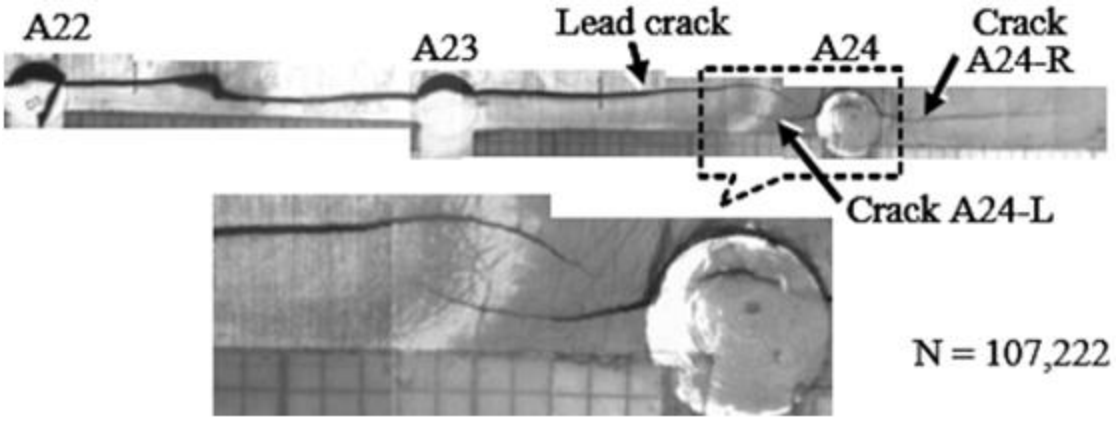


**Fig. 84**

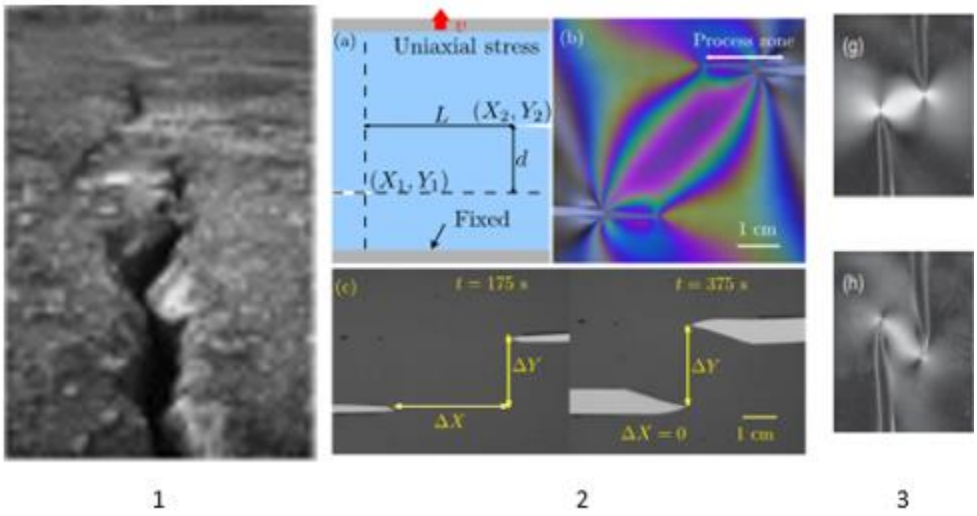


1 2 3

**Fig. 85**

Crack formation is considered in more detail in [1.9].

The photographs are showing in Fig. 83- Fig. 85 show cracks in objects, the size of which differs by thirteen orders of magnitude (from 10 nanometers to a dozen kilometers). The identity of the mechanism of the formation of such cracks is not in doubt. But the mechanism of crack formation, whose length is tens of nanometers, can be caused only by the exchange interaction of atoms. Thus, we conclude that such cracks are caused by atomic reactions that are independent of the size of the object. This conclusion saves us from the need to analyze geometric and mechanical models.

### 6.2. The growth dynamics of four cracks in the fuselage of the aircraft

A. Ahmed carried out careful measurements of crack growth A22 L (left), A22 R (right), A23 L, and A23 R [4.26]. These cracks get and grow contrary to the models prescribed in mechanics. Having noted this fact, he remained within the framework of these models, considering the crack growth rate da/dN as a function. Graphically, this semi-logarithmic relationship is shown in Fig. 86.

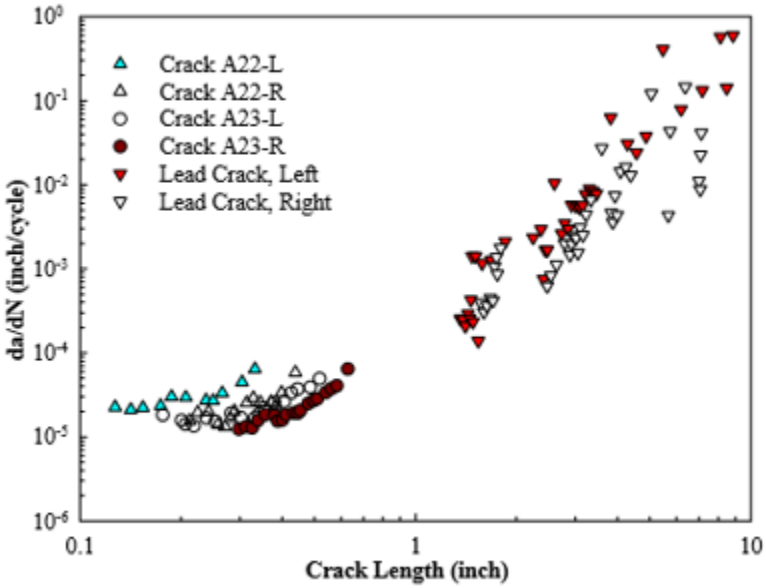


**Fig. 86**

The distinctive features of the four marked cracks can be establishing only partially, noting the general laws of the crack growth rate along their length. However, a crack that length was 1925 mm is not predictable.

The crack growth tables given in [4.26] provide complete information when calculating the energy spent on crack formation.

The results of calculating the energy spent on cracking A22-L and A22-R are showing graphically (A22-L and A22-R Crack Energy).

The information that we receive using these graphs more accurately reflects the process of cracking; this allows us to understand the mechanism of this process better; we can assess the danger of each of the cracks, having data on the energy and rate of its accumulation. Tables N and ΔN show that the interval between the maximums is mainly preserved even in such a cumbersome experiment.

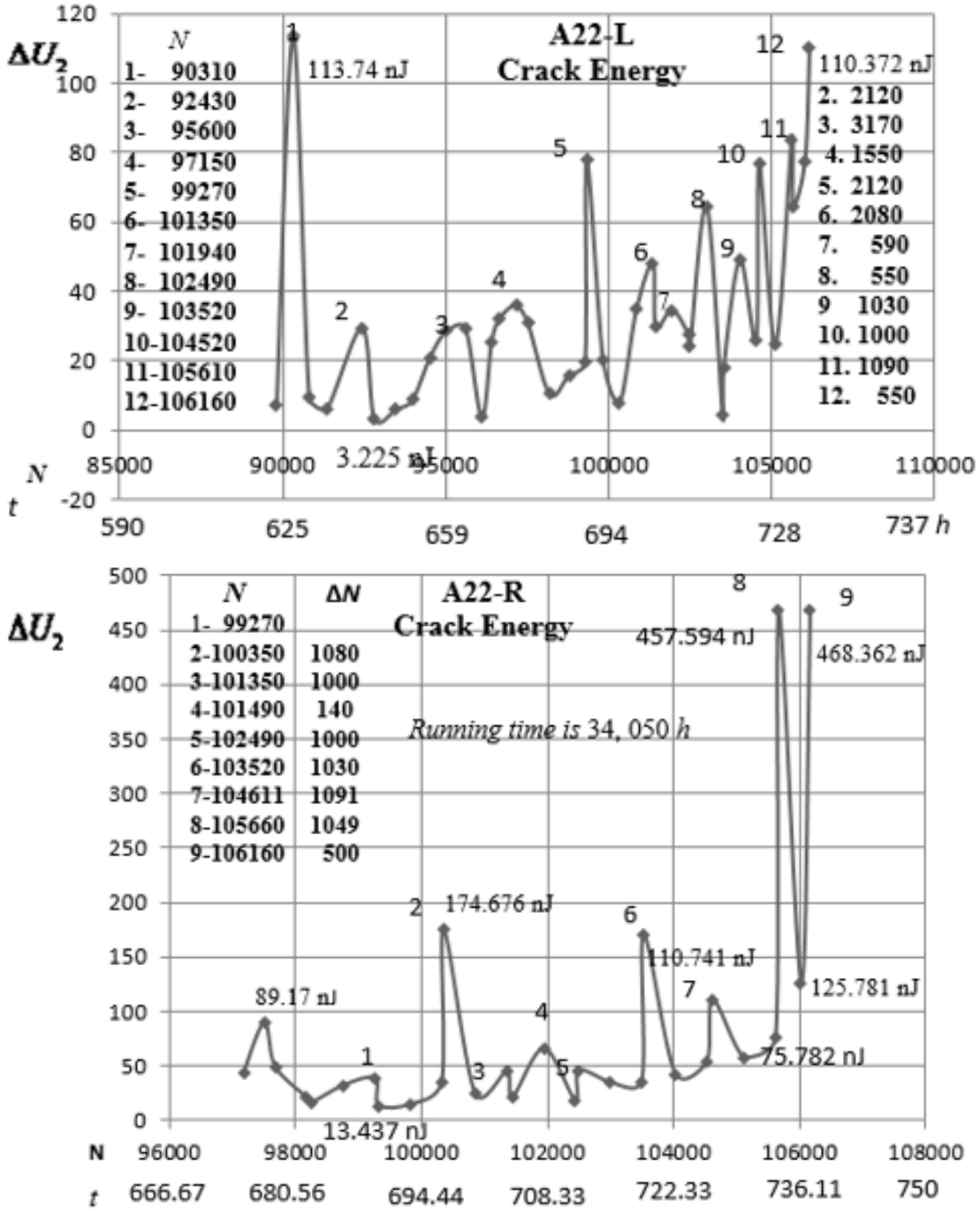


So, we see that its jumping radiation accompanies the accumulation of energy; the crack on the right grew four times faster than on the left; the study took 34050 hours**.**

.

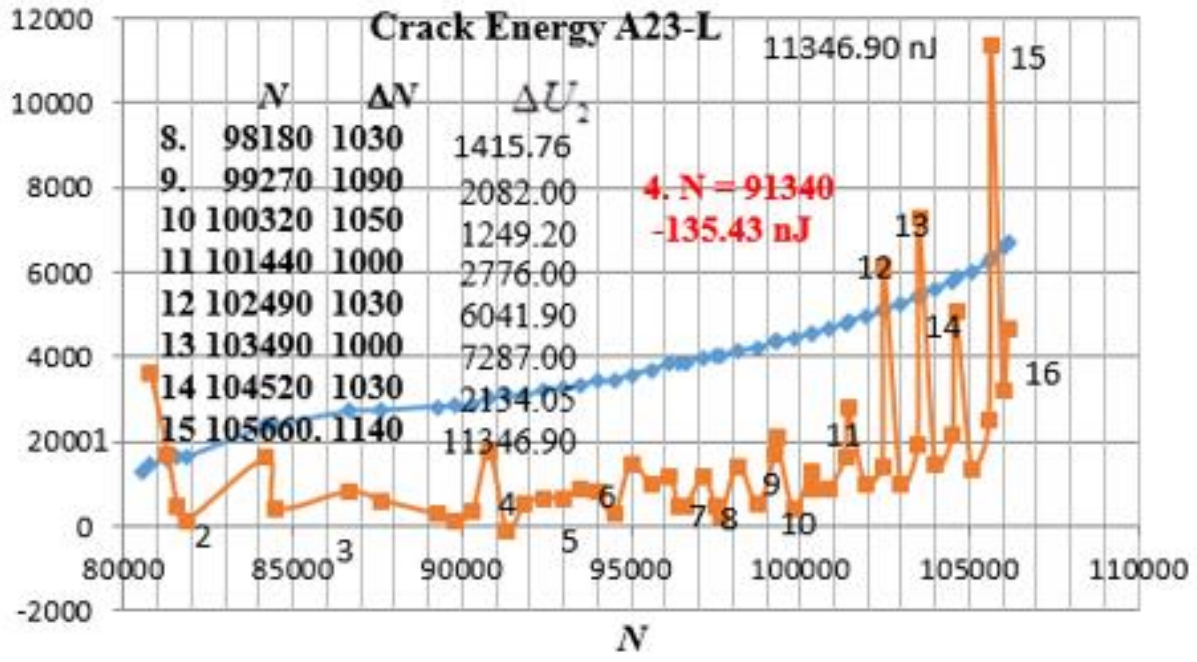


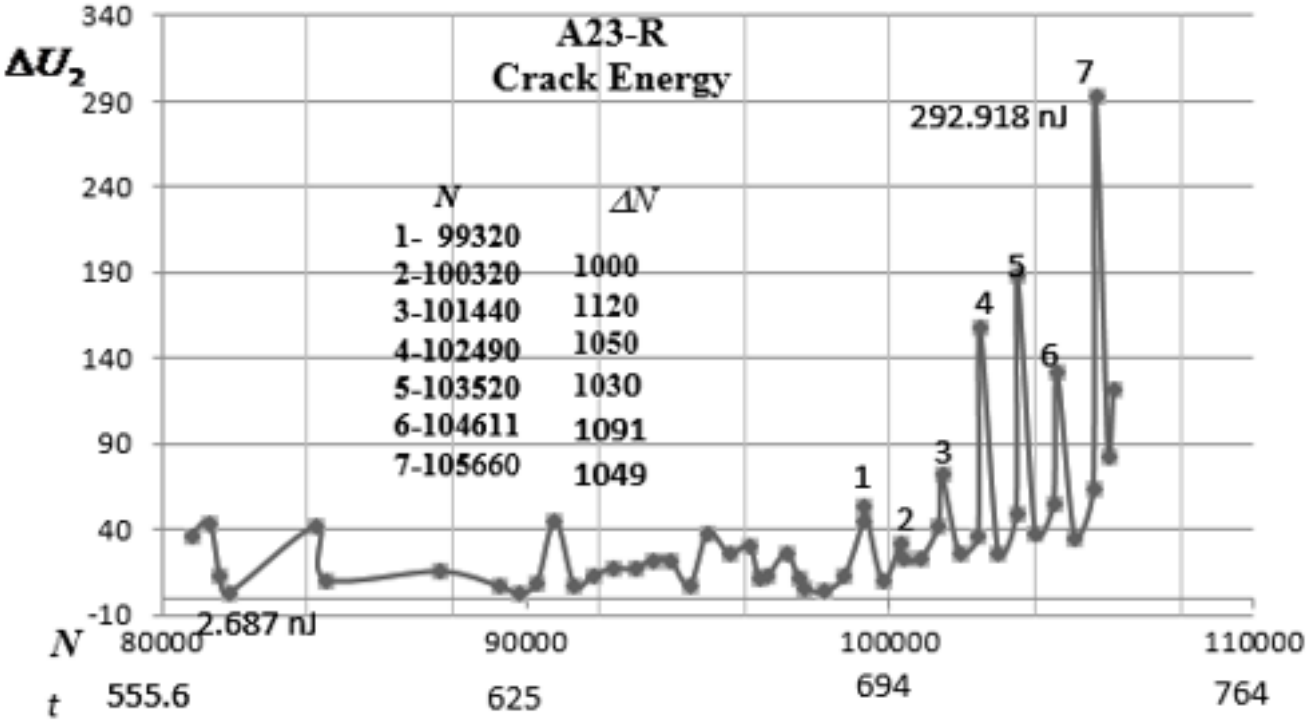


1) The blue graph shown on A23-L illustrates the change in crack length throughout the study. 2) An energy analysis of the processes of the formation of cracks A23-L and A23-R shows that the mechanism of these cracks has not changed compared to cracks formed near the hole A22, but the crack A23-L grew almost 39 times faster than A23-R and about 25 times faster than the oncoming A22-R crack.

The fact that a 1.925 m long crack originated to the left of the A23 hole requires individual studies. But the graphs are given to demonstrate once again the failure of mechanical models of cracking

### 6.3. Mistakes of state standards

1. An analysis of the works published until December 2019 shows that the most significant parameters in fracture mechanics remain: the rate of release of elastic energy G, the stress intensity factor K, the J-integral, the crack-tip opening displacement CTOD, and crack-tip opening angle CTOA.

2. The main mistakes in the development of state standards that guaranty the safe operation of structures and devices are due to the neglect of the fundamental laws of physics, based on which measurements of the necessary physical parameters are carried out, an attempt to replace the measurements of these parameters with mathematical polynomials.

3. Analysis of US standard E 399, based on publications [4.29, 4.30], showed that the number of parameters used to calculate the fracture toughness is 103, of which there are twelve intensity factors. The number of equations necessary for this, in [4.29] is 33, in [4.30] -87. The measured parameters are crack length, sample thickness, stress, Young's modulus. It means that all other parameters are mathematical. There is no indication based on which experiment the equations are proposing, or with what test they are confirmed.

4. It is especially important to note that even when the laser beam acts on the metal, the same parameters G, K, J, CTOD, and CTOA are using.

5. Numerous experiments described in this book and appendix prove that standards designed to ensure new ones should replace the safe operation of structures and devices that do not take into account the energy of atomic reactions.

6. The experiment showed that the main measured parameter is the potential energy due to a change in the electron shell of atoms, and not the position of the atoms.

7. The modern experimental base allows you to perform an expert assessment of any standard for compliance with physical laws.

Example. US patent 9,272,794 B2, Mar. 1, 2016, D.A. Froom, W. T. Manak, System and Methods for Non-Destructive Inspection of Airlines.

The patent is intending for periodic studies of defects in a model of an aircraft made of gold using radiography, neutron diffraction, and ultrasound.

The disadvantages of the method.

1. X-rays from an external source, ultrasonic waves, and neutrons do not detect an energy source whose radiation causes destruction.

2. Mathematical extrapolation during modeling is unacceptable for the study of the interaction of X-rays and neutrons with atoms. For example, the linear absorption coefficient of X-rays $\tau$ depends on the density of the substance $\rho$, the nuclear charge $Z$ and the wavelength $\lambda$ according to the formula $\tau = k\rho Z^3\lambda^3$. The ratio $\frac{\tau(gold)}{\tau(aluminum)} = 1603$. It means that the defects in the model and the real object are different.

3. Gold is not subject to corrosion. Therefore, the appearance of such a defect in the metal is not predicting.

4. There are no equations with which to predict the time of safe operation.

### 6.4. The ability to replace State standards

1. The result of the experiments performed by the author indicates electromagnetic radiation with a frequency of the order of $10^{18}$–$10^{19}$ Hz, which occurs during an atomic reaction. Therefore, the method of monitoring atomic reactions is universal. So, It is appropriate to all objects, regardless of size, composition, structure, and types of external influences.

2. The intensity of electromagnetic radiation and the luminescence caused by it is measured with maximum accuracy.

3. The spectral composition of the electromagnetic signal, allows you to determine the chemical element by which it is emitted.

4. Measurement of the intensity of electromagnetic radiation in a local region is a necessary and sufficient condition for assessing the energy state of this region.

5. Detection of defects and damages in structures and devices by non-destructive testing methods is based on the use of ultrasound, eddy currents, and X-ray radiation. The technique of monitoring atomic reactions is fundamentally different from them in that it controls the energy source formed by the atoms of that element, which is passively or actively used by humans. The body, which is exposed to external influences, absorbs energy. The energy absorbed by the body does the work, dissipates, or accumulates in it. The accumulation of energy is possible only when some of the atoms have changed. Changes in atoms are due to changes in the electron shell. It leads to the fact that the geometric position of the atoms changes.

*The most accurate information on changes in atoms is ensured by the absorption and emission spectra of atoms.*

*The task of monitoring is to accept this information and use it.*
The intensity of spontaneous electromagnetic radiation $I_v$ ($x$, $t$) is the main measured parameter. It is associated with accumulated energy, an equation that must be found (or confirmed) experimentally. A control test is carried out on the product, for the experimental determination of the product parameters: accumulated energy, energy storage rate of critical energy recovery. The test is performed until a defect occurs in which operation is not possible.

*We must remember that the intensity of spontaneous emission at the time of formation of pores, cracks, and fracture is minimal; the maximum power before the creation of crack pores and*

*fracture characterizes the critical value of the accumulated energy. The emission of energy, which also accompanies corrosion differs in frequency and penetration from p-radiation.*

Research laboratories have methods and devices for accurately estimating the energy balance, but in practice, the accumulated energy is assessing by the intensity of spontaneous radiation. The successful long-term use of electromagnetic radiation in various spectral regions facilitates the transition from methods based on classical mechanics to methods based on quantum mechanics. A characteristic feature of non-invasive monitoring of atomic reactions is due to the properties of hydrogen. The hydrogen molecule on the metal surface, as shown in the works of G. Ertl, dissociates and ionizes, turning into a proton. A proton moves randomly through the metal, but any external action increases its speed, increasing the likelihood of p-radiation and bond breaking between atoms. The absorption of hydrogen by palladium and its destruction occurs at room temperatures, the binding energy between the atoms of which is 3.936 eV. The binding energy between iron and oxygen ions is almost three times higher than that of palladium atoms. Therefore, such a reaction is possible at a higher temperature.

A large number of works have been devoting to the reduction of iron from $Fe_2O_3$ and $Fe_3O_4$ oxides using hydrogen.

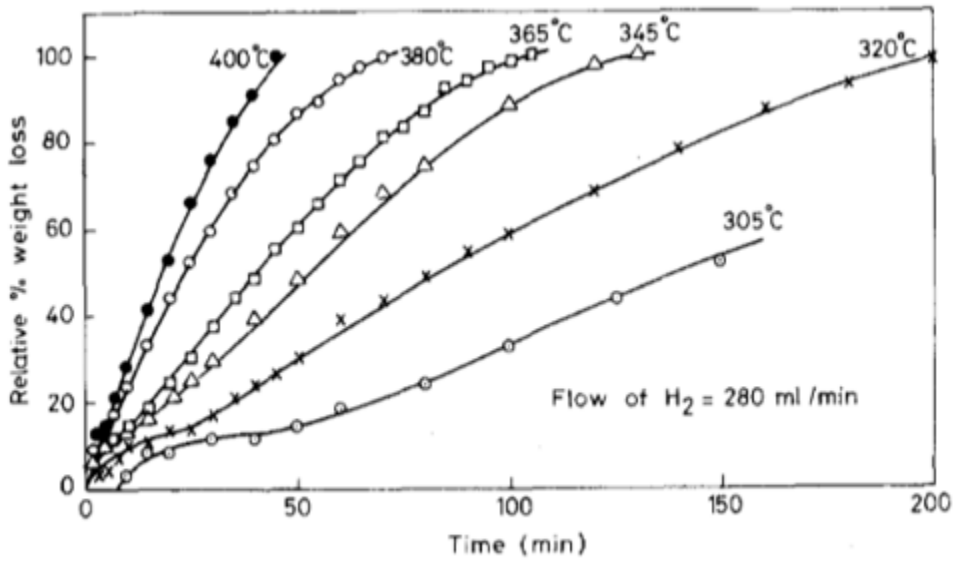


**Fig. 87**

The chemical reaction is represented by equations (1 *) and (2 *)

$$Fe_3O_4 + 4H_2 \rightarrow 3Fe + 4H_2O \quad (1^*)$$

$$Fe_2O_3 + 4H_2 \rightarrow 3Fe + 4H_2O \quad (2^*).$$

Analysis of works, including reviews, for example, [4.37. 4.38], published from 1962 to

January 2020, devoted to the problem of iron reduction, indicates that experiments were performing on both macroscopic and nanoscale samples. The authors publish the results obtained using X-ray diffraction analysis, electron microscopy, the Mössbauer effect, but the atomic mechanism of reactions is not considering.

More than a hundred photographs given in the first and second chapters of the book are obtaining in those experiments in which the participation of protons in the atomic reaction is undeniable. Using hydrogen in reduction reactions of iron from oxides is another confirmation of the p-radiation hypothesis. Redox reactions form the basis of plant growth and the life of cells of living organisms, but they cannot be realized without water.

The successful long-term use of electromagnetic radiation in various spectral regions facilitates the transition from methods based on classical mechanics to methods based on quantum mechanics. P- radiation is causing by an atomic reaction that does not require high voltage. The energy absorbed by the device or structure is spent on useful work, dissipated, and accumulated. The danger of possible destruction lies only in the stored energy. Research laboratories have methods and devices for accurately assessing the energy balance, but in practice, energy storage is estimated by the intensity of spontaneous emission.

### 6.5. Monitoring atomic reactions in the pipeline

The pipeline for transporting gas or oil products is subjected to strong external and internal influences, leading to corrosion, cracking, and destruction. External factors are deformations caused by soil displacement, temperature changes, stray currents, water, gases, and nuclear radiation from radioactive elements. The inner surface undergoes deformation, like the outer one, under the powerful influence of hydrogen, oxygen, and sulfur, which leads to corrosion.

Many-meter longitudinal cracks in pipelines testify to electromagnetic stimulated processes. The leakage of gas or oil leads to explosions, fires, deaths, and environmental disasters. The accumulation of paraffin on the walls of the pipeline has become one of the problems of its operation. The walls of the pipeline were cleaning with a device called a pig. A catastrophic crack, whose length was 4.8 m, formed in the pipeline after the passage of the pig. (See [1.9] and paragraph 3.1].

Long-term continuous operation of the pipeline leads to the fact that nanoscale defects, which are recognizing as acceptable at the beginning of the service, become dangerous, even if their size

has not changed. Its defects are called hidden cracks. The number of such cracks in the rivet holes seam of the fuselage reaches 85%. They are called fatigue cracks.

Non-destructive testing of structural elements of devices is designing to prevent catastrophic destruction based on an analysis of the results of studies of areas that are recognizing as reliable for future use and areas damaged during operation. The reliability and durability of the studied area can be estimated correctly only based on laws characterizing the bonding forces between atoms, and processes leading to a weakening of the bonding forces and the appearance of defects. We will call such regions a structural element, and we will mean by the structure the arrangement of atoms and their state due to the settlement of electrons in their shell.

Any effect on atoms is electromagnetic. Changes caused by exposure are an atomic reaction, the duration of which is millionths of a second. A change in the energy state of atoms leads to a change in their arrangement, at which a new dynamic equilibrium arises.
An experimental study of a structural element is carrying out using reflection or transmission of waves whose wavelength should be less than at least one of the dimensions of the region. Modern experimental devices allow us to study nanoscale areas, as shown above, but they cannot be used in practice.

Non-destructive monitoring of defects is carried out based on three methods: ultrasound, eddy currents, and radiography. The disadvantage of the ultrasonic method and the eddy current method is the large wavelength that does not allow the detection of areas less than 0.5 mm. The advantage of radiography is due to its high penetrating ability and the ability to detect defects located at a depth of the material. The absorption of X-rays depends mainly on the density of the material, the serial number of the element (core charge) $Z^4$. Radiography is a very effective way to detect bulk defects (for example, inclusions of slag, porosity, and unmelted metal) in the weld. The disadvantages of the X-ray method are the need for a high voltage source, the impossibility of detecting hidden cracks. The possibility of applying various processes in the pipeline was considering [4.34]. But the main drawback of these methods is the fact that the decisive role in violating the integrity of the structural element is energy sources whose core charge does not change.

The causes for a crack formation in the gas pipeline, the length of which was 11 meters, surprised the authors of [4.34]. They write,″ An uncommon blowout in a 24” diameter, 7 mm thick API 5L X52 gas pipeline was due to fracture at the longitudinal double submerged arc weld (DSAW). Oddly enough for gas pipelines, it was found that fatigue cracks had propagated from a large embedded weld defect of lack of fusion resulting from severe geometrical mismatch between inner and outer weld passes. What makes this failure particularly interesting is that: previous in line

inspections failed to detect any defect, no evidence of third party damage was found, and very few large pressure cycles had been recorded during the last 5 years of service, which were believed to be representative of the entire service life of the pipeline. *Fatigue tests were carried out to characterize propagation of fatigue cracks in weld metal, it was found that a large Paris exponent made the few large amplitude cycles most contributing to crack propagation. Crack growth path and striation patterns were studied."* (Italic supplied).

The analysis of the results of the study was based on the Paris equation, similar to that given in [3.1]. It has an erroneous hypothesis. So, it makes no sense to consider it.

In the article [4.35], it has pointed out that a search is doing for new methods of monitoring damage in pipelines.

### 6.5.1. Pipeline Safety

**1. Weld quality control**

Modern non-destructive testing methods include "three-axis high-resolution magnetic flux leakage (MFL) inspection, liquid ultrasonic crack inspection, electromagnetic acoustic transducer (EMAT) inspection, and remote field eddy current (RFEC) inspection technologies, in a bid to realize high detection accuracy of girth weld defects and repair the defects in advance."

The experiment showed that the cause of the destruction is electromagnetic p-radiation, which none of the methods detect, but the book and patent application are devoted to monitoring this radiation.

The experiment showed that solidification of the melt is accompanied by p-radiation, which can be detected from the liquid state to complete cooling around the entire circumference. Sensors are placed inside the device, as described in [4.35, 3.3. Electromagnetic Acoustic Transducer Inspection of Natural Gas Pipeline Girth Weld Defects] and shown in Fig. 88 a and b.

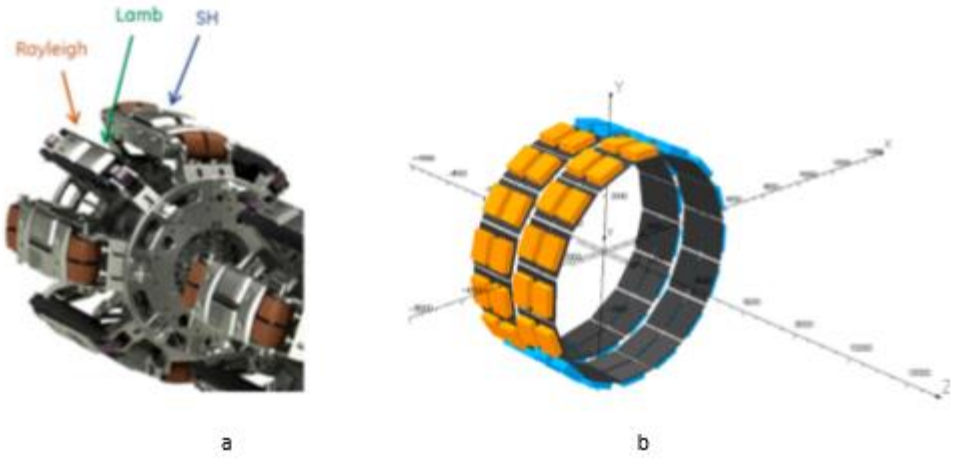


**Fig. 88**

Sensors at the research stage are replacing by photographic film.

It was established by the experiment that p-radiation caused by deformation at one point of a continuous material is also recording at other locations as a result of self-emission transparency, which exceeds the penetrating power of X-rays. This fact should not only be taking into account but also used to establish a connection between sensor readings and photographs. Sensors, or film frames, simultaneously record the response of the metal at the point at which they are locating. The second ring of sensors is locating on the outer surface of the pipeline. It has been experimentally showing that a heat-insulating layer can be located between the sensor and the metal or cooling can be performing.

**2. Control of the inner surface of the pipeline**

A modern smart pig is equipping with sensors for studying ultrasound, eddy currents, and a navigation system. It is complemented by p-radiation sensors, as described above.

**3. Monitoring the external surface of the pipeline and other devices**

*The addition of a smart pig with p-radiation sensors turns it into a robot that can monitor atomic reactions in the pipeline. It gives rise to the belief that a smart pig can be used as the first robot to monitor atomic reactions to prevent catastrophic destruction.*

4**. Advantages of non-invasive monitoring of atomic reactions**

Numerous experiments suggest the advantage of non-invasive monitoring of atomic reactions over other non-destructive testing methods.

1. Refusal from external sources of energy, since the source of energy, is the object itself. It ensures the absolute reliability of the energy source.

2. Applicability for research testing, and operation.

3. A wavelength comparable to X-ray radiation can detect the onset of defects before pores or cracks form.

4. High penetrating power, superior to the penetrating ability of X-ray radiation, allows you to investigate defects that originate inside the structural element.

5. Luminescence, stimulated by p-radiation, enables the use of screens that increase the sensitivity of the sensors.

6. The monitoring of atomic reactions allows you to create a universal robot for monitoring, which will complement or replace the control system in various industries.5. Luminescence, stimulated by p-radiation, enables the use of screens that increase the sensitivity of the sensors.

6. The monitoring of atomic reactions allows you to create a universal robot for monitoring, which will complement or replace the control system in various industries.

**SUMMARY**

**1**. *The book contains experimental confirmation of the author's hypothesis that the formation of pores, cracks in a solid, and its destruction is due to stimulated emission of photons by local groups of metastable atoms, the excitation of which occurred as a result of external exposure.*

**2**. ***The law of destruction of a solid body is formulated***.

**3**. *Numerous experiments performed by the author refute the hypothesis that the elastic energy concentrated in stress concentrators is sufficient for cracking and fracture.*

**4**. *Numerous tests conducted by the author refute all models of cracking and fracture in which electromagnetic energy is not taking into account.*

**5**. *It was found that atomic reactions are accompanying by electromagnetic radiation with an energy of* 50-100 *keV, which corresponds to a frequency of* $10^{18}$-$10^{19}$ *Hz.*

**6**. *It is shown that the penetrating ability of p-radiation generated in metal is millions of times greater than the penetrating ability of X-rays excited by electron impact.*

**7**. *The universality of monitoring atomic reactions and the possibility of practical application to prevent technological disasters, timely alerts about a possible earthquake or tsunami, and control of the nucleation and development of plant cells and living organisms have been proved.*

**8**. *Recommendations are given for the development of monitoring devices.*

## References to Chapter IV

**4.1**. Zhang, S. Zaefferer, D. Raabe, *A study on the geometry of dislocation patterns in the surrounding of nanoindents in a TWIP steel using electron channeling contrast imaging and discrete dislocation dynamics simulations,* Materials Science & Engineering A 636 (2015) 231–242.

**4.2**. А.А. Шибков, М.А. Желтов, М.Ф. Гасанов, А.Е. Золотов, *Динамика полосы Людерса и разрушение алюминий-магниевого сплава, инициированные концентратором напряжений,* М: Физика твердого тела, (2018), **60**, 315-323.

**4.3.** B. Sun, Y. Ma, N. Vanderesse, R. S. Varanasi, W. Song, P. Bocher, D. Ponge, D. Raabe, *Macroscopic to nanoscopic in situ investigation of yielding mechanisms in ultrafine grained medium Mn steels: Role of the austenite-ferrite interface,* Acta Materialia, (2019), **178**, 10-25.

**4.4**. S. Takaki, D. Akama, N. Nakada, and T. Tsuchiyama, *Effect of Grain Boundary Segregation of Interstitial Elements on Hall Petch Coefficient in Steels,* Materials Transactions Special Issue on Strength of Fine-Grained Materials-60 Years of Hall-Petch, 2013, pp. 7.

**4.5**. M-M. Wang, C.C. Tasan, D. Ponge, A. Kostka, D. Raabe, *Smaller is less stable: Size effects on twinning vs. transformationof reverted austenite in TRIP-maraging steels,* Acta Materialia **79,** (2014), 268–281.

**4.6.** V. Turlo, T. J. Rupert, *Grain boundary complexions and the strength of nanocrystalline metals: Dislocation emission and propagation*, Acta Materialia, **151**, (2018), 100-111.

**4.7**. W. Wang, W. Zhang, H. Wang, X. Fang, and X. Liang, *Influence of Grain Boundary on the Fatigue Crack Growth of 7050-T7451 Aluminum Alloy Based on Small Time Scale Method* Advances in Materials Science and Engineering (2016) V.2016, Article ID 7671530, pp. 7,

**4.8.** Y. Wang, D. Raabe, C. Klüber, F. Roters, *Orientation dependence of nanoindentation pile-up patterns and of nanoindentation microtextures in copper single crystals,* Acta Materialia, **52**, (2004)2229-2238.

**4.9**. Y. Gaillard, M. Anglada, and E. Jimenez-Pique, *Nanoindentation of yttria-doped zirconia: Effect of crystallographic structure on deformation mechanisms,* Mater. Res., **24**, No. 3, (2009), 719-728

**4.10.** A.F. Gerday, M. B. Bettaie, L. Duchêne, N. Clement, H. Diarra, A.M. Habraken, *Material behavior of hexagonal alpha phase of titanium alloy identied from nanoindentation,* European Journal of Mechanics A/Solids **30**, (2011), 248- 255.

**4.11**. V. A. Glebov, A. S. Bakulina, I. V. Efremov, I. V. Shchetinin, Yu. D. Yagodkin, A. M. Glazers, Yu. Rashkovskii, and D. L. Vainshtein, *Study of the structure of steel 12Kh12M1BFP modified with additions of fullerenes and carbon nanotubes,* Metal Science and Heat Treatment, **52** (2010), No.7–8, 321-324.

**4.12**. L. Yuan, D. Ponge, J. Wittig, P. Choi, J.A. Jiménez, D. Raabe, *Nanoscale austenite reversion through partitioning, segregation and kinetic freezing: Example of a ductile 2 GPa Fe–Cr–C steel,* Acta Materialia **60** (2012), 2790-2804.

**4.13**. E. A. Ariza, S. S. Babu, J. D. Poplawsky, W. Guo, K. A Unocic, A. J. Ramirez, A. P. Tschiptschin, *Evaluation of Carbon Partitioning in New Generation of Quench and Partitioning (Q&P) Steels*, Qatarize *et al.* 2017_14_11_2017, pp.37.

**4.14**. Y.J. Li, P. Choi, S. Goto, C. Borchers, D. Raabe, R. Kirchheim, *Evolution of strength and microstructure during annealing of heavily cold-drawn 6.3 GPa hypereutectoid pearlitic steel wire,* Acta Materialia 60 (2012) 4005–4016.

**4.15**. **V**.V. Rybin, E.A. Ushanova, N.Y. Zolotorevskii, *EBSD Investigation of the Plastic Flow Vortex-Like Insabilites in the bond Zone of the Aluminun-Aluminum Weld Produced Expiosive Welding*, Sbornik_DFMN2017 (2017) 141-142.

**4.16.** Pańcikiewicz, A. Zielińska-Lipiec, E. Tasak, *Cracking of High-Strength Steel Welded* 10.2478/adms-2013-0013.

**4.17.** M.-Y. Choi, J.-H. Park, K. S. Kang, W.-T. Kim, *Application of Thermography to Analysis of Thermal Stresses in the NDT for Compact Tensile Specimen*, 12th A-PCNDT-2006-Asia-Pacific Conferenceon NDT, 5th-10th Nov 2006, Auckland, New Zeland.

**4.18.** M. Lalpoor, *Study of Cold Cracking during DC-casting of High Strength Aluminum Alloys*, PhD thesis. Delft University of Technology, 2010, P 150.

**4.19.** M. Lalpoor, D.G. Eskin, and L. Kargerman, *Cold Cracking Development in AA7050 Direct Chill–Cast Billets under Various Casting Conditions*, Metallurgical and Materials Transactions A, **41**, (2010) 2425-2434.

**4.20.** D. G. Eskin, L. Katgerman, Dr. Suyito, J. F. Mooney, *Contraction of aluminum alloys during and after solidification*, Metallurgical and Materials Transactions A, **35** (2004), 1325–1335.

**4.21.** M. Lalpoor, D.G. Eskin, D. Ruvalcaba, H.G. Fjær, A.Ten Cate, N. Ontijt, L. Katgerman, *Cold cracking in DC-cast high strength aluminum alloy ingots: An intrinsic problem intensified by casting process parameters***,** Materials Science and Engineering: A **528**, (2011), 2831-2842.

**4.22.** L. Zhang, D. G. Eskin, A. Miroux, T. Subroto, and L. Katgerman, *Effect of inlet geometry on macrosegregation during the direct chill casting of 7050 alloy billets: experiments and computer modelling*, IOP Conf. Series: Materials Science and Engineering **33** (2012) 012019.

**4.23.** T. A. Subroto, Connection between hot tearing and cold cracking in DC-casting of AA7050: Experiments and computer simulations, Thesis, Delf University of Technology, (2014), pp 186.

**4.24.** B. R. Mosinyi, *Fatigue Damage Assessment of High-Usage In-Service Aircraft Fuselage Structure,* A Thesis Submitted to the Faculty of Drexel University 2007, pp.423.

**4.25**. S. Reboh, *Defect engineering in H and He implanted Si,* Thesises Submitted to: Universidade Federal do Rio Grande do Sul – Brasilia, pp 169, (2008).

**4.26.** C.-D. Wu and H.-W. Tsai, *Atomic study of effects of crystal structure and temperature on structural evolution of Au nanowires under torsion,* J. of Applied Physics **123**, 214304 (2018).

**4.27.** A. Ahmed, *Initiation and Growth of Multiple-Site Damage in the Riveted Lap Joint of a Curved Stiffened Fuselage Panel: An Experimental and Analytical Study,* Thesis Submitted to the Faculty of Drexel University 2007, pp.328.

**4.28.** V. Acocella, A. Gudmundsson, R. Funiciello, *Interaction and linkage of extensional fractures: Examples from the rift zone of Iceland,* Journal of Structural Geology (2000), **22**,1233-1246.

**4.29.** M.-J.e Dalbe, J. Koivisto, L. Vanel, A. Miksic, O. Ramos, M. Alava, and S. Santucci, *Repulsion and Attraction between a Pair of Cracks in a Plastic Sheet,* Phys. Rev. Let., (2015) **114**, 205501.

**4.30**. M. L. Fender, F. Lechenault, and K. E. Daniels, *Universal Shapes Formed by Two Interacting Cracks,* Phys. Rev. Let. (2010) **105**, 125505

**4.31**. Standard Test Method for Plane-Strain Fracture Toughness of Metallic Materials, Designation: E 399 – 90 (Reapproved 1997).

**4.32**. X. K. Zhu, J. A. Joyce, *Review of fracture toughness (G, K, J, CTOD, CTOA) testing and standardization*, Engineering Fracture Mechanics **85** (2012) 1–46.

**4.33**. Y. Takashima, Mitsuru Ohata, F. Minami, *CTOD Toughness Correction for Laser Welded Joints with Narrow Hardened Zone*, Procedia Materials Science 3 (2014) 1009–1014.

**4**.34. P. Fazzini, J. L. Otegui, M. Teutonico, C. Manfred, *Fatigue Assessment of a Double Submerged Arc Welded Gas Pipeline*, Rio Pipeline Conference & Exposition (2005), pp. 9.

**4.35.** Q. Feng, R. Li, B. Nie, S. Liu, L. Zhao, and H. Zhang, *Literature Review: Theory and Application of In-Line Inspection Technologies for Oil and Gas Pipeline Girth Weld Defection*, Sensors (2017), 17, 50; doi:10.3390/s17010050, pp. 24.

**4.36.** M. V. C. Sastry, R. P. Viswanath, and B. Viswanatan, *Studies on the Reduction of Iron Oxide with Hydrogen,* Int. J. Hydrogen Energy, (1982) **7**, No. 12, pp. 951-955.

**4.37**. D. Raabe, C. C. Tasan, E. A. Olivetti*, Strategies for improving the sustainability of structural metals,* Nature, (2019) 575, 63-74.

**4.38**. D. Spreitzer and J. Schenr, *Reduction of Iron Oxides with Hydrogen- A Review,* Steel Research International, (2019), **90**, Issue 10.

**Contents**

**ATTACHMENT No. 1**

## COLOR AND BLACK AND WHITE PHOTOS

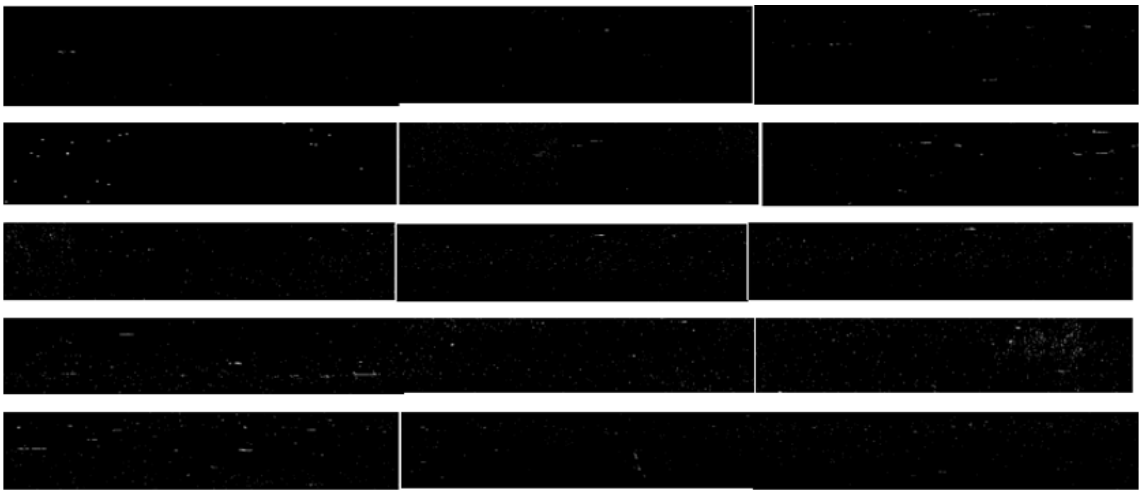

**Fig. 89**

The need to introduce this application is because a mistake was made in assessing the role that dark photographs play, due to the continuous radiation of high intensity.

It is known that continuous and line spectra take place in the infrared, visible ultraviolet and X-ray spectral regions. Colored (monochromatic) sections of the p-radiation spectrum are observed in numerous photographs.

Colored areas alternate with dark ones, which are caused by intense absorption of electromagnetic waves. Using contrast, including black and white, allows you to get additional information about the features of p-radiation. The self-emissive transparency in wood was illustrated on five frames, as shown in Fig. 17 and Fig 17 (1). Fifteen black-and-white frames 3, 5-18 illustrate defects in this interval, as shown in Fig. 89. Another example of defect detection using p-radiation using black and white contrast is shown in Fig. 90.

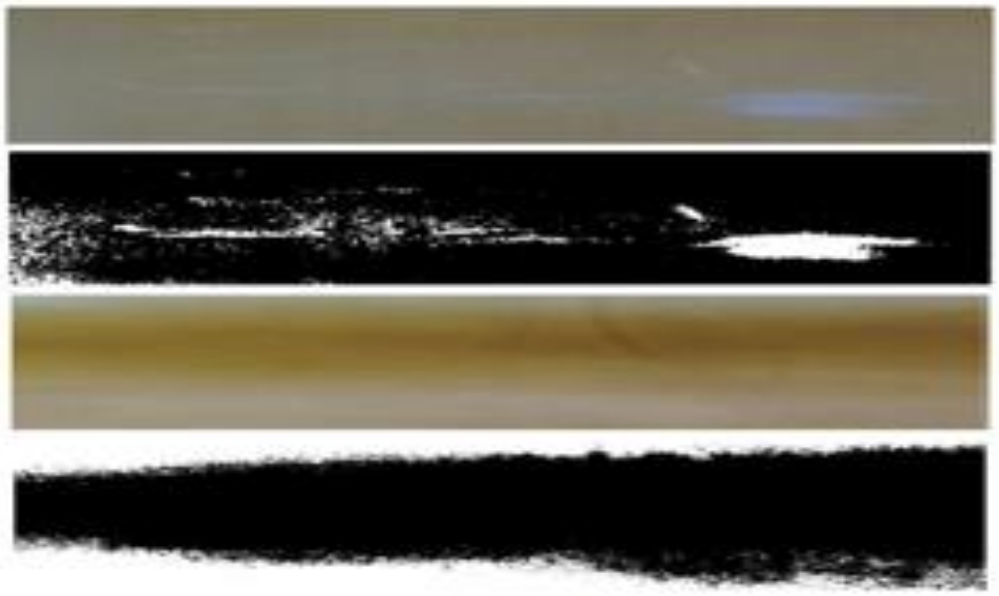

**Fig. 90**

Two photographs (first and third) obtained during the study are demonstrated using black and white contrast (second and fourth). This allows you to more accurately assess the danger of a defect.

**Protocols of experimental studies of electromagnetic radiation of atomic reactions**

| DVD Number | Date | Experimental Series | Number of Photos | | DVD Number | Date | Experimental Series | Number of Photos |
|---|---|---|---|---|---|---|---|---|
| 1 | 2/24/2016 | 1110 | 8 | | 31 | 10/26 | 3730 | 15 |
| 2 | 3/01 | 1111 | 7 | | 32 | 11/19 | 3799 | 28 |
| 3 | 3/02 | 1112 | 7 | | 33 | 12/11 | 3809 | 11 |
| | | | | | | | | |
| 4 | 3/04 | 1113 | 7 | | 34 | 1/23/2019 | 3875 | 27 |
| 5 | 3/14 | 1114 | 6 | | 35 | 1/29 | 3932-34 | 58 |
| 6 | 3/18 | 1115 | 6 | | 36 | 2/28 | 3954-59 | 129 |
| 7 | 5/25 | 1116 | 7 | | 37 | 3/22 | 2061-62 | 62 |
| 8 | 7/22 | 3757 | 16 | | 38 | 4/19 | 2064 | 11 |
| 9 | 9/13 | 3802 | 26 | | 39 | 4/22 | 2108 | 22 |
| 10 | 10/16 | 3817 | 27 | | 40 | 4/24 | 2186-87 | 22 |
| 11 | 10/20 | 3823 | 28 | | 41 | 5/03 | 2095-2101 | 67 |
| 12 | 10/22 | 4032 | 29 | | 42 | 5/07 | 2277 | 27 |
| 13 | 1/17/2017 | 4091 | 17 | | 43 | 5/12 | 2215 | 12 |
| 14 | 1/23 | 2691 | 17 | | 44 | 6/11 | 2390 | 25 |
| 15 | 1/27 | 2692 | 9 | | 45 | 6/17 | 2514 | 27 |
| 16 | 3/10 | 2695 | 20 | | 46 | 8/07 | 2608 | 14 |
| 17 | 3/15 | 2700 | 26 | | 47 | 8/12 | 2609 | 19 |
| 18 | 3/22 | 2705 | 25 | | 48 | 8/15 | 2615 | 13 |
| 19 | 4/21 | 2770 | 38 | | 49 | 8/21 | 2665-66 | 28 |
| 20 | 5/25 | 2811 | 30 | | 50 | 8/30 | 2703-04 | 28 |
| 21 | 11/15 | 3261 | 38 | | 51 | 9/09 | 2753-54 | 27 |
| 22 | 11/16 | 3303 | 3 | | 52 | 9/20 | 2772 | 12 |
| 23 | 2/23/2018 | 3428 | 27 | | 53 | 9/23 | 2777 | 12 |
| 24 | 2/28 | 3450-51 | 22 | | 54 | 9/25 | 2804-05 | 27 |
| 25 | 8/09 | 3682-83 | 58 | | 55 | 10/01 | 2812-2813 | 56 |
| 26 | 8/14 | 3952 | 18 | | 56 | 10/31 | 2971 | 24 |
| 27 | 8/20 | 2742-43 | 22 | | 57 | 11/08 | 3015-16 | 26 |
| 28 | 9/21 | 3753 | 15 | | 58 | 11/10 | 3022 | 24 |
| 29 | 9/25 | 2695 | 39 | | 59 | 1/02/2020 | 3137 | 28 |
| 30 | 10/23 | 3903-04 | 27 | | 60 | 1/28 | 3237 | 28 |

The table below shows that in an experimental study 1534 photographs were obtained, of which 508 must be analyzed using black and white contrast. It is impossible to neglect this fact.

**ATTACHMENT No. 2**

(43) International Publication Date
28 November 2019 (28.11.2019)

WIPO | PCT

WO 2019/226700 A1

(51) International Patent Classification:
*B61K 9/10* (2006.01) *G01N 23/02* (2006.01)
*G01B 5/30* (2006.01) *G01N 23/04* (2018.01)

(21) International Application Number:
PCT/US2019/033392

(22) International Filing Date:
21 May 2019 (21.05.2019)

(25) Filing Language: English

(26) Publication Language: English

(30) Priority Data:
62/674,107 21 May 2018 (21.05.2018) US

(72) Inventor; and
(71) Applicant: **ROMBAKH, Volodymyr Pavlovich** [US/US]; 8317 188th Street SW, Edmonds, Washington 98026-6025 (US).

(74) Agent: **ADAMS, Scott S.** et al.; c/o IP Docketing Dept., Davis Wright Tremaine LLP, 920 Fifth Avenue, Suite 3300, Seattle, Washington 98104-1610 (US).

(81) Designated States *(unless otherwise indicated, for every kind of national protection available)*: AE, AG, AL, AM, AO, AT, AU, AZ, BA, BB, BG, BH, BN, BR, BW, BY, BZ, CA, CH, CL, CN, CO, CR, CU, CZ, DE, DJ, DK, DM, DO, DZ, EC, EE, EG, ES, FI, GB, GD, GE, GH, GM, GT, HN, HR, HU, ID, IL, IN, IR, IS, JO, JP, KE, KG, KH, KN, KP, KR, KW, KZ, LA, LC, LK, LR, LS, LU, LY, MA, MD, ME, MG, MK, MN, MW, MX, MY, MZ, NA, NG, NI, NO, NZ, OM, PA, PE, PG, PH, PL, PT, QA, RO, RS, RU, RW, SA, SC, SD, SE, SG, SK, SL, SM, ST, SV, SY, TH, TJ, TM, TN, TR, TT, TZ, UA, UG, US, UZ, VC, VN, ZA, ZM, ZW.

(84) Designated States *(unless otherwise indicated, for every kind of regional protection available)*: ARIPO (BW, GH, GM, KE, LR, LS, MW, MZ, NA, RW, SD, SL, ST, SZ, TZ, UG, ZM, ZW), Eurasian (AM, AZ, BY, KG, KZ, RU, TJ, TM), European (AL, AT, BE, BG, CH, CY, CZ, DE, DK, EE, ES, FI, FR, GB, GR, HR, HU, IE, IS, IT, LT, LU, LV, MC, MK, MT, NL, NO, PL, PT, RO, RS, SE, SI, SK, SM, TR), OAPI (BF, BJ, CF, CG, CI, CM, GA, GN, GQ, GW, KM, ML, MR, NE, SN, TD, TG).

**Published:**
— *with international search report (Art. 21(3))*

(54) **Title:** NON-INVASIVE MONITORING OF ATOMIC REACTIONS TO DETECT STRUCTURAL FAILURE

WO 2019/226700 A1

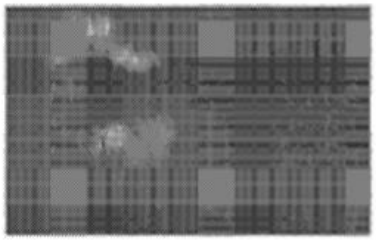

a

**(57) Abstract:** The method and device to ensure the safety of people's life and health is based on the measurements of spontaneous electromagnetic radiation caused by the deformation from a structure or device, the nucleation and growth of plant cells and living organisms; calculating energy stored in a portion of the structure or cells based on the measured intensity; performing a comparison of the energy stored with a critical value for the structure and pathological changes in the cells; and indicate potential failure of the structure or the level of pathological changes based on the performed comparison.



# NON-INVASIVE MONITORING OF ATOMIC REACTIONS TO DETECT STRUCTURAL FAILURE

## CROSS-REFERENCE TO RELATED APPLICATION

[0001] This application claims priority to and incorporates by reference for all purposes the full disclosure of U.S. Provisional Patent Application No. 62/674,107, filed May 21, 2018, entitled "METHOD AND SYSTEM FOR NON-DESTRUCTIVE REMOTE MONITORING THE WEAR OF STRUCTURES AND DEVICES."

## FIELD

[0002] The present disclosure relates to embodiments to ensure the safety of life and human activity on natural and man-made objects, regardless of their size, shape, composition, purpose and nature of external influences. This goal is achieved by the possibility of experimental continuous or periodic monitoring the energy of dynamic processes due to the atomic reaction, and accessing its magnitude using equations, in order to stop operation before the accumulated energy reaches a critical value. Electromagnetic, including X-ray, radiation accompanying atomic reactions in inorganic and organic objects is used to analyze the processes of wear and aging.

[0003] An experimental study carried out by the inventor showed that the method based on the analysis of atomic reactions is applicable in all areas of human activity. Analysis of atomic reactions leading to wear, aging, destruction of structures and devices; aging, pathological changes and death of plants and organs of a living organism are performed in the invention from the standpoint of quantum electrodynamics, which is an accurate physical theory that ensured the development of natural science, technology and medicine.

## BACKGROUND

[0004] Numerous structures in various contexts are relied upon for the safety of individuals, not to mention for other reasons. For example, people in an airplane rely on the integrity of the structures that make up the airplane. People crossing a bridge by car, truck, or other vehicle rely on the structural integrity of the bridge. Rail passengers rely on the integrity of the rails and structures that make up the trains on which they ride. Despite efforts to prevent structural failure, structures nevertheless do fail, too often resulting in injury and death. Prediction of structural failure has proven to be a difficult problem. Cracks in structures can be difficult to detect and often appear without warning after normal or even abnormal use.



## DETAILED DESCRIPTION

[0005] The experimental basis of the invention is the next use of an electromagnetic impulse for practical purposes. The number of such applications is huge. They cover almost all modern technical devices that people use. The first use was found by a primitive man, when, striking a piece of iron with a flint, he extracted a spark and lit a fire, repeating a natural phenomenon called lightning. Consequently, impact and friction give rise to electromagnetic impulse.

[0006] A lightning rod, invented by B. Franklin, was used as the second example of the use of a spark. The utility of this invention lies in the fact that the lightning rod increases the rate of energy dissipation in a thundercloud, the accumulation of which is caused by the impact (friction) of ice crystals.

[0007] The amplification of an electromagnetic pulse in a laser is due to the fact that in the process of pumping the accumulation rate exceeds the rate of energy dissipation. Energy accumulation is due to the fact that some of the atoms, having absorbed energy, moved to a higher energy level and do not emit it during a certain time interval, which is called the lifetime

of the metastable state.

[0008] If there are more atoms at the metastable level than at the bottom, then a random pulse emitted by one atom, called a photon, can stimulate the emission of other atoms in the same direction, with the same energy, phase and polarization. The energy of such photons is summed. Such a phenomenon, called stimulated or induced radiation, has no analogs beyond the limits of quantum systems.

[0009] The theoretical basis of the method proposed in the invention is the inventor's hypothesis that the loss of integrity of a solid , i.e. the formation of pores, cracks and destruction is due to the formation of local regions of metastable atoms, the stimulated emission of which, being absorbed by other atoms, is sufficient to break the bond between these atoms. Such a local group of atoms is called a destruction domain.

[0010] The transition of atoms from the normal to the metastable state is due to the absorption of photons, the birth of which occurs as a result of the transformation of the mechanical energy of deformation into the electromagnetic one.

[0011] All dynamic processes are initially due to the interaction of atoms, which are attracted to each other, but repel at some distance because the charges of all atomic nuclei are positive and the electron shells are negative. Dynamic equilibrium occurs when the forces of attraction are equal to repulsive forces.

[0012] It is proved that all processes in nature are caused by four types of interaction: strong, which is taken as 1; electromagnetic equal to 1/137; weak, equal to $1/10^{12}$ and gravitational, equal to $1/10^{40}$. Mechanical interaction in nature is absent not only between individual atoms, but also macroscopic bodies. This seemingly paradoxical conclusion is due to the fact that a layer of electrons with a thickness of up to two nanometers is formed above the surface of a solid. The convergence of bodies at this distance is accompanied by a change in the electric field and the appearance of a varying magnetic field. These two fields propagate in the form of an electromagnetic wave (photon).

[0013] The glow of two bodies caused by friction, called triboluminescence, serves to confirm this mechanism. This means that we can limit ourselves on the Earth by electromagnetic interaction in the analysis of dynamic processes.

[0014] Dynamic processes caused by atomic reactions provide for the safe operation of elements of structures and devices until changes occur in them, called fatigue, wear, or aging.

[0015] The term "fatigue" was introduced in 1839, it was widely used after Wöhler's work, published in 1860-1870. This term and the method of constructing *S-N* curves are still used both in State Standards and in scientific research.

[0016] This term cannot be considered a physical parameter, since for 150 years the quantitative value of fatigue and the method of its measurement have not been proposed.

[0017] Modern mechanics of strength and destruction are based on the hypothesis that damage to materials, such as fatigue cracks, is due to the emission of elastic energy accumulated in stress concentrators. The main parameter of the equations proposed for the analysis of the experimental results is the stress intensity factor (SIF), $K=\sigma\sqrt{m}$.

[0018] The dimension of this parameter in the International System of Units $Pam^{1/2}$.

[0019] Currently, a number of methods and computer programs are used, the main parameters of which are stress intensity factors, for example, NASGRO, AFGROW, FRANC2D. The disadvantage of the experiment designed to implement these methods is its low efficiency. The analysis of such methods is performed using for example of AFGROW Release 5.03.03.23, which was used to study the causes of cracking in the fuselage. The fuselage panels were deformed with a period of 25-30 seconds. The total number of cyclic tests for each of the nine panels ranged from 2.5 to 4.3 million. Therefore, the experiment was lasted 730 working weeks. The crack of length 1925 mm was formed in one of the panels, but

forecasting the time and place of cracking by these methods is impossible, since the equations do not contain time as a parameter and damage is detected after hundreds of hours.

[0020] Consider as an example the Paris-Erdogan equation $\frac{da}{dN} = C\Delta K^n$, where $da$ is the elongation of the crack, $dN$ is the increase in the number of test cycles, the $C$-coefficient of proportionality, which has the dimension m/cycle, $K$ is the stress intensity factor, $\Delta K = K_{max} - K_{min}$,

[0021] $N$ is the exponent. The NASGRO equation reduces to the Paris-Erdogan equation. Analysis of this equation is necessary to show the errors they contain.

[0022] The left side of the equation, called the crack growth rate, has the same dimension as $C$. Consequently, the dimensions of the left and right sides are different.

[0023] Analysis of the causes of crack formation, 4.8 m long, in the oil pipeline [See: M.D. Chapetti, *at al.*, Int. J. of Fatigue, (2002), 24, 21-28] was performed using the Paris-Erdogan equation. The authors gave one of the solutions: $n = 6$, $C = 3.818 \cdot 10^{-15}$ m/cycle, which contains gross errors: the cycle in which the elongation of the crack corresponds to the size of the atomic nucleus is meaningless, as is the measurement of length with an accuracy of $10^{-18}$ meters. But there are many such examples.

[0024] The NASGRO equation, which differs from the Paris-Erdogan equation only by a numerical factor, contains the same errors.

[0025] The gross errors of the modern theory of strength and destruction are associated with the neglect of the achievements of quantum theory, on the basis of which electron and atomic force microscopes, diffractometers, and field ion microscopes are created. The authors of the articles, using them, try to describe from the point of view of classical mechanics the results obtained using, for example, the electron backscattering effect.

[0026] The inventor's hypothesis and the method based on it is a quantum-mechanical interpretation of the idea of D. K. Maxwell that the potential deformation energy $U$ is equal to the sum of two energies:

$$U = U_1 + U_2 \quad (1),$$

where $U_1$ it is caused by symmetric compression and $U_2$ is caused by distortion without compressions. [ See: J. C Maxwell, Letter to William Thomson, 18 December 1856, The Scientific Letters &Papers of James Clerk Maxwell, v.1, 1846-1862, 487-491.]

[0027] Equation (1) forms the basis of the modern energy theory of strength. The energy $U_2$, the radiation of which leads to destruction, is considered in this theory as elastic energy, is stored in stress concentrators.

## DESCRIPTION OF THE EXPERIMENTAL RESEARCH

[0028] The emission of electrons and X-rays during the destruction of the adhesive layer and the separation of thin films was observed repeatedly [See: V. V. Karasev *et al*. DAN USSR, (1953), 88, 777-78; C. G. Camara *et al*., Nature, (2008) 455, 1089-1092]. It was assumed that the emission of X-rays was caused by discharge in gases.

[0029] The inventor's hypothesis is that X-rays are the cause of the damage and the consequence. Such a conclusion seems paradoxical, but only from the standpoint of classical mechanics. It is due to the quantum nature of electromagnetic waves and the wave properties of electrons.

[0030] The deformation of compression, tension, bending, torsion of the samples and their destruction was carried out on a special device made on the basis of a vice. Shear deformation and destruction of the samples was carried out when drilling or putting the sample with a rotating grindstone. In all cases, at room temperature and liquid nitrogen

[0031] A KODAK 400 color film or FUJIFILM SUPERIA X-TRA 400 color film was placed in a container that was opaque to visible and ultraviolet rays. The container was irradiated with a stream of particles that were caught by a sticky film located on its surface. The frames were diaphragmed using lead tiles 2/3″ thick (16.3 mm). A stream of particles from glass, alloys of iron, copper, aluminum, and zinc is directed above the surface of the container or outside of it to study direct electromagnetic radiation at the moment of destruction.

[0032] The absorption of electromagnetic radiation and luminescence was investigated using screens located on the surface of the container (FIG. 1 i and j; FIG. 2 f and j) and inside it (Fig 2 k).

[0033] X-ray radiation of varying intensity was recorded in all experiments before destruction and from fragments after destruction. At the time of destruction, X-ray was not recorded. This fact confirms the idea that the energy of this radiation is absorbed by the atoms between which the bond was broken.

[0034] The delay of radiation of particles as a result of destruction, calculated from the length of the span and velocity is 1.6-0.3 μs. This fact suggests that this energy of metastable atoms was not stimulated.

[0035] All experiments confirmed the inventor's hypothesis that X-rays cause a break between atoms, leading to a loss of integrity. The formation of regions with increased stress and the delayed emission of photons is a consequence of the change in the condition of dynamic equilibrium, caused by a change in the electronic structure of atoms in a local region.

## BRIEF DESCRIPTION OF FIGURES

[0036] The patent or application file contains at least one drawing executed in color. Copies of this patent or patent application publication with color drawing(s) will be provided by the Office upon request and payment of the necessary fee.

[0037] The present invention covers a wide range of dynamic processes in inorganic objects investigated in experiments No. 1 to No. 36 and in the growing pine-No. 37, in the roots of the growing strawberry-No. 38 and in human organs: the brain-No. 39, the spine-No. 40, the loin No. 41, and the chest No. 42.

[0038] The results of the experiment are shown in the table “Experimental study of X-rays emissions” chart.

[0039] FIG. 1a illustrates the moment of a copper plate rupture fixed in the upper and lower parts when it is stretched. Radiation in the upper and lower halves as a result of deformation before and after destruction.

[0040] FIG. 1b illustrates an internal crack-like defect in a steel beam caused by an impact.

[0041] FIG. 1c illustrates the moment of formation of a crack in a cobblestone, (dark region), divided into two parts during a sudden cooling from a temperature of 500°C down to 12°C.

[0042] FIG. 1d illustrates the moment of destruction of a high-strength steel rod. The rod fixed in the upper and lower parts was destroyed in the central part by the movement of the piston from left to right. The photograph illustrates the distribution of luminous regions not only in the metal, but also in the air space caused by retarded radiation from fragments formed after the destruction.

[0043] FIG. 1f illustrates the moment of formation of two cracks in a glass plate cooled in liquid nitrogen during a point impact.

[0044] FIG. 1g illustrates the moment of rupture of the top hole in the place of attachment of the aluminum plate when it is stretched.

[0045] FIG. 1h illustrates the moment of partial rupture of the upper right hole at the place of attachment of the aluminum plate, similar to the previous one, but fixed at two points during its stretching. The experiment was terminated before the plate was broken.

[0046] A container with photographic film was placed under a steel bar 1.55 ″ thick, on the upper surface of which one blow was struck with a hammer. FIG. 2 1 illustrates X-rays radiation recorded by the photographic film.

[0047] FIG. 2 (frame 2-frame 8) illustrates the X-rays emitted by an impact with the tip of an ax (frame 4) on the surface of a 4×9.5 I-steel beam, fixed by photographic film located on the opposite surface at a distance of 4″ from the impact point. FIG. 2 2 illustrates the X-ray radiation recorded on a film located on the left butt at a distance of 14″ (frame 2) from the impact point. FIG. 2 8 illustrates the X-ray radiation recorded on the film located on the right butt at a distance of the impact point 70″ (frame 8). Note. Only some frames, located between

butt at a distance of the impact point 70″ (frame 8). Note. Only some frames, located between the point of impact and the butts are shown.

[0048] FIG. 2 frame 9 illustrates the dark stripe of an ax striking a wooden rod and the green response 0.4 ″ to the left of it. The most remote response is located on the right at a distance of 11.4″ and is shown in FIG. 2 e.

[0049] A fragment of the hacksaw blade 0.5 mm thick, shown in FIG. 2, frame 11, was irradiated with X-rays from particles of the same alloy formed after destruction. The photo shows intense X-ray absorption.

[0050] Three photos shown in FIG. 2, frames 13, 14, 15, illustrate X-rays from strawberry roots. FIG. 2, frame 16, illustrates the luminescence of a steel washer located on the surface of the container when irradiated from particles formed upon contact of a copper alloy plate with a rotating grinding stone; FIG. 2, frame 12, illustrates the luminescence of a Pb-Sn alloy wire located inside a container when irradiated from particles formed upon contact of a steel plate with a rotating grinding stone.

[0051] The photos shown in FIGS.3-10 illustrate the X-ray radiation that occurred during the process:

[0052] solidification of molten plastics- FIG. 3a,

[0053] solidification of molten silumin-FIG. 3b,

[0054] solidification of molten aluminum alloy 7075-T651 - FIG. 3c,

[0055] destruction of flagstone at bending - FIG. 3 d, FIG. 3 e, and impact - FIG. 3 f,

[0056] drilling holes in concrete- FIG. 4 a,

[0057] luminescence in the X-ray of a steel washer irradiated with radiation from particles of a copper alloy after destruction- FIG. 4 b,

[0058] welding steel parts- FIG. 4 c,

[0059] pine growth - FIG. 4 d, FIG. 4 e, FIG. 4 f,

[0060] battery discharge FIG. 4 g, FIG. 4 h, FIG. 4 I,

[0061] chemical reaction of soda and vinegar FIG. 4 j,

[0062] chemical reaction between iron alloy and electrolyte FIGS. 4 k and 4 l.,

[0063] copper alloy corrosion- FIG. 5 a,

[0064] steel corrosion - FIG. 5 b, FIG. 5 c, FIG. 5 d, and FIG. 5 e,

[0065] some areas of the brain of the inventor - FIG. 5 f, FIG. 5 g, FIG. 5 h, and FIG. 5 i,

[0066] some areas of the spine of the inventor - FIG. 6,

[0067] some areas of the back of the inventor - FIG. 7 a, b, c, d, f; friction of aluminum container loaded with flagstone and asphalt-FIG. 7 g, h, and i,

[0068] some areas of the cell in the heart and lungs of the inventor- FIG. 8.,

[0069] at impact of a stone with mass 15 kg, which fell from a height of 5 m onto the surface of the water in the container filled with flagstone, in which the film was placed U-shaped at the bottom and up along the side surface- FIG. 9, and

[0070] hitting the stone in the same experiment, but the second film was placed on a circle on the outer surface of the container-FIG. 10.

[0071] 72 Photos shown in FIGS. 11- 16, are of particular interest, since they are obtained by X-ray radiation caused by the movement of a locomotive by rail road.

[0072] FIG. 11 illustrates the X-ray radiation recorded on a photographic film placed in a container located on the sleeper between the rails perpendicular to them.

[0073] FIG. 12 illustrates the X-ray radiation recorded on a photographic film placed in a container located on the web of the rail. Locomotive was stopped three meters before the film.

[0074] FIG. 13 illustrates the X-ray radiation recorded on a photographic film placed in a container located on the web of the rail, but in the snow.

[0075] FIG. 14 illustrates the X-ray radiation recorded on a photographic film placed in a container located on the rail foot.

[0076] FIG. 15 illustrates the X-ray radiation recorded on a photographic film placed in a container located on the rail web after the passage of a locomotive in the forward and reverse direction.

[0077] FIG. 16 illustrates the X-ray radiation recorded on a photographic film placed in a container located on the frame of the locomotive.

[0078] FIG. 17 a-f illustrates the X-ray radiation recorded on a film placed in a container located three meters from the railway, which was exposed for two days. FIG. 17 g-i illustrates the X-ray radiation recorded on a photographic film placed in a container 5, 9, 26 mm from the bottom surface of a 6 mm thick steel plate caused by an ax hit on the top surface; FIG. 17 j-l illustrates the X-ray radiation recorded on a photographic film placed in a container located 15, 18, and 21mm from the surface of this plate caused by a hammer impact on the butt.

[0079] FIG. 18 illustrates the X-ray radiation recorded on 14 frames of film, located in a container spirally on the surface of a cylinder with ice, in the center of which water vapor was passed through a tube having smaller diameter.

[0080] FIG. 19 illustrates the X-rays due to the deformation of the rail as the locomotive moves while performing the control experiment.

[0081] FIG. 20 illustrates the formation of three types of electromagnetic, including X-ray, radiation. Photos shown in FIG. 20 (frames 1-8) are used to demonstrate for the result of atomic processes during which the formation of pores, cracks and fracture occurs;

[0082] FIG. 20 (frames 9-16), are characteristic not only of the processes occurring during deformation, but also of those that caused the growth of plants and the vital functions of human organs.

[0083] FIG. 21 illustrates the dependence of the crack length in a rotating compressor disk on rotational energy.

[0084] FIG. 22 illustrates the use of the method proposed in the invention for a comparative assessment of the danger of two cracks formed to the right and left of the rivet hole A40 in an experimental study of the fuselage panel of the Boeing 737-232 (B727).

[0085] FIG. 23 illustrates the process of the formation of a crack to the left of the rivet hole A23 in an experimental study of another fuselage panel of the same aircraft.

[0086] FIG. 24 illustrates a scheme for measuring the intensity of electromagnetic radiation of structures and devices.

[0087] FIG. 25 illustrates a diagram of an experimental study of rail X-rays radiation during locomotive movement.

[0088] FIG. 26 is an illustrative, simplified block diagram of a computing device that can be used to practice at least one embodiment of the present disclosure.

ANALYSIS OF THE EXPERIMENTAL RESEARCH

[0089] The experimental study carried out by the inventor not only refuted conventional energy source hypotheses but also indicated the need to identify areas that radiate or absorb energy.

[0090] The final table of X-ray research results, is based on an analysis of 836 photographs obtained from experimental studies of the deformation and fracture of various materials, including 234 photographs recorded during locomotive movement. X-rays were observed in all materials studied, regardless of their composition and structure, in all dynamic processes in inorganic and organic materials, including cells of a living organism. This fact allows us to conclude that the proposed method is universal.

[0091] The difference between the number of tests and the number of photographs is due to the fact that in some trials more than forty photographs were observed at the same time, in other cases when the intensity of radiation was low, for example, 8-15 drills were required to get one frame. However, each photograph is not random — it was obtained to demonstrate the application of the method on each specific technological operation. Experts in each industry can perform similar experiments on a planned program.

[0092] FIG. 1a shows that the radiation in both upper and lower parts was caused by the deformation as before, as well as after destruction. There's no radiation at the moment of destruction because all the energy was used to break the connection between the atoms. Radiation in the lower part is caused by the transition of the electrons from the metastable level to the normal one, excluding the atoms, which weren't used in the process of the formation of the impulse that resulted in a crack.

[0093] FIG. 1d. The photograph illustrates the distribution of luminous regions not only in the metal, but also in the air space caused by delayed radiation from fragments formed after destruction. Thee dark region in the middle part of the rod indicates the absence of metastable atoms with increased energy in it. The experiment indicates that stress concentrators exist, but they are the result of changes in the energy state of local regions.

[0094] FIG. 1g. The plate had two notches, the right of which is visible in the photo. We see that the upper part of the plate has a red tint, indicating that the frequency of X-ray

photons is lower than the frequency of those photons that are emitted in the central part. A clear distribution of luminous regions characterizes the distribution of metastable atoms, the detailed study of which is of particular importance for understanding the processes of destruction and the design of the element of a structure or device

[0095] Pb-Sn alloy wire with a diameter of 3 mm flattened to a thickness of 0.004 mm was irradiated with radiation from steel particles formed upon contact with a rotating grinding stone. Photo shown in FIG. 1 i illustrates the result obtained by irradiation for 10 minutes. Fig 1j, illustrate irradiation for 30 minutes. This experiment allows to conclude that the energy of photons emitted from steel exceeded 100 keV.

[0096] Photos shown in FIG. 2 frames 1-10 demonstrate high penetrating power of X-rays

in metal and wood, caused by an impact. But the same rays emitted from the particles, intensely absorbed by the metal, cause luminescence or heating. This phenomenon, called the inventor of self-emissive transparency, has been observed for the first time and was not theoretically predicted. The number of experiments performed by the inventor for verification is so large that it excludes the possibility of error. The name given by the inventor is similar to self-induced transparency, which was theoretically predicted and experimentally confirmed using a femtosecond laser. The lack of a theoretical explanation of the observed phenomenon does not exclude the possibility of its use in practice.

11

[0097] Photos shown in the application characterizes the distribution of the intensity and frequency of the emission spectrum causing luminescence. The central part is white in all cases while the color of the luminescence of the peripheral regions is more specific for lower excitation frequencies. This happens due to the peculiarity of X-ray radiation. An electron removed from a deeper energy level may be replaced not by a free electron, but by an electron from a level above. White color indicates a cascade transition of electrons from higher to lower levels.

[0098] Of particular interest are the six photographs shown in FIG. 4g -FIG. 4 l.

[0099] The container with the photo film was placed under the PRO ECL series 29 battery, which was discharged during the day with a current of 1 ampere. The photographs of FIG. 4 g and FIG. 4 h illustrate X-rays in the anode region. Photo FIG. 4 i illustrates X-rays in the cathode region. A similar phenomenon is demonstrated by FIG. 5 f, obtained in the study of radiation due to biological processes in the brain of the inventor. The photo illustrates the operation of the hearing aid battery, the current strength of which is thousands of times less.

[0100] 60 g of baking soda in a cylindrical beaker placed on a container were poured with vinegar until the chemical reaction completely ceased. FIG. 4 j illustrates the X-rays due to the reaction.

[0101] This fact indicates that dynamic processes caused by atomic reactions are accompanied not only by the excitation of valence electrons that are participants in chemical reactions, but also by the excitation of electrons from deeper levels, the transition to which is the cause of the of X-ray photons emission.

[0102] The experiment performed to detect defects in rails and locomotive is of particular importance, demonstrating unlimited possibilities for obtaining important information about dynamic processes occurring in different parts of the rail and locomotive.

[0103] Five films located on different sections of the rail illustrate the appearance of similar and different energy emitters. FIG. 11 illustrates the X-ray radiation detected by a film located between the rails on the sleeper perpendicular to the rails. The radiation is caused by the deformation of the rails with a single pass locomotive over the film. Intense radiation recorded on frames 1, 2 on the one hand, and 17, 18 on the other hand, is caused by deformation of rails and fastenings to the sleeper. A clearly defined luminous channel is fixed on frames 3-16. The observed phenomenon is of practical interest, as on frame 2 there was one fixing defect, while on frame 17 six such defects and a small luminous area on the bottom of the frame were recorded. A similar area is observed in frame 15.

[0104] FIG. 12 illustrates the X-ray radiation recorded by the film located on the rail web in the place in front of which the locomotive stopped, not reaching three meters. "Fan-like" radiation, fixed at frames 2, 5, 6, 8, 10, 11, is identical with that recorded in FIG. 11 frames 15 and 17. The formation of such radiation is due to snow, that is, water. Such luminous regions are observed in FIG. 13, FIG. 14, FIG. 15.

[0105] "Fan-like" radiation was detected in 55 photographs obtained by condensation of steam on the ice surface and its melting, corrosion of alloys in aqueous solution containing chlorine, plant growth, body impact on the water surface, destruction of flagstone, and deformation of the rail on which surface was snow, and from the organs of a living organism. The nature of the radiation indicates that it occurred on the surface as a result of breaking the bond between the oxygen and hydrogen atoms forming the water molecule, and their subsequent ionization. The second stage is the formation of compounds, occurred as a result of exothermic reactions. The mechanism of chemical reactions with catalysts was discovered by G. Ertl [See: G. Ertl, Nobel Lecture, Reaction at Surfaces: From Atoms to Complexity, December, 2007]. Photographs of the oxidation of carbon monoxide $2CO + O_2 \rightarrow 2CO_2/Pt$ (110) on the surface of platinum, obtained by photoemission electron microscopy on a surface of 360×360 μm, testify that as a result of the reaction spiral figures are formed due by

chemical turbulence.

[0106] The difference between "Fan-like" and spiral-shaped figures indicates that in these two experiments there are various manifestations of atomic reactions.

[0107] The arc-shaped figures observed during deformation of a solid, plant growth, and reactions that cause energy processes in the cells of living organisms are not identical to those characteristics of chemical turbulence, not identical to vibrational chemical reactions of Belousov-Jabotinsky.

[0108] The photos shown in FIG. 17 and FIG. 11, witness that X-rays are emitted from the ground or emitted from a deformed rail will spread over a considerable distance in the ground.

[0109] The anisotropy of the response of the materials with respect to the direction of the acting force, as observed in the experiment with the I-beam (See FIG. 2 a, b, c), indicates the interaction of electromagnetic radiation with acoustic waves, leading to stimulated Brillouin scattering.

[0110] The identity of the response of the material during its hardening and destruction confirms the inventor's hypothesis that the energy of photons emitted during corrosion or spontaneously sufficient to locally melt the nanoscale region.

[0111] Numerous arc-shaped X-ray sources shown in FIG. 8 and FIG. 7, were observed in metals upon impact. The maximum number of such sources was recorded on a film located parallel to the direction of impact.

[0112] The disclosure of the mechanism of atomic processes caused by water-salt metabolism in plants and cells of a living organism is of particular importance. 14 photos from 22 shown in FIG. 18 demonstrate the processes that occur during vapor condensation at the border with ice (frames 1–4), the boundary between liquid and ice. But on all photos not nanoscopic, but macroscopic radiating areas are fixed. This fact suggests that in a certain area atomic reaction are identical.

[0113] Photographs (FIG. 18 frame 1 and Fig 18 frame 2) differ little from one another, but the rays fall on the surface of the films at an angle different by ~ 40 °. This means that the radiation source is spontaneous. The energy of such sources is partially absorbed and increases the temperature. The local temperature is sufficient for a phase transition, but not sufficient for the formation of cracks.

[0114] The fact that the interaction of water with organic and inorganic materials begins with the decomposition of water on the surface allows the use of pump-probe and plasmon resonance to study these processes.

[0115] The experimental study based on which an invention is proposed shows that it can be implemented only on the basis of quantum mechanics, since the laws of classical mechanics are inapplicable when bodies approach each other at a distance of 2 nanometers, due to the cloud between them electrons emitted by each of the bodies.

[0116] The interaction of one electron cloud with other leads to a change in the electric field, which is accompanied by a change in the magnetic field and the formation of electromagnetic waves. This hypothesis, formulated by Maxwell, is confirmed experimentally and forms the basis of classical electrodynamics.

[0117] Electromagnetic wave is considered in quantum electrodynamics as an energy quantum, called a photon. The interaction between atoms is due to the exchange of electrons and photons. In other words, the process of destruction originates in the nanodomain.

[0118] Electrification by friction, due to the displacement of the electron cloud together with the body from which they are emitted, is accompanied by a discharge and a glow, which is called triboluminescence. Any type of deformation causes a relative displacement of grains, twins, or other fragments separated by a heterogeneity boundary. This fact is confirmed by research performed using electron microscopes and described in the literature.

[0119] The intense emission of electromagnet waves, observed during deformation, indicates that it is due to the displacement and/or rotation of grains and twins. This phenomenon is called by the inventor as internal triboluminescence.

[0120] Particularly intense displacement or rotation of the grains or twins occurs upon impact, causing maximum acceleration and the maximum change in electrostatic induction, resulting in an electromagnetic pulse with maximum energy.

[0121] The table below shows (See No. 24) that with five blows on samples from iron alloys, 76 photographs were taken, both in the direction of impact and at different angles in planes drawn through the direction of impact.

[0122] Similarly, a single blow to the surface of the water (See No. 28) caused X-rays in all directions, recorded in 53 photographs.

[0123] A large number of photographs were obtained to demonstrate the phenomenon, it allows one to draw certain conclusions about defects that are observed with dynamic processes caused by deformation, and without it.

[0124] Eight photos FIG. 20 (1-8) confirm the inventor's hypothesis about the main source of energy, the radiation of which is the cause of man-made disasters [See: V. P. Rombakh, Damage of Metals: Atomic Nature, International Conference on Fatigue Damage of Structural Materials V, Hyannis, MA, USA (2004), Poster No 1; V.P. Rombakh, Atom Parameters and Metal Properties, Logistics Capital, Inc. Edmonds WA, USA, pp 311].

[0125] The formation of cracks occurs in the area in which energy is absorbed and cannot be fixed. The luminescence that is observed is due to spontaneous radiation that occurred before or after the destruction, just as it was recorded from particles many times.

[0126] The experiment refutes the hypothesis of the decisive role of the tip of a crack, which forms millions, or even billions, fractions of a second, the length of which depends on the energy absorbed by atoms; the accumulation of energy occurs in an area outside the crack. A clear boundary between these two regions is fixed in all observed experiments.

[0127] FIG. 20 8 illustrates the case when there were atoms in the damaged area, the radiation of which occurred with a delay.

[0128] Photos shown in FIG. 20, indicate that the number of types of defects that are detected by the shape of the radiator is limited. They can be classified and the effect on the material properties has been established experimentally.

ATOMIC REACTIONS OF DYNAMIC PROCESSES

[0129] Quantum mechanics allows us to estimate the energy state of an atom or group of atoms in the local region of the metal in theory and modern experimental base allows verification of this assessment. Therefore, by analogy with fatigue, we introduce the notion of normal *AN* and morbid (pathological, painful) atoms *AM*. A morbid atom is an atom that has changes that occurred in its electronic shell due to external influences.

[0130] Assume that all atoms (ions), under which the property of the material does not change a normal *AN* regardless of what they represent. Changing the properties of the material means that there was a change of parameters of a group of atoms.

[0131] We can describe all of the changes that occurred in the technical element of the structure or device using five atomic reactions:

[0132] 1. $AN + h\nu \rightarrow AN^* = AM$ (I). Electron transfer to the metastable level.

[0133] 2. $AN + h\nu_1 \rightarrow AM^+ + e^-$ (II). Forced additional ionization.

[0134] 3. $AN + e^- \rightarrow AM^- + h\nu_2$ (III). Ion and electron recombination.

[0135] 4. $AN^* - h\nu_3 \rightarrow AN$ (IV). Spontaneous or stimulated transition of an electron from the metastable level.

[0136] 5. $AM^+ + e^- \rightarrow AN + h\nu_4$ (V). Here $AM^+$ is a morbid atom (ion) the charge of which is increased; $AM^-$ is a morbid atom whose charge has fallen.

[0137] Only the induced radiation of energy from the destruction domain is sufficient to form a crack or fracture.

[0138] The law of destruction formulated by the inventor states: The loss of integrity of a solid and its destruction is the result of breaking the bond between atoms that have absorbed photons induced by local groups of metastable atoms, the excitation of which occurred as a result of the conversion of mechanical energy into electromagnetic and electromagnet energy into mechanical.

[0139] Cracking or fracture occurs when, after the bond is broken, the atoms are removed to a distance at which a new equilibrium state occurs. The formation of such a state is accompanied by acoustic oscillations, the frequency of which decreases from $10^{13}$ to $10^{4}$ Hz.

[0140] The reality of such a mechanism confirms the latent radiation of X-rays from fragments formed after destruction. This fact indicates that not all the accumulated energy was consumed.

[0141] The advantage of a method based on the use of a phenomenon whose law is revealed is due to the knowledge of cause-effect relationships. Empiric equations are proposed on the basis of statistical studies, but this does not exclude the possibility of the realization of an unlikely event at the beginning of operation, which leads to a disaster.

[0142] For example, the probability of an event due to which the shuttle Challenger crash occurred was estimated at 1: 100,000. Such a low probability ruled out the possibility of a catastrophe during the entire service life, but a catastrophe occurred.

[0143] The X-ray radiation caused by the deformation and the luminescence caused by it are used for the first time as parameters on the basis of which the technical state of the object under study is evaluated and possible changes are made. The practical application of this

phenomenon requires preliminary experimental studies to assess the basic parameters of the material, which is the accumulated energy and the rate of its accumulation. Material wear, its critical state, reliability and durability are not determined by strength, but by the ratio of energy accumulation rate to its dissipation rate.

[0144] Experiments performed by the inventor show that the use of modern experimental methods can reduce the testing time by tens of thousands of times, obtaining more accurate objective information about the processes leading to destruction.

[0145] The analysis of atomic reactions leading to destruction is possible on the basis of quantum mechanics. This fact dictates the need for voluntary or compulsory refusal to use erroneous methods in scientific and technical laboratories. This is the first step to solving the problem of forecasting and preventing man-made disasters.

[0146] The theory of spontaneous and stimulated radiation was developed by Einstein. The creation of a maser and a laser was an experimental confirmation of this theory.

[0147] The spontaneous radiation photons, not absorbed by the material, leave it. Measuring the intensity of spontaneous radiation $I_e(\nu)$ allows us to estimate the accumulated energy $U(\nu)$ and the rate of its accumulation, if the relationship between these parameters is established. The units of radiant intensity are watts per steradian. The total power (watts) emitted in a given frequency

$$U(\nu) = \int_0^S I_e(\nu) d\nu d\Omega \quad (2),$$

where the integral is taken over the closed surface $S$ of the region in which the atoms emitting energy are.

[0148] The total energy radiated spontaneously by a local group of identical $N_i$ atoms in the frequency interval is

$$U(\nu) = N_i A_i h\nu g(\nu) \quad (3)$$

[0149] Here $A_i = \sum_j A_{ij}$ where $A_{ij}$ is the Einstein coefficient, which characterizes the probability of electron transition from level $i$ to level $j$, which has dimension $s^{-1}$. $A_i$ characterizes all transitions from level $i$

[0150] Thus, if $N_i$ (0) electrons were at the level $i$ at the time $t = 0$, then the number of electrons at this level decreases exponentially $N_i = N_i(0)e^{-A_i t}$ (4).

[0151] The possibility of applying Einstein's theory to analyze the processes of destruction is demonstrated by examples of solving specific problems. The lifetime of a domain of destruction is different from the lifetime of the metastable state of an individual atom, just as the time of existence of a forest is different from the time of existence of a separate tree. Wear and aging are due to an increase in the ratio of the number of morbid atoms to the number of normal atoms.

[0152] The process of energy accumulation in a substance during its deformation and pumping in a laser is carried out by an electromagnetic pulse excited in a different way. This difference of principle does not matter. Therefore, the application of an equation similar to the Einstein equation

$$U_2(t) = U_2(0) \exp\left(D_1 \frac{h\nu_d}{kT} t\right) \quad (5)$$

is justified.

[0153] Here $D_1$ is the energy dissipation coefficient characterizing spontaneous radiation, having dimensions $s^{-1}$, $v_d$ is the frequency of the photon stimulating the radiation of energy accumulated in the domain of destruction, $k$ is the Boltzmann constant, $T$ is the absolute temperature. However, such a conclusion is provable via experimental verification. In connection with this, additional equations are proposed.

BASIC EQUATIONS OF DESTRUCTION MECHANICS

[0154] The absence of a quantum theory of strength and destruction led to the fact that the physical measurable parameters, on the basis of which equations can be proposed, are determined for the first time. Modern technical laboratories use instruments and methods for studying dynamic processes at the atomic, molecular, and nano level. Quantum mechanics allows the use of material parameters based on the measurement of spontaneous emission of atoms during operation. One of these parameters is wear due to the ratio of the number of morbid $N_m$ atoms to the number of normal $N_n$ atoms at each stage of the operation of an element of structure or device.

[0155] The total binding energy of a local group of atoms of an element at the initial time $t=0$ is due to the energy state of normal atoms. The experiment shows that the induced

radiation occurs in a narrow frequency interval, at which the frequency, phase, polarization and direction of the photons emitted induced, coincide with the parameters of the photon that stimulated the radiation. In this regard, we can restrict by one chemical element.

[0156] The energy of a local group of atoms, an element before the start of operation $t=t_0$, due to the energy of the bond $\varepsilon_b=h\nu_b$ of atoms, is equal to

$$U_1(v, t_0) = \varepsilon_b N_n(t_0) \quad (6),$$

where $N_n(t_0)$ is the number of normal atoms.

[0157] The energy of the morbid atoms at this time is equal to

$$U_2(v, t_0) = \varepsilon_m N_m(t_0) \quad (7),$$

where $\varepsilon_m = h\nu_m$ is the energy of the morbid atom, $N_m(t_0)$ is the number of atoms. The number of morbid atoms is extremely small,

$$N_m \ll N_n.$$

[0158] Experimental studies performed by S. P. Zhurkov showed that long-term strength is well described by the exponent Experimental studies performed by S. P. Zhurkov showed that long-term strength is well described by the exponent

$$\tau_p = \tau_0 \exp[(U_0-\gamma\sigma)/RT] \quad (8)$$

for various crystalline and amorphous bodies. Here $\tau_0$ is a constant, numerically close to the period of thermal oscillations, $U_0$ is the destruction energy, close to the sublimation energy, $\gamma$ is a structure coefficient, having the dimension of volume, $\sigma$-mechanical stress, $R$ is gas constant, $T$ is absolute temperature.

[0159] Attempts to improve Zhurkov's formula were made repeatedly, but without success, because the authors remained in the position of classical mechanics, which does not allow one to understand the physical meaning of the structural coefficient, which has the dimension

of volume.

[0160] The inventor proposes to treat this coefficient as the volume occupied by morbid atoms, i.e. the volume of destruction domain $V_d$. In this case, the Zhurkov's formula will be represented as follows:

$$\tau_p = D^{-1} e^{\frac{U_S - \sigma V_d}{kT}} \quad (9),$$

where $D$ is a parameter similar to the coefficients in the Einstein's theory of spontaneous and stimulated emission, $U_s$ is the sublimation energy. This allows us to postulate that the number of morbid atoms grows exponentially.

[0161] This allows us to postulate that the number of morbid atoms grows exponentially

$$N_m(t) = N_m(t_0) \exp(A/DkT) = N_m(t_0) \exp(U_2/t_c DkT') \quad (10)$$

Here $A = U_2/t$ is the energy accumulation rate, $B = DkT$ is its dissipation rate, $\Gamma = A/B$ is the degree of wear

of volume.

[0160] The inventor proposes to treat this coefficient as the volume occupied by morbid atoms, i.e. the volume of destruction domain $V_d$. In this case, the Zhurkov's formula will be represented as follows:

$$\tau_p = D^{-1} e^{\frac{U_S - \sigma V_d}{kT}} \quad (9),$$

where $D$ is a parameter similar to the coefficients in the Einstein's theory of spontaneous and stimulated emission, $U_s$ is the sublimation energy. This allows us to postulate that the number of morbid atoms grows exponentially.

[0161] This allows us to postulate that the number of morbid atoms grows exponentially

$$N_m(t) = N_m(t_0) \exp(A/DkT) = N_m(t_0) \exp(U_2/t_c DkT') \quad (10)$$

Here $A = U_2/t$ is the energy accumulation rate, $B = DkT$ is its dissipation rate, $\Gamma = A/B$ is the degree of wear.

[0162] The safe operation time $t_c$ is set during design. Based on this, the degree of wear

of wear and accumulated energy is estimated, $\ln N_m(t_c) - \ln N_m(0) = A/Dk_B T = U_2/t_c\, Dk_B T$ . $\ln N_m(t_c)$-$\ln N_m(0) = A/DkT = U_2/t_c DkT$

[0163] Neglecting the number of morbid atoms at the initial moment, we get:

$$U_2(t_c)/DkT = t_c \ln N_m(t_c) \quad (11).$$

[0164] However, the determination of the ultimate value of the energy $U_2^u(t_u)$, which leads to destruction, is possible only by experimental research, but the experiment should answer the question: when should the operation be terminated so it will be not too early, but not too late.

[0165] The theory cannot answer this question, for an atomic reaction can be stimulated even by solar radiation, especially during a solar storm.

[0166] Determining the moment of termination of the facility or device becomes so important that such a decision must be justified by a comprehensive experimental study, providing a computer program with all the data to determine when an emergency stop.

WAYS TO IMPLEMENTATION THE METHOD

**[0167]** Maxwell's work [J. C. Maxwell, III. On the Equilibrium of Elastic Solids, (1850) pp.31-74, The Scientific Papers of James Clerk Maxwell, Edited by W. D. NIVEN, M.A., F.R.S.] still remains the only theory in mechanics, the equations in which are derived on the basis of experiment and suggested experimental methods for their use.

[0168] Maxwell investigated the relationship between the pressure at various points in the body under mechanical action and the only optical response known at that time as the interference of polarized rays, putting the foundations of photoelasticity. He proposed the equation

$$I = \omega \frac{Mb}{2\pi r^2} \quad (12),$$

which relates the optical response $I$ to the moment of force $M$, which displaces the upper surface of the hollow cylinder relative to the fixed inner surface by an angle $\delta\theta$. Here $b$ is the length of the cylinder, $r$ is the distance from the axis of the cylinder to any point of the solid

part of the cylinder. The article concludes with the conviction that the study of the relationship between mechanical action and optical response for various materials might lead to a more complete theory of double refraction, and extend our knowledge of the laws of optics. The creation of quantum electrodynamics, which is the most accurate physical theory, confirmed Maxwell's prediction, but it is not used to solve the problems of strength and destruction.

[0169] Photoelasticity is used in strength mechanics as the main argument for the introduction of stress intensity factors.

[0170] This conclusion is erroneous, because birefringence is due to the anisotropy of atoms or molecules associated with a change in orbital or magnetic quantum numbers, which does not lead to a change in strength properties or destruction. Electro-optical and magneto-optic effects, leading to birefringence, were confirmed by Maxwell's prediction. He discovered an effect called dynamo-optic.

[0171] The use of the photoelasticity method simultaneously with the method proposed in the invention will help clarify the role of luminous regions and establish the coordinates of the domains of destruction using another Maxwell equation proposed in this paper:

$$\Psi(x,y) = I\frac{1}{z} = \omega(q-p)\frac{1}{z}, \qquad (13)$$

where $I$ is the difference of retardation of the oppositely polarized rays, and $q$ and $p$ the pressures in the principal axes at any point, $z$ being the thickness of the plate.

[0172] The equations proposed by Maxwell for the bending of rods were tested by him experimentally on samples of iron, brass, and glass with an accuracy of a fourth sign.

[0173] The X-ray radiation that occurs when a steel bar is destroyed is shown in FIG. 1 d. This experiment, performed by the author of the proposed method, confirmed the idea of Maxwell, formulated by him in a letter to Thomson (Lord Kelvin).

[0174] The theoretical prediction of quantum effects and experimental confirmation allows them to be used for experimental evaluation of the ultimate value $U_2^u(t_u)$, which is the main parameter on the basis of which the possibility of preventing catastrophic destruction is based. This allows the method of assessing the potential energy of destruction of the element of structure or device to be briefly called MAPED.

[0175] Spontaneous emission of morbid atoms is not the only response to deformation.

Additional information about atomic reactions in the deformed material during operation is provided by luminescence; in experimental studies, additional resonance methods are used, for example, gamma resonance, stimulated Brillouin scattering, X-ray diffraction, X-ray spectroscopy, etc.

[0176] The implementation of the proposed method consists in establishing a functional relationship between the radiation intensity and parameters characterizing an external effect, for calculating the accumulated energy and the rate of its accumulation with the maximum accuracy until a crack appears. A characteristic feature of the method is that it uses only measured parameters, a crack forms in millionths of a second, and no radiation is observed at the moment of the formation of a crack.

[0177] For example, one has to research:

[0178] • $I_e(v,t)=F_1(\sigma N)$ until cracks appear under cyclic deformation of stretching, bending, torsion, or shear, where σ is stress, N is the number of external influences;

[0179] • or $I_e(v,t)=F_2(Sh_1)$ when an indenter is immersed, where $S$ is the indenter footprint, $h_1$ is the immersion depth;

[0180] • the connection $U_2(v,t)=F_3[I_e(v,t)]$ when a crack appears is established only in an experimental study; in practice, an extremely admissible value of energy $U_{2\,ex}(v,t_{ex})=U_2^u(t_u)$, is used, at which the operation is terminated and the element is replaced.

[0181] • an accurate definition of $t_{ex}$ prevents catastrophe and provides the ability to use the entire resource.

[0182] Quantum electrodynamics is an accurate physical theory, on the basis of which processes of interaction of atoms can be explained. Every interaction of atoms is due by the exchange of electrons and photons.

[0183] The implementation of the method is based on a theoretical assessment of the potential energy, the accumulation of which is due to the deformation. The equations used for the calculations contain only the measured physical parameters characterizing the atomic reaction, and the proportionality coefficients found during experimental studies of the material.

[0184] The spectrum of electromagnetic radiation is the only objective characteristic of the energy state of the atom. The frequency of electromagnetic radiation is measured with such an accuracy that is not available for measuring other parameters.

[0185] The induced radiation is due to the quantum mechanical properties of local groups of atoms. It occurs at a certain concentration of metastable atoms in a region, for example, in a grain or in a twin, which is a resonator having two parallel boundaries on which electromagnetic waves are reflected.

[0186] It is particularly important to note that the amplification of electromagnetic radiation can occur when a small number of atoms are in the upper state in the local area, unlike in a laser. It is only important that there are more of them at the excited level than at the lower level. Energy absorption will be accompanied by breaking the bond between the number of atoms at which further exploitation is possible. This may be enough for high-power induced radiation to occur, but with little energy. This phenomenon is called in mechanics tolerance to damage, hidden or subcritical crack.

[0187] A similar phenomenon is possible with high concentration quenching of luminescence or under the influence of impurities.

[0188] These phenomena allow reducing the rate of accumulation the energy, increase the rate of dissipation by changing the composition of the material, the shape of the product and stimulating the safe radiation from the destruction domain.

[0189] The safety of structures and devices cannot be achieved without state standards, which must be changed due to the successes of science and new discoveries. US standards are becoming the basis of other countries' standards or are used unchanged, but a number of standards, such as E399, are based on the use of stress intensity factors. Such standards are erroneous. The basis of the new standards should be the experiments described in the present invention or similar to it.

[0190] The implementation of the method does not present fundamental difficulties in any technical field, for the experimental equipment for studying the *S-N* curves is supplemented by devices for studying electromagnetic, including X-ray, radiation, transmission, storage and analysis of information. This change turns the *S-N* method into the *U-N* curve method. This is the second step to preventing the man-made disasters.

COMPARATIVE ANALYSIS OF THE METHOD PROPOSED IN THE INVENTION WITH OTHER

[0191] Example No. 1. A titanium alloy compressor disc with 12 bolts holes was tested in accordance with the FASTRAN II program [W. Z. Zhuang et al., ICAS-98-5, 2, 3, A98-3162 (1998)]. The first crack on the edge of one of the holes was found after testing 8533 rpm. The disk was destroyed into five fragments after testing at the speed of 9462 rpm. The photo above demonstrates four points in which three cracks meet (or diverge) and the fact that the crack discovered first grew in one and the opposite direction. The main damage didn't occur in the area of the holes, the thickness of the metal in which is 3 mm, but in four points along the rim, which is 15 mm thick. This fact allows us to conclude that the cause of the destruction was the distribution of energy, but not stresses, as the authors believe.

[0192] FIG. 20 confirms this conclusion. The graph above characterizes the relationship between the crack length and the kinetic energy of a rotating disk. The proportionality ratio $C$ is used instead of the moment of inertia. The maximum crack length is lowered to show a parabola.

[0193] One of the causes of erosion, corrosion, and even destruction, turbine blades, propellers is an increase in electron density on the outer surface caused by centrifugal force. Increased electron density leads to the formation of $AM$ morbid atoms, the bond between which is weakened. This defect is eliminated by creating an electrostatic field of counter-polarity.

[0194] Example No. 2. The crack to the right of the A40 AET rivet was discovered when examining a panel of a riveting joint with an overlap of the fuselage of a Boeing 727-232 (B727) [See: B. R. Mosinyi, Aircraft Fuselage Damage Assessment In-Service Aircraft Fuselage Department, Drexel University (2007)] earlier than the crack to the left A40 FWD. The crack on the right, according to Griffiths theory, will reach the critical value earlier than the crack on the left, but Mosinyi received one solution of the NASGRO equation for two cracks.

[0195] Analysis of the processes of formation of these cracks was performed by the inventor using the equation relating changes in energy $\Delta U_2$ with metal thickness $h_1$, binding energy $\varepsilon_b$, lattice constant $a$, crack growth rate $\frac{\Delta l}{\Delta N}$

$$\Delta U_2 = h_1 \varepsilon_b a^{-2} \frac{\Delta l}{\Delta N} \quad (14).$$

[0196] Note that the crack growth rate (measured parameter) in the equations of fracture mechanics, including NASGRO, is used as a function of stress intensity factors and other parameters that cannot be measured.

[0197] The use of equation (14) for analyzing the A40 AET and A40 FWD crack formation processes is demonstrated in FIG. 21 in the form of graphs based on the tables given Mosinyi, and the parameters of the fuselage metal.

[0198] The maximums on the graphs indicate at the time when the energy was emitted by some atoms, was absorbed by other atoms, between which the bond was broken; minima correspond to the period of energy accumulation. Particular attention should be paid to the minimum at $N = 141229$ on the A40 FWD chart, which is actually located below the limits of the chart. The stored energy has a negative value of 12882 nanojoules. This minimum on the graph coincided with the maximum of A40 AET, whose energy of 5336 nanojoules was radiated. The coincidence is conditional, since the extension of the crack occurred in a millionth of a second during the experiment, which lasted 1176 hours.

[0199] Example No.3 Cracks growing towards each other were observed on nanofilms to tens of kilometers indicates that the nucleation and growth of cracks caused by a single mechanism which is independent of the size of the object. This mechanism is due to the atomic reaction, in which the accumulation and dissipation of energy occurs and its induced radiation.

[0200] Two pairs of such cracks A22Right –A23Left and A23 Right-A24Left was found when examining the Boeing 727-232 (B727) fuselage riveted panel, [See: A. Ahmed, Initiation and Growth of Multiple-Site Damage in the Riveted Lap Joint of a Curved Stiffened Fuselage Panel: An Experimental and Analytical Study, Thesis Submitted to the Faculty of Drexel University 2007, pp.328.] The analysis of these cracks was limited to a statement of the fact.

[0201] The tables in the cited paper were used by the inventor to analyze processes using equation (14). The graph of one of the cracks is shown in Fig 22. Comparative analysis of the volume of information and its quality using equations in which the crack length $l$ is used as a function of the number of cycles and other parameters, and equation (14) shows that a smooth crack growth does not represent the dynamic processes leading to destruction.

[0202] The minima characterizing the time of energy accumulation are replaced by maxima indicating the moment of induced radiation. Note that even though the measurements of crack elongation were carried out after hundreds of hours, the intervals between the peaks differ by no more than 10%.

[0203] However, the most important difference between MAPED and other methods is the ability to analyze not only the accumulated energy, but also the accumulation rate, which slowed down by 5 nJ/cycle between 13 and 14 measurements, while it increased to 13.6 nJ between 14 and 15 nJ/cycle.

## ANALYSIS THE MAN-MADE DISASTERS CAUSES

[0204] Problem No. 1. The railway accident (Hatfield, UK, 2000) is explained by the fact that the rail under the train broke into 300 fragments on a 35-meter section. Cracks were found on another 50-meter section. This happened despite the fact that, shortly before the accident, the rail was tested with ultrasound, but no defects were found. The cause of the catastrophe is called "rolling contact fatigue" (defined as multiple surface-breaking cracks). However, the nature of fatigue can be explained using quantum mechanics.

[0205] The distinctive features of the analysis of this catastrophe are: the impossibility of finding the cause, multiple homogeneous gaps in which the structure of the fracture surface of the fragments is different, as can be seen in the photos given in the first report published in October 2000. The surface of the fragment, characteristic of plastic fracture, was subjected to intensive corrosion, while the surface of the fragment, characteristic of brittle fracture, remained brilliant, as can be seen in the photographs published in the second report six years later.

[0206] Problem No. 2. The crash of the river bridge I-35 W across Mississippi (USA, 2007) was due to the rupture of eight rivet holes of the U10 gusset 40 years after its opening. The cause of the disaster, as defined by the State Commission, is a design error, which is that the thickness of the leaflet is insufficient. The conclusion is made on the basis of the analysis performed using the finite element method.

[0207] A photo of the U10 Gusset plate taken after extracting a fragment from water, not published in a report, shows that the nature of the breakdown of four even-riveted holes differs from the breakage of four odd holes. The rupture line passed through the centers of all the holes, but the shape of the even holes remained unbroken and the edges shiny, while the

metal near the odd holes was severely damaged and subject to intense corrosion, just as happened with rail fragments.

[0208] Coincidence is natural, since dark areas have been observed in the study of rail defects more than once, but the finite element method is purely mathematical, no containing physical parameters. This method did not reveal the damage that occurred during operation. The method proposed by the invention makes it possible to record the intensity of the radiation of energy, which is the main physical parameter, and the position of the radiating objects in space. These physical parameters are used in a computer program to calculate the accumulated energy and the rate of its accumulation.

TECHNOLOGICAL PROCESS CONTROL CAPABILITIES

[0209] Problem No. 3. Quality control riveting holes of the fuselage and the wings of the aircraft

[0210] The study of defects arising in the rivet holes of the aircraft wings, made using an external source of X-rays [See J. Xu et al, Automatic X-ray Crack Inspection for Aircraft Wing Fastener Holes, 2nd Int. Symposium on NDT in Aerospace 2010 Mo.5.A.4] revealed the damage of the holes edges, just as it was obtained using MAPED, but did not detect

hidden defects between them.

[0211] Two plates of aluminum alloy imitated a rivet joint with an overlap of the aircraft fuselage. Eighteen holes were drilled in this joint. One hole was intentionally damaged. 14 frames recorded the destruction of the hole and 11 defects between the holes. Studies of the fuselage have shown that in these places pitting defects of corrosion and cracks grow, growing towards each other.

[0212] The study of defects arising in the rivet holes of the aircraft wings, made using an external source of X-rays revealed the damage of the holes edges, just as it was obtained using MAPED, but did not detect hidden defects between them.

[0213] Eleven frames were obtained when installing 18 rivets, at which one defect was fixed, made intentionally.

[0214] Problem No. 4. Hot and cold chinks in cast aluminum

[0215] An analysis of the publications showed that attempts to understand the mechanism of the formation of hot and cold cracks in cast aluminum, while remaining in the position of classical mechanics, and creating a computer program to prevent them, were unsuccessful.

[0216] The experimental study, made by the inventor, of hot and cold cracks formation in silumin and aluminum alloy 7075-T651 during solidification of the ingot and cooling of the samples at a temperature gradient of 120K/cm showed that the mechanism of cracking is identical. A computer program for predicting the occurrence of hot or cold cracks is created on the basis of measurements the intensity of spontaneous X-ray radiation and luminescence intensity caused by radiation in various areas of the cooling melt or ingot.

[0217] Problem No.5 High-entropy alloys

[0218] High-entropy alloys consisting of five to six chemical elements, the concentration of each of which is from 5 to 35%, have high hardness, corrosion resistance, heat resistance, thermal and mechanical wear resistance. It is assumed that the unique properties of these materials are due to the successful combination of ductility and brittleness. The authors of the publications, offering different compositions, try to establish the natural influence of any physical parameter on the alloy property. The number of combinations is unlimited, but the trial and error method are not effective.

[0219] The electron backscattering method is one of the most effective for studying high-entropy alloys using electron microscopes. The study of Fe-30Mn-10Co-10Cr-0.5C (at. %). Alloy grains. [See: M. Wang et al., Acta Materialia 147 (2018) 236-146], showed that all metals form local regions whose color is different. This allows you to determine the chemical element whose atoms form a destruction domain and replace it with another analog.

[0220] The method of backscattering of electrons, like methods based on transmission, gives distorted information in cases where the material under study is deformed, because atoms in this case are subject to two electromagnetic effects. This distortion is especially great when the energy of a photon intended for research is comparable or exceeds the photon energy, which is the cause for the atomic reaction.

[0221] The method proposed in this invention is free from this disadvantage.

[0222] The fact that atoms of a single chemical element form a local nano-sized area in the grain makes it possible to experimentally estimate to what extent this concentration affects the rate of energy accumulation and its dissipation and change it to extend the time of safe

[0223] Theoretical and experimental methods developed to improve the quality of a laser help to develop methods for reducing the rate of energy accumulation and increasing the rate

MEASURING THE INTENSITY OF SPONTANE RADIATION

[0224] Measurement of the intensity of spontaneous electromagnetic radiation of a monitored object (MO) is shown in FIG. 22. The part of the object, the damage of which leads to a catastrophe, is called the structural element (SE). For example, the self-loosening of the nuts on the point 2182 A caused a catastrophe (Potters Bar, UK, 2002). The number of structural elements $n$ is due to the safety of MO operation. The signal from the sensor, for example, Sen 1, enters the converter Con 1 and is converted, encoded and transmitted to the TR 1 transmitter, then by wires or without them transferred to the computer (COMP).

[0225] Signal coding eliminates the possibility of unwanted interference and unwanted reading.

[0226] The computer program analyzes the data obtained, estimates the accumulated energy, its accumulation rate, compares with the limit values obtained as a result of the experimental study, and the control convector (CC), in case of danger, through the TR 2 transceiver and the RS receiver using wires or through air is transmitted an alarm and shutdown alarm (ASD). The limit values may be referred to as "critical values." The

MEASURING THE INTENSITY OF SPONTANE RADIATION

[0224] Measurement of the intensity of spontaneous electromagnetic radiation of a monitored object (MO) is shown in FIG. 22. The part of the object, the damage of which leads to a catastrophe, is called the structural element (SE). For example, the self-loosening of the nuts on the point 2182 A caused a catastrophe (Potters Bar, UK, 2002). The number of structural elements $n$ is due to the safety of MO operation. The signal from the sensor, for example, Sen 1, enters the converter Con 1 and is converted, encoded and transmitted to the TR 1 transmitter, then by wires or without them transferred to the computer (COMP).

[0225] Signal coding eliminates the possibility of unwanted interference and unwanted reading.

[0226] The computer program analyzes the data obtained, estimates the accumulated energy, its accumulation rate, compares with the limit values obtained as a result of the experimental study, and the control convector (CC), in case of danger, through the TR 2 transceiver and the RS receiver using wires or through air is transmitted an alarm and shutdown alarm (ASD). The limit values may be referred to as "critical values." The

measured value of accumulated energy (which may be expressed in various ways using various proxies, including intensity) may determined by the computer program to be indicative of potential structural failure in various ways, such as by reaching a threshold relative to the critical value, accelerating at a threshold rate toward the critical value, or in other ways. The threshold or other parameters for determining whether measurements are indicative of potential catastrophic failure may be dependent on context and may be determined experimentally. For example, statistical analysis can be performed to set the parameters such that measurements are determined to be indicative of potential structural failure if there is a certain probability of failure based on experimental measurement, where the probability can be set dependent on context (e.g., the potential for disaster). For example, the probability may be low in such cases where structural failure can lead to catastrophe (e.g., for an airplane) and higher when structural failure has less potential for catastrophe (e.g., in contexts where there is little chance for harm to humans or large-scale property damage). The parameters may also be set based on the availability of redundant systems that operate in case of failure, and based on other factors.

MEASURING THE INTENSITY OF SPONTANE RADIATION

[0224] Measurement of the intensity of spontaneous electromagnetic radiation of a monitored object (MO) is shown in FIG. 22. The part of the object, the damage of which leads to a catastrophe, is called the structural element (SE). For example, the self-loosening of the nuts on the point 2182 A caused a catastrophe (Potters Bar, UK, 2002). The number of structural elements $n$ is due to the safety of MO operation. The signal from the sensor, for example, Sen 1, enters the converter Con 1 and is converted, encoded and transmitted to the TR 1 transmitter, then by wires or without them transferred to the computer (COMP).

[0225] Signal coding eliminates the possibility of unwanted interference and unwanted reading.

[0226] The computer program analyzes the data obtained, estimates the accumulated energy, its accumulation rate, compares with the limit values obtained as a result of the experimental study, and the control convector (CC), in case of danger, through the TR 2 transceiver and the RS receiver using wires or through air is transmitted an alarm and shutdown alarm (ASD). The limit values may be referred to as "critical values." The

measured value of accumulated energy (which may be expressed in various ways using various proxies, including intensity) may determined by the computer program to be indicative of potential structural failure in various ways, such as by reaching a threshold relative to the critical value, accelerating at a threshold rate toward the critical value, or in other ways. The threshold or other parameters for determining whether measurements are indicative of potential catastrophic failure may be dependent on context and may be determined experimentally. For example, statistical analysis can be performed to set the parameters such that measurements are determined to be indicative of potential structural failure if there is a certain probability of failure based on experimental measurement, where the probability can be set dependent on context (e.g., the potential for disaster). For example, the probability may be low in such cases where structural failure can lead to catastrophe (e.g., for an airplane) and higher when structural failure has less potential for catastrophe (e.g., in contexts where there is little chance for harm to humans or large-scale property damage). The parameters may also be set based on the availability of redundant systems that operate in case of failure, and based on other factors.

[0227] The universality of the method proposed in the invention is due to the possibility of continuous non-destructive remote monitoring of atomic processes in all objects, regardless of their size, composition, structure, nature of external influences.

[0228] The main objective of the invention is to predict the critical state of the object under study and to prevent its destruction. The method is applicable to both experimental studies and facilities that are operated.

[0229] The maximum effect from the implementation of the MAPED will become possible when a functional connection between the areas emitting energy due to the deformation and the areas accumulating it is established. The search for such a connection is possible not only on laboratory models, but also on real technical objects.

[0230] Numerous experiments, the purpose of which is shown in the table above, allow us to propose a program of experimental studies for the implementation of the proposed method.

[0231] Problem No. 6. The next panel of the Boeing 727-232 (B727) fuselage is tested on the same experimental equipment as the previous ones, but using a different program. Electromagnetic radiation that occurs in the process of deformation, is fixed on the film and digital sensors. The signals from sensors are converted and transmitted by wire or without

them to a computer containing a program for measuring the intensity, storing information and analyzing it. The sensors, in an embodiment, are placed on structures of the plane using adhesive stickers (e.g., stickers as part of logos and other decorative aspects of the exterior of the plane) to reduce air resistance caused by the stickers.

[0232] The nature of the test samples varies to reduce their number, reduce time and increase efficiency. For example, the number of tests of the fuselage panel and the number of cycles before a crack appears decreases due to an increase in the stress.

[0233] Refusing to use the *S-N* method does not exclude the possibility of using the results obtained by this method. The tables obtained during the study can be used to clarify the time of safe operation, residual life and degree of wear. Only on the basis of experimental studies can the extent to which formula 12 b gives more accurate results than formula 12 a, but note that formula 12 b can be replaced by formula

$$\tau_p=D^{-1}e^{\frac{U_A-V_d\sigma^2}{EkT}} \text{ (12 c) or } \tau_p=D^{-1}e^{\frac{U_A-V_d\sigma^2}{GkT}} \text{ (12 d),}$$

proposed by the inventor.

[0234] Here, $E$ is the modulus of elasticity, $G$ is the shear modulus.

[0235] The volume of the domain of destruction can be calculated on the basis of experimental data, if they are sufficient for this.

[0236] Problem number 7.

[0237] Find the volume $V_d$ of the domain of destruction.

[0238] We use the experimental study which are given by Atre et al. [W. S. Atre et al. Finite Element Simulation of Riveting Process and Fatigue Lives, DOT/FAA/AR-07/56, V.3, 2009, pp. 166]

[0239] Initial data:

[0240] metal $M$

[0241] crack length $l$

[0242] crack depth $h_1$

[0243] bond energy $\varepsilon_b$

[0244] lattice constant $a$

[0245] spontaneous emission photon frequency $\nu$.

[0246] Solution

[0247] The sequence of mathematical transformations is given below.

[0248] The crack area is $S = lh_1$, the number of cells on it is $n=\frac{S}{a^2} = \frac{lh_1}{a^2}$, the energy radiated to form a crack is $U_2=\frac{lh_1}{a^2}\varepsilon_b$, the number of morbid atoms emit her: $N_m=\frac{lh_1}{a^2}\cdot\frac{\varepsilon_b}{h\nu}$.

[0249] If there is one morbid atom in each unit cell, then the total volume is $V_d=\frac{lh_1}{a^2}\cdot\frac{a^3\varepsilon_b}{h\nu}=alh_1\frac{\varepsilon_b}{h\nu}$. A numerical solution of the problem can be obtained after experimentally determining the frequency of the photon of spontaneous radiation.

[0250] The main task of the experimental study is to find the relationship between the accumulated energy and the intensity of spontaneous radiation, which is measured experimentally by $N_m=CI_e(\nu,t)$.

[0251] Problem number 8. Preventing railway disasters

[0252] The safety of the operation of the rail track today is based on the use of mainly two non-destructive control methods: ultrasonic and magneto dynamic, the main disadvantage of

which is the fact that they are designed to search and analyze cracks and other defects that are harbingers of catastrophic destruction, but not the cause. The wavelength of eddy currents and ultrasound, the minimum value of which is 1 millimeter, does not allow to detect micron cracks, while X-ray radiation from the material allows you to set the moment of nucleation of the nano-sized crack.

[0253] The ability to implement the method is due to the use of electromagnetic, including X-ray, radiation caused by the deformation, which is measured with maximum accuracy, data is transmitted by wire or without them at maximum speed using modern communication systems, including space.

[0254] It is known that the cause of a train accident is rail damage that occurs not only under the locomotive and wagons or after passing the train, but even before it. The inventor witnessed the prevention of a catastrophe that could have occurred on August 31, 1978 at Grebyonka station (Ukraine), when the rails curved in front of the passenger train, moving at

[0255] 15 m/s. Locomotive was stopped five meters before damage.

[0256] The photos shown in Fig 12 were taken when the locomotive stopped three meters from the film. Consequently, radiation occurred before the rail subjected to intense deformation.

[0257] Frames 3-16 of FIG. 11 illustrates the energetic connection between the rails, while frames 1, 2 and 17, 18 illustrate the displacement of rail fastenings.

[0258] Experimental research indicates that the energy radiated in one area as a result of mechanical action spreads in the rail to a considerable distance in the form of electromagnetic waves, causing acoustic waves in its path.

[0259] The fact that the driver, seeing the movement of the rails, managed to stop the train, allows predicting the formation of dangerous defects before approaching them.

[0260] The intensity of the radiation recorded in all the photos shown in FIG. 12 indicates that such radiation will be observed from a more distant source.

[0261] Problem number 8.1. Rail testing using locomotive, control experiment

[0262] An experimental test of this hypothesis was performed at the Northwest Railway Museum (Snoqualmie, WA) on ½ mile (800 m) railway track. The experimental scheme is shown in FIG. 24.

[0263] Two containers with photographic film were placed simultaneously on the surface of the rail head and the foot in the interval $Ax_0$. Locomotive, located at point $x_1$ at a distance of 20 feet, began to move towards point $B$, but stopped at point $x_d$, located at a distance of ¼ mile from point $x_1$. The containers with the film were replaced with similar ones, after which the locomotive began to move to the point $x_f$, located at a distance of 1/4 mile (400 m) from the point $x_1$. The containers were replaced a second time after the locomotive reached point $x_n$ and began braking. The seventh and eighth films fixed the start in the opposite direction for 15 seconds.

[0264] The results of the experiment in which 132 photographs were taken illustrate 24 (three from each film) shown in FIG. 19. Analysis of photographs shows that the film recorded radiation from a distance of 1/2 mile. This conclusion is the main argument for preventing a catastrophe. We see in Fig 19 2 and 3 "Fan-like" radiation; thin lines and wide areas similar to the crack shown in FIG. 19 1, 14, 15, 17, 19, 23, etc.

[0265] At the same time, we are witnessing a paradoxical phenomenon that requires an explanation. Repeated photographing of different objects in one frame distorts the image, but this did not happen, because the image is clear, like at a single blow. This fact is due to the locomotive and the synchronous effect.

[0266] Rail track damage is monitored using a device that measures the intensity of electromagnetic, including X-ray, radiation due to deformation, and/or the intensity of luminescence excited by this radiation, transmit data using radio signals to the spacecraft, which determines the coordinates of a point from which radiation occurred, and relays this information to the server, which analyzes, stores this information and makes decisions. The server may be located locally (e.g., on the train) or remotely, accessible over a wide area network, such as the Internet and/or a cellular network. Decisions may be, for instance, to alert an engineer (driver), transmit signals to cause brakes to engage, and/or perform other mitigating actions, which may be programmed to occur according to different contexts, which may be based on the level of danger encountered and/or potential catastrophes that feasibly could occur.

[0267] The device unit containing the sensors for measuring the intensity $I$ is located as close as possible to the side surface of the rail at the point of contact of the locomotive wheel and rail, but without touching it so that it is not damaged during movement. The unit is rigidly attached to the frame of the locomotive. Two sensors are placed vertically through the

[0263] Two containers with photographic film were placed simultaneously on the surface of the rail head and the foot in the interval $Ax_0$. Locomotive, located at point $x_1$ at a distance of 20 feet, began to move towards point $B$, but stopped at point $x_d$, located at a distance of ¼ mile from point $x_1$. The containers with the film were replaced with similar ones, after which the locomotive began to move to the point $x_f$, located at a distance of 1/4 mile (400 m) from the point $x_1$. The containers were replaced a second time after the locomotive reached point $x_n$ and began braking. The seventh and eighth films fixed the start in the opposite direction for 15 seconds.

[0264] The results of the experiment in which 132 photographs were taken illustrate 24 (three from each film) shown in FIG. 19. Analysis of photographs shows that the film recorded radiation from a distance of 1/2 mile. This conclusion is the main argument for preventing a catastrophe. We see in Fig 19 2 and 3 "Fan-like" radiation; thin lines and wide areas similar to the crack shown in FIG. 19 1, 14, 15, 17, 19, 23, etc.

[0265] At the same time, we are witnessing a paradoxical phenomenon that requires an explanation. Repeated photographing of different objects in one frame distorts the image, but this did not happen, because the image is clear, like at a single blow. This fact is due to the high speed of the electromagnetic signal and the constant distance between the wheels of the locomotive and the synchronous effect.

[0266] Rail track damage is monitored using a device that measures the intensity of electromagnetic, including X-ray, radiation due to deformation, and/or the intensity of luminescence excited by this radiation, transmit data using radio signals to the spacecraft, which determines the coordinates of a point from which radiation occurred, and relays this information to the server, which analyzes, stores this information and makes decisions. The server may be located locally (e.g., on the train) or remotely, accessible over a wide area network, such as the Internet and/or a cellular network. Decisions may be, for instance, to alert an engineer (driver), transmit signals to cause brakes to engage, and/or perform other mitigating actions, which may be programmed to occur according to different contexts, which may be based on the level of danger encountered and/or potential catastrophes that feasibly could occur.

[0267] The device unit containing the sensors for measuring the intensity $I$ is located as close as possible to the side surface of the rail at the point of contact of the locomotive wheel and rail, but without touching it so that it is not damaged during movement. The unit is

rigidly attached to the frame of the locomotive. Two sensors are placed vertically through the contact at a maximum distance from each other from the rail head along the web, including the foot, the other two sensors are located on either side of the vertical line.

[0268] The possibility of positioning the sensors above the radiation surface has been tested experimentally for two cases. The container with the film was fixed at two extreme points under the 6 mm thick steel plate located horizontally, so that the central part of the container was 26 mm away from the plate; three blows with the tip of the ax were applied at different points on the upper surface. 12 photographs were taken throughout the film. Three photos of the middle section are shown in Fig 17 g, h, i.

[0269] A similar plate and container were arranged vertically. The impacts with an ax and a hammer were applied to the butt surface. 10 photos were recorded, three photos of the middle part of the film are shown in Fig 17 j, k, l.

[0270] 22 these photographs show that the radiation is spontaneous and its intensity can be measured on the horizontal and vertical surfaces of the rail with repeated exposure.

[0271] Problem number 8.2. Research of radiation sources and determination of their intensity

[0272] In one example embodiment, the minimum number of sensors is eight. They are

located four to the left and four right of the locomotive to scan each rail at four points simultaneously. Denote the sensors located in the block to the left $\alpha$ and $\beta$, while the right are $\gamma$ and $\delta$.

[0273] Non-framed photographic films in containers, opaque to visible and ultraviolet rays, are placed on the vertical (web) and horizontal (foot) surface of the rail between points $x_0$ and $x_1$ in front of the locomotive.

[0274] Let me denote the intensity measured by the sensors in the horizontal plane on the left $I_{\alpha h}(x)$ $I_{\beta h}(x)$, and $I_{\gamma h}(x)$, $I_{\delta h}(x)$ on the right and the vertical plane on the left $I_{\alpha v}(x)$, $I_{\beta v}(x)$ and $I_{\gamma v}(x)$, $I_{\delta v}(x)$ on the right respectively. The peculiarity of the method designed to prevent fracture allows determination of the fracture energy only in an experimental study. This predetermines the fact that the most effective combination of using sensors can be proposed only on the basis of an experiment.

[0275] Simultaneously with the four-sensor unit, a three-sensor unit is tested, scanning the surface of the head, web and foot. The method does not limit the number of options, but the advantage sets the experiment.

[0276] Experiment No. 8.1. The locomotive is located at point $A$ to begin research. It moves forward until the rear wheels pass over the films. Sensors scan rails previously undeformed by the locomotive, while photographic films record radiation. Films are removed and the locomotive returns. New films are located just like before. Note that various embodiments may use digital imaging techniques to avoid the use of film and improve practicality. Generally, photographic sensors may be used in place of films and data may be obtained digitally.

[0277] Experiment No 8. 2. The locomotive passes over the films and stops. Films are replaced by sensors on the rails, the number and place of which is determined by the experimenter.

[0278] Such an arrangement of sensors and photographic films allows obtaining maximum information about the sources of radiation of energy for comparing the results of research obtained by photographic and sensory methods during the initial study.

[0279] Of particular interest are both energy-emitting and dark areas similar to those recorded in photos: FIG. 12 frames 8-11; FIG. 14 frames g, h, I; FIG. 15 frames a, j, k.

[0280] FIG. 11 shows that the energy radiated during the deformation of one rail is

transferred to another. Neglect of this energy without special experimental evidence is unacceptable.

[0281] Measuring the intensity of electromagnetic radiation at eight points on the rails allow to reveals sources of energy whose stimulated emission can lead to the formation of dangerous defects, using the fact that the signal intensity at each point of the rail is related to the intensity of radiation at other points where all wheels of the locomotive impact on rails.

[0282] However, FIG. 12-FIG. 15 shows that the total impact of the wheels is accompanied by the formation of a limited number of local luminous and dark areas. The continuous luminous region was formed only on the railway sleeper, as shown in FIG. 11.

[0283] This fact indicates the possibility of estimating the accumulated energy using a number of equations.

[0284] A system of possible equations for experimental studies based on data from eight sensors is proposed:

[0285] 1.1. $U_{\alpha h}=\Psi I_{\alpha v}(x)$, 1.2. $U_{\beta v}=\Psi I_{\beta v}(x)$, 1.3. $U_{\gamma v}=\Psi I_{\gamma v}(x)$, 1.4. $U_{\delta v}=\Psi I_{\delta v}(x)$, 1.5. $U_{\alpha h}=\Psi I_{\alpha h}(x)$,

[0286] 1.6. $U_{\beta h}=\Psi I_{\beta h}(x)$, 1.7. $U_{\gamma h}=\Psi I_{\gamma h}(x)$, 1.8. $U_{\delta h}=\Psi I_{\delta h}(x)$.

[0287] Here $\Psi$ is the coefficient of proportionality.

[0288] The number of equations and combinations of them is increasing to study the changes caused by the repeated effects of the wheels of the locomotive, the cars following it and repeated testing.

[0289] The distance $x_1$-$x_n$, after which the intensity of the pulses emitted at the locomotive location is insufficient for identification by fixed sensors, is used to establish the sensors at point $B$, is used to determine the position of the symmetric point $B$ and the similar arrangement of the sensors.

[0290] The intensity of the signals as the locomotive moves from point $x_n$ to point $B$ increases. The experimental section $A \leftrightarrow B$ is used in the forward and reverse direction the required number of times.

[0291] Thus, the experimenter receives information on the processes of accumulation and radiation of energy throughout the $AB$ section using the non-destructive method for the time

that the locomotive passes from point $A$ to point $B$.

[0292] The differentiation of hazardous and safe areas is of paramount importance.

[0293] Dangerous areas are those in which energy is accumulated. Such a region is detected by an increase in the intensity of spontaneous radiation. However, if the intensity of spontaneous radiation does not increase, this does not mean that accumulation does not occur. Therefore, additional, for example, X-ray, research is needed.

[0294] Experiments performed with the locomotive are complemented by experiments with the train, using sensors not only on the locomotive and rails, but also on the cars, including ultrasonic wagons, flaw detectors on eddy currents.

[0295] Experiment No. 8.3, designed to determine the zone of emergency braking in front of a sudden dangerous defect in the track, is performed only at the experimental railway section.

[0296] Point $x_d$ is located from point $A$ equipped with sensors, at such a distance $Ls$ that the locomotive is equipped with sensors also, moving from point $B$ to point $A$ with speed $v$, can stop at a safe distance from point $A$ during emergency braking.

[0297] Impacts inflicted on rails at point $A$ are recorded by sensors located on the rail and locomotive but with a delay $\Delta t = \frac{L_S}{c}$, where c is the speed of electromagnetic waves. The width of the pulse is due to the lifetime of the metastable atoms and the delayed radiation from fragments that were formed during cracking and destruction.

[0298] Comparison of the functions $U_l = \Psi I_l(x_l)$, which characterizes the energy accumulated as a result of the impact, and $U_l = \Psi I_l(x_l)$, which characterizes the energy recorded by the locomotive, allows you to set the distance at which the locomotive should begin emergency braking so that it is safe.

SELECTION OF SENSORS

[0299] The choice of sensors is determined by three factors: the maximum sensitivity at the frequency of the signal stimulating the emission of metastable atoms, location, shape and size. The frequency of the signal is due to the atomic number of the atom.

[0300] The sensors are located at the points of maximum absorption the stimulated radiation. An analysis of the causes of disasters has shown that the definition of such places is particularly important. The possibility of detecting such places is shown: in the aluminum alloy in FIG. 1, frame b; in cobblestone FIG. 1, frame c; in the rail FIG. 12, frames 8-12,

[0301] Recommendations for searching for particularly dangerous defects in rails are given by the Federal Railroad Administration (FRA) [See: Track Inspector Rail Defect Reference Manual, Juley 2015, Revision 2]. However, MAPED can detect the onset of defects at an early stage. We can assume that the total impact is due to the center of gravity, since signals from different wheels come to sensors with such a small-time interval, during which the sensor cannot resolve it. But all the hypotheses can be confirmed or refuted only by experiment.

FIG. 15 frames a, i, k; in the frame or wheels of the locomotive FIG. 16 frame h.

[0301] Recommendations for searching for particularly dangerous defects in rails are given by the Federal Railroad Administration (FRA) [See: Track Inspector Rail Defect Reference Manual, Juley 2015, Revision 2]. However, MAPED can detect the onset of defects at an early stage. We can assume that the total impact is due to the center of gravity, since signals from different wheels come to sensors with such a small-time interval, during which the sensor cannot resolve it. But all the hypotheses can be confirmed or refuted only by experiment.

[0302] Modern companies in the United States, creating sensors and equipment for them, such as Canon Industrial Sensors and Delphi Precision Imaging, are able to ensure the implementation of the method in all sections of the industry, crop production and medicine.

[0303] Problem No. 8.3. Evaluation of critical energy

[0304] Sensors located on the rail at the point of impact send signals $U_i^n = \Psi I_i^n(N)$, caused by repeated impacts, which are fixed by the sensors. A computer program explores the relationship of energies in successive hits

$$Z_2=\frac{U_i^2}{U_i^1}=\frac{I_i^2(2)}{I_i^1(1)}\ldots, Z_n=\frac{U_i^n}{U_i^{n-1}}=\frac{I_i^n(N)}{I_i^{n-1}(N-1)}, Z_{n+1}=\frac{U_i^{n+1}}{U_i^n}=\frac{I_i^{n+1}(N+1)}{I_i^n(n)} \quad (15),$$

[0305] which characterizes the ratio of the rate of accumulation of energy to the rate of its dissipation.

[0306] Changes in this relationship allows you to set the moment of formation of hidden cracks. The appearance of larger cracks is controlled additionally by ultrasound or eddy currents.

[0307] The critical energy $U_2^c$ is calculated according to the equation

$$U_2^c = \varepsilon_b S a^{-2} \quad (16),$$

where $\varepsilon_b$ is the binding energy of atoms, $S$ is the area of the formed crack, $a$ is the crystal lattice constant.

[0308] Comparison of the functions $U_i = \Psi I_i(x)$, which characterizes the energy accumulated at the impact site, and $U_l = \Psi I_l(x)$, which characterizes the energy recorded by the locomotive, allows you to set the distance at which the locomotive should begin emergency braking, which will be safe.

[0309] It should be noted that the intensity of spontaneous radiation depends on the direction. The total radiation power is estimated using the Ulbricht integration ball, in which the source is a luminescent screen surrounding the deformed body.

[0310] An important condition for the use of MAPED is the identification of luminous and dark areas in order to search for the destruction domain. One of the methods for its detection is the residual radiation of the surface of destruction. The lifetime of such atoms in the optical range is 1.6–0.3 μs. Radiation in the X-ray range is detected with the introduction of the indenter, as was confirmed by the inventor.

[0311] The decision on the practical application of the method is applied on the basis of the established State Standard.

[0312] The main advantage of MAPED compared with other methods is the objectivity of the assessment of the technical condition of structures and devices based on experimental energy measurements. The second advantage is efficiency.

[0313] For example, calculations of the strength of the rail according to GOST of Russia R 51685-2013 are performed on the basis of at least three tests, each of which includes at least

five million cycles with a frequency of 5-50 Hz. Therefore, testing one rail takes from 80 to 800 hours, whereas testing two rails 1/2-mile-long each was completed in 15 minutes.

[0314] The main danger is that the standards of other countries are also based on the use of stress intensity factors, but other equations and even polynomials are proposed. State standards, equations in which are based on a hypothesis, refuted by experiment, should be replaced.

[0315] The equations obtained in the study of rails using MAPED can be applied to all extended objects, such as support beams, ropes, bridges, regardless of their shape and composition.

[0316] Problem number 9. Prediction of the earthquakes and tsunamis

[0317] Earthquakes are the object, the prevention of which remains an unresolved problem, but earlier prediction is particularly important for saving people's lives.

[0318] The table above shows that ten experimental series were performed by the inventor to show that the energy storage mechanism, the emission of which leads to earthquakes, and behind it the tsunami, does not differ from the mechanism of the metal cracking. There were investigated deformation and destruction of solids: flagstone, granite, marble and

cobblestone; deformation of steam, water and ice; deformation under the friction of aluminum on asphalt, the propagation of electromagnetic waves in the ground. 176 photos show that X-rays were observed in all cases.

[0319] Attempts to use electromagnetic radiation to predict earthquakes, including via satellites, have been made repeatedly, [See: TE. Bleier US 6873265B2.] A distinctive feature of the proposed method is due to the use of X-ray radiation. The advantage of the earthquake prediction method proposed in this invention is the use of high penetrating power of X-rays, high sensitivity to all types of deformation, including internal friction and the phenomenon of self-emission transparency.

[0320] Electromagnetic radiation sensors, including those in the X-ray range, are located at any available depth of the seas and oceans, mines, and wells. Electromagnetic signals by wire or without them are transmitted to the station, including through spacecraft.

[0321] Sensors located at three points make it possible to calculate the coordinates of the radiation location of the signals. Sensors located near volcanoes in high tectonic zones make it possible to find a functional connection between small changes in X-ray intensity and earthquakes and predict them with higher accuracy.

[0322] The high penetrating power of X-rays and the high energy of atomic processes in the earthquake source and the Earth's core make it possible to fix these signals using sensors.

[0323] Problem 10. Pathology and aging of plants and living organs

[0324] The solution of these two problems has always been and remains important for humanity. Each discovery in experimental and theoretical physics is used in other natural sciences, but the discovery of galvanic electricity and the law of conservation of energy are made in medicine. X-ray radiation from plants and human organs, demonstrated in 102 photographs, expands the field of practical application of electromagnetic radiation in biology and medicine.

[0325] Discovering of self-emissive transparency in metal and wood indicates the possibility of such a mechanism in the organs of a living organism. This conclusion is based on the identity of atomic reactions, which result in the formation of luminous arcuate regions, shown for example, in 16 photographs with examples of phase transformations of water, human organs and metal deformation. Iron corrosion is accompanied by the formation of $Fe^{2+}$ and $Fe^{3+}$ ions. G. N. Petrakovich expressed the idea [See: Biofield Without Secrets, Moscow, "Public Benefit" 2009, pp. 305 (In Russian)], that transitions of $Fe^{2+} \leftrightarrow Fe^{3+}$ electrons occur at a frequency of 6 attohertz, which is a thousand times higher than the frequency of a femtosecond laser, with the help of which self-induced transparency is observed.

[0326] The problem of energy in mitochondria is one of the most important not only in biology, but also in technology, in order to understand the mechanism of energy concentration and develop similar devices. The efficiency of mitochondria greatly exceeds the efficiency of generators created by man. The study of the energy processes of plants, animal cells and humans by a non-invasive method allows us to understand the mechanism of this phenomenon and create a similar one.

[0327] In the preceding and following description, various techniques are described. For purposes of explanation, specific configurations and details are set forth in order to provide a thorough understanding of possible ways of implementing the techniques. However, it will also be apparent that the techniques described below may be practiced in different configurations without the specific details. Furthermore, well-known features may be omitted or simplified to avoid obscuring the techniques being described.

[0328] Note that, in the context of describing disclosed embodiments, unless otherwise specified, use of expressions regarding executable instructions (also referred to as code, applications, agents, etc.) performing operations that "instructions" do not ordinarily perform unaided (e.g., transmission of data, calculations, etc.) denote that the instructions are being executed by a machine, thereby causing the machine to perform the specified operations.

[0329] FIG. 26 is an illustrative, simplified block diagram of a computing device 2600 that can be used to practice at least one embodiment of the present disclosure. In various embodiments, the computing device 2600 may be used to implement any of the systems illustrated and described above. For example, the computing device 2600 may be configured for use as a data server, a web server, a portable computing device, a personal computer, or any electronic computing device. As shown in FIG. 26, the computing device 2600 may include one or more processors 2602 that, in embodiments, communicate with and are operatively coupled to a number of peripheral subsystems via a bus subsystem. In some embodiments, these peripheral subsystems include a storage subsystem 2606, comprising a memory subsystem 2608 and a file/disk storage subsystem 2610, one or more user interface input devices 2612, one or more user interface output devices 2614, and a network interface subsystem 2616. Such storage subsystem 2606 may be used for temporary or long-term storage of information.

[0330] In some embodiments, the bus subsystem 2604 may provide a mechanism for enabling the various components and subsystems of computing device 2600 to communicate with each other as intended. Although the bus subsystem 2604 is shown schematically as a single bus, alternative embodiments of the bus subsystem utilize multiple buses. The network interface subsystem 2616 may provide an interface to other computing devices and networks. The network interface subsystem 2616 may serve as an interface for receiving data from and transmitting data to other systems from the computing device 2600, such as sensor data, control signals (e.g., to apply brakes to a locomotive), transmitting information (e.g., message indicating warnings about structural failure, and other examples). In some embodiments, the bus subsystem 2604 is utilized for communicating data locally and/or over a network.

[0331] In some embodiments, the user interface input devices 2612 includes one or more user input devices such as a keyboard; pointing devices such as an integrated mouse, trackball, touchpad, or graphics tablet; a scanner; a barcode scanner; a touch screen incorporated into the display; audio input devices such as voice recognition systems, microphones; and other types of input devices. In general, use of the term "input device" is intended to include all possible types of devices and mechanisms for inputting information to the computing device 2600. In some embodiments, the one or more user interface output devices 2614 include a display subsystem, a printer, or non-visual displays such as audio output devices, etc. In some embodiments, the display subsystem includes a cathode ray tube

(CRT), a flat-panel device such as a liquid crystal display (LCD), light emitting diode (LED) display, or a projection or other display device. In general, use of the term "output device" is intended to include all possible types of devices and mechanisms for outputting information from the computing device 2600. The one or more user interface output devices 2614 can be used, for example, to present user interfaces to facilitate user interaction with applications performing processes described and variations therein, when such interaction may be appropriate. For example, a display interface may provide a graphical representation of a warning to an operator, a technician, or other employee to indicate results of measurements taken in accordance with embodiments described herein and conclusions derived therefrom.

[0332] In some embodiments, the storage subsystem 2606 provides a computer-readable storage medium for storing the basic programming and data constructs that provide the functionality of at least one embodiment of the present disclosure. The applications (programs, code modules, instructions), when executed by one or more processors in some embodiments, provide the functionality of one or more embodiments of the present disclosure and, in embodiments, are stored in the storage subsystem 2606. These application modules or instructions can be executed by the one or more processors 2602. In various embodiments, the storage subsystem 2606 additionally provides a repository for storing data used in accordance with the present disclosure. In some embodiments, the storage subsystem 2606 comprises a memory subsystem 2608 and a file/disk storage subsystem 2610.

[0333] In embodiments, the memory subsystem 2608 includes a number of memories, such as a main random access memory (RAM) 2618 for storage of instructions and data during program execution and/or a read only memory (ROM) 2620, in which fixed instructions can be stored. In some embodiments, the file/disk storage subsystem 2610 provides a non-transitory persistent (non-volatile) storage for program and data files and can include a hard disk drive, a floppy disk drive along with associated removable media, a Compact Disk Read Only Memory (CD-ROM) drive, an optical drive, removable media cartridges, or other like storage media. Memories of the system 2600 may be non-transitory and store instructions that are executable by one or more processors to cause the system to perform operations herein, such as applying logic to sensor data to infer conclusions to cause further operations (e.g., providing messages indicative of such conclusions, updating a graphical user interface, transmitting control signals to cause operation of another system (e.g., a brake subsystem, a

warning alarm, and/or other such system). The logic can be in various forms, such as a rules engine, a decision tree, a neural network or other machine learning model, and/or other such computer-executable applications of logic to data.

[0334] In some embodiments, the computing device 2600 includes at least one local clock 2624. The at least one local clock 2624, in some embodiments, is a counter that represents the number of ticks that have transpired from a particular starting date and, in some embodiments, is located integrally within the computing device 2600. In various embodiments, the at least one local clock 2624 is used to synchronize data transfers in the processors for the computing device 2600 and the subsystems included therein at specific clock pulses and can be used to coordinate synchronous operations between the computing device 2600 and other systems in which the computing device is used. In another embodiment, the local clock is a programmable interval timer.

[0335] The computing device 2600 could be of any of a variety of types, including a portable computer device, tablet computer, a workstation, or any other device described below. Additionally, the computing device 2600 can include another device that, in some embodiments, can be connected to the computing device 2600 through one or more ports (e.g., USB, a headphone jack, Lightning connector, etc.). In embodiments, such a device includes a port that accepts a fiber-optic connector. Accordingly, in some embodiments, this device is that converts optical signals to electrical signals that are transmitted through the port connecting the device to the computing device 2600 for processing. Due to the ever-changing nature of computers and networks, the description of the computing device 2600 depicted in FIG. 26 is intended only as a specific example for purposes of illustrating the preferred embodiment of the device. Many other configurations having more or fewer components than the system depicted in FIG. 26 are possible.

[0336] The specification and drawings are, accordingly, to be regarded in an illustrative rather than a restrictive sense. However, it will be evident that various modifications and changes may be made thereunto without departing from the scope of the invention as set forth in the claims. Likewise, other variations are within the scope of the present disclosure. Thus, while the disclosed techniques are susceptible to various modifications and alternative constructions, certain illustrated embodiments thereof are shown in the drawings and have

been described above in detail. It should be understood, however, that there is no intention to limit the invention to the specific form or forms disclosed but, on the contrary, the intention is to cover all modifications, alternative constructions and equivalents falling within the scope of the invention, as defined in the appended claims.

[0337] The use of the terms "a" and "an" and "the" and similar referents in the context of describing the disclosed embodiments (especially in the context of the following claims) is to be construed to cover both the singular and the plural, unless otherwise indicated or clearly contradicted by context. The terms "comprising," "having," "including" and "containing" are to be construed as open-ended terms (i.e., meaning "including, but not limited to,") unless otherwise noted. The term "connected," when unmodified and referring to physical connections, is to be construed as partly or wholly contained within, attached to or joined together, even if there is something intervening. Recitation of ranges of values in the present disclosure are merely intended to serve as a shorthand method of referring individually to each separate value falling within the range unless otherwise indicated and each separate value is incorporated into the specification as if it were individually recited. The use of the term "set" (e.g., "a set of items") or "subset" unless otherwise noted or contradicted by context, is to be construed as a nonempty collection comprising one or more members. Further, unless otherwise noted or contradicted by context, the term "subset" of a corresponding set does not necessarily denote a proper subset of the corresponding set, but the subset and the corresponding set may be equal. The use of the phrase "based on," unless otherwise explicitly stated or clear from context, means "based at least in part on" and is not limited to "based solely on."

[0338] Conjunctive language, such as phrases of the form "at least one of A, B, and C," or "at least one of A, B and C," unless specifically stated otherwise or otherwise clearly contradicted by context, is otherwise understood with the context as used in general to present that an item, term, etc., could be either A or B or C, or any nonempty subset of the set of A and B and C. For instance, in the illustrative example of a set having three members, the conjunctive phrases "at least one of A, B, and C" and "at least one of A, B, and C" refer to any of the following sets: {A}, {B}, {C}, {A, B}, {A, C}, {B, C}, {A, B, C}. Thus, such conjunctive language is not generally intended to imply that certain embodiments require at least one of A, at least one of B and at least one of C each to be present.

[0339] Operations of processes described can be performed in any suitable order unless otherwise indicated or otherwise clearly contradicted by context. Processes described (or variations and/or combinations thereof) can be performed under the control of one or more computer systems configured with executable instructions and can be implemented as code (e.g., executable instructions, one or more computer programs or one or more applications) executing collectively on one or more processors, by hardware or combinations thereof. In some embodiments, the code can be stored on a computer-readable storage medium, for example, in the form of a computer program comprising a plurality of instructions executable by one or more processors. In some embodiments, the computer-readable storage medium is non-transitory.

[0340] The use of any and all examples, or exemplary language (e.g., "such as") provided, is intended merely to better illuminate embodiments of the invention and does not pose a limitation on the scope of the invention unless otherwise claimed. No language in the specification should be construed as indicating any non-claimed element as essential to the practice of the invention.

[0341] Embodiments of this disclosure are described, including the best mode known to the inventors for carrying out the invention. Variations of those embodiments will become apparent to those of ordinary skill in the art upon reading the foregoing description. The inventors expect skilled artisans to employ such variations as appropriate and the inventors intend for embodiments of the present disclosure to be practiced otherwise than as specifically described. Accordingly, the scope of the present disclosure includes all modifications and equivalents of the subject matter recited in the claims appended hereto as permitted by applicable law. Moreover, any combination of the above-described elements in all possible variations thereof is encompassed by the scope of the present disclosure unless otherwise indicated or otherwise clearly contradicted by context.

[0342] All references, including publications, patent applications, and patents, cited are hereby incorporated by reference to the same extent as if each reference were individually and specifically indicated to be incorporated by reference and were set forth in its entirety.

## CLAIMS

WHAT IS CLAIMED IS:

1. A method, comprising:

using a sensor to measure intensity of electromagnetic signals emitted from a structure;

calculating energy stored in a portion of the structure based on the measured intensity;

performing a comparison of the energy stored with a critical value for the structure; and

indicating potential failure of the structure based on the performed comparison.

2. The computer-implemented method of claim 1, wherein the electromagnetic signals are x-rays.

3. The computer-implemented method of claim 1, wherein the sensor is mounted to vehicle that traversing the structure.

4. The computer-implemented method of claim 4, wherein the vehicle is a locomotive or rail car.

5. The computer-implemented method of claim 1, wherein the sensor is mounted to the structure.

6. The system of claim 5, wherein the structure is a component of an aircraft.

7. The system of claim 6, wherein the sensor is secured to the sensor of the aircraft by a decal of the aircraft.

8. A system, comprising:

one or more processors; and

memory including executable instructions that, if executed by the one or more processors, cause the system to:

use a sensor to measure intensity of electromagnetic signals emitted from a structure;

calculate energy stored in a portion of the structure based on the measured intensity;

perform a comparison of the energy stored with a critical value for the structure; and

indicate potential failure of the structure based on the performed comparison.

9. The system of claim 8, wherein the executable instructions that cause the system to indicate potential failure cause the system to update a user interface.

10. The system of claim 8, wherein the executable instructions that cause the system to indicate potential failure cause the system to transmit a message that causes a device to brake.

11. The system of claim 10, wherein the device is a vehicle.

12. The system of claim 8, wherein the system comprises a vehicle onto which the sensor is mounted.

13. The system of claim 8, wherein the system comprises a vehicle having a frame onto which the sensor is mounted to monitor the structure during operation of the vehicle.

14. A non-transitory computer-readable storage medium having stored thereon executable instructions that, if executed by one or more processors of a computer system, cause the computer system to at least:

use a sensor to measure intensity of electromagnetic signals emitted from a structure;

calculate energy stored in a portion of the structure based on the measured intensity;

perform a comparison of the energy stored with a critical value for the structure; and

indicate potential failure of the structure based on the performed comparison.

18. The non-transitory computer-readable storage medium of claim 15, wherein the instructions cause the system to indicate potential failure by transmitting a signal that causes a vehicle to change operation.

19. The non-transitory computer-readable storage medium of claim 18, wherein the signal that causes the vehicle to change operation causes the vehicle to brake.

20. The non-transitory computer-readable storage medium of claim 13, wherein the executable instructions that cause the computer system to indicate the potential failure cause the system to update a user interface to present information indicative of potential failure.

**ATTACHMENT No. 3**
**COLOR PHOTOS OF THE APPLICATION FOR A PATENT**

The black and white photographs given in the patent application do not allow us to show features due to the energy (frequency) of the photons involved in the atomic reaction. In connection with the book, black and white photographs are replaced by color ones.



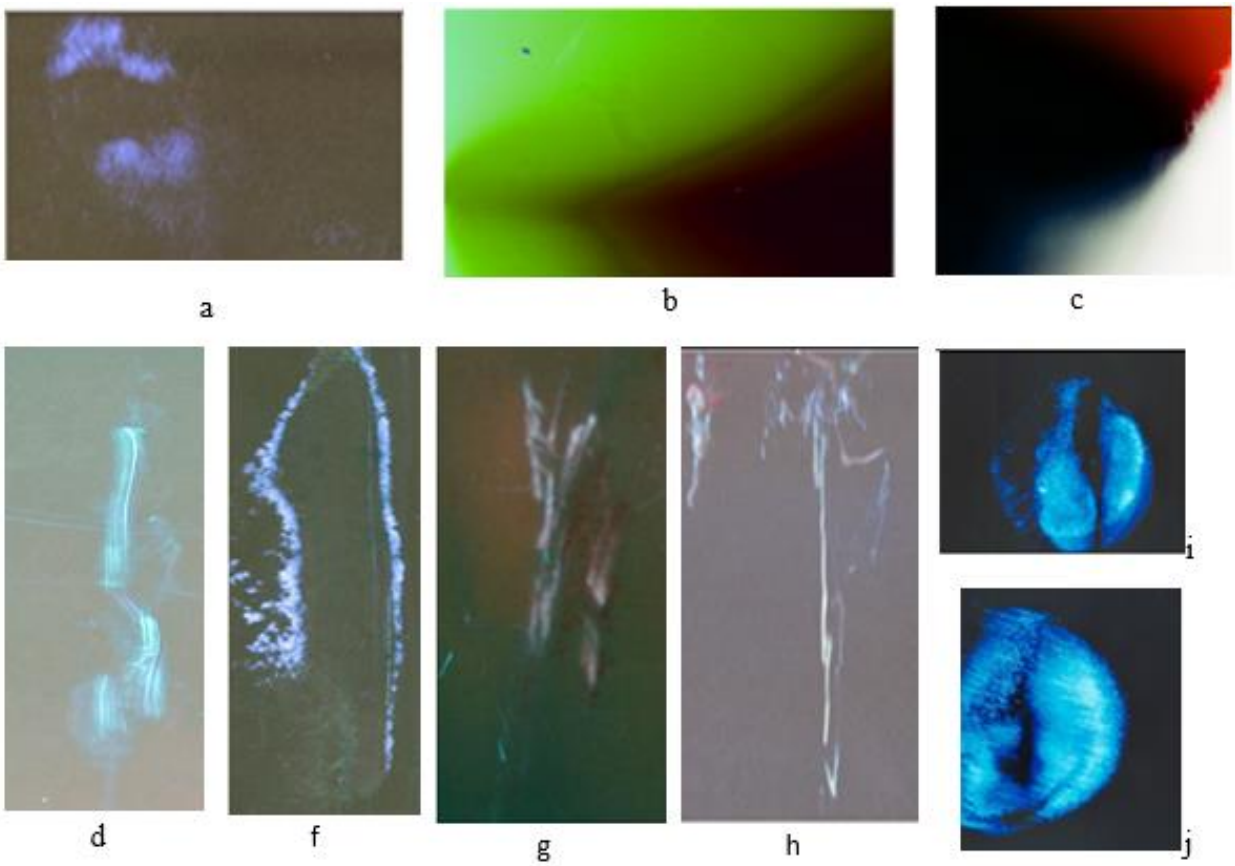


FIG. 1

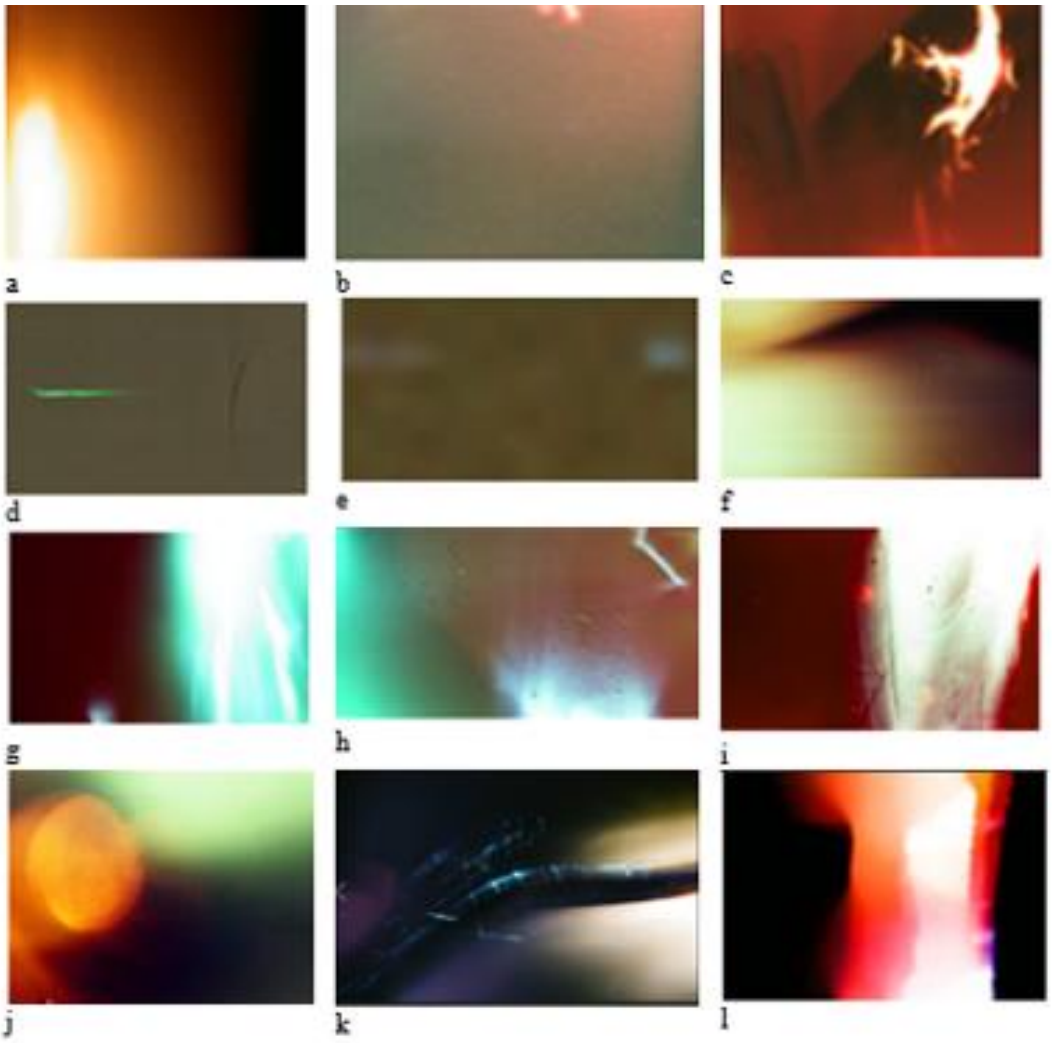


FIG. 2

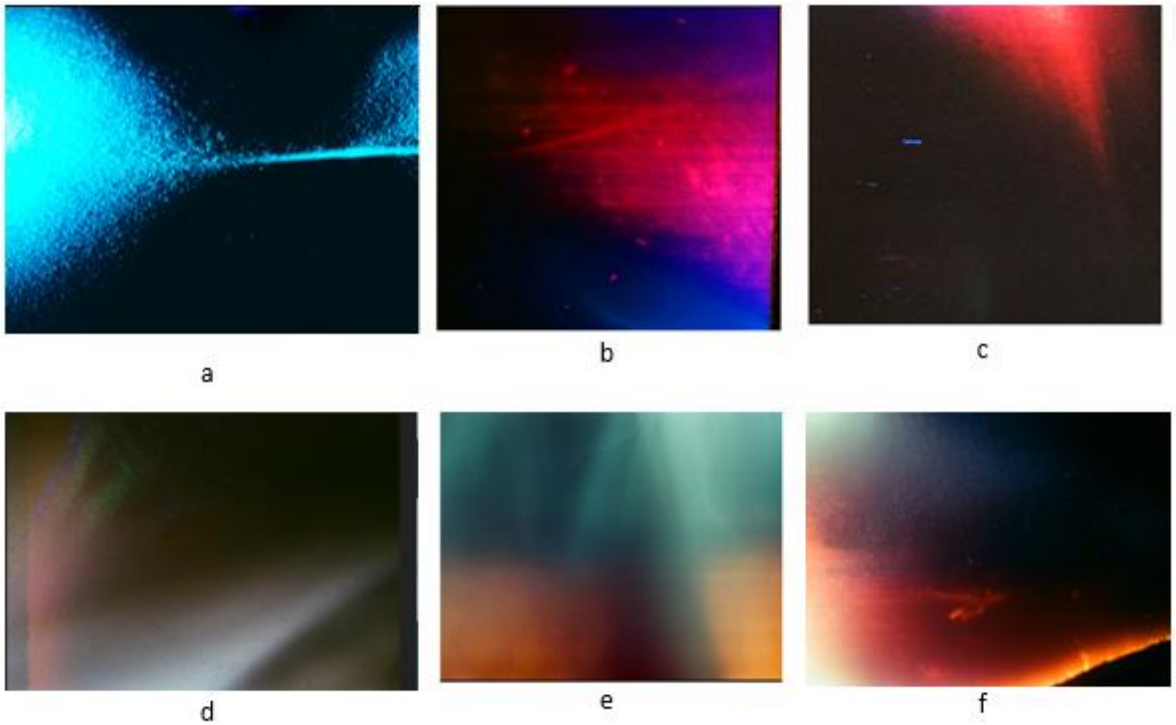


FIG. 3

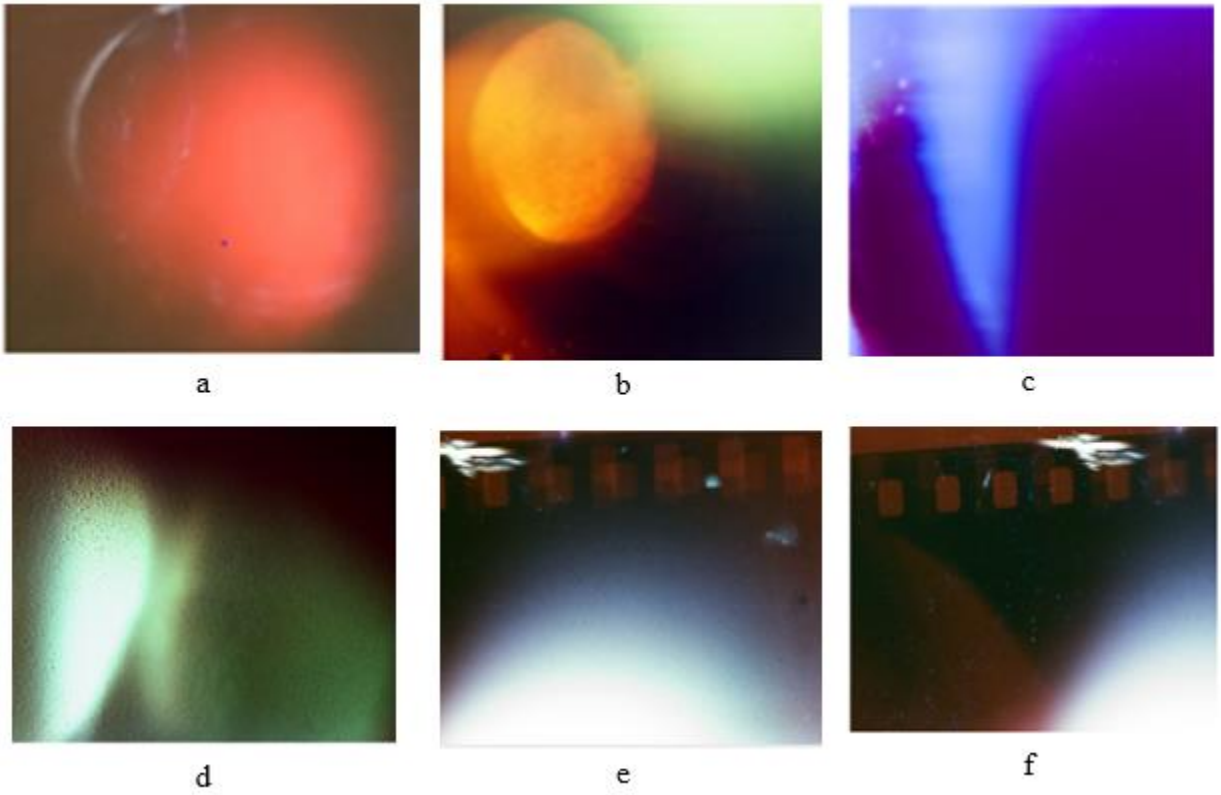


FIG. 4

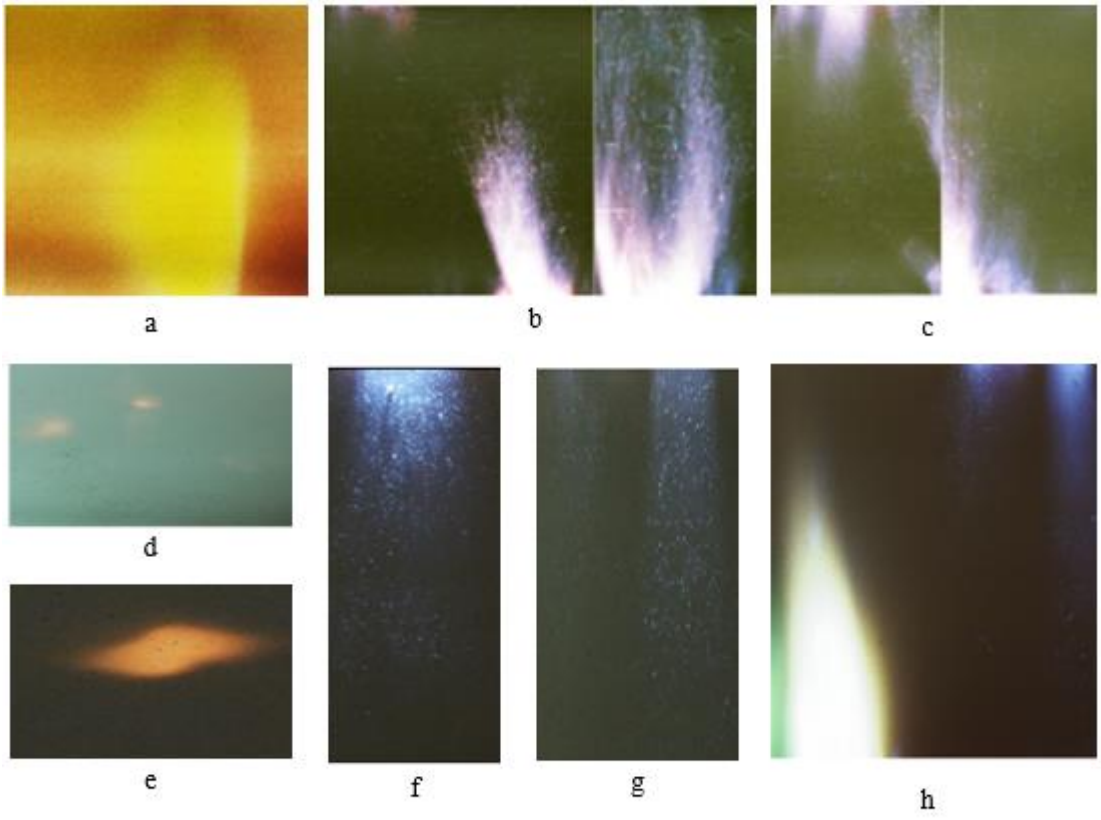


FIG. 5

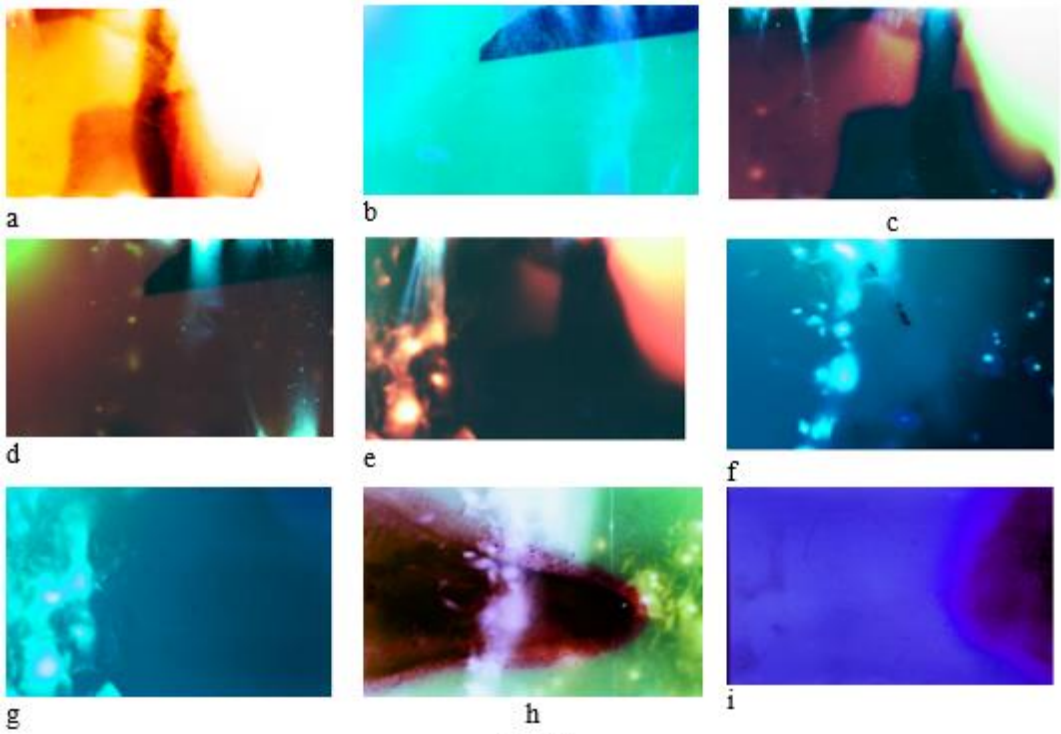


FIG. 6

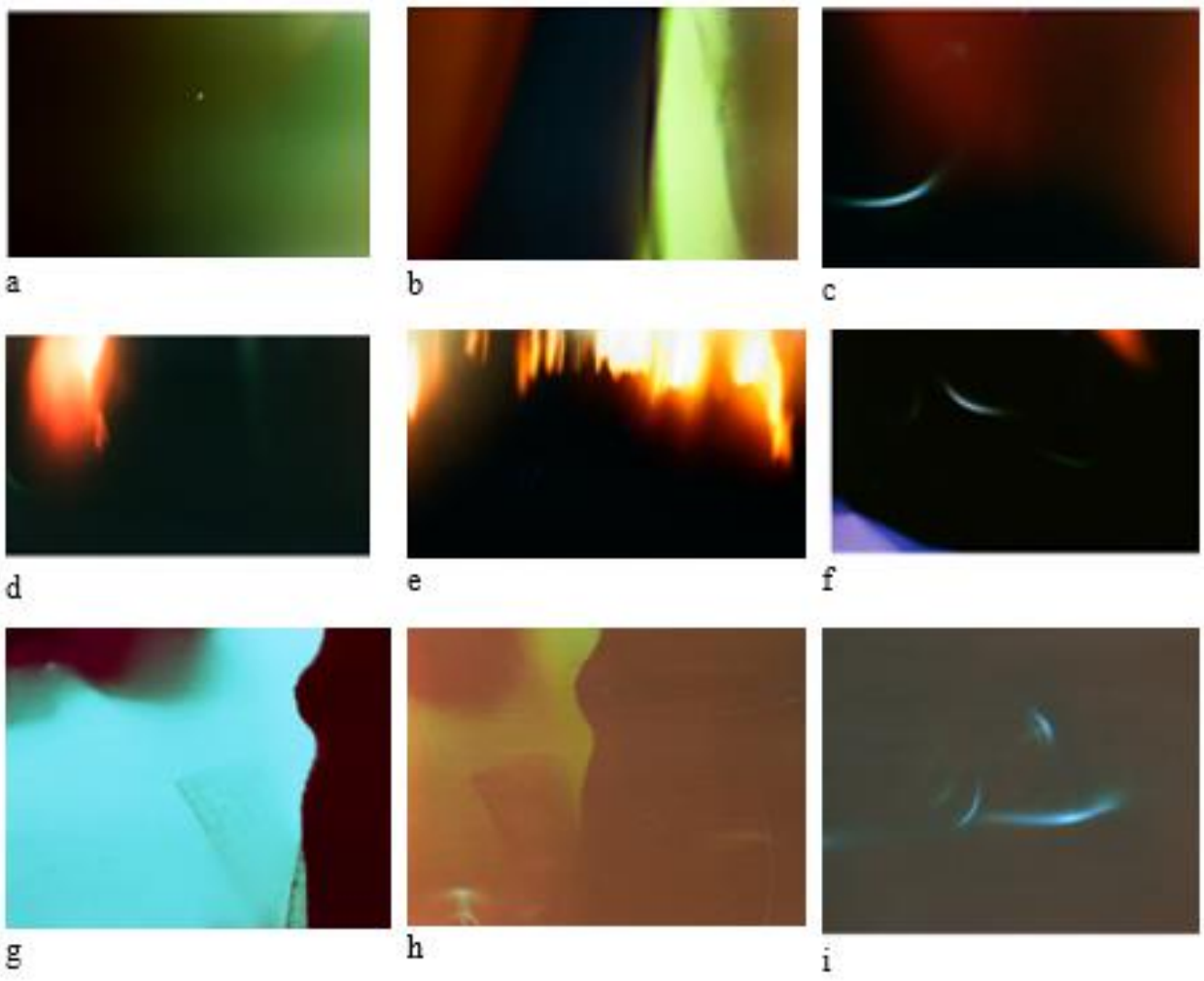


FIG.7

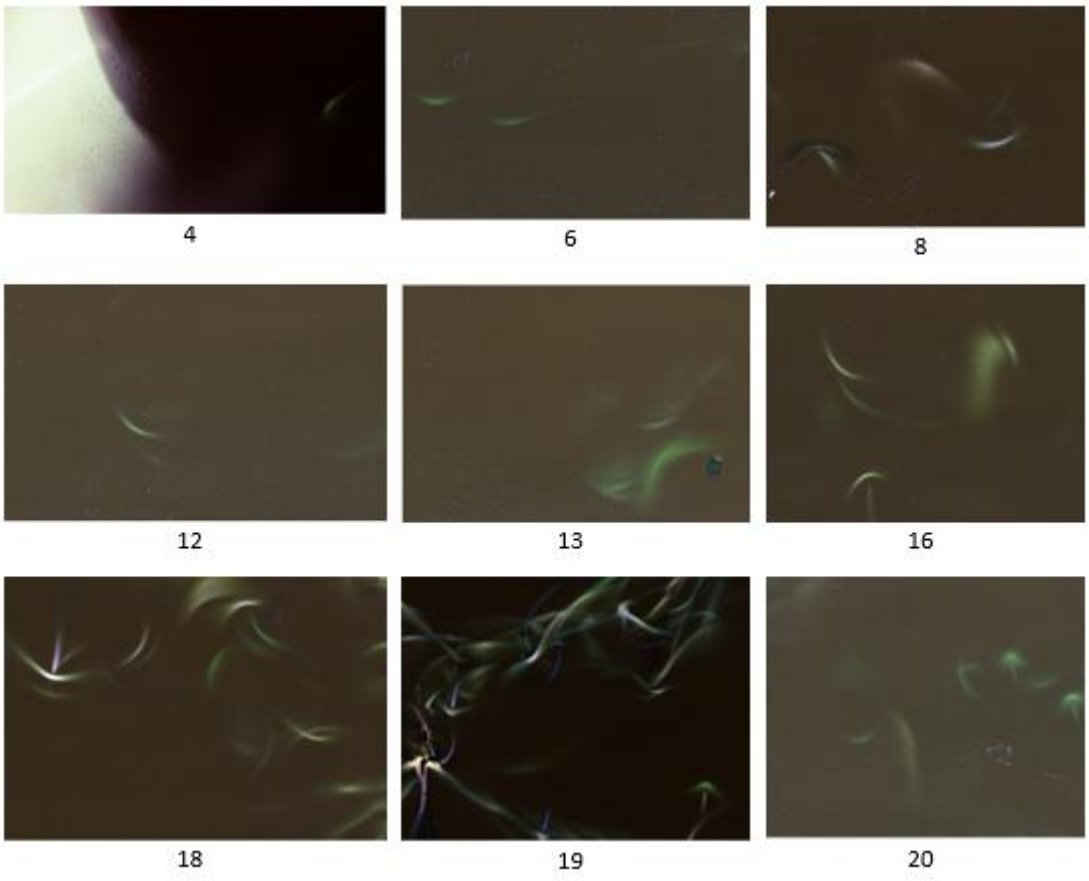


FIG. 8

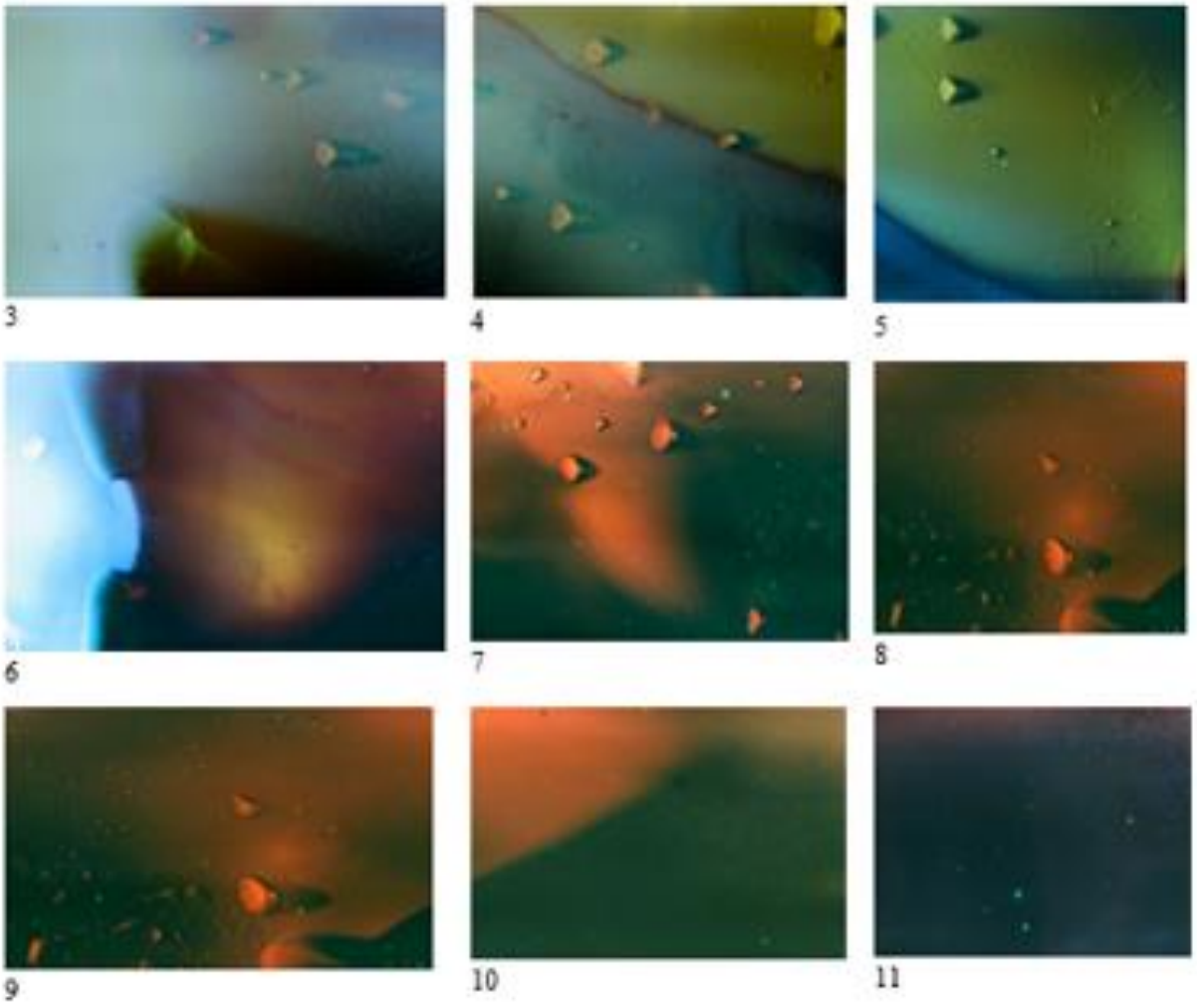


**Fig. 9**

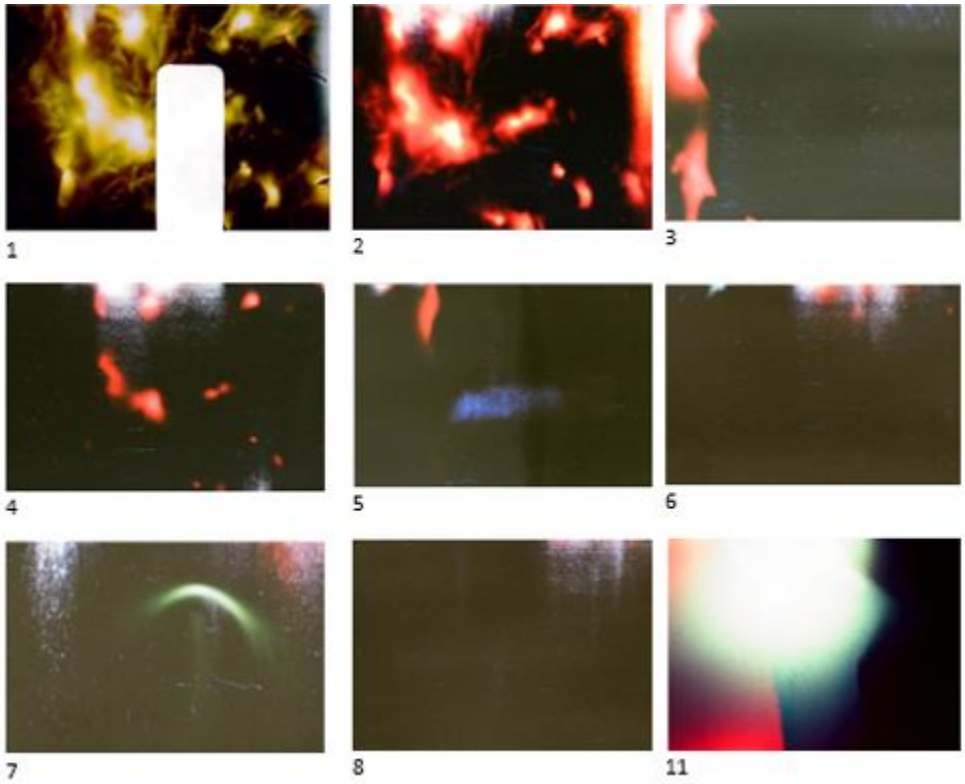


**Fig 10**

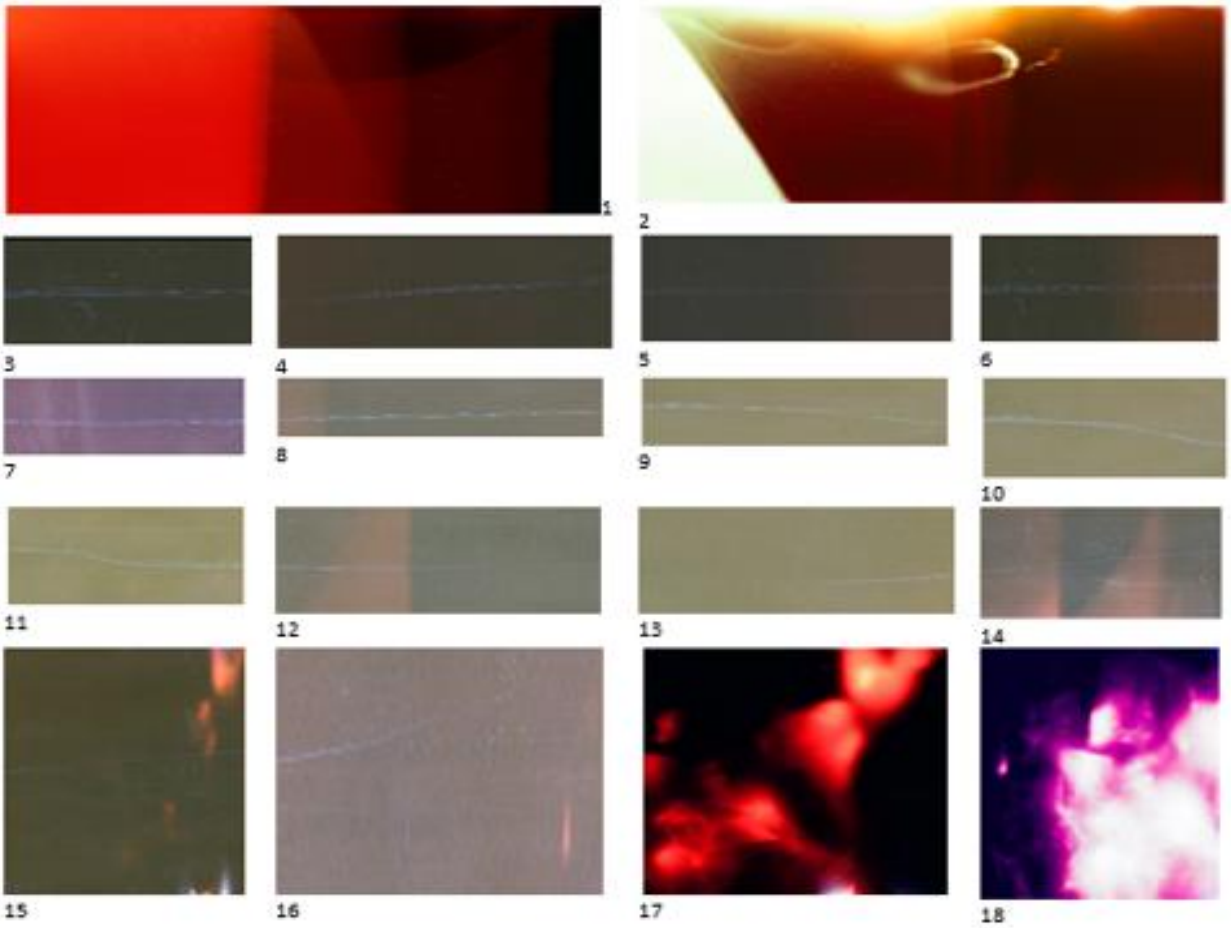


FIG. 11

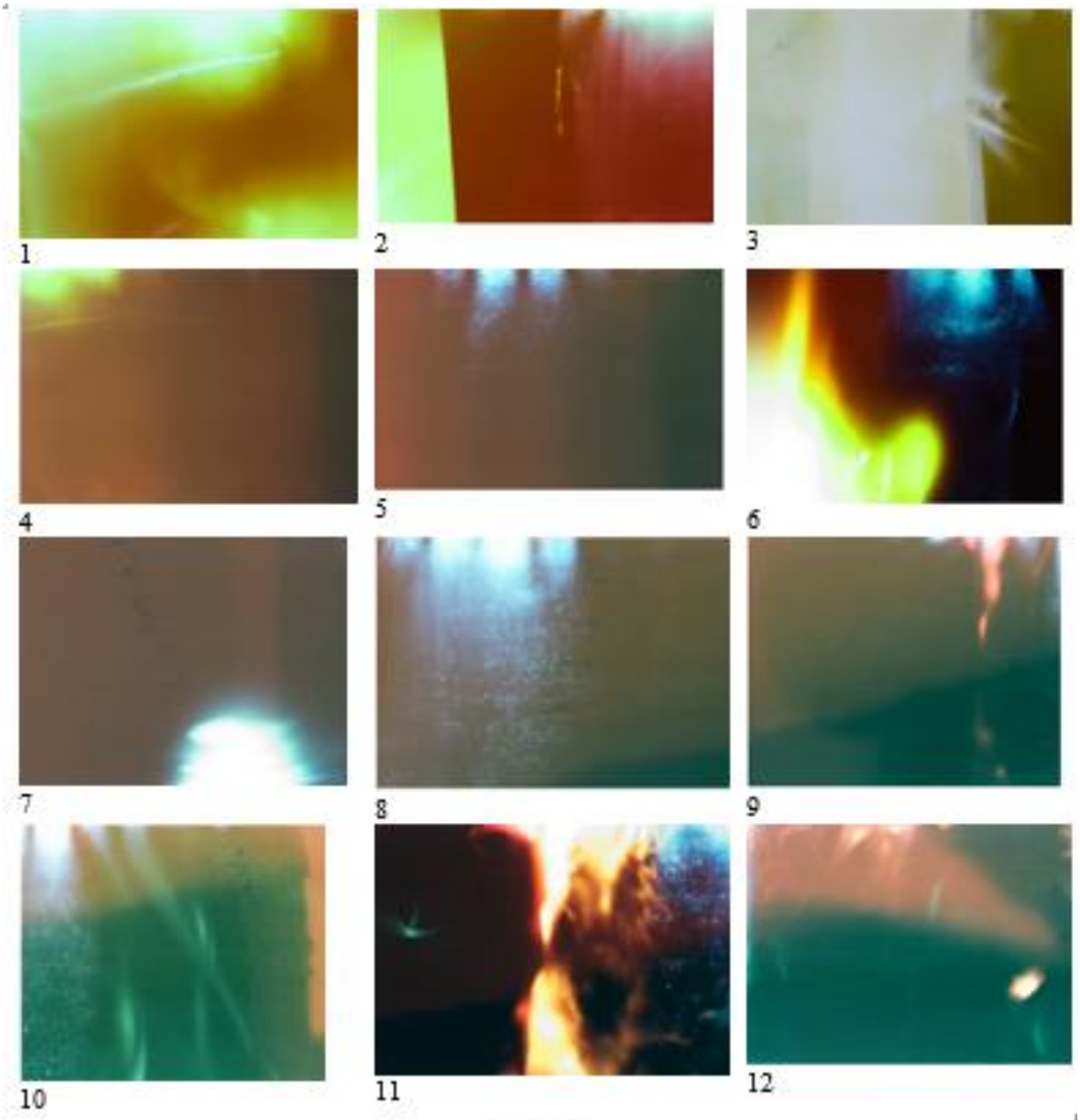


Fig. 12

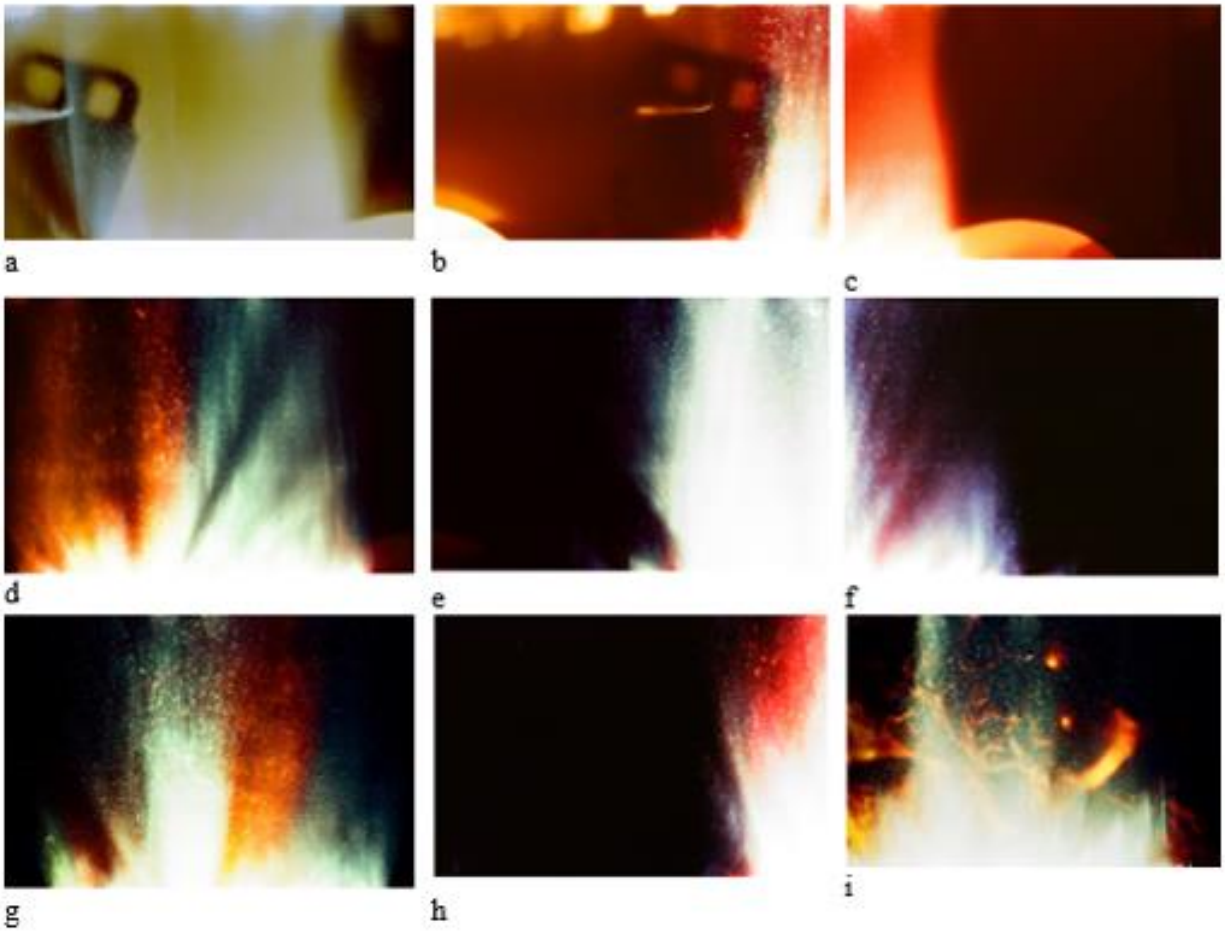


FIG. 13

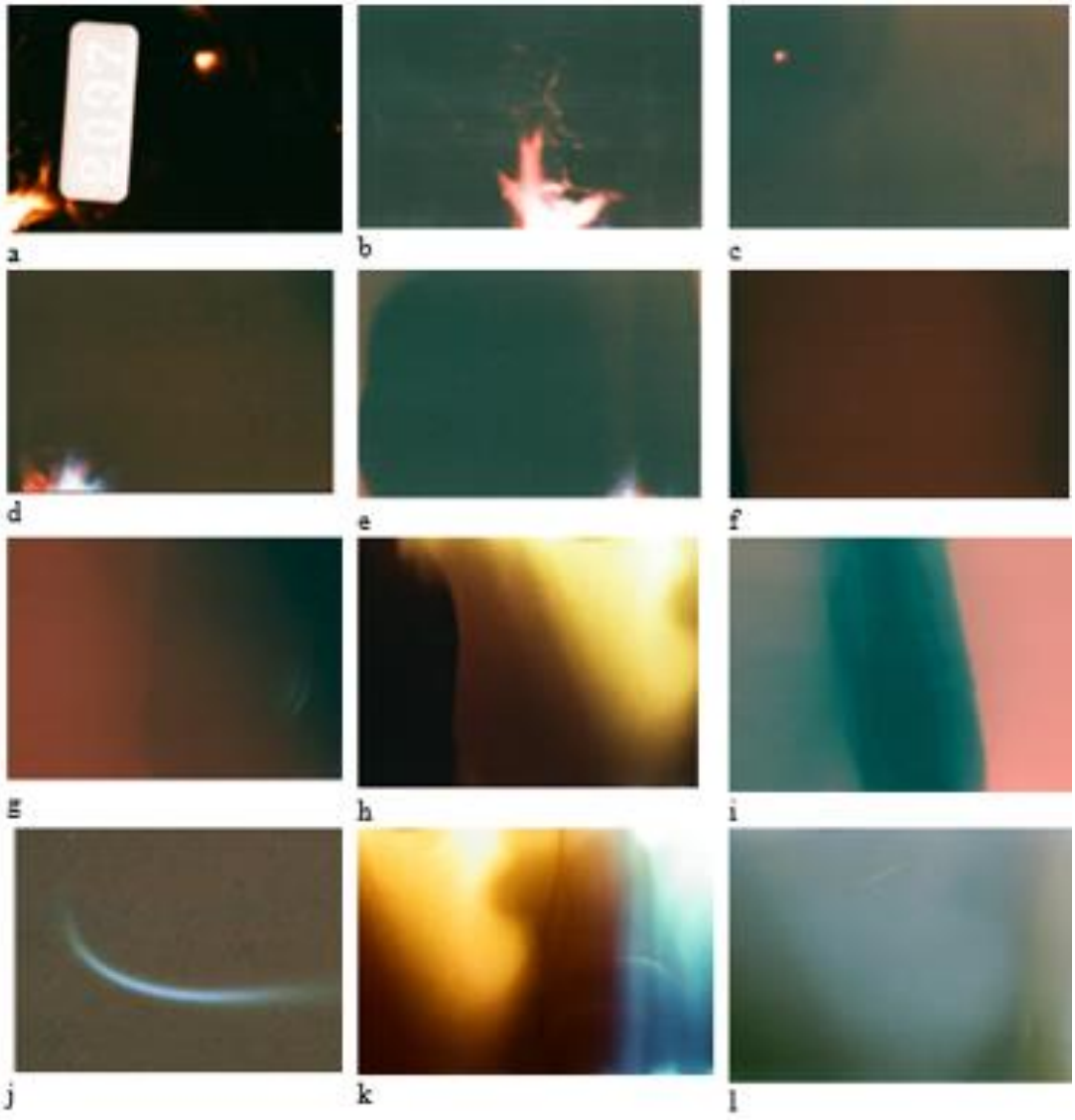


FIG. 14

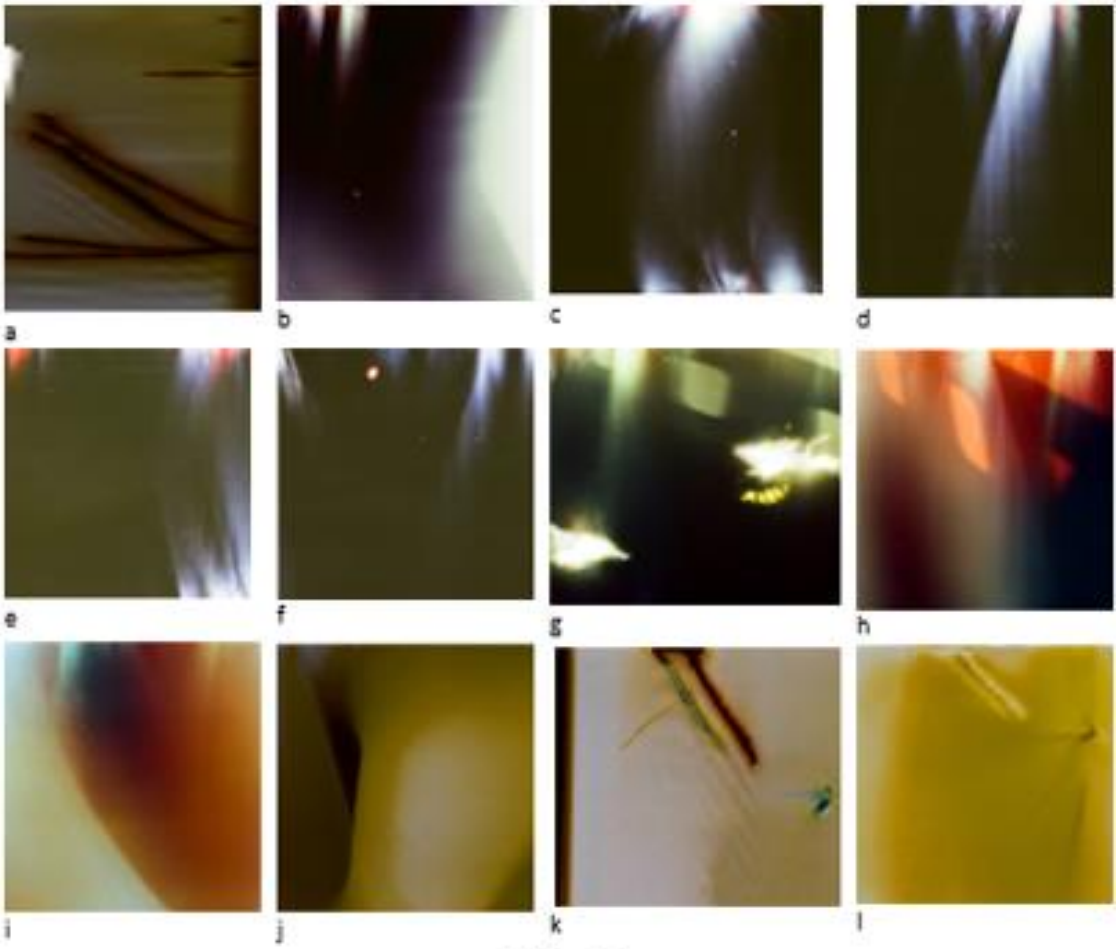


FIG. 15

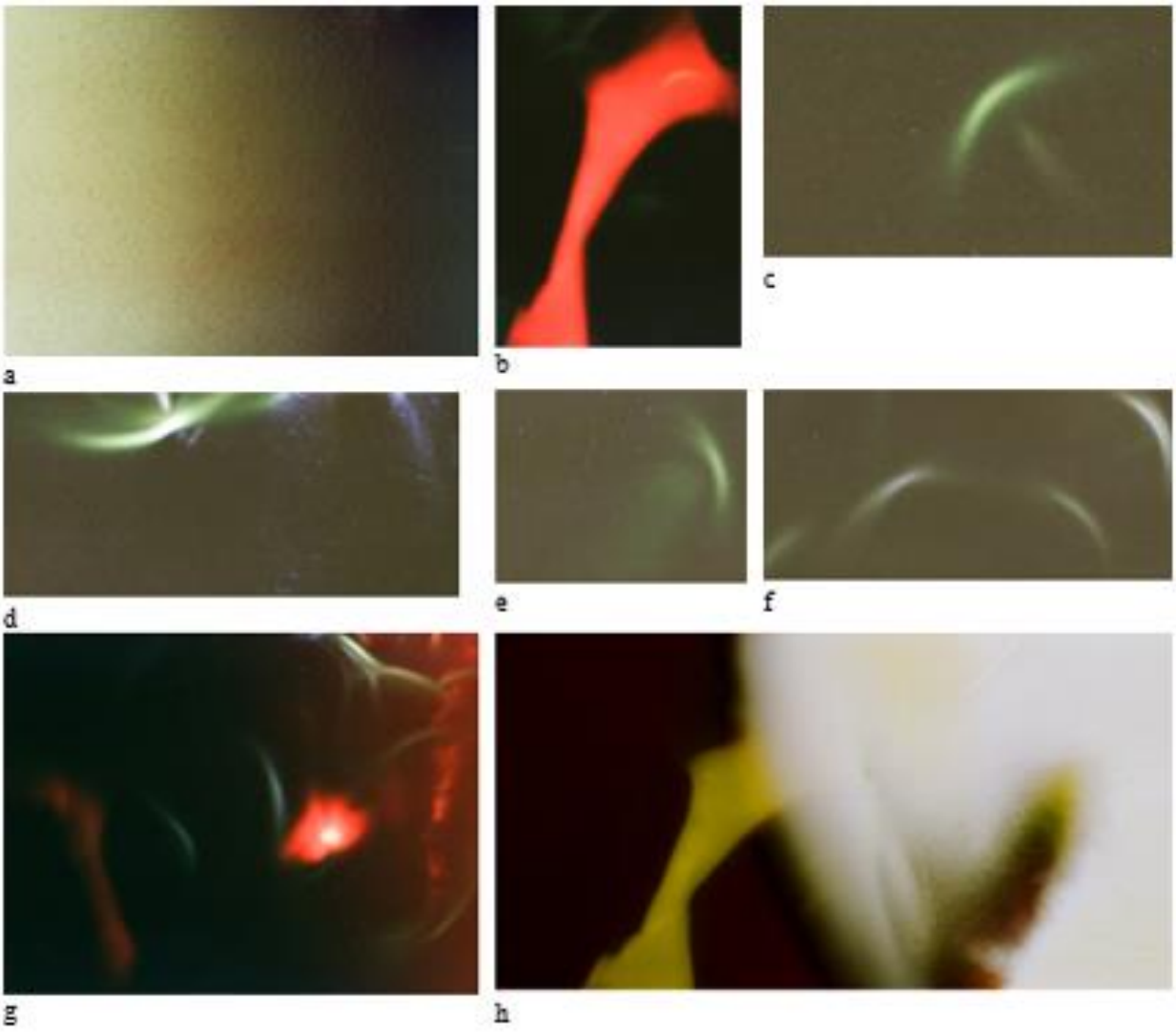


FIG. 16

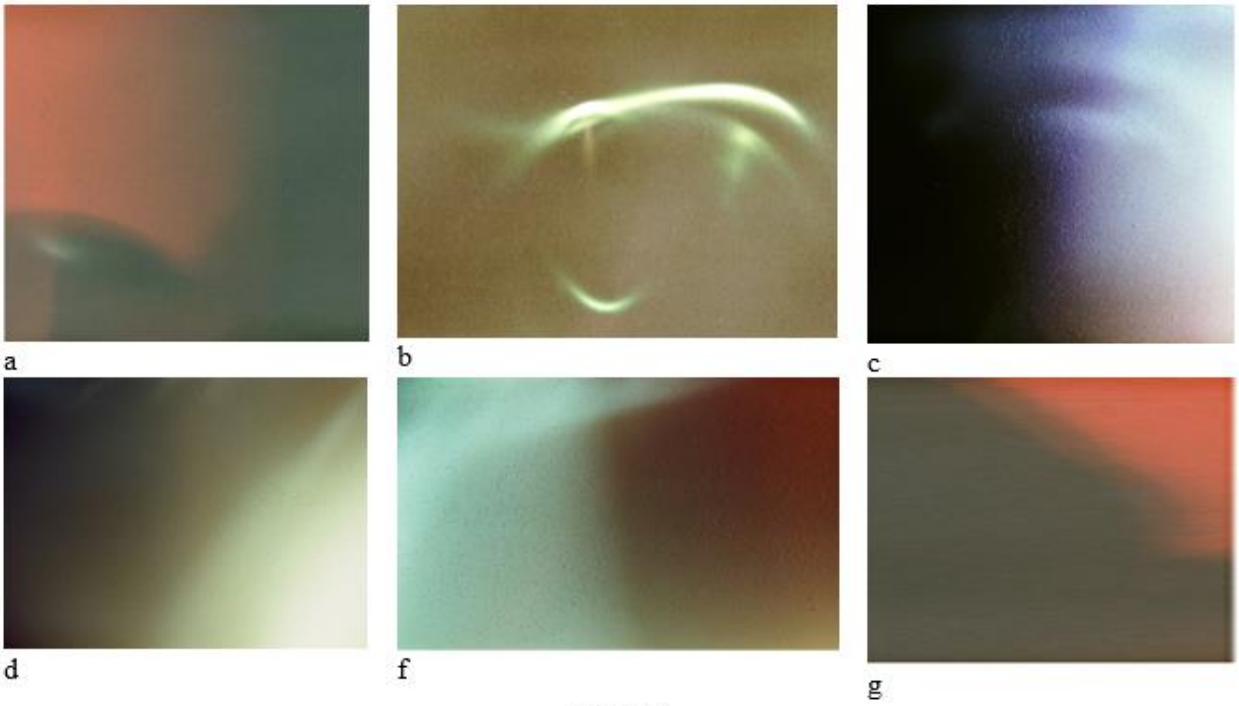


FIG. 17

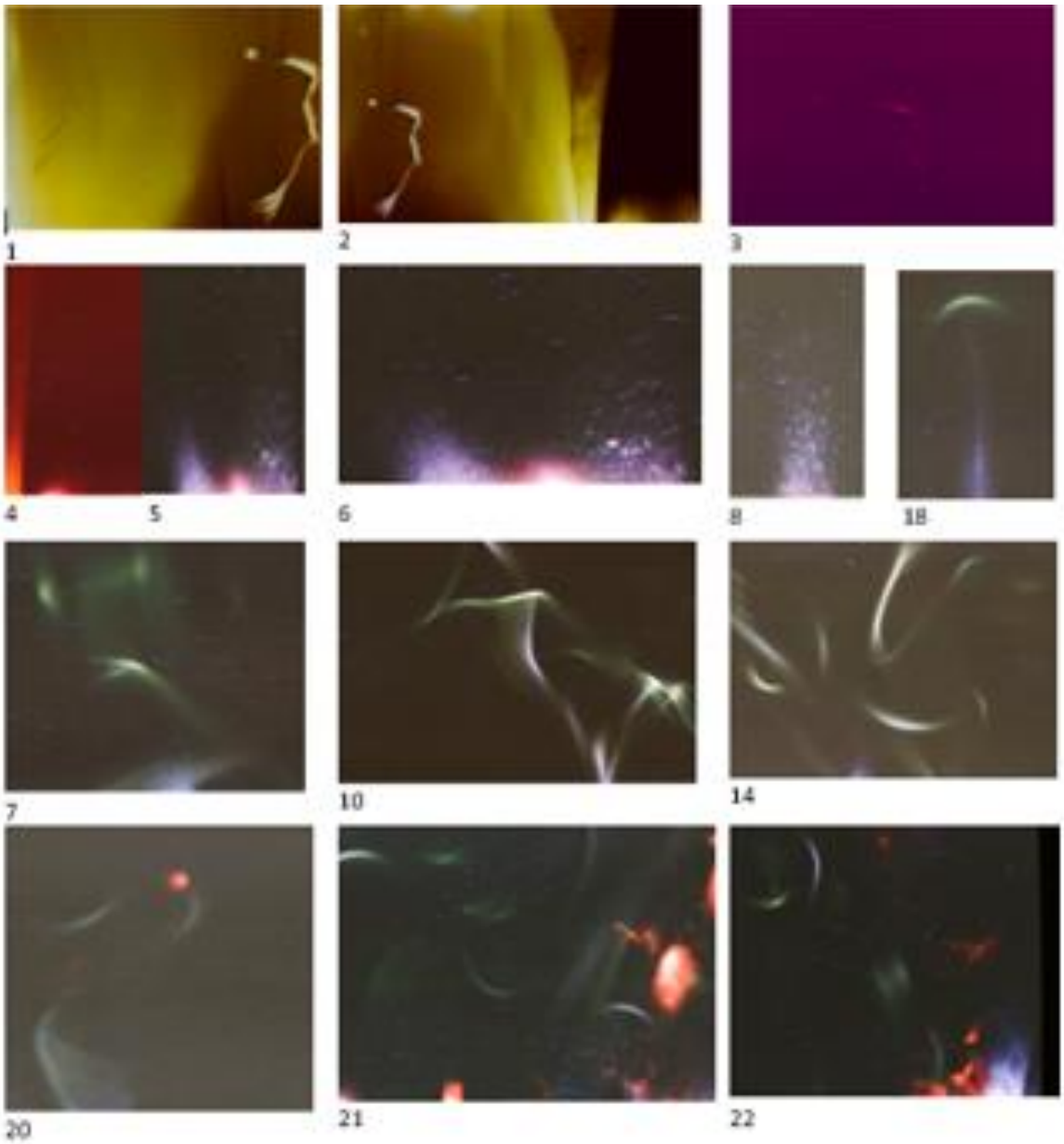


FIG. 18

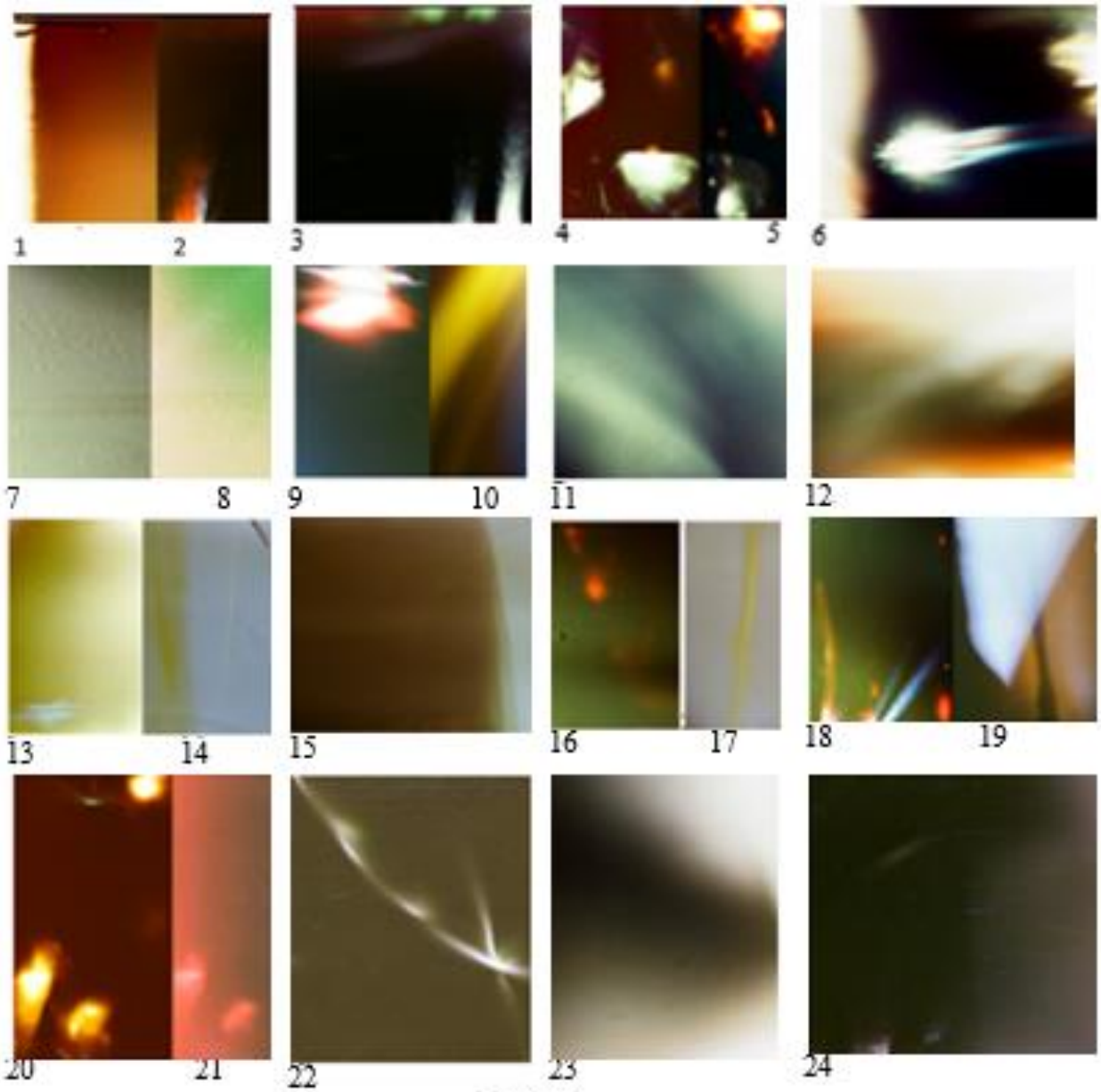


FIG.19

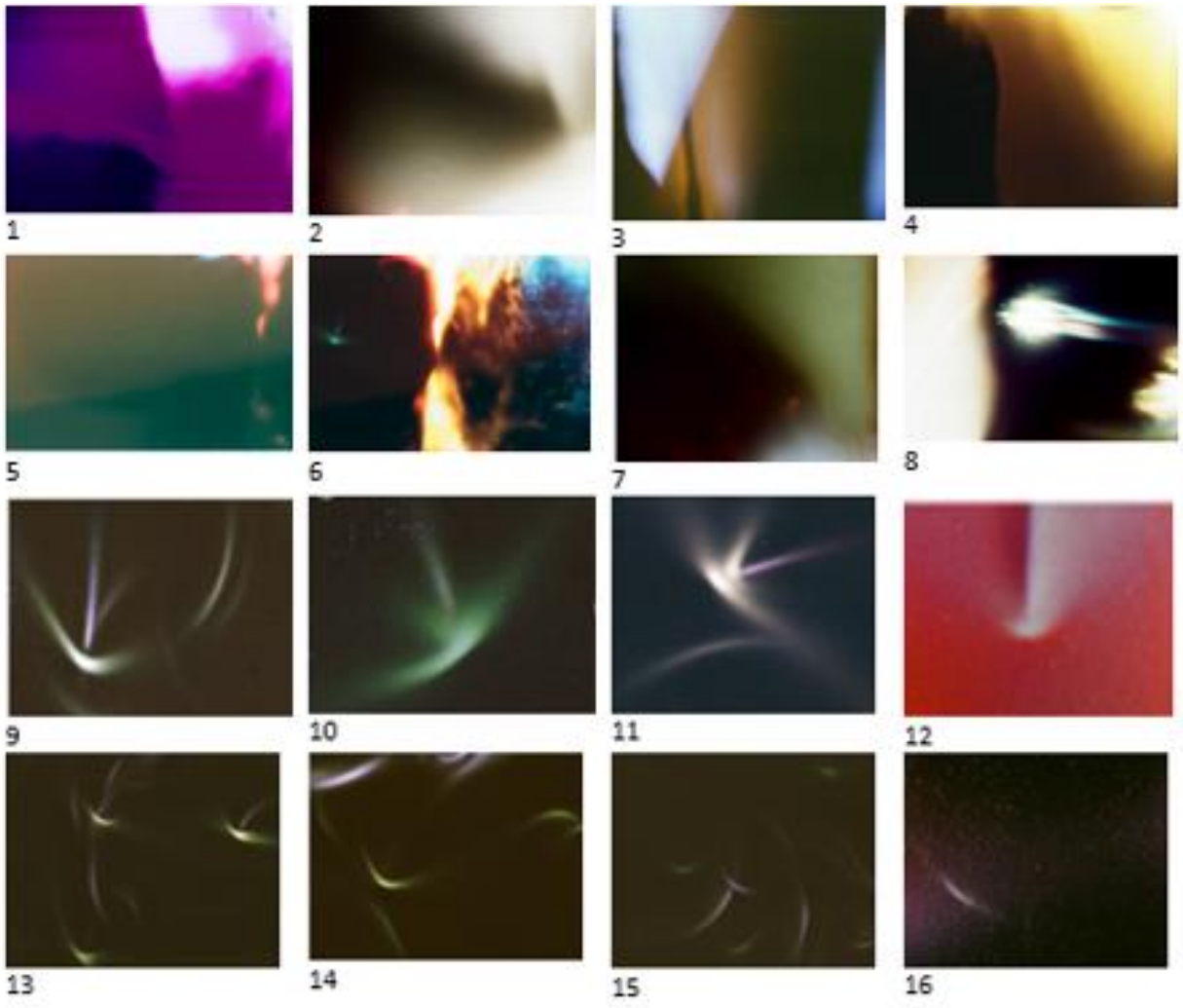


FIG. 20

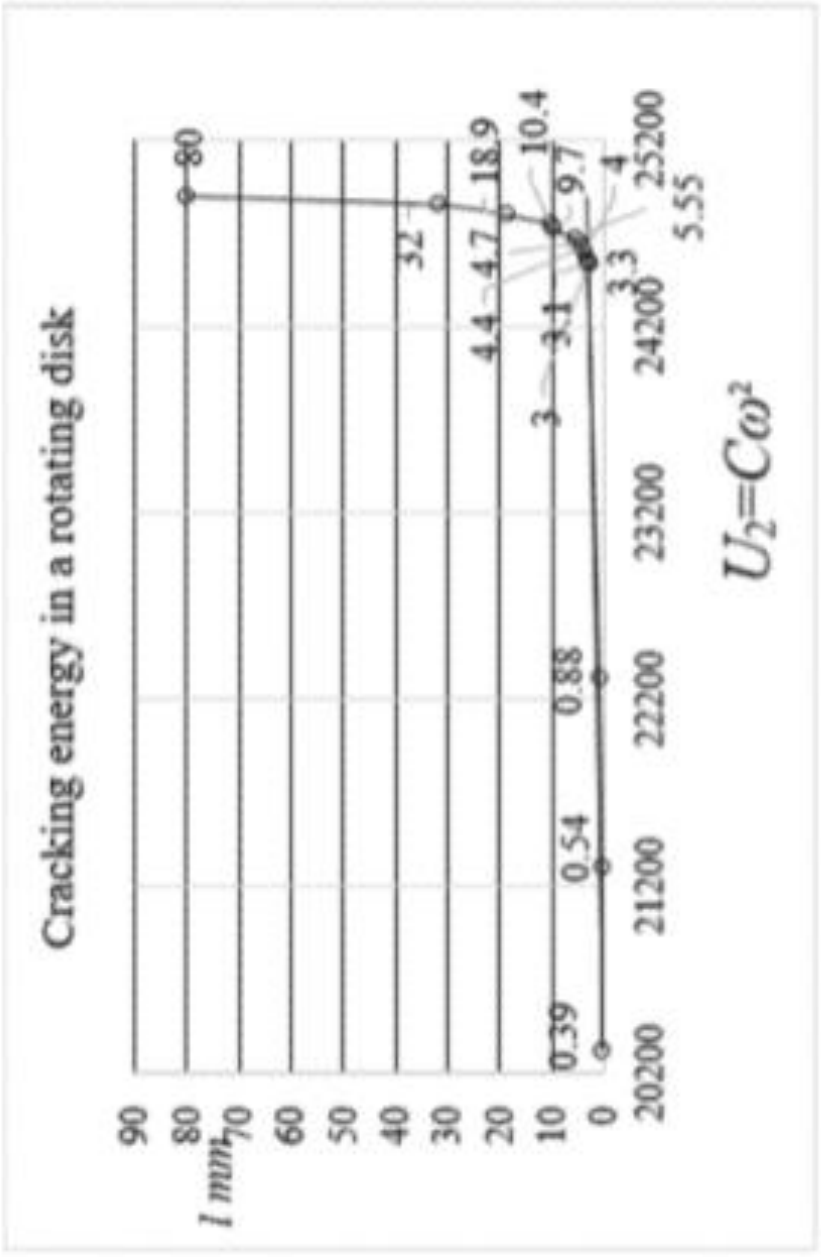
Cracking energy in a rotating disk
l mm
90
80
70
60
50
40
30
20
10
0
20200
21200
22200
23200
24200
25200
$U_2=C\omega^2$
80
32
18.9
10.4
9.7
4
5.55
4.7
4.4
3.3
3.1
3
0.88
0.54
0.39

FIG. 21

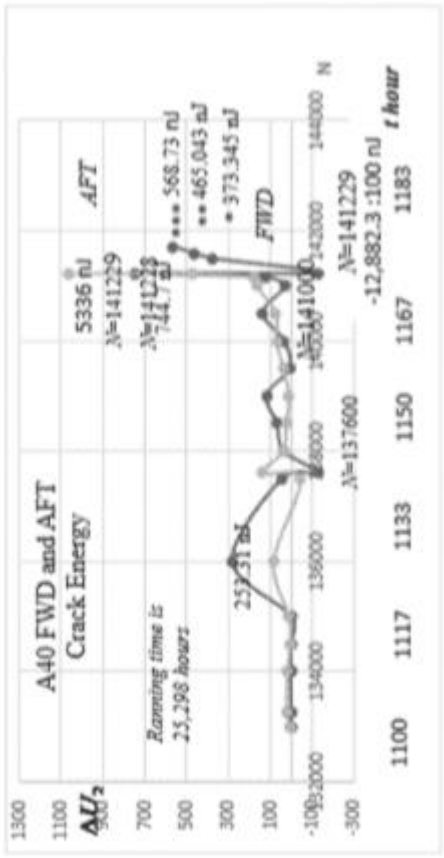
A40 FWD and AFT
Crack Energy
ΔU2
Running time is
25,198 hours
5336 nJ
λ=141229
568.73 nJ
465.043 nJ
373.345 nJ
FWD
AFT
λ=141229
-12,882.3 :100 nJ
λ=137600
1300
1100
900
700
500
300
100
-100
-300
134000
136000
138000
140000
142000
144000
N
1100
1117
1133
1150
1167
1183
t hour

FIG. 22

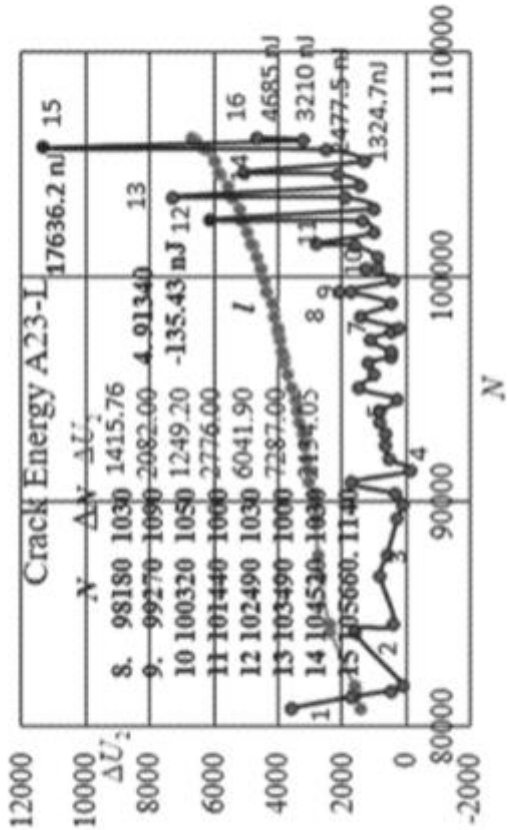


FIG. 23

SUBSTITUTE SHEET (RULE 26)

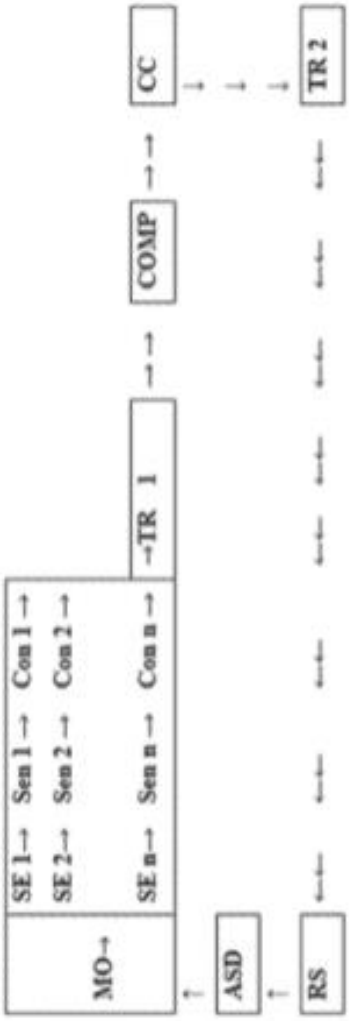
MO→
SE 1→
SE 2→
SE n→
Sen 1→
Sen 2→
Sen n→
Con 1→
Con 2→
Con n→
→TR 1
COMP
CC
TR 2
ASD
RS

FIG. 24

FIG. 25





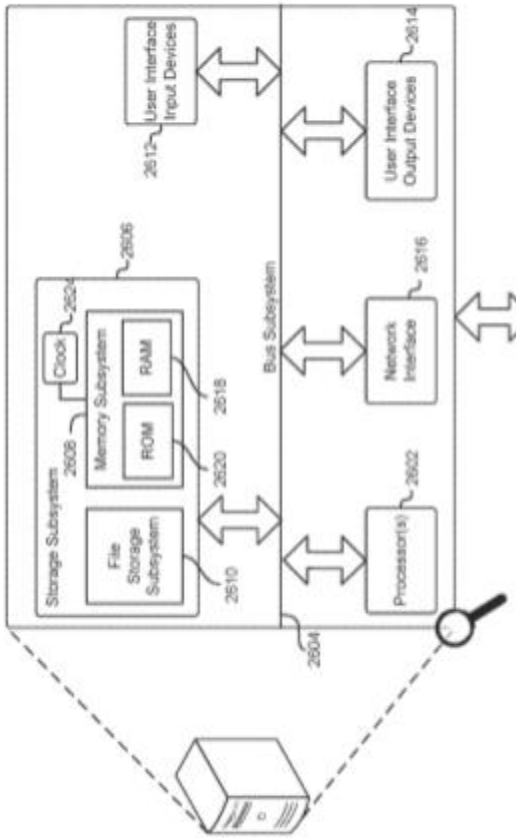
User Interface Input Devices
2612
User Interface Output Devices
2614
2606
Clock
2624
Memory Subsystem
RAM
2618
ROM
2620
Storage Subsystem
2606
File Storage Subsystem
2610
Bus Subsystem
Network Interface
2616
Processor(s)
2602
2604

FIG. 26